The University Of Sheffield.

Characterisation of DNA Repair Deficient Zebrafish for the Investigation of Neurological Disease

R Thomas

Submitted for the Degree of Doctor of Philosophy (PhD)

December 2022

Characterisation of DNA Repair Deficient Zebrafish for the Investigation of Neurological Disease

By Ruth Thomas

Submitted for the Degree of Doctor of Philosophy (PhD)

The University of Sheffield

Faculty of Science

School of Biosciences

Formally Biomedical Science

December 2022

Declaration

Some of the work included in this thesis has already appeared in published form in (Zaksauskaite *et al.*, 2021). I am a contributing author to the paper, supplying the work required for CRISPANT analysis of APEX2 in *tdp1*$^{-/-}$ larvae (Supplementary figure 5). The data in this thesis pertaining to that work is presented in Chapter 5. An unpublished zebrafish line used in this thesis is produced by Ringailė Zakšauskaitė. Mass-Spectrometry analysis was performed by the Kriaucionis Lab at the University of Oxford. When either of these are the case, it is stated in the text and/or figure legend.

I can confirm that all other work presented in this thesis is my own work.

Acknowledgements

First and foremost my thanks go to Dr Fredericus van Eeden and Professor Sherif El-Khamisy for their constant support, willingness to impart knowledge and faith that I would produce something worthwhile. I extend that thanks to all members of the van Eeden and El-Khamisy labs, past and present, you were all part of this journey. In particular I would like to thank Dr Davide Marchi. You met me with a warm smile on my first day and were always available for a coffee and a chat, a ritual that continued to keep me sane long after you left.

I've come to realise that the PhD cohort that started this journey in September 2018 were a rare kind. We found firm friendships early and consistently supported each other through experimental failures and publication success. I'm indebted to your collective ramblings on niche topics at lunch and weekly pub trips for keeping me grounded. I look forward to our next adventures, you are truly friends for life.

I would also like to thank Dr Philip Bassindale and Dr Bob Davies. Although you may not know it, the enthusiasm you showed for your own PhD research, before I even started, played a large part in my decision to undertake a PhD of my own. It also gave me confidence that the experience was something to be enjoyed and embraced, not feared, an opinion that was hard to find.

Ben Wesson, current fiancé and future husband. You were there at the start of this journey and have supported me throughout the highs and lows that came with it. A continuous reminder that the failure of an experiment was not the end of the world and that there was always cheese in the fridge.

Finally, I would like to thank my family. Firstly my brothers, Sam and Nick. Despite the fact that it came in the form of "sibling style" motivation, it was always welcome break from the PhD bubble. Dad, you are one of the most resilient people I know, a reassuring constant in a very unpredictable world and for that I can't thank you enough. Mum, although you passed away in May 2020, you have always been a key factor in my love for Biology. A botanist by training, many a holiday was spent identifying various species, primarily lichen! Although I discovered a love for the more molecular side, I certainly inherited your enthusiasm for the subject as a whole. I wish I could share this with you.

Abstract

An individual cell acquires approximately 1 million DNA lesions per day. Most lesions are resolved with little or no negative effects. Nonetheless, mutations that render important DNA repair constituents non-functional can result in debilitating diseases. Despite the advancements made through cell culture analysis, animal models are required to enable the study of redundancy and interactions at an organismal level. The small size of the zebrafish, rapid reproduction and ease of genetic manipulation has led them to be a less expensive alternative for mammalian systems.

A zebrafish model, an RNaseH2a mutant, is expected to be defective in the removal of ribonucleotides from DNA which are speculated to be a driver of the neurodegenerative disease, Aicardi Goutières Syndrome (AGS).

Surprisingly, I found that homozygous RNaseH2a mutants are phenotypically normal at adulthood, unlike previous AGS models. However, their resulting offspring show reduced development, increased ribonucleotide incorporation and upregulation in inflammatory markers, resulting in both maternal and paternal embryonic lethality. Homozygote adults show an accumulation of ribonucleotides in both the brain and testes that is not present in early development.

I hypothesized that the surviving homozygotes may have RNaseH2 like compensatory mechanisms that allow them to survive. Such mechanisms may not be activated or are overwhelmed by the inherited ribonucleotides in their offspring. I investigated a secondary repair pathway utilising topoisomerase 1 and findings from this thesis suggest a non-TOP1 dependent repair pathway.

I also investigated the repair of TOP1 associated DNA breaks in the absence of its repair factor, TDP1 and describe the use of CRISPANTs to identify two factors, APEX2 and ERCC4 in the repair of these protein linked DNA breaks.

Finally, I studied a novel TDP1 interaction factor, NuMA, via the creation of a novel zebrafish knockout to investigate the *in vivo* contributions of NuMA to the repair of oxidative stress.

Table of Contents

Table of figures

Abbreviations

8-oxo-G - 7, 8 dihydro-8-oxoguanine

Abasic, AP - apurinic/apyrimidic sites

AGS - Aicardi-Goutières Syndrome

AIM2 - Absent in melanoma 2

Alt-EJ - Alternative end-joining

AO - Acridine Orange

Ape1 - AP endonuclease 1

APEX2 - Apurinic/Apyrimidinic Endodeoxyribonuclease 2

APTX - Aparataxin

ATM - ataxia-telangiectasia-mutated kinase

ATP - Adenosine triphosphate

ATR - ATM-and Rad3-Related

ATRi - ATR inhibitor

Cdk - Cyclin dependent kinase

cGAMP - cyclic GMP-AMP

cGAS - cyclic GMP-AMP synthase

CPT camptothecin

CRISPR – Clustered Regularly Interspaced Short Palindromic Repeats

dCAPS - derived cleaved amplified polymorphic sequence

ddH_20 – double distilled water

DDR - DNA Damage Repair

dpf – Days post fertilisation

DNA - Deoxyribonucleic Acid

dNMP - Deoxynucleotide monophosphate

dNTP - Deoxynucleotide triphosphate

dr - Danio rerio

dsDNA - double-strand DNA

ER - Endoplasmic Reticulum

GG-NER - Global genome NER

gRNA - Guide RNA

GTP - Guanine triphosphate

H_20 - Water

H_2O_2 - Hydrogen peroxide

HCC - hepatocellular carcinoma

hs - Homo sapien

HU – Hydroxyurea

IF - Immunofluorescence

IFN - Interferon

IKK - IκB kinase

indels - insertions and deletions

IRF3 - Interferon regulatory factor 3

ISG - Interferon Stimulated Gene

ISGs - Interferon stimulated genes

LWT - London wild-type

MEFs - Mouse embryonic fibroblasts

MGMT - O^6-methylguanine transferase

MMR - Mismatch Repair

mpf – Months post fertilisation

MRN - Mre11-Rad50-Nbs1

Mrnaseh2a - Maternal RNaseH2a

MZrnaseh2a - Maternal zygotic RNaseH2a

NaAc - Sodium Acetate

NH4Ac - Ammonium Acetate

NER - Nucleotide Excision Repair

NFκβ - Nuclear factor-κβ

NHEJ - Non-Homologous End Joining

NRGs - NuMA Regulated Genes

NuMA - Nuclear mitotic apparatus protein

OGG1 - 8-oxoguanine glycosylase

PAR - Polymerization of ADP-ribose

PARP - Poly (ADP) ribose polymerases

PARP1 - Poly ADP Ribose Polymerase

PCNA - Proliferating Cell Nuclear Antigen

PCR – Polymerase Chain Reaction

PDB - Protein-linked DNA break

PER - Photoenzymatic repair

PIKK - Phosphatidylinositol 3 kinase-like kinases

PNKP - polynucleotide kinase 3'phosphate

Prnaseh2a - Paternal RNaseH2a

PTU - 1-Phenyl-2-thiourea

qPCR – quantitative Polymerase Chain Reaction

RAD23B - Radiation sensitive 23B

RED – Ribonucleotide Excision Repair Defective

RER - Ribonucleotide Excision Repair

RNA - Ribonucleic Acid

RNaseH2 - Ribonuclease H2

RNaseH2a – Ribonuclease H2 Subunit A

RNaseH2b – Ribonuclease H2 Subunit B

RNaseH2c – Ribonuclease H2 Subunit C

rNMP - Ribonucleotide monophosphate

rNTP - Ribonucleotide triphosphate

ROS - Reactive Oxygen Species

RPA - Replication protein A

RTP – Room temperature and pressure

SCAN1 - spinocerebellar ataxia with axonal neuropathy

SSBR - Single strand break repair

ssDNA- single-strand DNA

STING -Stimulator of Interferon Genes

TBE - Tris Borate EDTA

TBK1 - TANK binding kinase 1

TBST - Tris-buffered saline Tween 20

TC-NER - Transcription-coupled NER

TDP1 - Tyrosyl-DNA phosphodiesterase

TFIIH - transcription initiation factor IIH

TLR9 - Toll-like receptor 9

TOP1 - Topoisomerase 1

TOP1-cc -TOP1 covalent complex

UV - ultraviolet

γH2AX - Phosphorylated Histone2AX

Chapter 1

Introduction

1.1 Introduction to genome stability

DNA damage is constantly occurring and can cause approximately 1 million lesions in the DNA of each cell every day. Damage can be caused by both internal sources, such as transcription and replication, but also external sources like ultraviolet (UV) light and chemicals, such as those found in cigarette smoke. Damage can include the modification or loss of nucleotide bases, hydrolysis of the N-glycosidic bonds or damage to the DNA backbone itself. These can lead to single-strand DNA (ssDNA) breaks or the more toxic double-strand DNA (dsDNA) breaks **(Figure 1.1)**.

Organisms rely on the faithful transmission of genetic material to reproduce, develop and survive. To maintain the conservation and inheritance of genetic material, organisms have evolved several repair pathways to maintain DNA stability. This DNA Damage Repair (DDR) system includes the sensing of initial damage, followed by a signalling cascade to activate downstream repair components of several different, yet overlapping pathways. Key pathways include the repair of bases that no longer obey the Watson-Crick pairing laws or removal of whole bases in Nucleotide and Base Excision Repair (NER/BER). Finally, repair of both single and double strand breakage is also vital for maintaining DNA stability. In the case of the level of damage being too high to repair, systems such as apoptosis are key for removal of potentially malignant cells.

As indicated, much of the damage that occurs is repaired with little or no negative consequences due to the DNA damage response pathway. Their importance is underlined by the fact that defects in these pathways can lead to premature aging, immunodeficiency, tumorigenesis and cell death. Due to the importance of DNA repair pathways, they are highly conserved in eukaryotes which allows for translational research between model organisms.

The main focus of this thesis will be on the use of zebrafish to study the removal and repair of incorporated ribonucleotides. It will also cover key interaction partners and the clinical relevance of failures in these pathways.

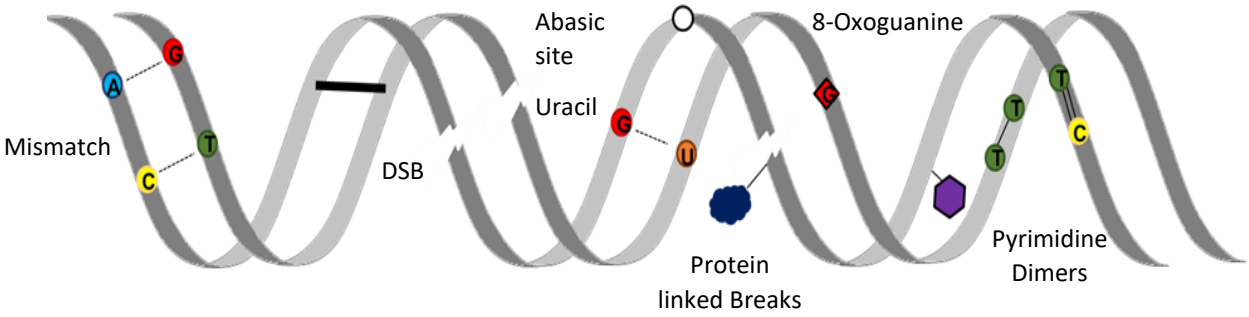

Figure 1.1: Types of DNA Damage occurring from endogenous and exogenous factors

Watson-Crick pairing can be disrupted by modification of bases such as methylation, formation of abasic sites, oxidisation to form 8-oxoguanine (8-oxo-G) as a result of reactive oxygen species and spontaneous deamination that can be induced by UV radiation. The DNA backbone can be effected by interstrand crosslinking and the formation of single-strand breaks. These can be formed through spontaneous cleavage of incorporated ribonucleotides or via enzymatic processes such as Topoisomerase 1-mediated relaxation of DNA (El-Khamisy *et al.*, 2005). Double strand DNA breaks can arise from two single-stand breaks in close proximity.

1.2 Types of DNA damage

1.2.1 Ribonucleotide incorporation

The concentrations of ribonucleotide triphosphates (rNTPs) in a cell vastly outnumber those of deoxyribonucleotide triphosphates (dNTPs), leading to the incorporation of single ribonucleotides during DNA replication (Chabes *et al.*, 2003). The structural and charge differences between the two nucleotides is utilised by polymerases to help limit the rate of this incorporation as they have evolved steric-gate and polar gate filters (Brown and Suo, 2011; Johnson, Kottur and Nair, 2019). Despite this, *in vitro* experiments have revealed the incorporation of ribonucleotides into the genome of eukaryotic cells at a rate of approximately 1 every several thousand base pairs (Kunkel, 1999; Nick McElhinny *et al.*, 2010; Reijns *et al.*, 2012). Also during replication, 30-50 million Okazaki fragments of 10 ribonucleotides in length are used to initiate synthesis of short strands of lagging strand DNA, resulting in their attachment to the newly synthesised DNA stand. Although these are usually transient, removal of the fragments can be incomplete, contributing to the overall rNMP (ribonucleotide monophosphate) incorporation rate (Rumbaugh *et al.*, 1997). Ribonucleotides are also incorporated during repair via Non-Homologous End Joining (NHEJ) and are required for Ligase4 dependent repair of DNA breaks repaired by Pol μ (Pryor *et al.*, 2018).

During transcription, the mRNA strand produced has been shown to 'invade' the DNA duplex at the transcription bubble and anneal to the opposing DNA strand creating an RNA:DNA hybrid or 'R-loop'. However, given that the RNA strand is not directly incorporated into the DNA stand, it is unlikely that this can produce stably incorporated rNMPs. Despite this, R-loops are still considered to be threats to genome stability due to the exposure of a single DNA strand (Aguilera and García-Muse, 2012). However, RNA:DNA hybrids are also utilised in a positive manner, namely at telomeres. Here, they act as primers for the 3' extension of the complementary DNA strand. Like Okazaki fragments, if not efficiently removed, they can become incorporated and have been shown to result in telomere reduction and increased cellular senescence (Balk *et al.*, 2013).

1.2.1.1 Negative Consequences of ribonucleotide incorporation

Ribonucleotides are intrinsically more unstable then their deoxyribonucleotide counterparts as they contain a 2' OH moiety, not present in dNTPs. Given the structural differences

between dNTPs and rNTPs, the helical shape produced by two dNTP is disturbed via the incorporation of an rNTP, resulting in the inability of proteins to interact with the new helical shape (Egli, Usman and Rich, 1993; Meroni *et al.*, 2017). This can cause problems with processes such as transcription, whilst also stalling replication forks (Hovatter and Martinson, 1987).

The 2'OH also acts as an electron donor, causing spontaneous stand cleavage via a nucleophilic attack on the sugar-phosphate backbone of the DNA creating a 5'hydroxyl and 2'-3'-cyclic phosphate flanked single stranded DNA break (Li and Breaker, 1999). If these ssDNA breaks are in close proximity to each other, they can lead to the more aggressive dsDNA breaks (Li and Breaker, 1999). Groups of rNMPs can also cause stalling of the replication fork leading to cell cycle arrest and apoptosis. This is particularly evident when it occurs in mtDNA (Holmes *et al.*, 2015).

Removal of ribonucleotides via inefficient or error prone mechanisms is also a large cause of mutations produced via rNMPs and will be discussed in more detail later.

1.2.1.2 Ribonucleotide incorporation has important roles in normal cell biology

Despite the negative consequences described above, incorporation of ribonucleotides have been shown, in yeast, mice and humans, to be an enhancer of the Mismatch Repair (MMR) pathway. Here they are thought to act as a signalling molecule, labelling the nascent DNA strand (Lujan *et al.*, 2013). The rNMPs are also cleaved by Ribonuclease H2, generating a single strand nick allowing the loading of Exo1, and subsequent removal of nearby mismatches. For this to be the case, the rNMPs and base errors are required to be within 1KB, suggesting that this mechanism is a small part of the overall MMR pathway (Ghodgaonkar *et al.*, 2013). They are also implicated in NHEJ, mentioned earlier (Pryor *et al.*, 2018). Ribonucleotides have also been shown to play in key role in the mating type switching phenomenon seen in yeast. They aid this by stalling replication forks, allowing for a replication coupled recombination event to aid type switching (Dalgaard, 2012).
These 'positive' consequences of rNMP incorporation are one of the main cause of debate that ribonucleotides are not always 'mis'-incorporated, but perhaps are intentionally included for specific biological roles, including DNA repair. However, their over-incorporation is known to cause cell cycle arrest and neurological disease in humans, so

removal of un-intentionally incorporated ribonucleotides is still essential (Goutières *et al.*, 1998).

1.2.1.3 Ribonucleotide removal

1.2.1.3.1 Single rNMPs

The first method of removal is by the 3'-5' exonuclease activity by DNA polymerases, after DNA replication (Kunkel, 2004, 2009, 2011) . Shown to be present in both yeast and humans, this activity can be performed by various Polymerases (ε/δ) but to differing efficiencies. They also remove rNMPs less efficiently than incorrectly incorporated dNTPs (Williams *et al.*, 2012; Clausen *et al.*, 2013).

The most efficient pathway of single ribonucleotide removal, is the Ribonucleotide Excision Repair (RER) pathway. This requires cleavage of the rNMP by Ribonuclease H2 (RNaseH2), flap removal by FEN1/EXO1 and ligation of the two exposed DNA strand ends by DNA ligase (Stephanie A. Nick McElhinny *et al.*, 2010). Although proof of this mechanism has only been established via *in vitro* work, it is thought to be highly conserved as the removal of RNaseH2 from yeast has shown an increase in the number of stable rNMPs incorporated whilst knockouts in mouse models have shown it to be essential for survival (Stephanie A. Nick McElhinny *et al.*, 2010; Uehara *et al.*, 2018). This method of removal can occasionally go awry and premature ligation results in adenylated-5'-RNA-DNA junctions. Aprataxin has been shown to resolve such RER-intermediates (Tumbale *et al.*, 2014).

In the absence of RNaseH2, previous literature has shown that Topoisomerase 1 (TOP1), usually involved in the release of torsional stress from DNA, can cleave single ribonucleotides (Williams *et al.*, 2013). This process however can be error prone, particularly at repetitive sequences, leading to the deletion of 2-5 base pairs (Reijns *et al.*, 2022). Other enzymes have been linked with the TOP1 removal of ribonucleotides including APN2/APEX2. APEX2 has endonuclease activity that can resolve the 2'-3' cyclic phosphate that forms as a result of TOP1 rNMP cleavage. This resolution allows for a reduction in the number of cases in which short DNA stands are deleted during repair, thus acting in a protective manner against the mutagenic TOP1 repair process (Li *et al.*, 2019). Recent literature has also shown that the DEAD-box helicase DDX3X has ribonucleotide excision

repair activities, similar to RNaseH2, which may allow it to act as an alternative pathway of removal (Riva *et al.*, 2020).

1.2.1.3.2 Multiple rNMPs

The removal of multiple rNMPs occurs in several instances. One is the removal of Okazaki fragments after their use in replication of the lagging strand. In yeast, RNaseH2 is able to, but not essential for, the removal of these fragments via cleavage of one ribonucleotide at a time with final removal occurring via FEN1. They can also be removed via Pol δ displacement and FEN1/Dna2 removal (Qiu *et al.*, 1999; Garg *et al.*, 2004; Liu *et al.*, 2017).

Other RNA:DNA hybrids such as R-loops can also be resolved by RNaseH2. It has been reported that RNaseH2 becomes a part of the PolII complex and is involved in the removal of R-loops that form at a subset of transcribed genes. A second Ribonuclease, RNaseH1, has a more primary role in the removal of R-loops and its overexpression is often used as a negative control in S9.6 immunofluorescent experiments. However studies have suggested that RNaseH1 and RNaseH2 may resolve specific subsets of R-loops at nascent levels (Lockhart *et al.*, 2019; Cristini *et al.*, 2022). In yeast, both RNaseH enzymes have been implicated in the removal of RNA:DNA hybrids at telomeres (Balk *et al.*, 2013).

1.2.2 Topoisomerase 1 linked DNA breaks

As mentioned, TOP1 is involved in removing single ribonucleotides in the absence of RNaseH2. However, its main role in maintaining DNA stability is the release of the torsional stress that occurs to the DNA helix during replication. TOP1 is known to relieve such stress via the cleavage of one strand of DNA to aid relaxation via unwinding. During this process TOP1 becomes covalently bound to the DNA to form a TOP1 covalent complex (TOP1-cc). Although usually reversible, this protein linked DNA break can become permanent in the event of collision with replication machinery, close proximity to another TOP1-cc or via chemical inhibition. These protein linked DNA breaks can have negative consequences on a cell such as the stalling of transcription. If this occurs on highly transcribed genes, it can lead to a large number of dsDNA breaks forming and subsequent cell death.
Resolution of TOP1-cc's is reported to occur via tyrosyl-DNA phosphodiesterase (TDP1),

mutations in which can cause severe neurological damage in humans (Takashima *et al.*, 2002).

1.2.3 Oxidative DNA Damage

Cellular metabolism is critical for survival and is also the main internal source of Reactive Oxygen Species (ROS). Production of ROS can come from the generation of superoxides during the electron transport chain as well as hydroxyl radicals, hydrogen peroxide (H_2O_2) and single oxygen species. ROS can also be produced via external sources such as UV light and ionizing radiation that cause production of intracellular ROS (Mccormick *et al.*, 1976). ROS can be beneficial to the cell at low levels, being involved in signalling reactions and used as a defence mechanism against virally infected cells (Segal, 2005). However, these low level benefits can easily become damaging at higher levels.

Formation of oxidative damage mainly occurs via the highly reactive OH radical (Imlay, Chin and Linn, 1988). Methods of damage include addition to the double bonds of DNA bases, modification of their methyl groups and even targeting the sugar backbone (Breen and Murphy, 1995). The most commonly oxidized base is Guanine, forming 7, 8 dihydro-8-oxoguanine (8-oxo-G). This base no longer obeys the laws of Watson-Crick base paring and instead mis-pairs with Adenine, leading to transversion mutations in replicating cells (Cheng *et al.*, 1992). The removal of oxidative damage such as 8-oxoG is reported to occur via the 8-oxoguanine glycosylase (OGG1). Persistent oxidative DNA damage has been linked to cancer, neurodegeneration and aging (Cooke *et al.*, 2003).

1.2.4 Other DNA damage lesions

1.2.4.1 Base damage

Mismatch of DNA bases can occur during replication resulting in an inserted base that does not obey the Watson-Crick pairing laws. However, even correctly paired bases can undergo modifications such as methylation. This can lead to bulky adducts such as 7-methylguanine and 3-methyladenine that can cause spontaneous cleavage and inhibition of DNA synthesis respectively (Rydberg and Lindahl, 1982; Park and Ames, 1988).

Total removal of bases via breakage of the N-glycosyl bond between a nitrogenous base and the sugar phosphate backbone result in an apurinic/apyrimidic sites (Abasic, AP). This can either be due to spontaneous hydrolysis, or intentional cleavage during the Base Excision Repair pathway. AP sites readily convert to single strand DNA breaks due to their instability (Lindahl, 1993).

1.2.4.2 Backbone damage

Single strand breaks frequently occur at TOP1-cc's, ribonucleotide cleavage and during the repair of mismatch bases. Although usually repaired, if they are in close proximity to one another, they can lead to the more deleterious dsDNA breaks.

Formation of dsDNA breaks can occur due to the attempted repair of two oxidized bases on opposing strands (Yang, Galick and Wallace, 2004; Cannan *et al.*, 2014) or collapse of the replication fork (Mirkin and Mirkin, 2007; García-Muse and Aguilera, 2016). DsDNA breaks can also be formed by exogenous factors such as ionizing radiation and chemical mutagens. Despite being one of the most mutagenic forms of DNA damage, dsDNA breaks are utilized by the cell to perform events such as immunoglobulin class switching (Keeney and Neale, 2006) and in meiosis during V(D)J recombination (Dudley *et al.*, 2005).
Even when dsDNA are actively created (V(D)J recombination) and tightly controlled, errors can still occur and they can become permanent. Due to the ability of the DNA ends to completely separate from one another, this can lead to further DNA instabilities such as translocation of fragments and large deletions (Jackson, 2002). The consequences of large numbers of dsDNA breaks can be extremely detrimental due to the loss of genomic stability, subsequently leading to tumorigenesis or programmed cell death.

1.3 DNA damage response

As discussed, there are a large number of different ways the DNA can become damaged. This requires a similarly large number of different repair pathways, each specific to a certain subset of lesions. In order to activate the correct pathways for the damage, signalling cascades are utilized to activate the correct repair components. Although each transduction pathway is activated by a specific lesion, there is overlap in the enzymes and chemicals used to regulate each one. Two of the key families are the poly(ADP)ribose polymerases (PARP) and phosphatidylinositol 3 kinase-like kinases (PIKK).

1.3.1 Signal transduction

1.3.1.1 Poly(ADP)ribose polymerase

One of the key roles of PARP proteins is their activation via the recognition of single stranded DNA breaks by their zinc-finger binding motifs. PARP has been shown to catalyse the polymerization of ADP-ribose (PAR) polymers utilizing NAD+ as the substrate and this PARylation occurs both on itself and on other factors. These PAR chains recruit repair components to the site of damage and regulates their activity (Luo and Lee Kraus, 2012; Bai, 2015; Ray Chaudhuri and Nussenzweig, 2017). PARP activity has been particularly well characterized in Base Excision Repair and is known to facilitate the recruitment of XRCC1 and more recently in the repair of stalled TOP1-cc's through the formation of TDP1-PARP1 complexes (Das *et al.*, 2014). Although PARP1 is thought of as a DNA repair factor, the accumulation of PAR polymers can become cytotoxic (Ray Chaudhuri and Nussenzweig, 2017). One of the key downstream factors activated by PARP1 is the PIKK enzyme Ataxia-Telangiectasia-Mutated kinase (ATM).

1.3.1.2 Phosphatidylinositol 3 kinase-like kinase

The phosphatidylinositol 3 kinase-like kinase (PIKK) enzyme Ataxia-Telangiectasia-Mutated kinase (ATM) and ATM-and Rad3-Related (ATR) are two of the earliest proteins involved in the DDR pathway and are key factors is activating downstream components (Lempiäinen and Halazonetis, 2009; Lovejoy and Cortez, 2009). Much of this regulation requires phosphorylation of proteins at Ser/Thr-Glu motifs by ATM and ATR (Matsuoka *et al.*, 2007). Together, ATM and ATR also induce a second round of phosphorylation through key cell cycle regulators such as Chk1/2, MK2 and H2A.X (Matsuoka, Huang and Elledge, 1998; Liu *et*

al., 2000; Matsuoka *et al.*, 2007; Reinhardt *et al.*, 2007).

In terms of responding to damage, ATM has been shown to rapidly localize to dsDNA breaks, resulting in its activation. This activation is known to occur via the Mre11-Rad50-Nbs1 (MRN) complex that is one of the earliest protein complex recruited to double strand breaks and is thought to be responsible for the localization of ATM at dsDNA breaks (Uziel *et al.*, 2003; Lee and Paull, 2005).

ATR has a more pronounced role in response to replication fork collapse and the repair of single strand breaks. This recruitment occurs via the coating of ssDNA with replication protein A (RPA) and interaction with the, ATR interacting protein (ATRIP) (Cortez *et al.*, 2001).

Other members of the PIKK family include DNA-PKs, mTOR, SMG1 and TRRAP that have roles in non-homologous end joining, metabolism, nonsense medicated mRNA decay and chromatin remodelling (Imseng, Aylett and Maier, 2018), all of which are involved in DNA repair mechanisms present in eukaryotic cells.

1.3.2 Repair of nucleotide bases

1.3.2.1 Direct Reversal

This method of damage correction is specific and does not involve the breakage of the DNA backbone. One time use enzymes such as O^6-methylguanine transferase (MGMT) are used to remove methyl groups from DNA, returning them to their original state.

1.3.2.2 Mismatch Repair

A slightly more invasive repair mechanism is that of mismatch repair. In mammals, MMR is instigated by the MutSα (MSH2-MSH6) or MUTSβ (MSH2-MSH3). Directed by MSH2 binding directly to the PCNA, the MutS complex recruits the MutLα which nicks the DNA either side of the mismatched base. Resection then occurs in a 5'-3’ direction via Exo1 resulting in a single stranded DNA. This is cover by RPA, displacing the Mut complexes and recruiting downstream repair factors including DNA ligase 1, allowing gap-filling to occur resulting in restoration of a stable dsDNA (Zhang *et al.*, 2005).

1.3.2.3 Base Excision Repair

BER is involved in the removal of lesions that do not cause significant alteration to the DNA helix. These include the oxidative damage lesion 8-oxoG. These damage sites are recognized by a glycosylases that remove the damaged bases, leaving an AP site. This site undergoes 5' cleavage by AP endonuclease 1 (Ape1) which is then edited by DNA polymerase β before being sealed by LIG1 or a complex made up of XRCC1 and Ligase III (Gueven *et al.*, 2004).

1.3.2.4 Nucleotide Excision Repair

Nucleotide Excision Repair (NER) is mainly used to remove bulky lesions from DNA such as those produced by UV radiation.

Two distinct NER pathways have been identified. These are determined by whether the lesion causes transcription stalling, transcription-coupled NER (TC-NER) or if the break is present on the rest of the genome, a situation in which the cell would use global genome NER (GG-NER). Both undertake a 'cut and patch' mechanism of repair, excising a small, single stranded section of DNA containing the lesion and using the second strand as a template for repair.

Activation of the pathways is where they differ. TC-NER is activated by the stalling of RNA polymerase II which then recruits ERCC6 (CSB) and ERCC8 (CSA) whereas GG-NER identifies lesions through the use of two complexes, Xeroderma Pigmentosum, complementation group C (XPC) and the UV repair protein radiation sensitive 23B (RAD23B). (Fousteri and Mullenders, 2008) The two pathways then converge into one common repair pathway. Initially transcription initiation factor IIH (TFIIH) is recruited which contains bi-directional helicase activity. This results in the unzipping of around 30 nucleotides surrounding the lesion which is then stabilized by XPA and RPA. Endonucleases XPG and ERCC1-XPF then cleave at the 3' and 5' ends respectively, excising the 30 nucleotides including the lesion. This gap is then filled by DNA polymerases δ, ε or κ before being sealed via DNA ligase I or II. (Giglia-Mari, Zotter and Vermeulen, 2011).

1.3.3 Repair of DNA breaks

1.3.3.1 Single Strand Break Repair

Single strand break repair (SSBR) is primarily activated by the recruitment of the previously described Poly ADP Ribose Polymerase 1 (PARP1). Activation of PARP results in the recruitment of Ape1, polynucleotide kinase 3'phosphate (PNKP) and Aprataxin (APTX) before FEN1 excision of the damaged ends, followed by gap-filling with POL β/δ/ε and relegation via XRCC1 dependent LIG1. A secondary, similar mechanism known as short patch SSBR requires recognition by APE1 and gap filling via POLβ and LIGIII. **(Figure 1.2)**
A more specific variant of the long patch pathway is that performed by TDP1 processing of a 3'-phosphodiester bond which will be discussed later.

1.3.3.2 Double strand DNA Break Repair

Recognition of a dsDNA break initiates activation of ATM, phosphorylation of H2AX and recruitment of repair factors such as 53BP1.

Non-homologous end joining is a method of repair used to solve double strand breaks via re-ligation of DNA ends with no requirement for a homologous template. Initial recognition is performed by the Ku (Ku70 and Ku80) complex. This then recruits other repair factors such as Artemis and DNA protein kinase catalytic subunit (DNA-PKcs) that are involved in the stabilisation and resection of damaged ends. Gap filling is performed by POLλ before ligation with LIG4 **(Figure 1.3)**. NHEJ has the capability to resolve several different types of dsDNA breaks from blunt ends to incompatible 5' and 3' ends. Each require a slightly different sub-set of repair proteins but all employ the key Artemis/DNA-PKc complex (Chang *et al.*, 2017).

Homologous recombination is the far more accurate repair of dsDNA breaks, but requires the cell to be in G2/S phase of the cell cycle. Recognition occurs via the MRN complex that subsequently recruits ATM. The downstream signalling cascade recruits factors required for 5'-3' degradation of the DNA strand (CtIP, Exo1 and DNA2) to produce 3' overhangs that are subsequently surrounded by repair factors (RPA, RAD51 and BRCA2) to produce a nucleoprotein filament. This then invades a dsDNA section via the action of RAD54/B and polymerases. The subsequent Holliday junction is processed with DNA repair synthesis

factors (SLX1-SLX4, MUS81-EME1, GEN1, BLM-TOPOIII-RMI1-RMI2) via the use of the intact strand as a template (Chatterjee and Walker, 2017) **(Figure 1.3)**.

Finally, there is an inaccurate, alternative end-joining (Alt-EJ) method of repair. This process is thought to be a Ku-independent method of NHEJ involving recognition by PARP1. Mre11 and CtIP are then recruited and resect fewer than 20 bases before DNA synthesis by POlq and ligation by DNA ligase I or III (Thyme and Schier, 2016). If end joining is mediated by the use of 5-25 base pair (bp) regions of micro homology, it can result in small deletions (Truong *et al.*, 2013) **(Figure 1.3)**.

1.3.4 Activation of the inflammatory response pathway via cytosolic DNA

In response to pathogen infection, recognition of nucleic acids (DNA, RNA and RNA:DNA hybrids) is essential in the protection of the cell. Several pathways exist to recognize these aberrant nucleic acids including Toll-like receptor 9 (TLR9) Absent in Melanoma 2 (AIM2). However, of main interest to this thesis is the cyclic GMP-AMP (cGAMP) synthase (cGAS). Upon direct binding to DNA, cGAS undergoes a conformational change that allows the activation of its enzymatic activity. This converts Adenosine triphosphate (ATP) and Guanine triphosphate (GTP) into cGAMP. cGAMP binds to the Stimulator of Interferon Genes (STING) which is situated on the Endoplasmic Reticulum (ER) (Wu *et al.*, 2013). Oligomerisation of STING causes it's transportation to the Golgi. TANK binding kinase 1 (TBK1) and IκB kinase (IKK) are recruited and phosphorylate Interferon regulatory factor 3 (IRF3) and nuclear factor-κβ (NFκβ) inhibitor Iκβα respectively. IRF3 and NFκβ then translocate into the nucleus and activate inflammatory response genes such as IL-6, TNFα and Type 1 Interferons (Ishikawa, Ma and Barber, 2009; Motwani, Pesiridis and Fitzgerald, 2019).

Although I have described the activation of cGAS/STING via viral DNA, this pathway can also be activated by cGAS binding of host DNA that has entered the cytoplasm after being fragmented. Evidence suggests that this occurs via the formation of micronuclei, created via the recruitment of the nuclear envelop to chromosome fragments. This occurs during cell division, and results in micronuclei within the cytoplasm of newly formed cells (Fenech *et al.*, 2011). Further studies have shown that approximately 60% of micronuclei membranes break during interphase, resulting in the release of chromosomal fragments into the

cytoplasm (Hatch *et al.*, 2013) and that the normal mechanisms of nuclear membrane repair present in the nucleus, are not active in micronuclei (Raab *et al.*, 2016). The release of fragments can cause aberrant activation of STING as described earlier, resulting in continuous upregulation of interferon stimulated genes which can ultimately result in increased cell death, senescence, neuroinflammatory disease and cancer (Li and Chen, 2018).

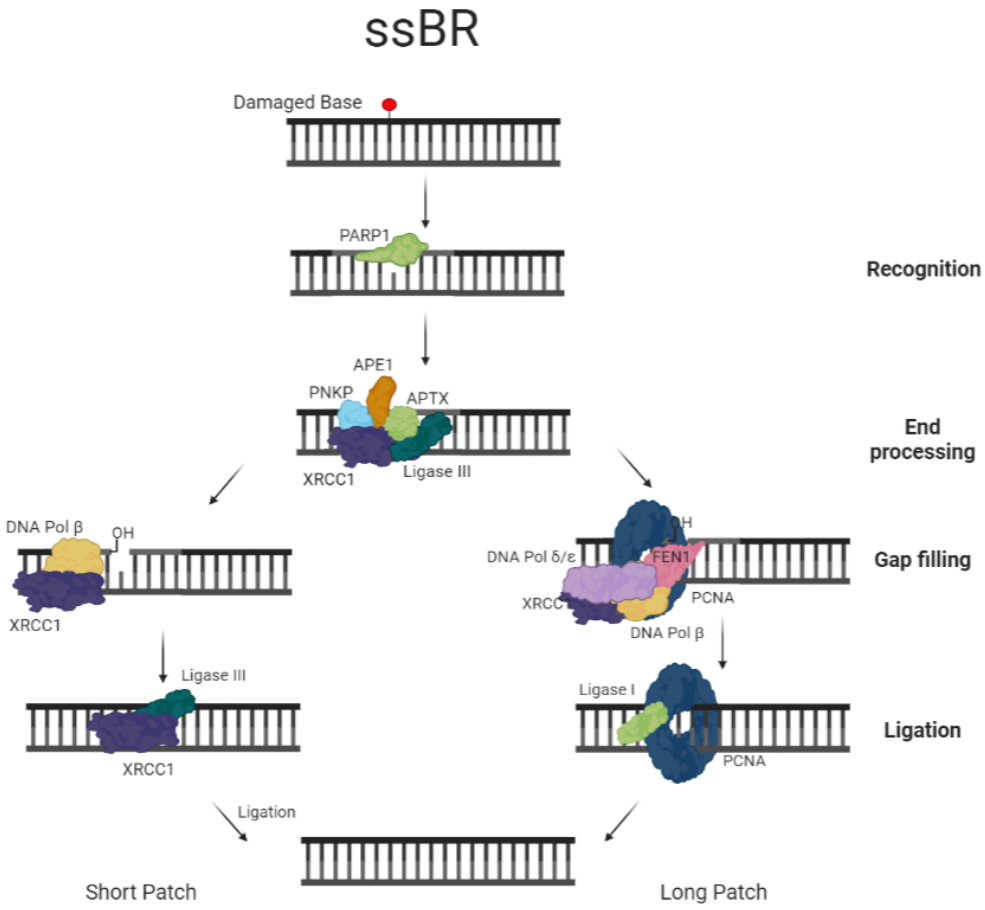

Figure 1.*2*: Single *strand break repair pathway for the resolution of a damaged base*

Single strand breaks can arise from damaged bases (e.g. 8-oxoG) that are converted into AP sites. Repair starts with recognition by PARP1 (lime) which actively recruits APE1 (Orange) PNKP (Blue) APTX (Green), XRCC1 (Purple) and Ligase III (Dark Green). These perform end processing via resection of the DNA strands. In long patch repair, gap-filling occurs via DNA Pol β (Yellow), Fen 1 (Red) and DNA Pol δ/ε (lilac) and ligation by PCNA (Dark blue) and ligase 1 (light green). In short patch, gap-filling only requires DNA Pol β (Yellow) and XRCC1 (Purple) with ligation performed by Ligase III (Dark green). Figure created with BioRender.com and adapted from (Caldecott, 2008).

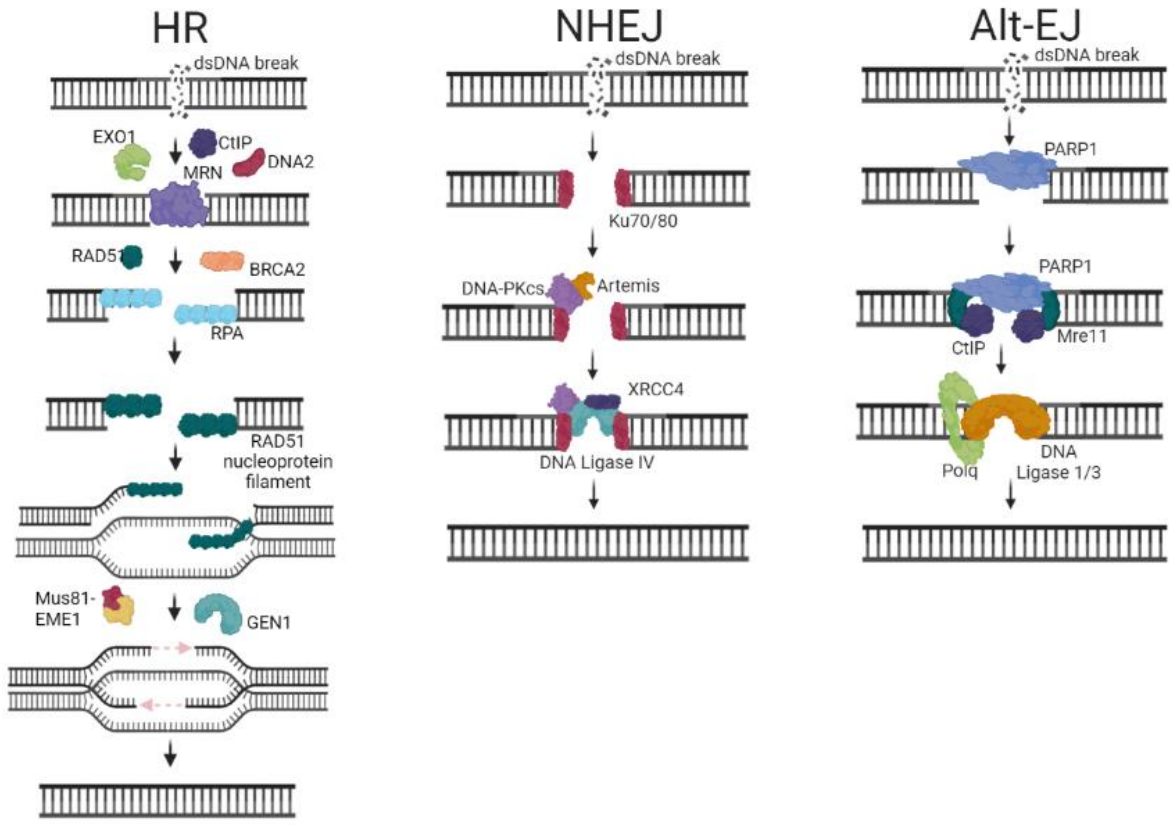

Figure 1.3: Mechanisms of dsDNA break repair

A) Homologous recombination (HR) initiated via the MRN complex recognising and binding the dsDNA break. This then activates ATM (not shown). ATM recruits downstream factors including Exo1 (green), CtIP (dark blue) and DNA2 (red) that resect the DNA strand. RPA (light blue) coats the single stand and subsequently recruits RAD51 (dark green) and BRCA2 (orange) to create a nucleoprotein filament. The filament invades a dsDNA section to create a Holliday junction that is processed by the Mus81-EME1 complex (Yellow/Red) and GEN1 (Blue). **B)** Non-Homologous End Joining (NHEJ) utilises the Ku complex (Red) to recruit repair factors DNA-PKcs (Purple) and Artemis (Orange) involved in strand resection before gap-filling and ligation with Polλ (not shown) and Ligase IV (Teal). **C)** Alternative End-Joining (Alt-EJ) is a Ku independent method of repair that utilises PARP1 (Blue), resection by Mre11 (Purple) and CtIP (Green) with Polq (green) and DNA ligase 1/3 (orange) perform gap-filling and ligation. Figure created with BioRender.com.

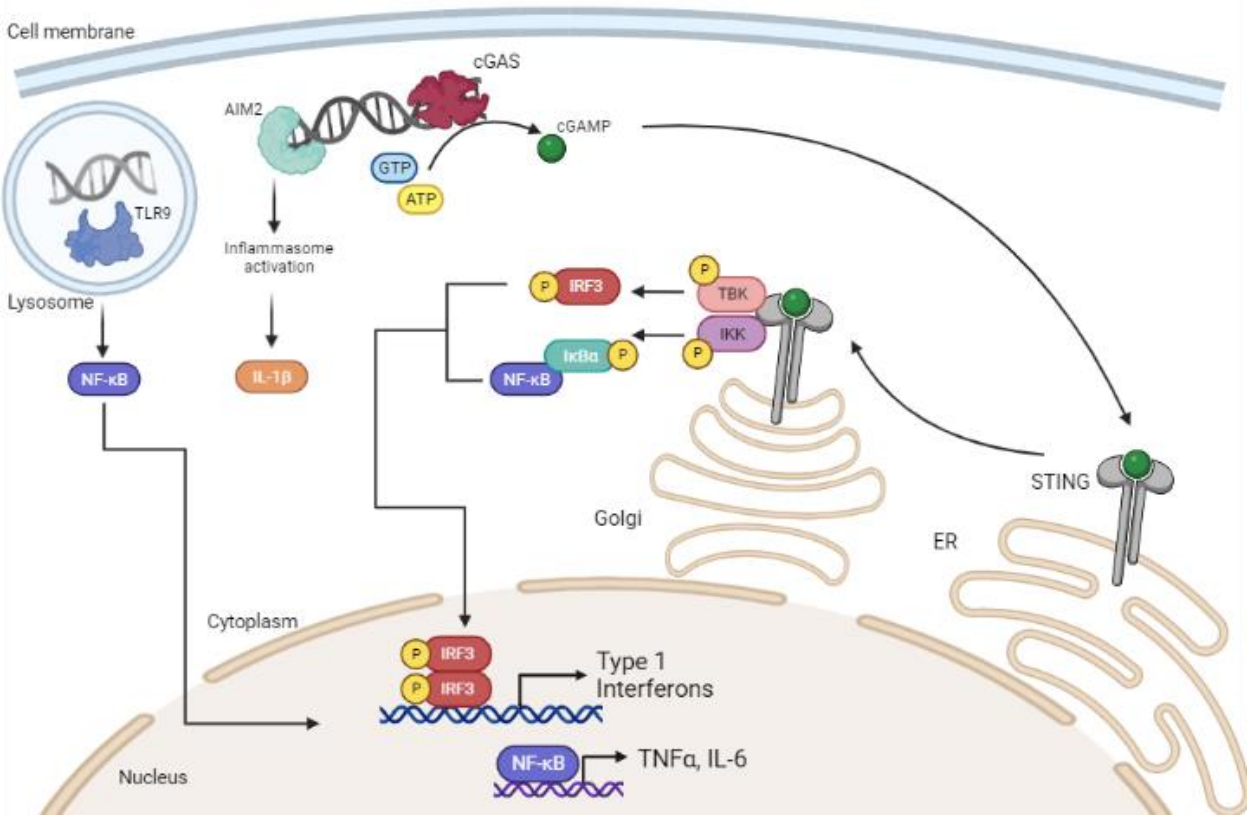

Figure 1.4: Activation of the cGAS/STING inflammatory response pathway

Recognition of nucleic acids (DNA, RNA and DNA:RNA hybrids) is essential in the protection of the cell from external infections. Toll-like receptor 9 (TLR9) is located in the lysosome and targets methylated substrates. Absent in melanoma 2 (AIM2) and cyclic GMP-AMP (cGAMP) synthase (cGAS) both recognise dsDNA. AIM2 causes activation of the inflammasome and maturation of IL-1 β. Once bound to DNA, cGAS converts Adenosine triphosphate (ATP) and Guanine triphosphate (GTP) into cGAMP. cGAMP binds to the Stimulator of Interferon Genes (STING) on the Endoplasmic Reticulum (ER) Upon binding, oligomerisation of STING occurs resulting in its transportation to the golgi. TANK binding kinase 1 (TBK1) and IκB kinase (IKK) are recruited and phosphorylate Interferon regulatory factor 3 (IRF3), causing dimerization, and nuclear factor-κβ (NFκβ) inhibitor Iκβα respectively. IRF3 and NFκβ then translocate into the nucleus and induce the expression of IL-6, TNFα and Type 1 Interferons. Modified from (Motwani, Pesiridis and Fitzgerald, 2019) and created in Biorender.com.

1.4 Ribonuclease H

1.4.1 Structure and mechanism of action

Single ribonucleotides incorporated into DNA are repaired mainly via the Ribonucleotide Excision Repair pathway (RER). This is mediated by Ribonuclease H2, a restriction endonuclease that cleaves ribonucleotides at the 5' end. There are two classes of Ribonuclease H, RNaseH1 and RNaseH2 (Cerritelli and Crouch, 2009). RNaseH1 is involved in solving multiple consecutive, four or more, rNMPs whereas RNaseH2 can remove single rNMPs that have been incorporated. RNaseH2 is a heterotrimeric protein (Subunits A, B and C) in eukaryotes (a single protein in Bacteria and Archaea) (Jeong *et al.*, 2004; Crow *et al.*, 2006). RNaseH2a contains the catalytic site required for cleavage (Sparks *et al.*, 2012). Nevertheless, the two accessory subunits, RNaseH2B and RNaseH2C are also essential for activity. Subunit B has a PIP box, required for binding to the Proliferating Cell Nuclear Antigen (PCNA) which will scan and identify the incorporated rNMP (Chon *et al.*, 2009; Bubeck *et al.*, 2011; Reijns *et al.*, 2011). The RNaseH2 complex will then cleave at the 5' side of the ribonucleotide to produce a 3' hydroxyl and a 5' phosphoribonucleotide. Following this cleavage, Fen1/Exo1 removes the rNMP and DNA ligase repairs the single strand break (Sparks *et al.*, 2012) **(Figure 1.5)**.

1.4.2 Clinical significance

Mutations in any of the three RNaseH2 subunits have been associated with the rare neurological disease, Aicardi-Goutières Syndrome (AGS) (Crow *et al.*, 2006) which has clinical characteristics including progressive microcephaly, motor neuron defects and an altered interferon response (Goutières *et al.*, 1998). In this manner, it mimics an *in utero* viral infection and systemic lupus erythematosus. Over 50% of AGS patients have biallelic mutations in the RNaseH2a complex but AGS can occur from mutations in other repair components such as TREX1(Morita *et al.*, 2004; Stetson *et al.*, 2008; Gall *et al.*, 2012), SAMDH1(Behrendt *et al.*, 2013; Rehwinkel *et al.*, 2013; Wu, 2013), ADAR1 (Hartner *et al.*, 2004; Walkley, Liddicoat and Hartner, 2012; Mannion *et al.*, 2014; Liddicoat *et al.*, 2015) and IFIH1 (Livingston and Crow, 2016). The structure of the RNaseH2 trimer shows that 7 of the 29 known AGS mutations are located on the interface of the A and C subunits which interferes with the formation of the heterotrimer and therefore its activity. A more specific mutation is that of G37S which is near the catalytic centre of the RNaseH2a subunit

(Nowotny *et al.*, 2005) and was found to cause AGS in patients.

Initial investigations *in vivo* revealed embryonic lethality of *rnaseh2b* and *rnaseh2c* null mice. Further analysis revealed increased incorporation of rNTPs, DNA damage and activation of p53 (Hiller *et al.*, 2012; Reijns *et al.*, 2012). Next, characterisation of homozygous null mice for RNaseH2a, found them to be embryonic lethal at the stage of gastrulation, in which it was identified that there was a threshold limit to the quantity of rNTPs incorporated before a p53 response was activated and resulted in embryonic arrest. (Uehara *et al.*, 2018). RNaseH2 can also remove single rNMPs as described but it also has a role in R-loop resolution. One of the main questions posed is which of the two roles, and therefore which form of RNA incorporation is most detrimental to the embryos. The creation of a Ribonucleotide Excision Defective (RNaseH2^{RED}) mutant allows the distinction between the two roles as it has no ability to remove single ribonucleotide but can still resolve R-Loops. Utilising this models, it was identified that the RNaseH2$^{RED/RED}$ mice were still unable to survive, suggesting that the continued incorporation of single ribonucleotides was the main cause the of inflammation and embryonic lethality observed (Uehara *et al.*, 2018).

It was also found that RNaseH2b deficient cells accumulate cytosolic DNA, surrounded by a nuclear envelope. These micronuclei are detected and bound by cGAS which induces cGAMP production which in turn, increases the expression of Interferon genes via a STING, a key characteristic used to identify AGS (MacKenzie *et al.*, 2017). Incubation of murine RNaseH2 knockout cells with mTOR inhibitors increases autophagy of the micronuclei present, therefore reducing the inflammation activation (Bartsch *et al.*, 2017). It is thought that mTOR inhibitors may be useful in the treatment of the inflammatory symptoms in AGS patients.

A homozygous knockout zebrafish model against RNaseH2a was previously created in the lab but has not yet been characterised. I will aim to characterise the knockout and separate the two functions of RNaseH2a.

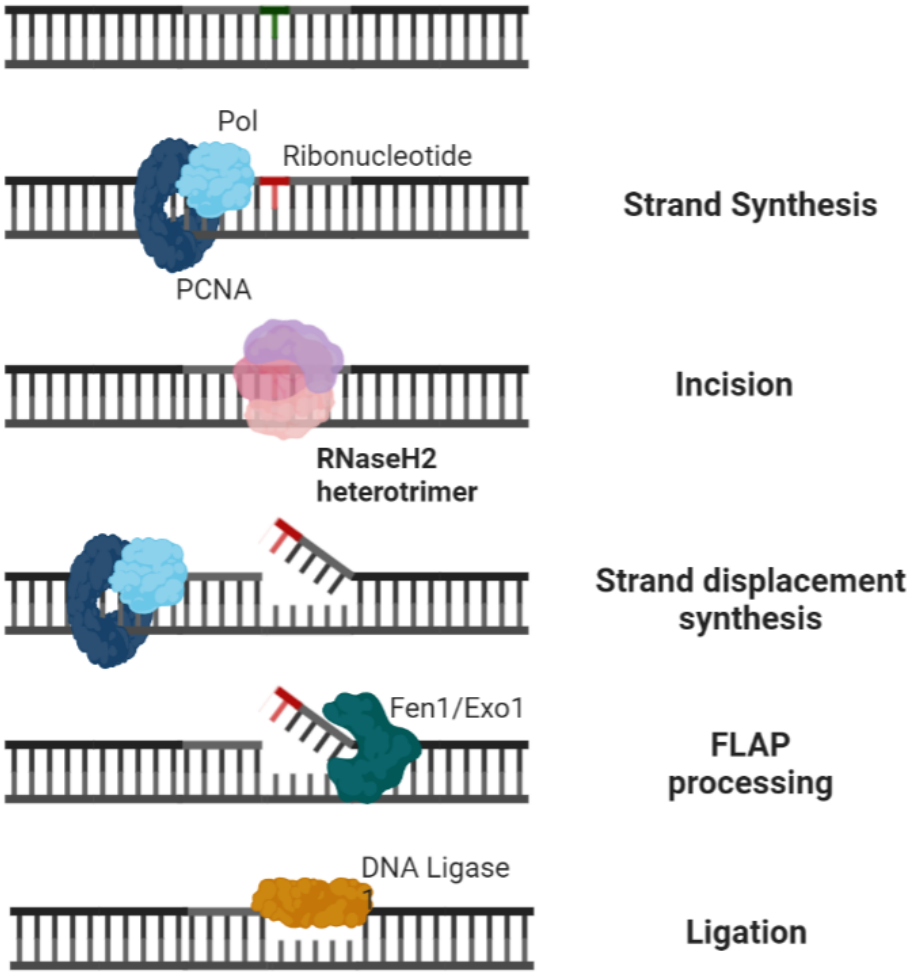

Figure 1.5: Removal of single ribonucleotides by RNaseH2

Mechanism of ribonucleotide removal mediated by the RNaseH2 complex (Purple) resulting in a DNA overhang that requires Fen1/Exo1 (Green) and DNA ligase (Orange) to complete the repair. Figure created with BioRender.com.

1.5 Topoisomerase 1

1.5.1 Structure and mechanism of action

Topoisomerases are key in the relaxation of torsional DNA stress which arises through biological processes such as gene transcription and replication. The human genome encodes for three types of topoisomerases: type IA, type IB and type IIA. All are similar in their mechanism of action which involves the cleavage and resealing of one (Type I) or both (Type II) nucleic acid strands. During this they become covalently bound to the 3' (Type IB) or 5' (Type IA and IIA) terminus of the nucleic acid via a Tyr residue in a transesterification reaction. This structure is known as a topoisomerase cleavage complex (Champoux, 2001). These complexes are transient as the 5'OH created by the initial cleavage deprotonates the phosphotyrosine, repairing the DNA phosphodiester linkage **(Figure 1.6).**
Although meant to be transient, these complexes can become permanent if they become trapped on the DNA. This can occur through encountering replication and transcription machinery or being in the close vicinity of another DNA lesion. This can result in a single stranded protein-linked DNA break (PDB) or dsDNA break. Stalled topoisomerases can be freed via a nucleophilic attack by the tyrosyl-DNA phosphodiesterase (TDP1) (Takashima *et al.*, 2002; Pommier *et al.*, 2016)

Although its main role remains in the relief of torsional stress , TOP1 has also been implicated in the removal of single ribonucleotides in the absence of RNaseH2 (Lippert *et al.*, 2011; Takahashi *et al.*, 2011)(Williams *et al.*, 2013). TOP1 can cleave embedded rNMPs to still result in the 3'-phosphotyrosyl linkage which can be released via the non-mutagenic pathway involving reversal by TDP1(Kim *et al.*, 2011).

Alternatively, the 2'OH on the ribose then attacks the phosphotryosyl linkage, releasing the Top1 complex and leaving a 2',3' cyclic phosphate and a 5' OH (Sekiguchi and Shuman, 1997; Kim *et al.*, 2011). If this occurs at a repetitive (tandem) sequence (i.e. ATAT) then, after processing of the cyclic phosphate and 5'OH, realignment of the intact DNA strand can cause 2bp of the repetitive sequence to be 'pushed out' of the DNA strand. After ligation of the gap and replication of the DNA stand, these 2bp will be lost (Kim *et al.*, 2011; Jinks-Robertson and Bhagwat, 2014)

Alternatively, the 2'-3' cyclic phosphate can also be processed by a second TOP1 cleavage event. This occurs upstream of the original nick and remains irreversible as the small oligonucleotide fragment between the two cleavage sites is readily released, resulting in a 2-5bp deletion. In a similar mechanism as described above, strand realignment allows for the release of TOP1 and via re-ligation of the single strand DNA gap, but at the consequence of losing the 2-5bp oligonucleotide (Sparks and Burgers, 2015) **(Figure 1.7)**.

Having only been studied *in vitro*, this mutagenic processing was then shown to be relevant in human disease via the association of defective rNMP repair with the characteristic 2-5bp deletions. This was also linked to ID4, (Indel Signature 4, Catalogue of Somatic Mutations in Cancer (COSMIC) database) (Alexandrov *et al.*, 2020), a mutational signature present in cancer (Reijns *et al.*, 2022). In higher eukaryotes, it has been suggested that TOP1 preferentially cleaves at the 3' of a ribouridine resulting in the 2'OH performing a nucleophilic attack on the bound TOP1. This subsequently releases the TOP1 and leaves a 2'3'-cyclic phosphate. As described above, TOP1 then cleaves further upstream, usually 2-5bp, preferentially at a Thymidine (TNT model). This then follows the model for realignment and TOP1 release (Reijns *et al.*, 2022).
A second mutagenic method of TOP1 removal of rNMPs involves cleavage on opposing strands, resulting in a dsDNA break (Huang *et al.*, 2017; Reijns *et al.*, 2022). However, this is not thought to be associated with the ID4 mutational signature seen in cancer **(Figure 1.7).**

1.5.2 TDP1

As mentioned, although TOP1 cleavage is usually reversible, it can become stalled upon collision with replication or transcription machinery (El-Khamisy and Caldecott, 2006). These complexes can interfere with processes such as replication which, if they occur in large numbers, can become toxic to the cell. Repair of these can occur via TDP1 through the cleavage of the phosphodiester bond.
TDP1 is a member of the phospholipase D superfamily that contains two catalytic HKD (HXK(X)4D(x)6GSXN) motifs, essential for their activity (Interthal, Pouliot and Champoux, 2001). In order to resolve TOP1-ccs the histidine at position 263 in TDP1 initiates a nucleophilic attack of scissile phosphate and histidine 493 protonates the tyrosyl group

(Interthal, Pouliot and Champoux, 2001). TDP1 becomes bound to the DNA via a phosphohistidine linkage, allowing the release of TOP1. The 493 Histidine now activates a water molecule allowing hydrolysis of the linkage and release of TDP1 from the DNA. PNKP and DNA ligase are recruited to complete repair. TDP1 also has alternative roles in the repair of other peptide bound by 3'phosphotyrosyl, phosphohistidine or phosphogycolate bonds, AP sites and also possesses DNA and RNA exonuclease activity (Interthal *et al.*, 2005; Interthal, Chen and Champoux, 2005).

1.5.3 Clinical significance

A mutation at the previously described H493 of TDP1 (*TDP1*^{H493R}) has been found in spinocerebellar ataxia with axonal neuropathy (SCAN1), a progressive neurodegenerative disease (Takashima *et al.*, 2002). SCAN1 is inherited in an autosomal recessive manner and is characterized by the slow development of cerebellar ataxia that is present from late childhood. MRI scans also reveal marked cerebellar atrophy.

Disease symptoms are thought to be caused by a mutation to the active site Histidine, 493, creating instead a R493. This *TDP1*^{H493R} has impaired activity and has been shown to be 25-fold less efficient in the cleavage of TOP1-ccs. SCAN1 cell lines have been shown to accumulate TOP1-ccs and it is these lesions that are thought to cause cell death and subsequent reduction in size of the cerebellum (Interthal, Chen and Champoux, 2005; Hirano *et al.*, 2007)

It was originally thought that the *TDP1*^{H493R} was a loss of function mutation, removing the ability to repair stalled TOP1-ccs, and that these protein linked ssDNA breaks were responsible for the phenotypes seen in patients. Analysis has revealed that the *TDP1*^{H493R} has a longer half-life, 13 minutes, and remains bound to the DNA, producing a protein linked DNA adduct that is the cause of cellular toxicity (Takashima *et al.*, 2002). A combination of these two functions may promote the cellular death of post-mitotic neurons.

Previous work in the lab has established a zebrafish *tdp1*$^{-/-}$ knockout line in an aim to study the effect of ineffective TOP1 repair. These fish have a mild phenotype at adulthood when stressed with TOP1 chemical inhibitors but this appears to be indispensable during their larval stages (Zaksauskaite *et al.*, 2021). I will be aiming to identify any alternative pathways that are being utilised to repair aberrant TOP1 activity.

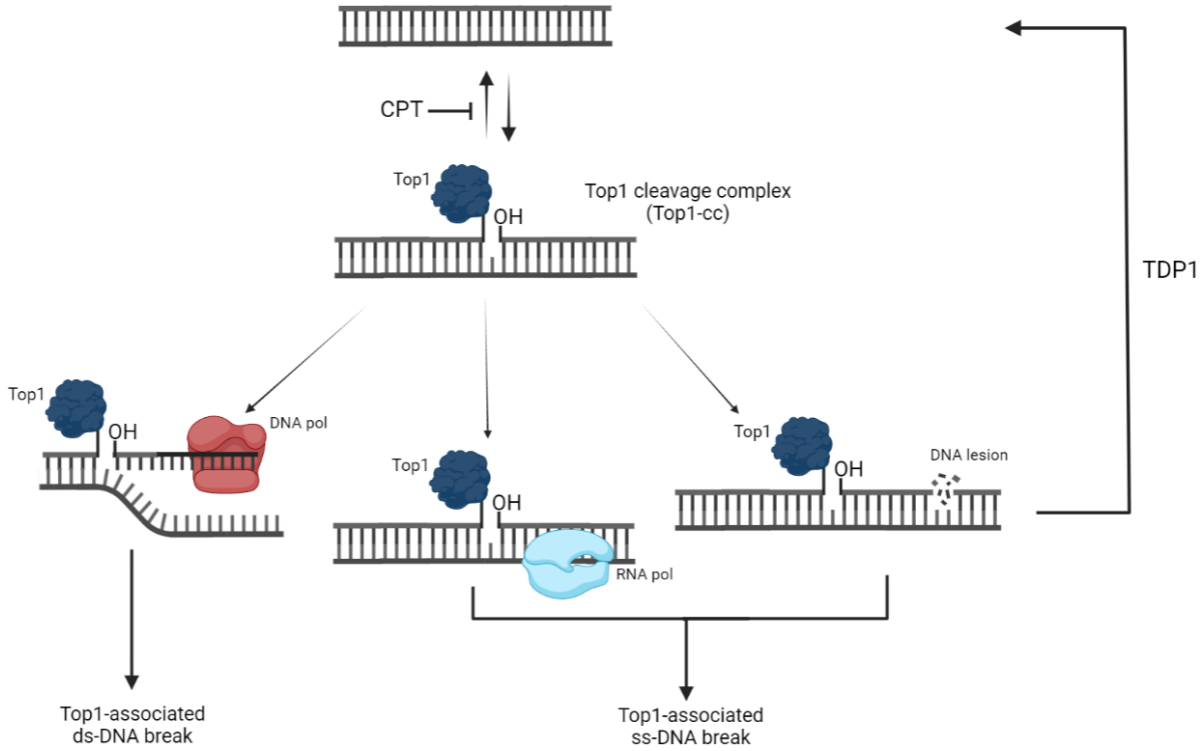

Figure 1.*6*: Resolution of torsional *stress by TOP1*

Formation of a TOP1 cleavage complex (TOP1-cc) via TOP1 cleavage of a single DNA strand to relieve torsional stress that occurs during DNA replication. Formation of TOP1-ccs are reversible but can become permanent due to collision with DNA or RNA polymerases or close proximity to a second single stranded DNA lesion. These permanent TOP1-cc lesions can be reversed via TDP1. Figure created with BioRender.com and adapted from (El-Khamisy and Caldecott, 2006).

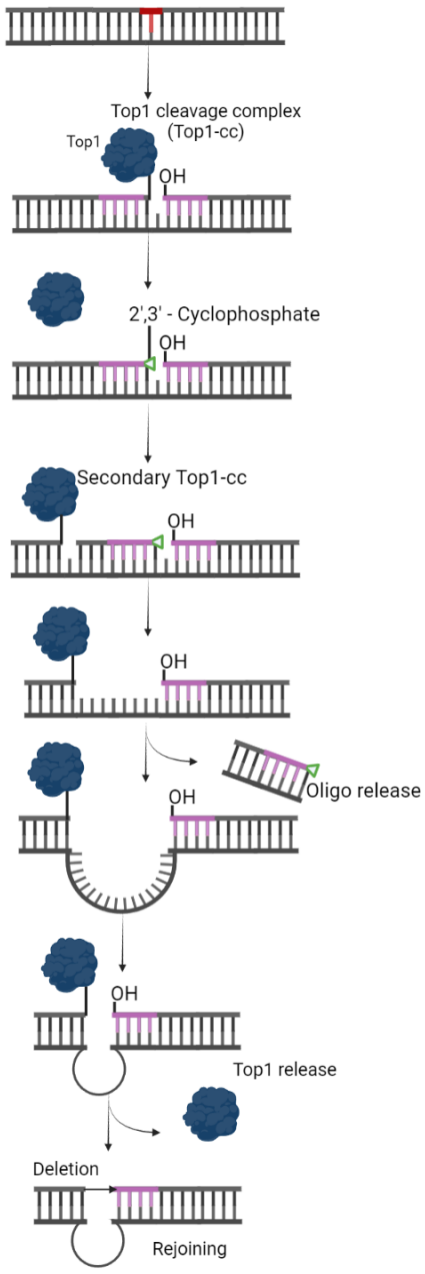

Figure 1.*7*: TOP1 removal of ribonucleotides can result in deletion of sma*ll fragments*

Initial TOP1 cleavage at the 5' side of the ribonucleotide forming a TOP1-cc. Reversal of this reaction occurs via the 2'OH of the ribose sugar. Subsequent release of TOP leaves a 2'3'-cyclophosphate in its place. Second cleavage by TOP1 5' to the original nick results the release of a 2-5bp fragment. Re-joining of repeated sequences (pink) results in the deletion of 2-5bp, an Indel Signature 4 (ID4). Created with BioRender.com and adapted from (Pommier *et al.*, 2022)

1.6 Novel TDP1 interaction partners

Recent work in the lab has revealed a novel interaction partner of TDP1, the Nuclear mitotic apparatus protein (NuMA). Although primarily known as a regulator of mitotic spindle function, it has now been revealed that NuMA is closely involved with the regulation of DNA damage response factors, particularly when dealing with oxidative damage (Ray *et al.*, 2022).

1.6.1 Structure and mechanism of action

NuMA is a large, 236kDa, protein and was initially discovered as a protein that localized to the interphase nucleus but to the spindle poles during mitosis. It comprises of globular head and tail domains that are separated by a 1500 amino acid (aa) coiled-coil (Yang, Lambie and Snyder, 1992). A nuclear localization signal is situated in the c-terminal domain along with a key stretch of 100aa identified as a region of binding microtubules (Gueth-Hallonet, Weber and Osborn, 1996; Du *et al.*, 2002). The first identified role of NuMA was the physical tethering of spindles and their maintenance at the centrosomes. Truncated versions of NuMA, both N and C, along with inhibitory molecules all resulted in aberrant spindle formation, concluding the essential role of NuMA in cell division (Du *et al.*, 2002). Knockout of NuMA *in vivo* also resulted in the early embryonic lethality of mice (Silk, Holland and Cleveland, 2009).

The speculation of the role of NuMA during it's time in the interphase nucleus has been unresolved for many years. There have been suggestions that it performs an organizational role in the form of a nuclear matrix, or perhaps a role in gene regulation, through the S/TPXX sequence, a motif found in proteins involved in gene regulation (Luderus *et al.*, 1994). More recently it has been reported to have roles in nuclear shape, chromatin remodelling and even homology-directed repair (Vidi *et al.*, 2014; Moreno *et al.*, 2019; Serra-Marques *et al.*, 2020).

Recent work in the lab has combined these ideas to reveal a new role of NuMA in DDR. It was identified that in humans, *numa* was upregulated in the cerebellum along with other SSBR components such as *TDP1* and *XRCC1*. The cerebellum is particularly sensitive to oxidative damage and therefore the lab wanted to investigate the potential role of NuMA in the DDR mechanism. They discovered that *numa* knockout cells were less efficient in repairing oxidative damage after H_2O_2 treatment, creating more ssDNA breaks. They also

identified the downregulation of a subset of genes labelled NRGs (NuMA Regulated Genes) in the absences of NuMA. These genes have been found to have a significant increase in the quantity of oxidative damage such as 8-oxoG in their promoters and enhancers in the absence of NuMA (Ray *et al.*, 2022). These 8-oxoG sites are particularly prevalent at guanine rich promoters and have been implicated in the upregulation of pro-inflammatory genes (Pan *et al.*, 2016; Fleming, Ding and Burrows, 2017).

1.6.2 Clinical significance

As mentioned, the depletion, inhibition or total deletion of NuMA leads to aberrant spindle formation *in vivo* and early embryonic lethality in mice (Silk, Holland and Cleveland, 2009). NuMA expression has also been linked to several cancer types, mainly through the upregulation of the 'guardian of the genome', p53 and its downstream factor, p21. Although the study of NuMA in oxidative DNA repair is relatively young, proteins related to its predicted roles, such as nuclear lamins, do have known clinical consequences. Lamins are nuclear matrix proteins, known to create a network between the inner nuclear membrane and chromatin and have roles in genome organization and stability (Dechat *et al.*, 2010). Diseases stemming from mutations in lamins are known as laminopathies and they include Emery-Dreyfus Muscular Dystrophy and Hutchinson Guilford Progeria Syndrome that universally display defects in cell proliferation, apoptosis and senescence (Bonne *et al.*, 1999; Rankin and Ellard, 2006; Dechat *et al.*, 2010). Due to the similarities of NuMA and nuclear lamins, it is predicted that mild dysregulation of NuMA may show similar phenotypes.

I will aim to create an *in vivo* model to corroborate the *in vitro* findings. If the *numa* knockout proves to be embryonic lethal, due to the external development of the zebrafish, the initial stages of the phenotype can be visualized and gene expression analysis still performed.

1.7 Zebrafish as a model organism

Danio rerio (zebrafish) are freshwater fish, native to Southern Asia, named after their five distinctive horizontal stripes. As an adult, they have an average body length of 3cm and a lifespan in captivity of 2-3 years. The transparent nature of their embryonic stages makes them a sought after model in many areas of research.

1.7.1 Development

The generation time of *D.rerio* from embryo to adult is approximately 3 months. With fertilisation occurring externally, embryos can be studied from the initial formation of the zygote through to adulthood. The one cell stage lasts for approximately 20 minutes during which cytoplasmic movements begin to separate out the embryo forming section (blastodisc). After 45 minutes, the cleavage period begins which consists of six cleavage events, spaced around 15 minutes apart, resulting the a 64-cell embryo. The blastula period that follows has several key steps including the midblastula transition (MBT). Here, interphase lengthens and RNA synthesis increases. Formation of the yolk syncytial layer (YSL) also occurs with epiboly following as the final stage in the blastula period, during which the YSL and blastoderm begin to migrate around the yolk, forming a 'cap'. At around 5 hours, the gastrula period begins which results in the formation of the primary germ layers and establishment of the tail bud. At 10 hours the embryo transitions into the segmentation period where it begins to develop somites and stays until 24hpf (hours post fertilisation). The pharyngula period stretches from 24hpf to 48hpf and at this point the embryo appears phenotypically relatable to a vertebrate with five distinct lobes to its brain. As the embryo enters 3 days post fertilisation (dpf) it also enters the hatching period where the embryo emerges from the protective chorion that is has, up until now, been surrounded by. Day four of fertilisation displays the inflation of the swim bladder, protruding of the mouth and an increase in embryo movement. By 5.2dpf the embryo requires external feeding (Kimmel *et al.*, 1995).

1.7.2 Advantages

Practically, the zebrafish has several advantages over other disease models. The use of human cell lines has greatly advanced our knowledge in many pathways but does not provide an accurate representation of the functionality of a particular gene within a whole organism and the effect of its removal or mutation in terms of specific tissues and organ

systems. Zebrafish are more genetically and pathologically similar to humans than a cheaper model, *Drosophila melanogaster* and are able to be stored via sperm freezing which is also not possible with the fruit fly. Compared with rodents, in particular mice, the husbandry and cost per animal is much lower for zebrafish, resulting in the ability to create much higher n numbers. The affordability and feasibility of large scale screens is far greater for zebrafish than mice and the fact that fertilization occurs *in vitro*, coupled with the transparent nature of the embryos enables the visualization of phenotypes and transient *in vivo* assay are far easier. Genetic modification has become far more achievable in zebrafish over recent years and they are very genetically tractable, allowing the creation of double and triple knockout mutants through the CRISPR/Cas9 system, enabling the *in vivo* analysis of potentially compensating mechanisms.

1.7.3 Disadvantages

The zebrafish is not a perfect model. Despite 71.4% of human genes having at least one zebrafish orthologue (Howe *et al.*, 2013), many of these have an additional copy due to the whole genome duplication event that occurred in teleost fish resulting in subfunctionalization and neofunctionalization. In particular, 70 of the 648 DNA damage repair genes have been found to be duplicated. This can lead to difficulties creating knockouts or specific gene modifications as more than one gene may have to be targeted (Cayuela *et al.*, 2019). Zebrafish are also less genetically and anatomically similar to humans than their rodent counterparts sometimes limiting their phenotypic representation of some human disease.

1.7.4 Zebrafish in DNA damage Repair

Zebrafish have been identified as an excellent model for studying DNA damage repair as they contain orthologues for components of all higher eukaryote DNA repair mechanisms.

1.7.4.1 Base repair

Zebrafish contain an *mgmt* gene but no studies have been done to date. Photoenzymatic repair (PER) is a key mechanism in zebrafish. Using deoxyribodipyrimidine photolyase, transcribed from the *phr* gene, this system reverses UV-induced DNA damage such as pyrimidine dimers (Lucas-Lledó and Lynch, 2009). PER however is not conserved in mammals who have to use the less efficient NER mechanism (Giglia-Mari, Zotter and Vermeulen, 2011). Zebrafish also utilise NER for non UV-induced base damage. Zebrafish

contain homologs for both *msh2* and *msh6*, essential for function of the MMR pathway. Homozygous knockouts of either gene show neoplasm development (Feitsma *et al.*, 2007).

1.7.4.2 DNA strand break repair

The error prone NHEJ, particularly the preferred Alt-EJ pathway in embryos, has been utilised in the creation of knockout mutations within zebrafish lines Using the CRISPR/Cas9 system, double strand breaks are induced in genes of interest. Error prone Alt-EJ repair then leads to the formation of indels that may disrupt the reading frame and truncate the protein. The more faithful HR pathway is also known to occur in embryos at early developmental stages (Michael Hagmann *et al.*, 1998).

1.7.5 Zebrafish as a disease model for DNA repair and neurological disease

In terms of the nervous system and related behaviour, the zebrafish have an anatomy that is representative of humans. They have a fore-, mid- and hind brain including the cerebellum and peripheral nervous systems with both motor and sensory components. They perform conditioned responses and social behaviours, indicating higher neural functioning (Lieschke and Currie, 2007). However, the zebrafish only contains a basic cortex and limited sensory organs leading to much simplified behaviour compared with humans. That said, many disease models have been created for Parkinson's disease, tauopathies such as Alzheimers, Huntington's and Motor Neuron Disease (Xi, Noble and Ekker, 2011; Babin, Goizet and Raldúa, 2014; Martín-Jiménez, Campanella and Russell, 2015) as well as peripheral neuropathies such as Charcot-Marie-Tooth Disease (Chapman *et al.*, 2013).

1.8 Aims and Objectives

1.8.1 A new *in vivo* model to study the role of RNaseH2a

Studies surrounding the role of RNaseH2 have been well studied using *in vitro* methods to determine its mechanism of action and the effects of complete knockout in mammalian cell lines (Sparks *et al.*, 2012; Bartsch *et al.*, 2017; MacKenzie *et al.*, 2017). Knockouts of each of the three subunit have also been created in mouse models, each resulting in early embryonic lethality (Hiller *et al.*, 2012; Reijns *et al.*, 2012; Uehara *et al.*, 2018). To date, no published models exist, studying the role of RNaseH2 in a zebrafish model.

Whilst initially studying the role of TOP1, previous work in the lab has created a knockout of subunit A of RNaseH2 in zebrafish which, surprisingly, unlike all other published *in vivo* knockout models, are able to survive to adulthood. Using a new *in vivo* system may help provide further insight into the molecular effects of RNaseH2a loss in whole organisms. Below I have outlined the aims of this thesis in studying this new model.

- Characterisation of *rnaseh2a*$^{-/-}$ zebrafish at both adult and embryonic stages using immunohistochemistry, biochemical assays and behavioural analysis
- Examination of adult *rnaseh2a*$^{-/-}$ for any AGS related phenotypes and monitor their ability to remove ribonucleotides
- Investigation of potential alternative mechanisms involved in the removal of ribonucleotides that allow for the survival of *rnaseh2a*$^{-/-}$ zebrafish including TOP1

1.8.2 Investigation into alternative mechanisms in the absence of TDP1

In an aim to study the role of TOP1, previous work has established an *in vivo* zebrafish knockout of *tdp1*, a key repair mechanism in the TOP1 pathway. Although able to survive to adulthood, *tdp1*$^{-/-}$ zebrafish show mild locomotive defects when stressed with topoisomerase inhibitors. This is not the case during their larval stages (Zaksauskaite *et al.*, 2021).

The mechanistic reasoning as to why larvae are not sensitive to TOP1 stalling is unknown, this is what I will investigate during this thesis using the methods stated below:

- Identification of secondary mechanisms that are responsible for the survival of *tdp1*$^{-/-}$ zebrafish via drug treatment and CRISPANT analysis

1.8.3 Creation of an *in vivo* model to study the role of NuMA in DNA repair

NuMA was first identified as a key component of spindle maintenance during mitosis (Yang, Lambie and Snyder, 1992). Since then, work performed *in vitro* has established a role in the repair of oxidative damage, particularly 8-oxoguanine sites, and the subsequent regulation of a set of NuMA Regulated Genes (Ray *et al.*, 2022). Although clinically NuMA has not yet been directly linked to neurological disease, it has shown to be upregulated in the cerebellum, an area of high oxidative stress, and interact with TDP1, mutations in which cause SCAN1 (Ray *et al.*, 2022). The only *in vivo* knockout mouse model to have been created to date resulted in embryonic lethality due to errors in mitosis and upregulated p53. They did not study the role of NuMA in oxidative damage (Silk, Holland and Cleveland, 2009).

In this thesis I will aim to create an *in vivo* model to support the *in vitro* findings surrounding the repair of oxidative damage. Given previous knockout models were embryonic lethal, this is predicted to be similar for a zebrafish lacking NuMA. However, due to the external development of the zebrafish, the initial phenotype, gene expression and oxidative damage levels can still be analysed.
The aims of this thesis regarding generation and characterisation of a new *in vivo* model to study NuMA are outlined below:

- Generation of *numa*$^{-/-}$ zebrafish to study the effect of *numa* in an *in vivo* model organism and its role in oxidative DNA damage
- Separation of the two functions of NuMA via reintroduction of truncated versions previously utilised in *in vitro* techniques to consolidate findings in an *in vivo* setting

Chapter 2
Materials and Methods

2.1 Zebrafish husbandry and maintenance

All adult zebrafish work was carried out in the Bateson Centre aquaria at the University of Sheffield. The zebrafish facilities were maintained at a constant temperature of 28°C on a 14:10 hour light:dark cycle. Fish were kept at a density of 4 animals per 1 L or less and fed artemia or dry food *(ZEBRAFEED*) twice a day.

2.1.1 Zebrafish strains and lines

Wild type lines used were London wild-type (LWT) or AB line ZDB-GENO-960809-7. All mutant lines were generated from LWT fish. All mutant lines were created using the CRISPR/Cas9 system as described in the relevant chapters and can be found in **Table 1.**

Zebrafish ID	Target gene	Mutation
SH478	*rnaseh2a*	49bp deletion
SH475	*tdp1*	4bp deletion
SH678	*numa*	112bp insertion

Table 1: Zebrafish lines

A table showing the zebrafish lines used in this thesis, the relative ID number and the mutations present in the target genes.

2.1.2 Zebrafish embryo collection and maintenance

Multiple pairs of males and females were set up in breeding tanks overnight, separated by dividers. The dividers were pulled out in the morning to allow the fish to mate, as stimulated by the start of the light cycle. Alternatively, trays of marbles were placed in the tanks overnight for collection of embryos in the morning. Embryos were collected using a fine sieve, washed with aquarium water and incubated in 1x E3 medium (500 µM NaCl, 17 µM KCl, 33 µM $CaCl_2$, 33 µM $MgSO_4$) with 0.0001 % methylene blue at 28°C. A maximum density of 60 embryos per 10 cm petri dish was maintained in approximately 30 ml of E3 medium. Unfertilized, dead or abnormal embryos were removed each day. Animals were kept no longer than 5.2 dpf, unless they were subsequently raised to adulthood in accordance with the UK Home Office Animals (Scientific Procedures) Act 1986. Addition of 12 µL PTU (1-Phenyl-2-thiourea) was added to 24hpf embryos in 30 mL of E3 medium (stock concentration 75 mg/ml) if pigment was to be prevented from forming as described in Karlsson *et al.,* 2001.

2.1.3 Zebrafish anaesthesia

If required, embryos were anaesthetized by addition of 1 mL of 0.4% w/v tricaine (PharmaQ, Hampshire) to 25 mL E3 medium. If they were then required for further use, they were transferred to a petri dish with fresh E3 medium. Adults were anaesthetized in 0.017% tricaine in aquarium water and monitored during recovery.

2.1.4 Zebrafish fin clipping

Adult zebrafish (>2 months) were anesthetized in 200 mL of 0.4% w/v tricaine, no more than three at a time. Once they had become unresponsive, they were individually picked out with a metal spoon and the last third of their tails cut off with scissors. Fish were then placed in an individual tank and its recovery monitored. Fin clips were placed in a corresponding 96 well plate with a pair of tweezers. Scissors and tweezers were both then washed in 70% ethanol followed by aquarium water before being used on the next fish. If the fish needed to be re-clipped, they were left for at least 1 month to allow correct regeneration of the tail. If fish required genotyping before raising, a 3dpf fin clip was performed. Embryos were anesthetized with 1mL tricaine in a Petri dish along with 10 µL Tween-20. Embryos were transferred onto masking tape on a petri-dish lid and excess media removed. A scalpel was used to cut along the break in pigment in the tail to prevent loss of circulation. Embryos were placed in 24 well plates with 3 mL fresh E3 medium whilst fin clips were transferred to a corresponding 96-well plate using a glass Pasteur pipette. Fish were monitored throughout recovery.

2.2 Zebrafish movement

2.2.1 Adult zebrafish locomotion

Five wild-type and five *rnaseh2a*$^{-/-}$ adult zebrafish were placed in single tanks and placed in front of the Adult Viewpoint Video system (Viewpoint Behaviour Technology) for 4 hours. Tanks were taped between fish to prevent any shoaling influence on their movement. The first hour was treated as habituation time and discarded. Total distance moved via video tracking was calculated using Microsoft Excel 2016 and statistical analysis performed using GraphPad Prism.

2.2.2 Photomotor response analysis

5dpf embryos were placed in individual wells of a 96 well plate (Corning® 3595) with 400 µL E3 medium. The embryos were transferred into the ZebraBox Viewpoint system (Viewpoint Behaviour Technology) and left to acclimatise for 1 hour. The embryos were then subjected to three cycles of five minutes of light (80%) followed by 5 minutes of darkness (0%) and the total distance travelled by each embryo was quantified. Analysis of total distance moved in each light/dark cycle was performed using Microsoft Excel 2016 before statistical analysis was performed using GraphPad Prism.

2.3 Zebrafish genome editing

2.3.1 gRNA design for CRISPR/Cas9

Suitable exon targets for CRISPR/Cas9 restriction were identified via ensembl (https://www.ensembl.org/). Chop-Chop (https://chopchop.cbu.uib.no/) was used to find high ranking gRNA sequences (Sigma-Aldrich). The sequences can be found in **Table 2**.

2.3.2 Microinjection of embryos

Thin-wall single-barrel borosilicate glass capillaries (World Precision Instruments, TW120-4) were used to form injection needles by use of a micropipette puller (P-97, Sutter Instrument Co., Novato, USA). Solutions were loaded into the glass needles via microloader pipette tips (Eppendorf, 930001007) and the needles inserted into a PV820 Pneumatic Pico-Pump injector (World Precision Instruments). The tip of the needles were broken off with tweezers and the volume of solution expelled measured via immersion in mineral oil on a 10 mm graticule. The injection volume was adjusted 0.5 nL (expelled injection mix with a diameter of 0.1 mm) in the 'timed' mode. One cell stage embryos were collected and arranged against a microscope slide on the lid of a 10 cm petri dish. Excess aquarium water was removed, and the required volume of solution was injected directly into the yolk. The embryos were then transferred into a 10 cm petri dish containing 1xE3. Injection solutions were prepared with 0.5 µL Cas9 (NEB, M0386, 20 µM), 1 µL gRNA (IDT, 100 µM), 1 µL tracrRNA (IDT, 100 µM) and 0.5 µL Phenol Red, up to a final volume of 5µL. CRISPANT embryos were produced via injection of three additional guides to a total final guide volume of 2 uL. Efficiency of CRISPANT knockout was determined by using ImageJ to calculate the

percentage of PCR product above and below the expected size, normalised against the total product per lane.

2.3.3 Determination of germline transmission of desired mutations

Embryos injected with the Cas9 and gRNA were raised to adulthood (~3 months) and then outcrossed with WT. Subsequent embryos were genotyped and sequenced for the identification of indels that would produce an early stop codon.

Target	Sequence	Source
Numa (Coding Exon 2)	GGCGGGACCACTTTTGACAT	Sigma Merck, Dorset, UK
NuMA (Coding Exon 14)	GGCAATCGGAGACCTTCAGG	Sigma Merck, Dorset, UK
lamb1b	TTGTTAATAGCATAGTACAT GGAGAACAAGCAAAACGATG GCGTGGTGCAGGGTTTGTAG TCACAATGACATGTGTGCG	Sigma Merck, Dorset, UK
apex2	AGTTTTAGCCGAGGACGAAGTGG ACTCCATTTCTGGCCGAGGAAGG AAGCCATCTTGAGCTCAGGGAGG GAGAGGTGTTCACGTCACCCAGG	Sigma Merck, Dorset, UK
ercc4	GGCATTCATGATGTCCAGAA TATCATTGAGTCTGTCAGG TGTCACUAGCCGAATCCTAG	Sigma Merck, Dorset, UK

Table 2: CRISPR guide RNAs

A table showing the sequences and sources of guide RNAs used during this thesis

2.4 Staining of embryos

2.4.1 γH2AX staining

24hpf embryos were dechorinated and fixed in 50% MeOH:Acetone which had been pre-incubated at -20°C overnight. Embryos are kept at -20°C for 5 days before staining. Embryos were washed in 50% MeOH:PBS for 5 minutes with gentle rocking. They were then washed briefly with 1x PBS. Following this they are washed 3 times for 5 minutes at RT with rocking in 1% Triton:PBS. Embryos are then incubated in 2% Blocking Buffer with 5% FCS and 1% DMSO for 3 hours at 4°C.

Primary antibody for γH2AX (Sigma-Aldrich, Anti-phospho-Histone H2a.x (Ser139) Antibody, clone JBW301, 05-636-I) was added at a 1:1000 dilution and incubated overnight at 4°C. The next day, embryos are washed eight times for 15 minutes with PBST and gentle rocking. The secondary antibody (Alexa 488, goat anti-rabbit) was added in blocking buffer at a dilution of 1:2000 for 2 hours at 4°C in the dark. Finally, the embryos are washed four times for 15 minutes in PBST before storage in 80% glycerol. Embryo tails were then mounted as described in **Section 2.9.2**.

2.4.2 Acridine Orange

Acridine Orange (AO) (Sigma Aldrich, 494-38-2) was used at a 1x concentration (10µg/ml) in E3 with no methylene blue and PTU. 24hpf embryos were incubated with 1x AO for 30 minutes in the dark. Following this, the embryos were moved to new petri dishes and fresh E3 media was added and the embryos were incubated for 10 minutes in the dark. This was repeated 3 times. Embryos were them imaged under a fluorescent microscope at 460-500 nm wavelength

2.5 Extraction of nucleic acids

2.5.1 Zebrafish genomic DNA extraction

Quick DNA extraction was performed via the Hot-Shot DNA isolation method. Individual embryos were transferred into a 96 well plate and excess water was removed via a fine pipette. 25 µL of 1x Base Solution (1.25 M KOH crystals and 10 mM, EDTA in ddH_20) was added to each tube and incubated for 30 minutes at 95°C. Tubes were then vortexed for a few seconds to ensure complete embryos lysis. 25 µL of 1x Neutralisation Solution (2 M TrisHCl in ddH_20) was then added and the tubes before they were vortexed again and the

DNA isolates were kept on ice. Before use, the extracts were centrifuged for 2 minutes at 4200rpm. In some cases, a proteinase K extraction would be used.

2.5.2 Proteinase K DNA extraction

A thermocycler was pre-heated to 98°C before 25 µL of 2950 µL of TE buffer (10 mM Tris, 1 mM EDTA, pH 8), mixed with 50 µl of 33.3% Tween (Sigma-Aldrich, 9005-64-5) , was added to the embryos and was incubated in the thermocycler for 15 minutes at 98°C. The samples were then removed, being careful not to disturb the solution, and 2 µL of Proteinase K (20 mg/ml) was added and mixed into the solution by pipetting up and down. The sample was then incubated for 3 hours at 55°C followed by 10 minutes at 80°C in order to denature the Proteinase K. Once completed, the samples were vortexed thoroughly. Samples were stored at -20°C.

2.5.3 Genotyping

Large indels that would be identifiable through band shifts were done so via PCR of the CRISPR cut site and gel electrophoresis (Sections 2.6.7, 2.7.3). Smaller deletions were identified via a prior restriction enzyme digest and separated using 3% agarose gel electrophoresis (Section 2.7.3). Some of these deletions were identified using the derived cleaved amplified polymorphic sequence (dCAPS) method (Neff *et al.*, 1998) that allowed for the distinction of deletions via the creation of restriction enzyme sites in the relevant PCR products. All genotyping primers can be found in **Table 3** alongside their PCR conditions.

Target	Sequence	F/R	Tm	Source	Purpose
numa (coding exon 2)	CCTTTTTCTCTCATGTGCTTCA	F	54	IDT	Genotyping
	TCTGTCAAAAGAGCAACCGTAA	R		IDT	Genotyping
numa (coding exon 14)	TGGTAGCAGAAAACAATTCCCT	F	51	IDT	Genotyping
	CAGAATCTCAGTCTGGAGGCTT	R		IDT	Genotyping
rnaseh2a	GTTTGTGGACACTGTGGGTC	F	53	IDT	Genotyping
	CTCCCGTTTTCTCCACCTCT	R		IDT	Genotyping
apex2	ACAACCTCATGTTGCCCATAAC	F	54	IDT	Genotyping
	TGGTCACCATAGCAACCAATAA	R		IDT	Genotyping
tdp1	CCCCTGCTGTAAAAAGGAAGAGAGAAGCT	F	52	IDT	Genotyping
	CATTAAGTTGGTCTCAAAGAAATCAG	R		IDT	Genotyping
lamb1b	TTGTTAATAGCATAGTACAT	F	50	IDT	Genotyping
	GGAGAACAAGCAAAACGATG	R		IDT	Genotyping
ercc4	TCAAACTGTGACCAGTGATGTG	F	54	IDT	Genotyping
	CCTGTTACTAGGTGAGCAGGGA	R		IDT	Genotyping
H2a_del557-558_R	ttgacagcatggtctctccacctttgcacagatg	F	62	IDT	Site Directed Mutagenesis
H2a_del557-558_F	catctgtgcaaaggtggagagaccatgctgtcaa	R		IDT	Site Directed Mutagenesis

Table 3: PCR primers

A table showing the sequences and sources of DNA primers used during this thesis used for PCR

2.5.4 Total RNA extraction

15 embryos were anesthetized in tricaine before being homogenized in 500 µL of TRIzol reagent for 5 minutes. 100uL of chloroform was added and the tubes shaken vigorously for 15 seconds before being left at room temperature for 2-3 minutes. The samples were then centrifuged at 12,000xg for 15 minutes at 4°C. The aqueous layer was then transferred to a fresh tube before being mixed with 250uL of isopropanol and incubated at room temperature for 10 minutes. The sample was then centrifuged at 12,000xg for 10 minutes at 4°C. The supernatant was carefully removed and the pellet washed with 1 mL of 75% ethanol. The sample was centrifuged at 7,500xg for 5 minutes at 4°C. The ethanol was removed and the samples were spun again at 7,500xg for 2 minutes to remove excess ethanol. Again, the remaining supernatant was removed and then the sample was left to air dry for two minutes. The pellet was then re-suspended in 15 µL of nuclease-free H2O.

2.5.5 Total Nucleic Acid Extraction

Up to 20 embryos were rinsed in sterile water and homogenized in 100 µl of lysis buffer (100mM Tris-HCL (pH 8.0), 100 mM EDTA, 250 mM NaCl, 1% SDS) with a sterile plastic micro-pestle. An additional 300ul of lysis buffer was added and the embryos homogenized further. The sample was incubated for 3 hours at 50°C with 200 µg/ml Proteinase K. 200ul of phenol:chloroform:isoamyl-alcohol (50:48:2) was added and gently inverted to mix before being centrifuged at 13000rpm for 15 minutes, RTP. The aqueous phase was removed and mixed with 200ul of chloroform before being centrifuged again. The aqueous phase was removed again and mixed with 100 µl NaAc (3M, (pH7) and precipitated with 800ul EthOH. The nucleic acid precipitate should be immediately visible. Centrifuge (13,200 rpm, 4°C, 30 minutes) and resuspend the pellet in 20 µl TE buffer (10mM Tris, 1 mM EDTA, pH 8).

2.5.6 Quantification of nucleic acid concentration

Both DNA and RNA concentrations were quantified using the NanoDrop ND-Spectrophotometer at a wavelength of 260nm.

2.5.7 Preparation of whole cell extracts from zebrafish embryos

100 embryos per condition were anesthetised in Tricaine and de-yolked by pipetting up and down in ice-cold Phosphate Buffered Saline (PBS, Sigma-Aldrich, P4417). Embryos were then washed twice with 1mL PBS and homogenised with a micropestle. 100 µl of lysis buffer (200 mM Hepes, 40 mM NaCl, 2mM MgCl2, 0.5 % Triton X-100, 1 x protease inhibitor cocktail (Roche, 4693159001), 1 x phosphatase inhibitor cocktail (Roche, 4906837001)) was then added for 30 minutes on ice. The samples were then centrifuged at 13,300rpm for 15 minutes at 4°C. The supernatant was transferred to a fresh tube and stored at -20°C.

2.5.8 Protein quantification

The Bradford Assay was used to quantify the protein concentration in samples. 2 µL of lysate was mixed with 998 µL of Coomassie Plus™ Protein Assay Reagent (Thermo Scientific, 23200) and OD595 was measured in the Jenway visible spectrophotometer at 292 nm (Genova, 6320D). Lysis buffer was used as a blank.

2.6 Molecular Biology techniques

2.6.1 Plasmids

All plasmids used in the thesis are listed below in **Table 4.**

Plasmid Construct	Source	ID	Antibiotic Resistance	Use
pME18S-FL3-rnaseH2a	Source Bioscience	IRBOp991C0421D	Ampicillin	Zebrafish *rnaseh2a*
pCS2+	Stone Elworthy	N/a	Ampicillin	Expression plasmid
pCS2+_RNaseH2a_WT	This thesis	N/a	Ampicillin	Active RNaseh2a for rescue
pCS2+_RNaseH2a_Del	This thesis	N/a	Ampicillin	Non-functional RNaseh2a control
pDONR™221	Steve Renshaw	N/a	Kanamycin	Gateway donor vector
pDestTol2CryCFP	Nik Ogryzko	N/a	Ampicillin + Chloramphenicol	Gateway destination vector
NuMA_FL_EGFP_CryCFP	This thesis	N/a	Ampicillin + Chloramphenicol	Attempted rescue of *numa*$^{-/-}$
NuMA_1700_EGFP_CryCFP	This thesis	N/a	Ampicillin + Chloramphenicol	Attempted rescue of *numa*$^{-/-}$

Table 4: Plasmids

A table showing the source and antibiotic resistance of key plasmids used during this thesis.

2.6.2 Transformation of DNA plasmids

A 50 µL vial of chemically competent (NEB, C3019) *E.coli* cells were thawed on ice for 10 minutes. 100-500 ng of plasmid DNA was added before being incubated for 20 minutes on ice. Cells were heat-shocked for 90 seconds at 42°C before being returned to ice for 2 minutes. 500 µL of LB broth was added to the cells and subsequently incubated at 200 rpm at 37°C for 1 hours. Selective LB agar plates were warmed for 20 minutes at 37 after which,

50 µL of the cells were spread onto them. The plates were incubated at 37°C overnight. Selective plates were made with 50 µg/mL of relative antibiotic.

2.6.3 Bacterial culture and plasmid DNA extraction

Single colonies were inoculated into 5 mL of selective LB broth and shaken overnight at 200rpm. The culture was then used for plasmid DNA extraction using the QIAprep® Spin Miniprep (Qiagen, 27104) kit, according to the manufacturers' protocol.

2.6.4 Glycerol stocks

750 µL of liquid culture and 250 µL of 70% glycerol were combined in a vial and stored at -80°C.

2.6.5 Multisite Gateway assembly

Plasmids that were injected into 1-cell stage embryos were created via the Multisite Gateway Assembly technology using the Multisite Gateway Three-Fragment Vector Construction Kit. Entry clones were created via a BP reaction between attB-flanked DNA fragment and the appropriate attP-containing donor vector. 20 fmoles of the attB-flanked PCR product was incubated with 150ng of the pDONRTM vector in TE buffer (10mM Tris, 1 mM EDTA, pH 8). 2 µL of the BP ClonaseTM II enzyme was added after being briefly vortexed twice. The reaction was incubated for 1hr at 25°C before 2 µg of Proteinase K solution and then incubated for 10 minutes at 37°C. The reaction was transformed into competent E.coli according to manufacturer's instructions. 50 µL was spread onto agar plates containing the correct antibiotic and incubated at 37°C overnight. Colonies were picked the next day and incubated overnight in 5 mL of LB media and appropriate antibiotic. DNA extraction was performed using the QIAprep® Spin Miniprep (Qiagen, 27104) kit according to manufacturer's instructions. Entry clones then underwent an LR reaction (as per the manufacturer's instructions) to generate the final expression plasmids. Details of the final plasmids can be found in **Table 4.**

2.6.6 Tol2 transgenesis

The Tol2 system was used to create transgenic lines in association with desired plasmids (NuMA_FL_EGFP_CryCFP, NuMA_1700_EGFP_CryCFP) as described in Kwan et al., 2007 via microinjection of 75-25pg plasmid, 25pg TOL2 mRNA and 10% phenol red.

2.6.7 DNA agarose gel electrophoresis

Unless otherwise stated, 100 ml of 1% w/v agarose in 1x TAE buffer (Tris-Acetate-EDTA, 40 mM Tris base, 20 mM Acetic Acid, 1mM EDTA) with 2 µg/mL ethidium bromide was set in a gel tray with a 20 well comb. The comb was removed and DNA samples were loaded with 1x loading buffer (ThermoFisher Scientific, R0611) into individual wells alongside 2 µL of 1 Kb/100 bp DNA ladder (ThermoFisher Scientific, SM0241). The samples were electrophoresed for 30 minutes at 120V in 1xTAE and UV bands were visualized via UV transillumination (Bio-Rad, 1708280).

2.6.8 DNA restriction digestion and fragment purification

0.1-2 µg of DNA was digested with 0.2-1U of restriction enzyme in 1x appropriate buffer in a total volume of 20 µL. Optimal digestion temperature and length were determined via the manufacturer's instructions. Electrophoresis was used to determine complete digestion, alongside an undigested control. Required DNA fragments were cut out and purified using the QIAquick® Gel Extraction Kit (Qiagen, 28704), according to the manufacturer's instructions.

2.6.9 Phenol/chloroform DNA purification

One volume of phenol: chloroform: isoamyl alcohol (25:24:1, VWR, A0944.0100) was added to the sample and mixed well. The sample was then centrifuged for 5 minutes at 13,300 rpm, RTP (room temperature and pressure). The supernatant was moved into a fresh tube and one volume of chloroform was added. The sample was mixed well and centrifuged for 5 minutes at 13,300 rpm, RTP. Again, the aqueous layer was moved to a fresh tube and sodium acetate, pH 5.2 was added to a final concentration of 0.3M followed by 1.5 volumes of 100% ethanol. The sample was mixed well and precipitated overnight at -80 ºC. The DNA was pelleted at 4 ºC for 30 minutes and washed with 500 µL 70% ethanol and centrifuged for 5 minutes at 13,300rpm RTP. Once the supernatant had been removed, the pellet was centrifuged again for 2 minutes at 13,300 rpm. The remaining ethanol was removed and the pellet was air dried for 2 minutes. Resuspension was performed with 20 µL ddH_20 and stored at -20 ºC.

2.6.10 Ammonium acetate RNA precipitation

The reaction volume was made up to 100 µL with ddH_2O and ammonium acetate and ethanol were added to finals concentrations of 0.3 M and 70% respectively. The

precipitation reaction was carried out at -80°C for at least 1 hour. The samples were centrifuged at 13,300 rpm for 30 minutes at 4°C. The pellet was then washed with 500 µL of 70% ethanol and centrifuged at 13,300 rpm for 10 minutes at 4°C. The supernatant was removed and the pellet was centrifuged again for 10 minutes at 4°C to remove and excess ethanol. The remaining supernatant was then carefully removed and the pellet air dried for 2 minutes before being resuspended in 100 µL ddH2O.

2.6.11 RNaseH2a activity assay

Protein lysate of varying concentrations were incubated in a total final volume of 25 µL with 1X ThermoPol®Reaction Buffer (NEB, B9004SVIAL), 0.5 µL 100x BSA, 0.5 µL DTT and 0.45 µL substrate (5' Cy5-GGTAACGCCAGGGTTTTCTCrGTTCACGACGTTGTAAAACGA) for 2 hours at 37°C. 13 µL of 2x Termination buffer (10mM EDTA, 80% formamide, 1 drop bromophenol blue) was added and incubated for 20 minutes at 65°C. 2 µL of 100 µM competitive DNA (5'-GGT AAC GCC AGG GTT TTC TC) was added and boiled at 95°C for 5 minutes. A 20% polyacrylamide 12 M urea gel was created by mixing 8 mL concentrated, 1 ml Dilute and 1 ml complete Ultrapure Urea Gel components. 40 µL of 10% APS was added before gas extraction occurred for 30 minutes on a magnetic stirrer. 4 µL TEMED was added and mixed via three inversions before being poured into a gel cassette containing 0.75 mm plates, previously cleaned with EthOH. The comb was added immediately and the get left to set for 2 hours. The gel was pre-run for 15 minutes at RT before being run at 180V for 1hr in hot TBE (45mM Tris-borate, 1mM EDTA). The TBE was then heated to 55°C before the wells were cleaned by pipetting up and down with a p200 and 12 µL of the sample was loaded and the gel run for 180V for 1 hour 15 minutes. A positive control of purified RNaseH2 (NEB, M0288) was used in each assay.

2.6.12 Real-Time-qPCR

Total RNA was initially extracted using the TRIzol method described in **Section 2.5.4**. 500 ng of RNA was then reverse transcribed using the Photoscript II cDNA synthesis kit (NEB, E6560S/L) according to manufacturer's instructions with 500 ng RNA. cDNA was then diluted 1:10 before 1 µL was added to a mix containing 500 nM of primers, 1x HOT FIREpol Master Mix (Solis Biodyne, DS-08-31) with a final volume of 20 µL in a single well of a 96 well qPCR plate (BioRad, HSP9601). A list of the primers used can be found in **Table 5**. To produce a standard curve, 100%, 10%, 1% and 0.1% cDNA dilutions were used as templates for each

primer pair. Each reaction was run in triplicate in a CFX96 Touch™ Real-Time PCR Detection System for 95°C for 10 minutes, followed by 45 cycles of 95°C for 15 seconds, 55°C for 15 seconds, and 72°C for 30 seconds. Quantification cycle (Cq) values were calculated via with CFX Maestro™ Analysis Software. Cq values were used to calculate Fold Change. The difference between the target gene Cq and the Cq for the reference gene was calculated (ΔCq) for both control and mutant samples. The difference between the average ΔCq for both sample sets was used as a normaliser and create a ΔΔCq value. As qPCR is exponential, Fold Change is calculated via 2^- ΔΔCq.

Target	Sequence	F/R	Source
rps29	TTTGCTCAAACCGTCACGGA	F	(Bower *et al.*, 2017)
	ACTCGTTTAATCCAGCTTGACG	R	
ISG15	AAC TCG GTG ACG ATG CAG C	F	(Hamilton *et al.*, 2020)
	TGG GCA CGT TGA AGT ACT GA	R	
mxa	GAC CGT CTC TGA TGT GGT TA	F	(Hamilton *et al.*, 2020)
	GCA TGC TTT AGA CTC TGG CT	R	
IL1β	TGGACTTCGCAGCACAAAATG	F	(Safari, Hoseinifar and Kavandi, 2016)
	GTTCACTCCACGCTCTTGGATG	R	
IFNΦ1sec	ACG GCA GCC TGA AAT ACG TT	F	(Hamilton *et al.*, 2020)
	GTC CTC CAC CTT TGA CTT GT	R	
Il16	GCTCATCCAGCAGGGTCCG	F	(Zhang *et al.*, 2016)
	CGACACACACTGTTTGGCCTTG	R	
tnfα	GCGCTTTTCTGAATCCTACG	F	(Dorsemans *et al.*, 2017)
	TGCCCAGTCTGTCTCCTTCT	R	
p21	AGGAAAAGCAGCAGAAACG	F	(Morsli *et al.*, 2022)
	TGTTGGTCTGTTTGCGCTT	R	
tdp1	GCTCCTCAATTGGCTTCCCT	F	(Zaksauskaite *et al.*, 2021)
	ATGTTCCAGATCCAA GGCCG	R	
rnaseh2a	CAGCAGAGAAGTATCAGGACAAG	F	This thesis
	GCGCTGACGATTGGGAATA	R	
DDX3X	ATTCTGGCCCGTGACTTTC	F	This Thesis
	CTCTTCTACCCAAACCACCTTC	R	
Δ113p53	CAAGACCAGGAGGTATTCACCGGAC	Taqman probe	(Kim *et al.*, 2020)
APEX2	ATCCAGCCACTTTCTCCCAG	F	(Zaksauskaite *et al.*, 2021)
	TGAACACCTCTCACAGACCC	R	
APEX2-201	TCCTGGATTCATTTGATGCGG	F	(Zaksauskaite *et al.*, 2021)
	CAGGTCGCGGGTAACTTTG	R	

Table 5: Quantitative PCR primers

Table of primers used in RTqPCR analysis during this thesis

2.6.13 Alkaline Assay

Samples are prepared via Total Nucleic Acid Extraction in **Section 2.5.5**. Quantification of samples is performed via visualization on an agarose gel, equal quantities of samples are prepared in TE (Tris-EDTA) to a volume of 10 µl. NaOH or NaCl (control) were added to a final concentration of 0.3 M and incubated at 55°C for 15 minutes. Samples were centrifuged briefly. 3 µl of 80% glycerol and 3 µl of 6x Loading Dye (Thermo Scientific™) was added and the entire samples run on a 1% agarose gel for 20 hours at 1V/cm, 1x TAE. Gels were stained with SYBERGold (ThermoFisher, S33102) overnight. Bands were visualized via UV transillumination.

2.6.14 SDS-polyacrylamide gel electrophoresis

A 4-20% polyacrylamide gradient gel was cast in a 1 mm XCell SureLock Mini-Cell cassette (Fisher Scientific, VXNC2010) following the Sambrook and Russell method. 10 µg of total protein was used per lane. Protein loading buffer was added to each sample to a final concentration of 50 mM Tris pH 8.0, 200 mM DTT, 2 % w/v SDS, 10 % glycerol and 0.1 % w/v bromophenol blue and the samples were denatured for 5 minutes at 90°C. The gel was placed in a Bio-Rad Mini-PROTEAN Tetra electrophoresis cell (Bio-Rad, 1658004) and samples loaded in addition to a Precision Plus Protein Dual Colour Standard (Bio-Rad, 1610374) protein marker. SDS running buffer (25 mM Tris, pH 8.3, 192 mM glycine, 0.1 % w/v SDS) was used and the gel run for 15 minutes at 120V followed by 45-60 minutes at 170V.

2.6.15 Protein transfer

Trans-Blot Turbo® transfer™ system (Bio-Rad, 17001915) was used according to the manufacturer's instructions to transfer protein from the gel onto a 0.45 µm nitrocellulose membrane (Bio-Rad, 170-4271).

2.6.16 Immunoblotting

The nitrocellulose membrane was blocked in 5% w/v milk dissolved in TBST (200 mM Tris, 140 mM NaCl, 0.1 % Tween-20, pH 7.4) for 1 hour at room temperature. The membrane was then incubated with the appropriate primary antibody **(Table 6)** in fresh 5% w/v milk overnight at 4°C. The next day the membrane was washed 3x 5 minutes in TBST before being incubated for 1 hour at room temperature with appropriate secondary antibody **(Table 6)** in 5% w/v milk. The blot was once again washed 3x 5 minutes in TBST before

Clarity Western ECL blotting substrate (Bio-Rad, 1705060) was added onto the membrane, Membranes were visualized using the ChemiDoc MP imaging system (Bio-Rad, 1708280).

Primary antibody	Host	Supplier	Concentration	Application
DIG-AP	Sheep	Roche (11093274910)	1:5000	ISH
TOP1-CC	Mouse	Merck (MABE1084)	1:2000	SB
γH2AX	Rabbit	Genetex (GTX127342)	1:1000	WB
GAPDH	Rabbit	Genetex (GTX100118)	1:1000	WB

Secondary antibody	Reactivity	Host	Supplier	Concentration
Anti- IgG (H+L)-Alexa Fluor 488	mouse	goat	Molecular Probes (A28175)	1:2000
IgG (H + L)-HRP Conjugate	mouse	goat	Bio-Rad (170-6516)	1:4000
IgG (H + L)-HRP Conjugate	rabbit	goat	Bio-Rad (170-6522)	1:4000

Table 6: Antibodies

A table showing the primary and secondary antibodies used during this thesis

2.7 Synthesis of capped RNA

2.7.1 Template plasmid linearization

10ug of DNA plasmid was digested using 30U of a restriction endonuclease, known to only cut once in the sequence (Not 1) in the appropriate buffer in a total volume of 30 µL. This was incubated at 37°C overnight with no agitation. 1µl of the reaction mixture was run on an agarose gel against an undigested sample to confirm the linearization. This was them purified by phenol: chloroform precipitation.

2.7.2 *In vitro* transcription

1 µg of linearized plasmid was used as a template for *in vitro* mRNA synthesis with the mMESSAGE mMACHINE® SP6 or T3 kit (Life Technologies, AM1340). Once the reaction had finished, it was incubated with 10U of TURBO DNase for 30 minutes at 37°C. RNA was precipitated as described in **Section 2.5.4.**

2.7.3 Polymerase chain reaction

Unless otherwise stated, all reactions were carried out in the BioRad T100™ thermal cycler using FIREpol PCR master mixes (Solis Biodyne, 04-12-00S15), according to the manufacturer's instructions.

2.7.4 PCR purification

PCR reactions were purified with the QIAquick® or MinElute® PCR Purification Kits (Qiagen, 28104, 28004) or, if subsequently sent for sequencing, with exonuclease 1 (Exo1) (Thermo Fisher Scientific, 15513677) and shrimp alkaline phosphatase (SAP) purification (NEB, M0371S).

2.7.5 Site-directed mutagenesis

Site-directed mutagenesis was performed via a protocol provided by Dylan Webster (Adapted from QuickChange II XL Site-Directed Mutagenesis Kit Protocol). The Agilent webpage was used to design mutagenic primers. Which can be found in **Table 3**. Mutant strand synthesis was performed via PCR. The reaction mix contained 1X Phusion HF buffer, 1 nM of dNTPs, 500 nM of the relevant primers, 1.5 µL DMSO, 10 ng of template plasmid, 1U Phusion polymerase and ddH_2O up to a total reaction volume of 50 µL. The tube was gently flicked to mix and spun down in a microcentrifuge. Pre-heating of the thermocycler to 98°C

before addition of the reaction mix and the following parameters were set: 98°C 1 minute, then 18 cycles of 98°C for 30 seconds, 62°C for 50 seconds, and 72°C for 2 minutes finishing with 72°C for 10 minutes. Once completed, the reaction mix is kept at 4°C for at least 5 minutes before DpnI was added directly to the reaction mix and mixed by pipetting up and down. Once again, the mix was spun down in a microcentrifuge before being transferred to a thermocycler for 1 hour at 37°C. Dpn1 is heat inactivated at 80°C for 20 minutes. 1 µL of the reaction mix is then transformed into chemically competent cells as in **Section 2.6.2.**

2.8 Whole-mount *in situ* hybridization

Probes were amplified using plasmid stocks through linearization of the plasmid before purifying with phenol chloroform (Section 2.6.9). Transcription was then performed using 1 µg linearized plasmid DNA, 4 µL of the relevant transcription buffer, 0.5 µL RNase inhibitor, 2 µL 10xDIG labelling mix, 2 µL of the correct polymerase and RNase free water up to a total of 20 µL. The reaction mixture was incubated for 2hours at 37°C before 1 µL was removed and kept on ice. 1 µL of DNase was added to the remaining sample for 30 minutes at 37°C. A further 1 µL aliquot was removed post treatment and both underwent electrophoresis to determine DNA digestion. Precipitation of the RNA was performed via the addition of 80 µL RNase free water, 33 µL of 10uM NH4Ac and 350 µL 100% EtOH. The solution was mixed by pipetting up and down before being stored at -80°C for 2 hrs or overnight. After incubation the samples were centrifuged for 30 minutes at 4°C. The supernatant was removed and the remaining pellet was washed with 70% EtOH and spun for 5 minutes at 4°C. The supernatant was removed and the pellet air dried for 5 minutes before being resuspended in 100 µL RNase-free water. Long term storage of RNA samples occurred at -80°C.

48hpf zebrafish were fixed in 4% w/v PFA in PBS overnight at 4°C. The fish were then washed with PBST before dehydrated in successive 10 minute incubations with 30%, 60% and 100% methanol in PBST before being stored at -20°C overnight. Rehydration to 100% PBST is required before continuation can occur. Embryos were incubated with 10 µg/ml Proteinase K for 30 minutes and then washed with PBST for 5 minutes. Next, they are re-fixed in 4% w/v PFA in PBS for 20 minutes and then washed three times with PBST for a total of 15 minutes.

Embryos were then pre-hybridized in HM^+ (50 % formamide, 5 x SSC, 9.2 mM citric acid, 0.1 % Tween-20, 0.5 mg/mL tRNA (Invitrogen, 15401029), 0.05 mg/mL heparin) for at least 1 hour at 70°C. This was removed and replaced with HM^+ containing 500ng of RNA probe which had been pre-mixed at 70°C for 10 minutes. The solution was left on the embryos overnight at 70°C.

The embryos were then washed briefly in 100% HM^- (50 % formamide, 5 x SSC (ChemCruz, SC296419), 9.2 mM citric acid, 0.1 % Tween-20, pH 6) then for 15 minutes at 70°C in 75% HM^-/25% 2x SSC, 50% HM^-/50% 2x SSC, 25% HM^-/75% 2x SSC and 2x SSC. They were then washed for 2x 30 minutes with 0.2x SSC at 70°C followed by 10-minute washes at room temperature with 75% 0.2xSSC/25%PBST, 50% 0.2xSSC/50%PBST, 25% 0.2xSSC/75%PBST and 100%PBST. 1 mL of blocking buffer (2% Blocking reagent (Roche, 11096176001) dissolved in 1x malate Buffer at 70°C) was added and incubated for 3 hours at room temperature with shaking. The blocking buffer was replaced with a 1:5000 dilution of α-DIG antibody (Roche, 11093274910) in blocking buffer and the sample was incubated overnight with gentle rocking at 4 °C.

The samples were washed briefly with PBST at RT to remove any antiserum before undergoing four 30 minutes washes with PBST at RT in the dark. AP $buffer^-$(100 mM Tris pH 9.5, 100 mM NaCl, 0.1 % Tween-20) was added for 15 minutes, RT in the dark before two 10 minute washes with AP^+(100 mM Tris pH 9.5, 100 mM NaCl, 50 mM MgCl2, 0.1 % Tween-20).

Embryos were then transferred to a 24 well plate and incubated with 0.5ml Staining Solution (3.4 µL NBT and 3.5 µL BCIP in 1mL $AP^=$ buffer. Embryos were monitored with a dissecting microscope and checked every 30 minutes- 1 hour for stain development. Once sufficient stain had appeared, the embryos were washed three times in PBST for 5 minutes each at 4°C in the dark. Embryos were post fixed in 4%w/v PFA in PBS for 20 minutes at room temperature before undergoing successive incubations in 25%, 50% and 80% glycerol in PBS. Long term storage at -20C.

2.9 Microscopy

2.9.1 Microscopy

All whole embryo brightfield and fluorescent images were taken using a Leica M165FC fluorescent stereo microscope, with a digital colour camera (DFC310FX) and a Leica external fluorescent light source (EL6000). Images were taken with Leica Application Suite v.4.3.0. If live embryos were being imaged, they would first be anesthetized in Tricaine methanesulfonate (MS-222) and placed on a drop of 2% methylcellulose (Sigma). Whole mount embryos were imaged in 80% glycerol. A confocal (Olympus) microscope was used to image γH2AX tissues at 40X magnification.

2.9.2 Mounting

Small channels were created on microscope slides (Sigma-Aldrich, CLS294875X25-72EA) with Diamond Tape. Tails from embryos were mounted in liquid set Vectashield with DAPI (Vector Labs, H-1200-10) and enclosed with a coverslip (Sigma-Aldrich, BR470045). Small points of nail varnish were used to secure the coverslip in place.

2.10 Image Analysis

Fiji (Image J) software v.2.0 was used for image analysis. Tail lengths were measured from the base of the yolk to the tip of the tail. To measure γH2AX foci, initially a mask was created, outlining the visible nuclei. The maxima points were then identified in the 460-500nm channel with a suitable parameter set. Maxima points within the outlined nuclei were then counted and averaged over several samples.

2.11 Statistical Analysis

Quantification and statistical analysis were performed using GraphPad Prism version 8.4.0 for Windows 10 (GraphPad Software, La Jolla, California, USA, www.graphpad.com). Students t-tests were used for comparison of two normally distributed samples. One-Way or Two-Way ANOVAs were used for multiple comparisons with Sidak's post hoc analysis test.

Chapter 3

Characterisation of an RNaseH2a knockout zebrafish

3.1 Introduction

Ribonuclease H2 is a heterotrimeric protein complex that has a well-defined role in the removal of single ribonucleotides that are incorporated into the DNA during replication by polymerases, Okazaki fragments and also during Non-Homologous End Joining (Sparks *et al.*, 2012). Whilst some of these are intentional (see NHEJ) and aid repair, an abundance of rNMPs in the genome can increase its fragility leading to increased strand breakage and cell death (Klein, 2017; Pryor *et al.*, 2018). RNaseH2 also has a less well characterized role in the resolution of RNA:DNA hybrids that occur during transcription. Although these hybrids expose a single DNA strand, which is susceptible to breakage, they are also predicted to be important regulators of transcription (Crossley, Bocek and Cimprich, 2019).
Mutations in any of the three subunits of the complex (RNaseH2a, RNaseH2b and RNaseH2c) have been found to be associated with the severe neurological auto inflammatory disorder Aicardi Goutières Syndrome (AGS). Over 50% of mutations in AGS patients are found to be in subunits of RNaseH2 which result in AGS4 (Crow *et al.*, 2015).

One of the hallmarks of AGS is an increase in Type 1 interferon stimulated genes (ISG) (Lebon *et al.*, 1988) leading it to be defined as a Type 1 interferonopathy. The uncontrolled stimulation of these interferon regulated genes can lead to the destruction of the myelin sheath surrounding nerves and is responsible for many of the symptoms seen in AGS patients. The activation and upregulation of interferon stimulated genes is often seen in viral infections and AGS patients have a phenotype that has been described as comparable to an in-utero viral infection and systemic lupus (GoutièRes *et al.*, 1998). In the case of AGS, rather than an external viral genome being the cause of interferon stimulation, the cell may recognise aberrant DNA fragments formed via a large quantity of DNA damage.

Previously, a number of models to study the role of RNaseH2 have been created. Yeast cells that are deficient for RNaseH2 were shown to have increased rNMP incorporation into their genome (Stephanie A Nick McElhinny *et al.*, 2010) and exhibit increased replicative stress (Stephanie A Nick McElhinny *et al.*, 2010; Lazzaro *et al.*, 2012). Fibroblasts isolated from a conditional knockout RNaseH2b mice (RNAseH2$^{\Delta GFAP}$) also showed an increase in DNA damage, a reduction in their ability to proliferate and increased senescence. However, they did not display upregulated ISGs (Hiller *et al.*, 2012).

Several groups have also created knockout mouse models for RNaseH2a, RNaseH2b and RNaseH2c (Hiller *et al.*, 2012; Reijns *et al.*, 2012; Uehara *et al.*, 2018). A striking similarity between all these animal models is that the null knockouts are embryonic lethal. RNaseH2b and RNaseH2c mice provided evidence that removal of these subunits lead to a significant increase in embedded ribonucleotides in the genomes of effected animals. It also lead to an increase in their constitutive levels of DNA damage and increased expression of p53 (Hiller *et al.*, 2012; Reijns *et al.*, 2012). Removal of the RNaseH2a subunit was also discovered to have similar effects on mice (Uehara *et al.*, 2018). Given the two roles of RNaseH2 (RER and R-loop resolution) an RER defective (RED) mouse was produced via the mutation of two key amino acids (P40D, Y211A) in the RNaseH2 active site. This RNaseH2a^{RED} mouse also displayed large levels of incorporated ribonucleotides and an increased p53 response that ultimately led to embryonic lethality, confirming the increased rNMP incorporation as the main cause of lethality in this and previous RNaseH2 null mice (Uehara *et al.*, 2018).

Although these null *in vivo* models have revealed the essential nature of RNaseH2 during early development, they are not AGS specific models. The mutations in AGS patients identified so far show a reduction, not a total loss, of RNaseH2 activity. An *Rnaseh2b*^{A174T} mouse model was used to establish that the A174T point mutation, the most common missense mutation found in humans, showed increased ISG induction in several different tissues, although not in the brain (Mackenzie *et al.*, 2016). A second model, *Rnaseh2a*^{G37S}, showed increased survival compared with null models although still displayed perinatal lethality. They also showed increased induction of ISGs which, when reduced after ablation of STING, partially rescued the perinatal lethal phenotype (Pokatayev *et al.*, 2016).

In contrast to the findings that ISG reduction improves the murine phenotypes, specific neuronal knockouts have shown no recovery in cerebellum reduction after knockout of cGAS, suggesting that the high levels of DNA damage are more responsible for the detrimental phenotypes than the inflammatory response (Pokatayev *et al.*, 2016). Specific knockouts in astrocytes however have shown accumulation of DNA aggregates in their cytoplasm which are thought to activate the cGAS/STING pathway and subsequent ISGs (Bartsch *et al.*, 2017). Treatment of AGS patients with mTOR inhibitors aims to reduce the formation of these cytosolic micronuclei and subsequently reduce the large upregulation of ISGs seen in patients.

RNaseH2a is also heavily implicated in cancer. Studies have reported the overexpression of RNaseH2a in brain, breast and bladder cancer. It has also been reported in leukaemia's, melanomas and seminomas along with head and neck squamous cell carcinoma (Flanagan *et al.*, 2009) and hepatocellular carcinoma (HCC) (Hua *et al.*, 2020). It has also been considered as a marker for kidney cancers and colorectal cancer patients (Yang *et al.*, 2018; Zhang *et al.*, 2018). Knockout of RNaseH2a in leukemic cells caused a reduction in cell viability and suggests RNaseH2a to be a potential inhibitor target (Ghosh, Kumari and Raghavan, 2022).

The range of models displayed from null models to cell-type specific knockouts show a breadth of phenotypes in mice. So far, no zebrafish model has been characterised to study any of the three subunits of RNaseH2. Along with their small size and rapid development, zebrafish allow for easy genetic manipulation and study of development given their embryonic transparency and external fertilization giving a simpler yet still genetically similar alternative to mice.
Here I will describe the creation of a zebrafish containing a knockout of subunit A of RNaseH2 and subsequent characterization of this DNA repair model.

Hypothesis: Zebrafish lacking RNaseH2a will suffer from increased ribonucleotide incorporation resulting in an increase in DNA damage and AGS phenotypes such as upregulation of Type1 interferons.

Aims:

- Characterisation of *rnaseh2a*$^{-/-}$ zebrafish at embryonic and adult stages
    - Quantification of ribonucleotide incorporation at embryonic and adult stages
    - Identification of any changes in DNA damage
    - Investigation of any AGS related phenotypes including upregulation of Type 1 interferons

3.2 Results

3.2.1 RNaseH2a knockout zebrafish are viable

Like humans, zebrafish contain one gene for each subunit of the RNaseH2 complex. The RNaseH2a gene contains nine exons creating a protein that is 309 amino acids in length (www.ensembl.org). There is 76% amino acid similarity between *Homo sapien (hs)* RNaseH2a and *Danio rerio (dr)* RNaseH2a including conservation of key AGS mutation site suggesting that they would be a good model for investigating to effects of RNaseh2a knockout **(Figure 3.1)**. The expression pattern of *rnaseh2a* in 24hpf zebrafish embryos was determined using in-situ hybridization. This revealed the universal expression of *rnaseh2a* throughout the embryo with a slight increase in mRNA concentration in the head **(Figure 3.2)**. This is in accordance with previously published data from mouse models showing the universal expression of RNaseH2a (Yue *et al.*, 2014).

Work performed previously by a PhD student in the El-Khamisy lab, Ringailė Zakšauskaitė, utilised the CRISPR/CAS9 system to target exon six **(Figure 3.3A)** and establish a 49bp deletion (SH478) **(Figure 3.3B)**. This created an early stop codon and truncated protein of 206 aa in length, compared with the wild type at 307 aa **(Figure 3.3C).** Exon six was chosen as it is early enough to prevent alternative start sites creating a functional protein. The early stop codon is situated 52a.a downstream of the deletion and removes key residues that are known to be mutated in AGS patients (amino acid positions 231,236,241,298) and Y211, known to be essential for RER related cleavage. **(Figure 3.3C)** (Coffin et al., 2011) This strongly indicates that this mutation will be deleterious towards RNaseH2a function.

In contrast to previous models, the homozygote mutant adults are viable, appearing indistinguishable from the *wild-type* at both their embryonic and adult stages at the gross morphological level, with genotype ratios of both embryos and adults occurring at Mendelian ratios. The spots visible in some *rnaseh2a*$^{-/-}$ adults (*rnaseh2a*$^{SH478/SH478}$) are a background mutation present in the laboratory zebrafish so should not affect any of the findings presented in the rest of this thesis **(Figure 3.4A,B).** In humans, AGS mutations cause reduced development of the brain resulting in the structure being smaller than usual (Aditi *et al.*, 2021). When looking at the brain of adult *rnaseh2a*$^{-/-}$ zebrafish there was not a significant difference in the size of their brain compared with their wild-type siblings **(Figure 3.5A,B)** or in their overall development **(Figure 3.5C,D)**. This viable phenotype is distinct

from those that have been previously seen in animal models and leads to interesting opportunities to study the molecular causes behind their survival.

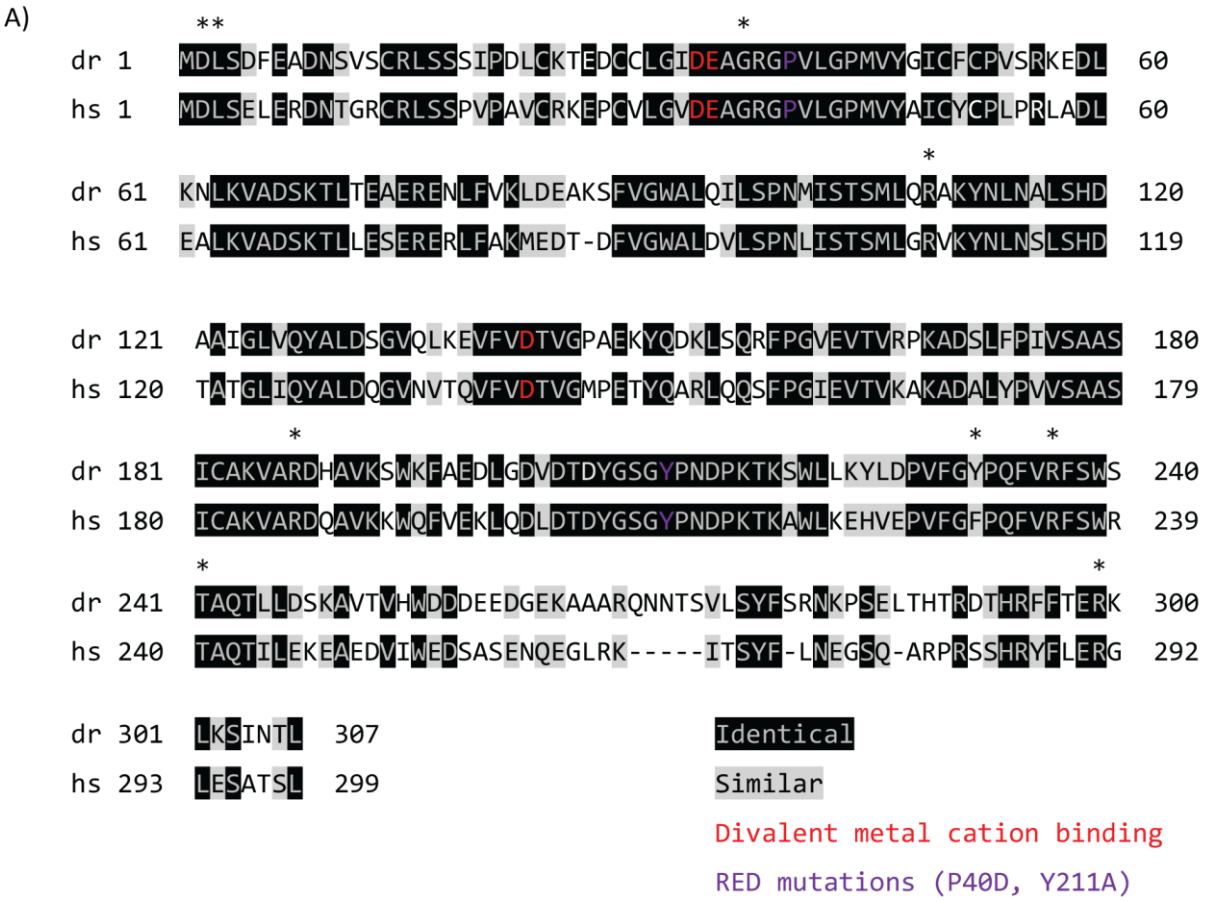

Figure 3.1: Zebrafish RNaseH2a amino acid sequence alignment against human RNaseH2a

Protein alignment between zebrafish, *Danio rerio* (dr) and Human, *Homo sapien* (hs) RNaseH2a. Identical amino acids highlighted in black (61%) and similar amino acids in grey (17%). Asterix show sites of AGS mutations. Divalent metal cation binding sites (Red). Mutations required to remove RER activity (Purple). Accession numbers: hsRNaseH2a: ENST00000221486.6 drRNaseH2a: ENSDART00000045894.7. Sequence aligned using Protein BLAST

Figure 3.2: RNaseH2a is universally expressed in wild-type zebrafish embryos

Whole Mount In Situ Hybridisation of RNaseH2a mRNA in wild-type, 24hpf zebrafish embryos. Antisense RNaseH2a mRNA used as a negative control. *Rnaseh2a* expression seen in blue (top) is universal throughout the embryo with a mild emphasis in the head. Scale bar 0.5mm.

My thanks to master's student Patricia Zheng for performing this experiment

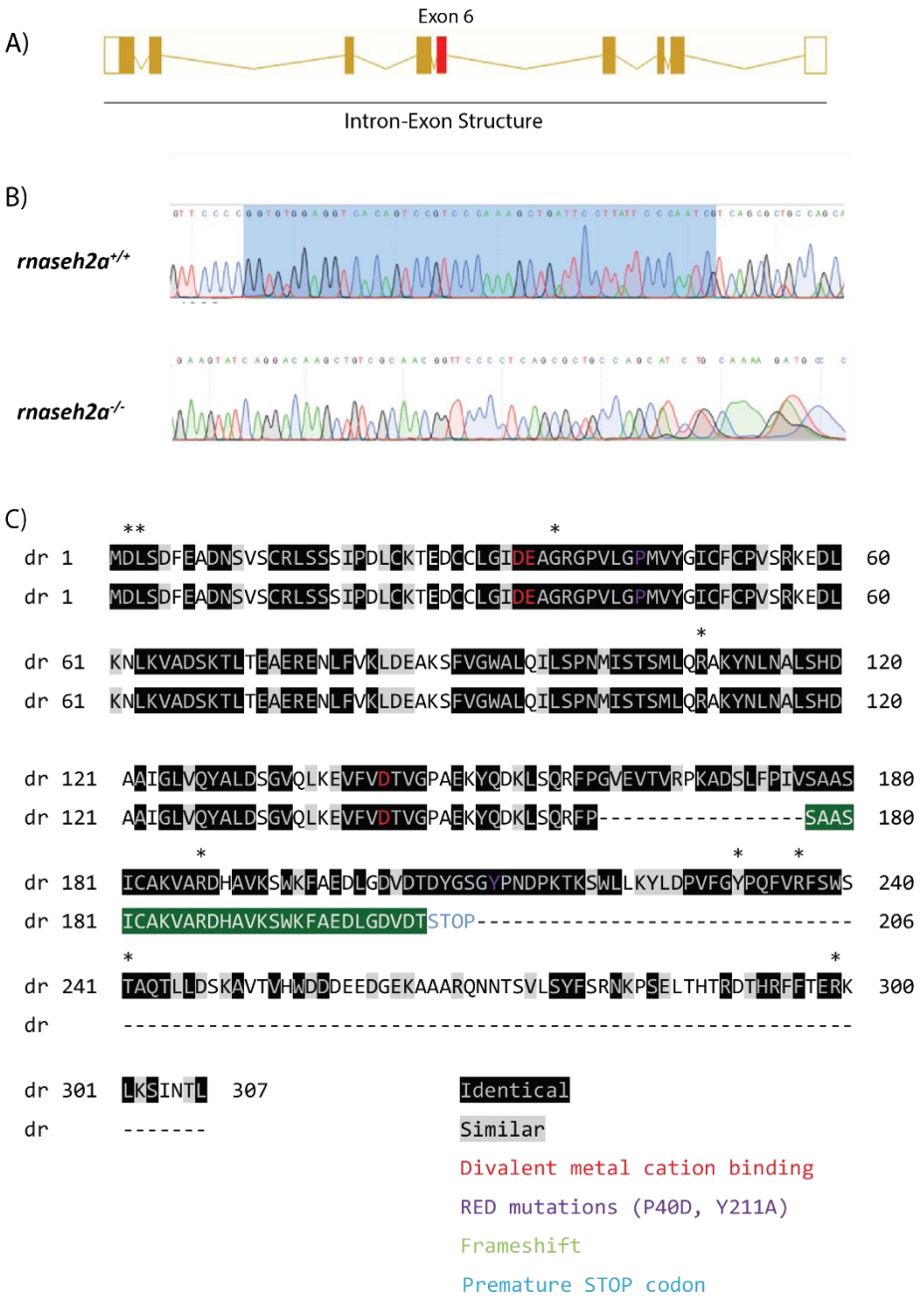

Figure 3.3: Creation of a homozygous knockout zebrafish using the CRISPR/Cas9 system

A) Intron-Exon structure of the zebrafish *rnaseh2a* gene with targeted area for cleavage by Cas9, Exon 6, highlighted in red. **B)** Sequence of wild-type and mutated RNaseh2a. The blue box indicates the 49bp deletion at the site of cleavage resulting in the frame-shit and early stop codon 52 amino acids downstream. **C)** Protein alignment between full length and mutated zebrafish RNaseH2a showing the positions of the deletion amino acids (158-175), the resultant frameshift (Green) (177 – 205) and premature STOP codon (blue), ultimately resulting in a truncated protein.

Sequences in **B)** provided by Ringailė Zakšauskaitė.

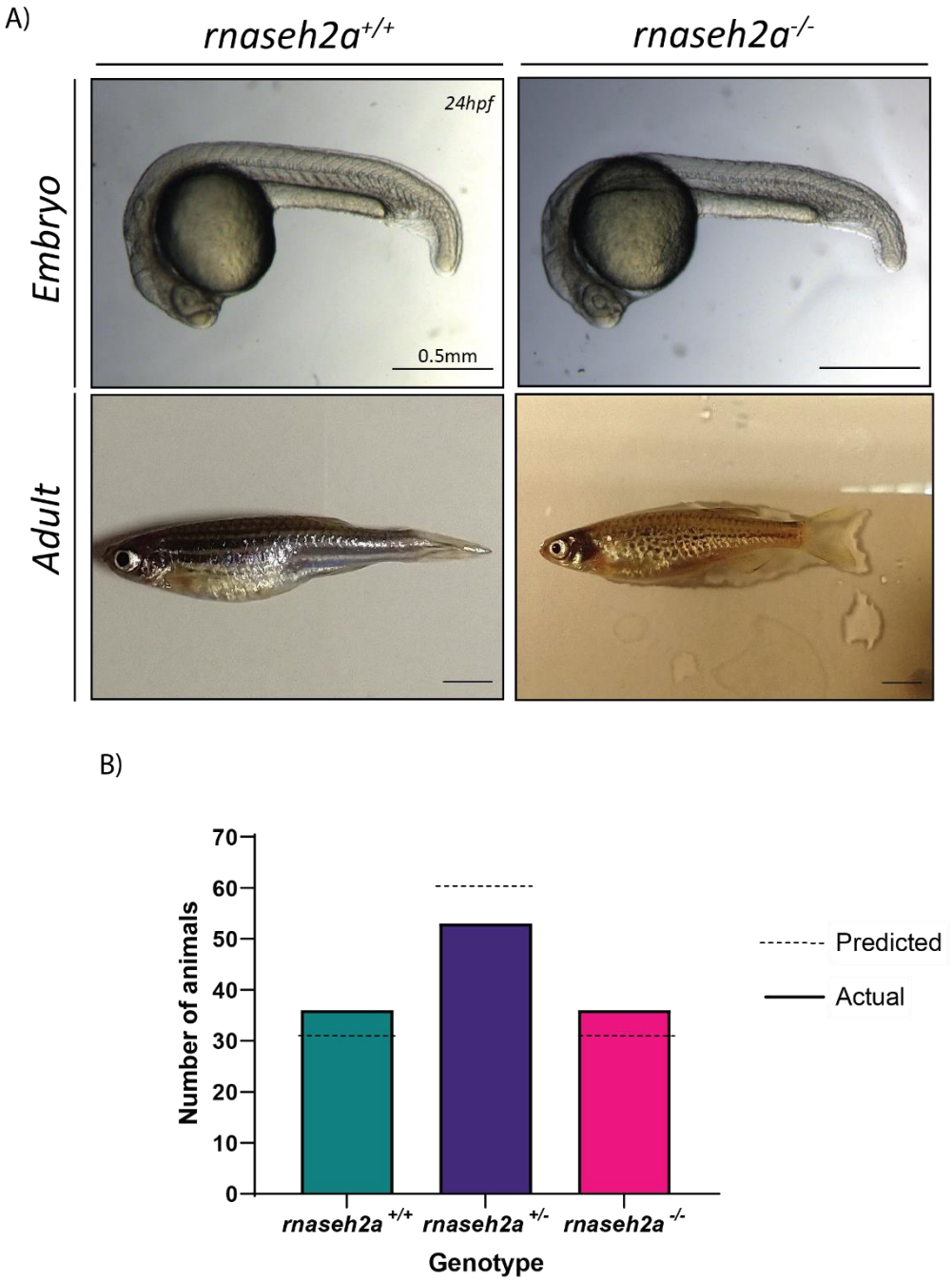

Figure 3.4: Homozygous knockouts are indistinguishable from wild-types

A) Embryos at 24hpf resulting from *rnaseh2a*$^{+/-}$ parents do not show any visibly detrimental phenotype and are able to develop to adulthood where they continue to have no gross morphological differences. Spots in *rnaseh2a*$^{-/-}$ adults caused by background mutation. **B)** Genotype ratios at 5dpf are not significantly different from those predicted, confirming inheritance in a Mendelian Ratio. $X^2 = 2.66$, with two degrees of freedom; 2-tailed P value of 0.529. Scale bar 0.5mm (Embryo) and 0.5cm (Adult).

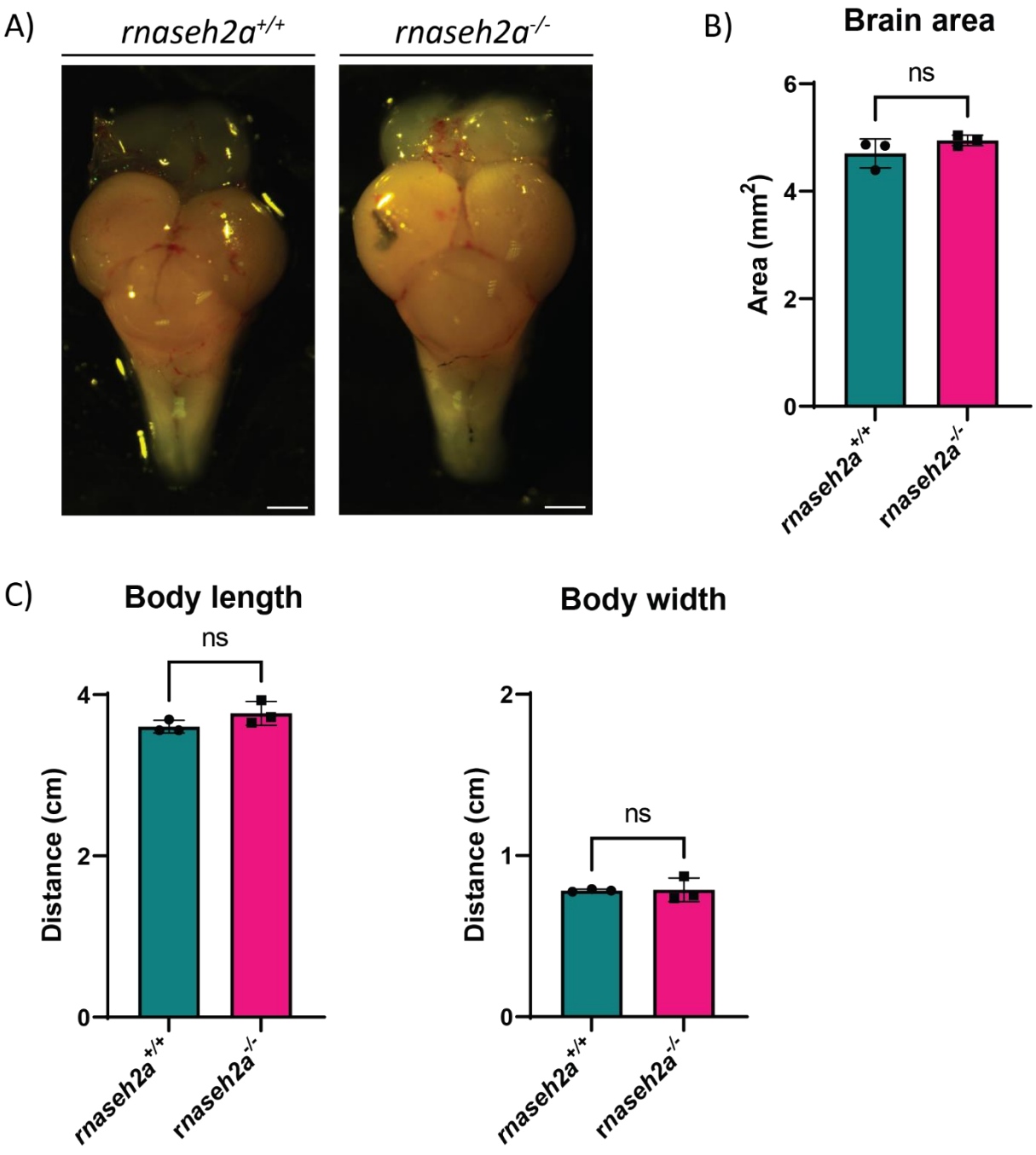

Figure 3.5: Brain size is not reduced in *rnaseh2a*$^{-/-}$ adults

A) Images of whole brains from 15 month old adult zebrafish show gross morphological changes. **B)** Quantification of whole brain area from three individual fish shows no significant difference in size between *rnaseh2a*$^{-/-}$ and *rnaseh2a*$^{+/+}$. Quantification performed using ImageJ freeform tool. **C+D)** Body length and width of individual adult zebrafish show no significant difference between *rnaseh2a*$^{-/-}$ and *rnaseh2a*$^{+/+}$ *adults* indicating no gross morphological phenotypes at adulthood. Scale bar, 0.5mm, n=3, individual adults, ±SD, Unpaired T-test, $p<0.05$

3.2.2 RNaseH2a homozygotes do not produce viable offspring

We have successfully created homozygous knockout zebrafish line in which individuals are able to survive to up to 3 years (studies limited by law). Zebrafish receive a large number of maternally contributed factors that support development during early embryogenesis. RNaseH2a mRNA is detectable in fertilised oocytes (www.ensembl.org), I therefore checked if there is a maternal requirement for RNaseH2a.

The *rnaseh2a*$^{-/-}$adults are able to breed and produce maternal zygotic (*MZrnaseh2a*) fertilized embryos that develop normally up until gastrulation **(Figure 3.6A,B)**. From here, their reduced development is visible by 24hpf, resulting in short tails, small heads and severe necrosis resulting in all of the embryos dying by 3dpf **(Figure 3.6B).** RTqPCR analysis revealed a significant decrease in the mRNA expression of the *rnaseh2a* gene in *Mzranseh2a* embryos suggesting nonsense mediated decay of the mutant transcripts **(Figure 3.6C)**.

The *rnaseh2a*$^{-/-}$ embryos from heterozygous parents however, are indistinguishable from their *rnaseh2a*$^{+/+}$ siblings **(Figure 3.6B).** Therefore, it was predicted that the surviving *rnaseh2a*$^{-/-}$ either have 1) A strong requirement for maternally contributed RNaseh2a function during the early rapid cell divisions that is not required during later larval stages 2) They are tolerating the large quantities of ribonucleotides, providing they remain below a critical threshold or 3) *rnaseh2a*$^{-/-}$ embryos have a secondary mechanism of rNMP removal from their DNA, maintaining genome stability and allowing them to age and reproduce. Finally, a combination of these scenarios may be true.

3.2.3 *Mzrnaseh2a* embryos are unable to efficiently cleave a single rNMP substrate

RNaseH2 has a key role in the cleavage and repair of single ribonucleotides incorporated into DNA. Subunit A of this complex contains the active site and therefore, upon removal via CRISPR/Cas9, it would be expected that the *rnaseh2a*$^{-/-}$ were no longer able to cleave single rNMPs. To confirm that the *rnaseh2a*$^{-/-}$ fish are null in this cleavage activity, confirming a successful RNaseH2a knockout, a cleavage assay was used **(Figure 3.7a)**. Whole cell lysate from *wild-type* and MZ*rnaseh2a* embryos was incubated with a dsDNA substrate with a single ribonucleotide incorporated and a 5'Cy5 tag. Active RNaseH2 would cause a cleavage on the 5' side of the incorporated ribonucleotide, resulting in a 20bp cleavage product. If *rnaseh2a* has been successfully knocked out and the resulting truncation has resulted in a non-functional protein, then the substrate will remain at 42bp in length.

In *MZrnaseh2a* embryos, it was observed that cleavage of the dsDNA substrate was below 20% cleavage across all concentrations. This was over 50% lower than the cleavage observed in embryos from an *rnaseh2*$^{+/+}$ incross and the positive control of purified RNaseH2 **(Figure 3.7B,C)**.

However, when *rnaseH2a*$^{-/-}$ adults from *rnaseh2a*$^{+/-}$ parents were tested, it was found that despite having a lack of functional RNaseH2a, they are able to cleave single ribonucleotides as efficiently as their wild-type siblings in an *in vitro* setting, in multiple tissues (**Figure 3.8A,B,C,D)**. To determine whether this cleavage activity was present from an earlier developmental stage, we looked at 5dpf *rnaseh2a*$^{-/-}$ embryos from an *rnaseh2a*$^{+/-}$ incross. Here, I observed that the ability to cleave single ribonucleotides is present in the *rnaseh2a*$^{-/-}$ offspring from an early embryonic stage as lysate from 5dpf embryos showed the same cleavage ability as their *rnaseh2a*$^{+/+}$ siblings **(Figure 3.9A,B)**. It was also noticeable that the overall cleavage efficiency in 5dpf embryos, even in the *rnaseh2a*$^{+/+}$ samples, was lower than seen at both 24hpf and in the adult tissue samples. As well as the uncleaved (41bp) and cleaved (20bp) bands, I observed a central, approximately 30bp, band. This consistently appeared in all samples using zebrafish lysate. This is predicted to be non-specific degradation of the dsDNA substrate by exonucleases present in the whole-cell lysate, therefore not related to the presence of the single rNMP.

The data shown here suggests that any such mechanism that is removing the single rNMPs is present from the embryonic stage all the way through to adulthood. Therefore, this indicates that scenario 3, the presence of a secondary mechanism of removal, appears to be true.

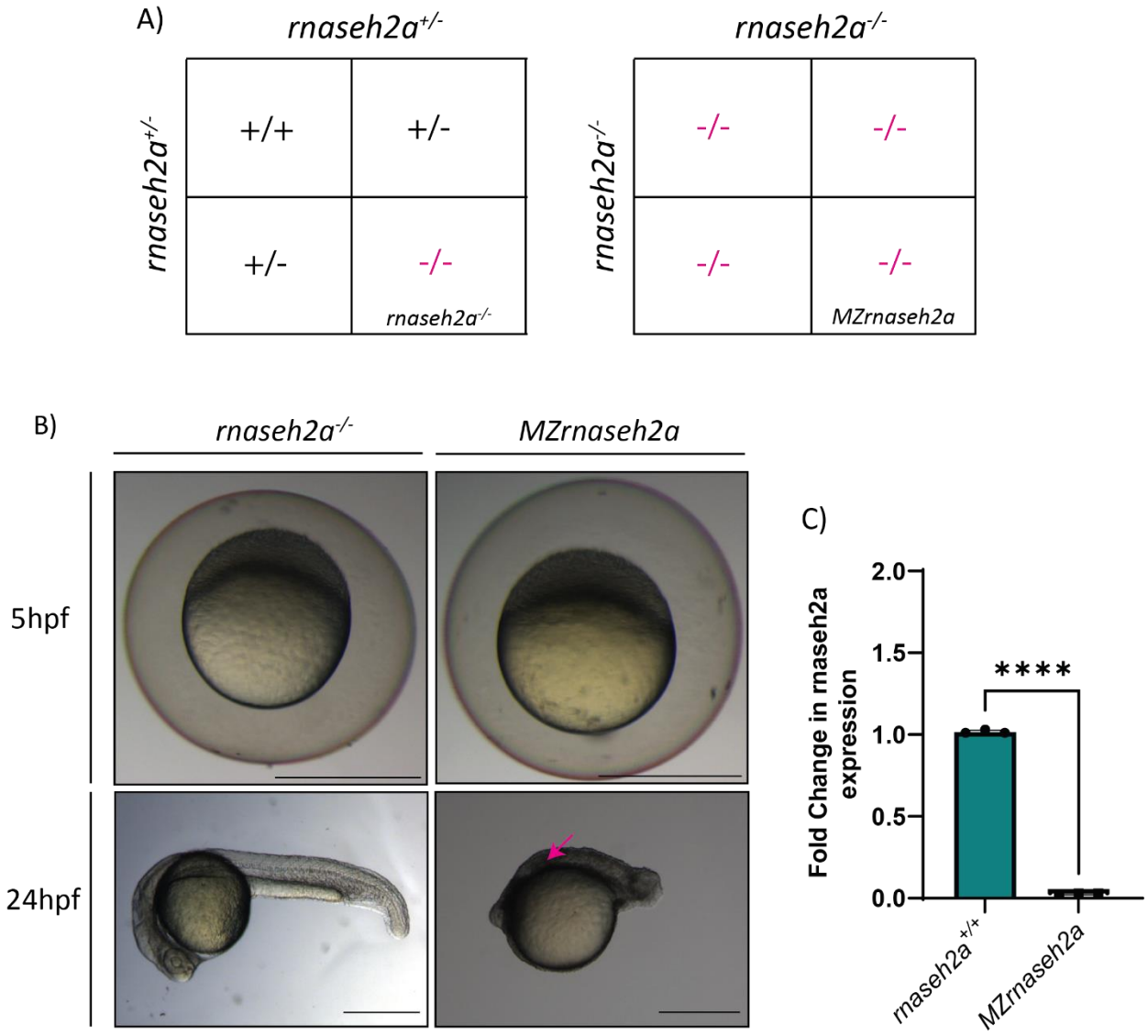

Figure 3.6: Embryos from two *rnaseh2a*$^{-/-}$ adults are poorly developed

A) Homozygous embryos resulting from heterozygous parents are phenotypically normal and are indistinguishable from their wild-type siblings and occur in Mendelian Ratios. **B)** 5hpf embryos are fertilised and develop normally. 24hpf *MZrnaseh2a* homozygote embryos are significantly underdeveloped with small heads, malformed tail growth and high level of cell death (pink arrow). Scale bar 0.5mm. **C)** RT-qPCR analysis of *rnaseh2a* expression in *MZrnaseh2a* embryos showed a significant reduction in expression, suggesting nonsense-mediated decay of the mutant transcript. n=3, 20 pooled embryos, ±SD Unpaired t-test, ****p<0.001

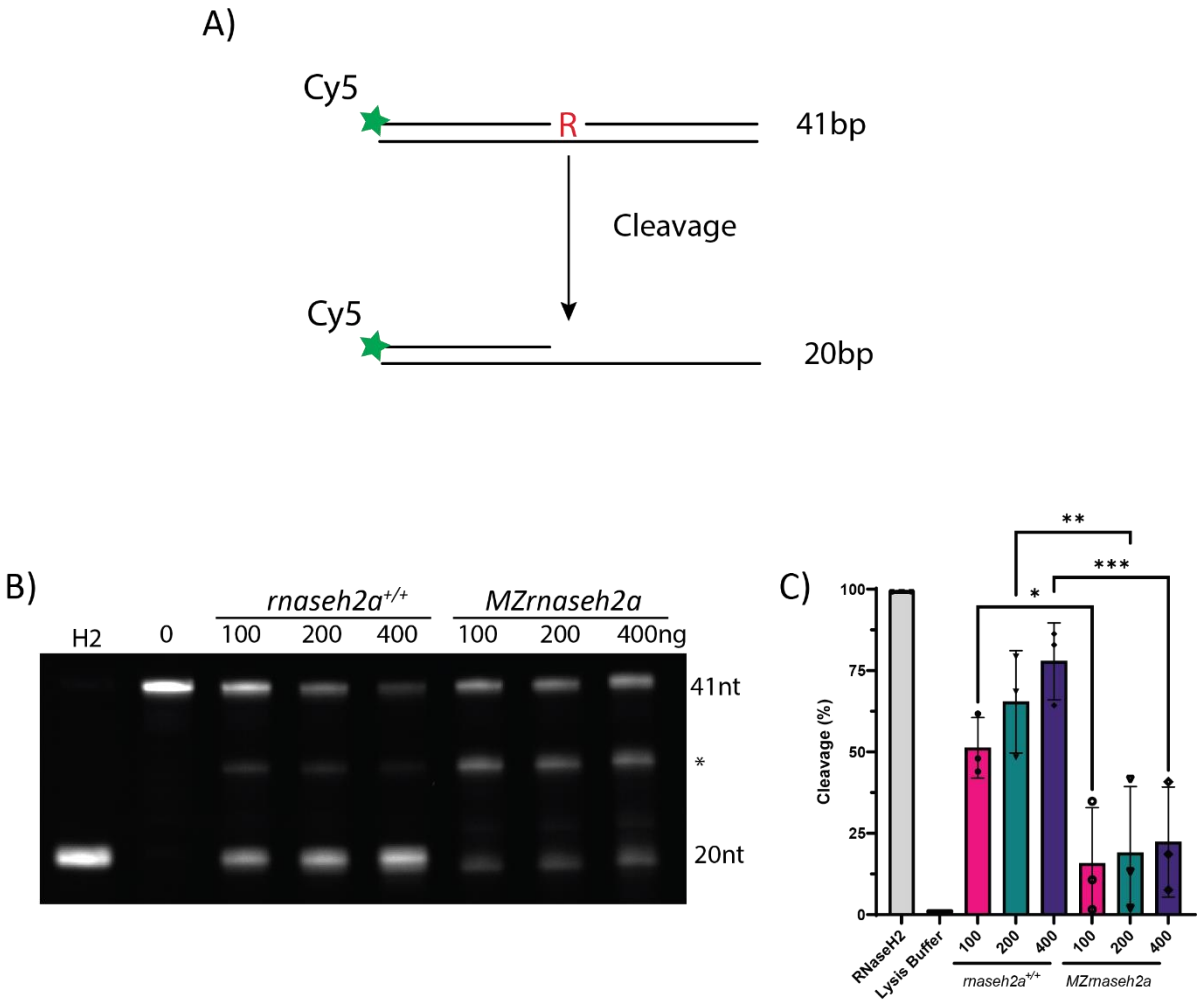

Figure 3.7: *MZrnaseh2a* embryos are unable to efficiently cleave a single rNMP substrate

A) Schematic of the cleavage assay showing the 41bp starting substrate and the expected 20nt product after cleavage. **B)** Denaturing UREA gel showing cleavage by *rnaseh2a*$^{+/+}$ increasing with lysate concentration but not by *MZrnaseh2a* embryos. * Indicates a middle band, predicted to be non-specific to rNMP cleavage **C)** Quantification of cleavage by embryo lysate seen in B showing a significant difference in rNMP cleavage between *MZrnaseh2a* and *rnaseh2a*$^{+/+}$ embryos at 24hpf. n=3, 20 pooled embryos, ±SD One-Way ANOVA, ns p>0.05, *p<0.01, **p<0.001, ***p<0.0001.

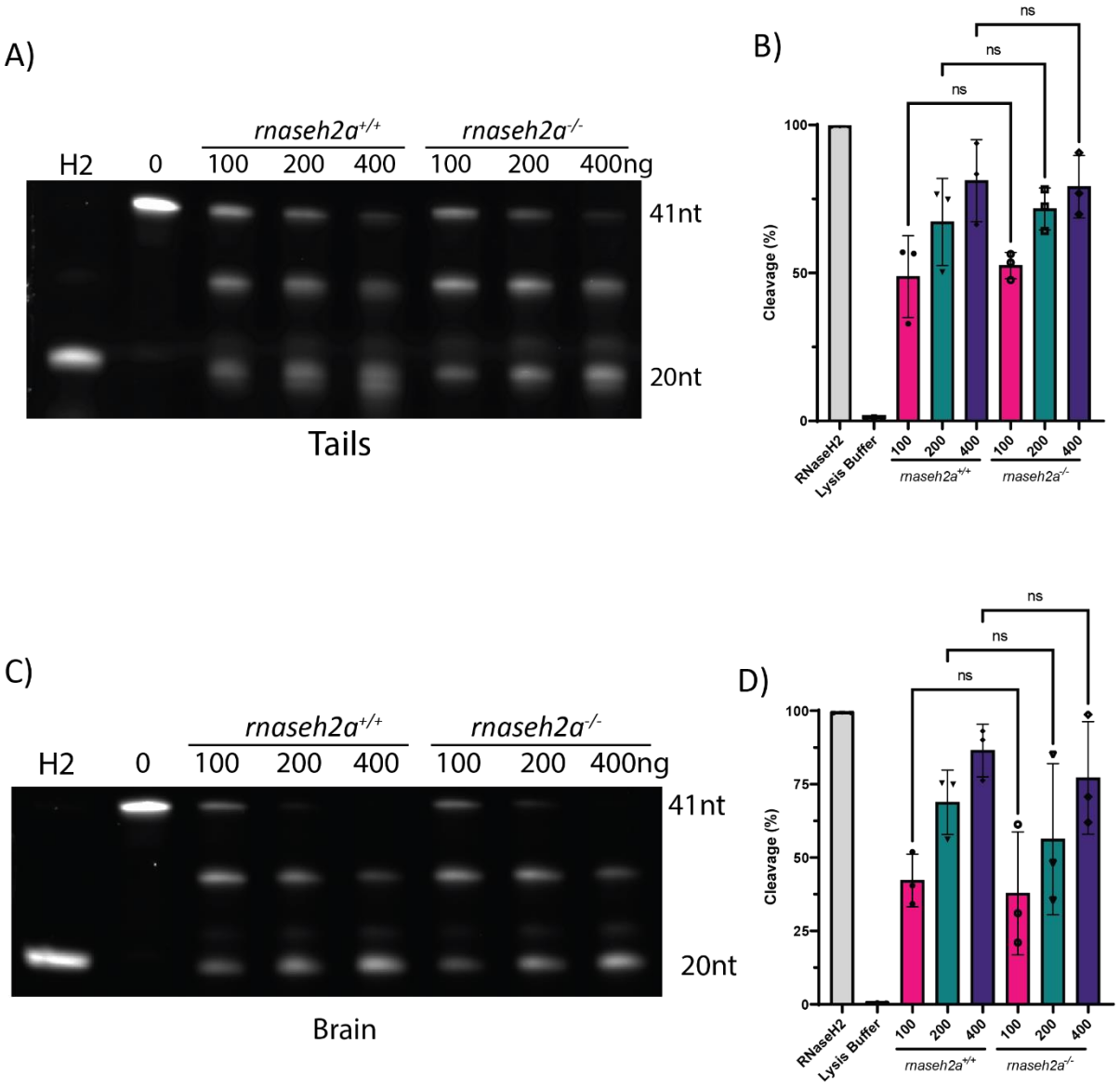

Figure 3.8: *rnaseh2a*$^{-/-}$ adults are able to efficiently cleave a single rNMP substrate in multiple tissues

A) Denaturing UREA gel showing cleavage by lysate from tail clips of 15 month old zebrafish. **B)** Quantification shows that lysate from *rnaseh2a*$^{-/-}$ fish are able to cleave the single rNMP substrate as efficiently as their *rnaseh2a*$^{+/+}$ siblings in lysate from adult tails. **C)** UREA gel showing cleavage by lysate from adult zebrafish brains. **D)** Quantification of the cleavage shown in C reveals no significant difference in cleavage ability by *rnaseh2a*$^{+/+}$ and *rnaseh2a*$^{-/-}$ in lysate from brain tissues. n=3, individual adults, ±SD, One-Way ANOVA, ns p>0.05.

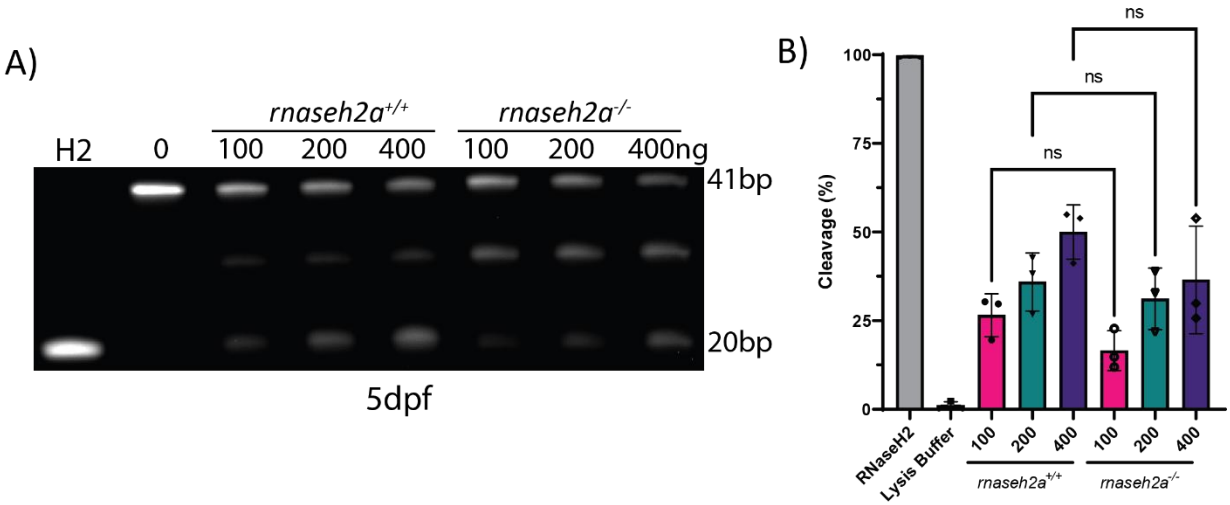

Figure 3.9: *rnaseh2a*$^{-/-}$ embryos from a heterozygous cross are able to efficiently cleave a single rNMP substrate

A) Denaturing UREA gel showing cleavage by lysate from 5dpf zebrafish larvae after genotyping via 3dpf fin-clipping. **B)** Quantification shows that lysate from *rnaseh2a*$^{-/-}$ embryos are able to cleave the single rNMP substrate as efficiently as their *rnaseh2a*$^{+/+}$ siblings. n=20 pooled embryos, ±SD, One-Way ANOVA, ns p>0.05

3.2.4 *MZrnaseh2a* embryos show higher levels of ribonucleotide incorporation

The main role of RNaseH2 is the removal of single ribonucleotides from DNA. Upon the removal of this key DNA repair protein, it has been shown that, during replication, the number of persistent rNMPs increased (Stephanie A Nick McElhinny *et al.*, 2010). However, given that I have identified the potential for a backup activity, it is predicted that this may be sufficient to remove rNMPs and therefore be one explanation for the viability of the homozygote mutants.

Ribonucleotides are very susceptible to spontaneous hydrolysis due to the hydroxyl group at the 2' position. Alkaline conditions exacerbates this hydrolysis and causes DNA with large numbers of rNMPs to fragment (Stephanie A Nick McElhinny *et al.*, 2010). Therefore, if DNA fragments from *rnaseh2a*$^{-/-}$ embryos are treated with NaOH and run on an agarose gel, the fragments would be expected to run further as the DNA would be in smaller fragments if repair is incomplete, or the same distance as their siblings if the repair if efficient **(Figure 3.10A)**.

First I explored as to whether the *MZrnaseh2a* embryos that showed severe developmental defects, also contained a large number of rNMPs by use of an alkaline assay. Samples were taken from pooled whole embryos from an *rnaseh2a*$^{-/-}$ incross (*MZrnaseh2a*) and an *rnaseh2a*$^{+/+}$ incross as well as *rnaseh2a*$^{-/-}$ embryos from a heterozygous incross. In addition, brain samples from adults were also isolated via Total Nucleic Acid Extraction **(Section 2.1.10)**. After treatment in high alkaline conditions, samples were run overnight on an agarose gel.

The 24hpf *MZrnaseh2a* embryos showed a significantly higher density of smaller DNA strands, suggesting high levels of fragmentation compared with the *rnaseh2a*$^{+/+}$ sample which accumulate above 10kb (**Figure 3.10B,C)**. This also occurred in the control samples treated with NaCl which may suggest that the density of incorporated rNMPs in *MZrnaseh2a* embryos is so high that spontaneous hydrolysis frequently occurs without alkaline treatment or the level of apoptotic cells in *MZrnaseh2a* embryos is high enough to create large quantities of DNA fragmentation.

Unexpectedly, despite not showing any visible phenotypes, *rnaseh2a*$^{-/-}$ adults also showed a mild increase in ribonucleotide incorporation in their brains compared with their wild-type counterparts, although to a lesser extent than the *MZrnaseh2a* embryos **(Figure 3.11A,B)**.

To test whether this was apparent from an embryonic stage, we performed the same experiment in 5dpf *rnaseh2a*$^{-/-}$ embryos from an *rnaseh2a*$^{+/-}$ incross. Surprisingly, the embryos were able to remove ribonucleotides as efficiently as their wild-type siblings, resulting in no significant build up and subsequent damage from the alkaline conditions **(Figure 3.11C,D)**.

Overall the data support a scenario where from embryonic stages to adulthood, there is a slow accumulation of rNMPs over time in *rnaseh2a*$^{-/-}$ animals. This also leads to the hypothesis that the previously proposed secondary mechanism of rNMP removal in *rnaseh2a*$^{-/-}$ fish from a heterozygous incross is insufficient to prevent this accumulation.

Due to the large numbers of rNMPs found to be incorporated into the genome of *MZrnaseh2a* embryos, it is thought that their spontaneous hydrolysis will lead to a large number of single, and potentially double stranded DNA breaks, these will be more damaging during early development when cells are replicating quickly. I speculate that this in turn, may activate the apoptosis of a large number of cells and overall contributing to their lack of development.

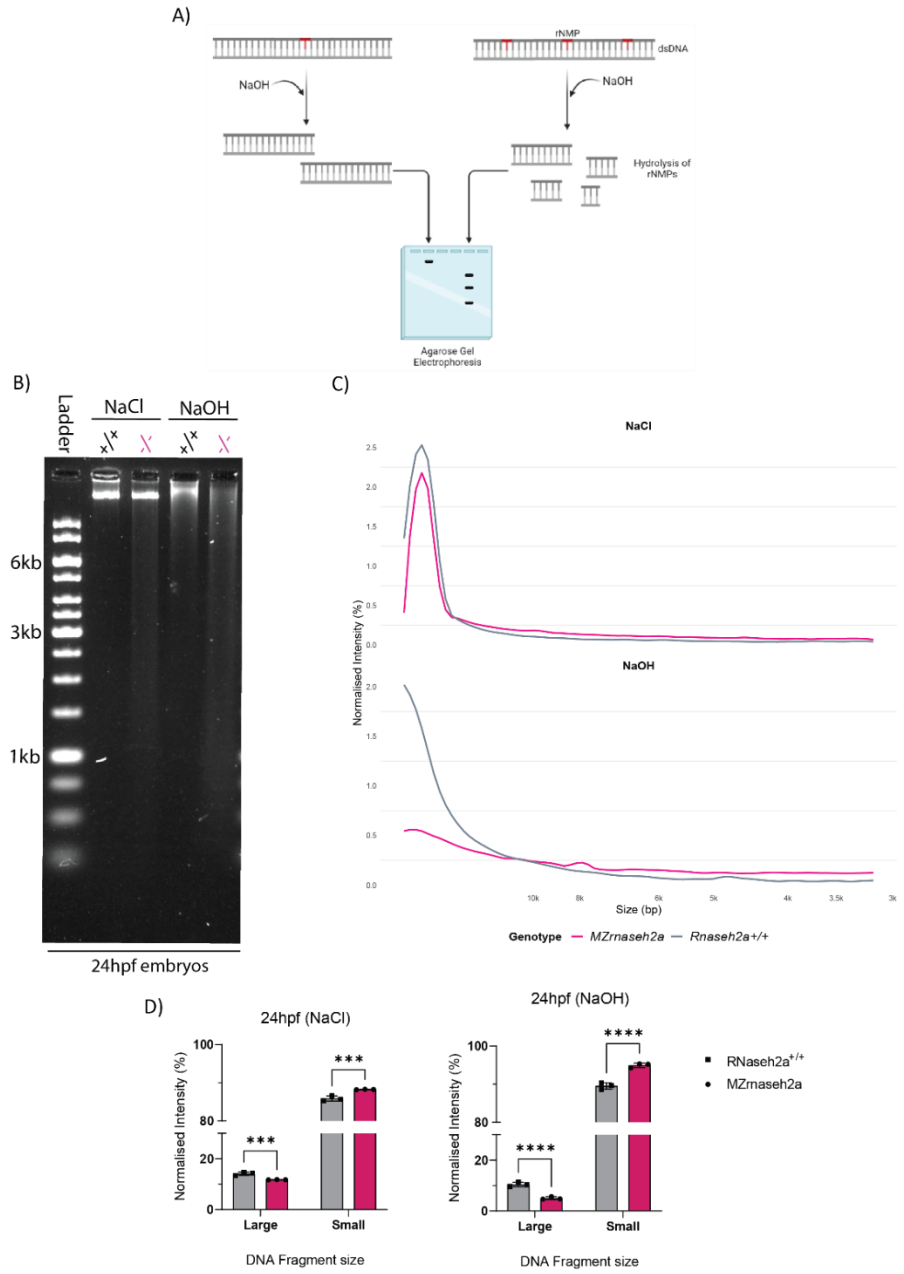

Figure 3.10: *MZrnaseh2a* embryos have increased rNMP incorporation in their genomes

A) Schematic of workflow for a gel assay following alkaline treatment with NaOH with expected outcomes, also described in Section 2.6.13 **B)** Representative DNA agarose gel of *MZrnaseh2a* and *rnaseh2a*$^{+/+}$ 24hpf embryos. Individual samples split into Control (NaCl) and Alkaline Treated (NaOH). **C)** Quantification of intensity from 3.10B. Intensity of DNA normalised to total DNA per lane. Mean Normalised Intensity calculated from three biological replicates and plotted using R Studio (20 pooled embryos per replicate). **D)** Total normalised intensity of large and small DNA fragments. Fragmentation size defined as above (large) or below (small) the x value at which Normalised Intensity has halved in the relative *rnaseh2a*$^{+/+}$ sample. n=3, 20 pooled embryos, Unpaired t-test, ±SD, ***p<0.001, ****p<0.0001

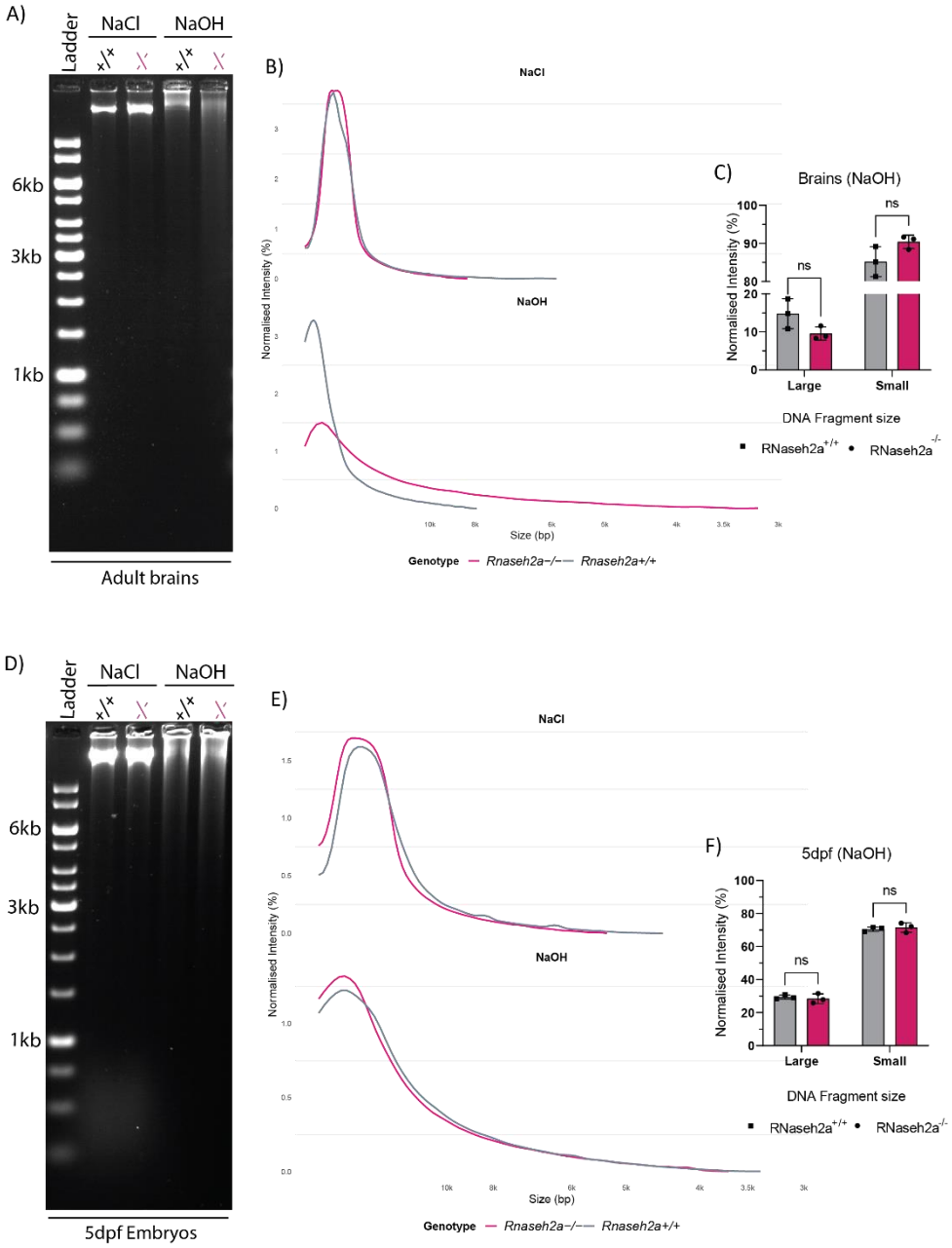

Figure 3.11: *rnaseh2a*$^{-/-}$ embryos have a mild increase in rNMP incorporation at adulthood but not at 5dpf

A) Representative agarose gel of DNA extracted from adult (19 month) *rnaseh2a*$^{-/-}$ and *rnaseh2a*$^{+/+}$ brains **B)** Quantification of intensity from 3.11A and graphing of mean Normalised Intensity calculated from three biological replicates using R Studio (1 brain per replicate). **C)** Total normalised intensity of large and small DNA fragments as described in 3.10D. n=3, individual adults, Unpaired t-test, ±SD, p>0.05 **D)** Representative agarose gel of DNA extracted from 5dpf embryos from *rnaseh2a*$^{+/-}$ parents. Genotype determined using 3dpf fin clipping. **E)** Quantification of intensity from 3.11D. n=3, 20 pooled embryos, Unpaired t-test, ±SD, p>0.05.

3.2.5 MZ*rnaseh2a* embryos have an increase in DNA damage

My previous experiments show that *MZrnaseh2a* embryos from have a significantly larger number of ribonucleotides incorporated into their DNA than wild-type embryos, or zygotically mutant (*MZrnaseh2a)* larvae. Due to the susceptibility of these nucleic acids for spontaneous hydrolysis, it is predicted that these hydrolysis events cause single stand DNA breaks. If these are in close proximity to each other, these breaks can result in the more toxic, double stranded DNA break. These breaks are recognized by the cell via several pathways including the activation of ATM via autophosphorylation (Burma *et al.*, 2001). This in turn phosphorylates the histone.2AX (H2AX) to yH2AX.

Immunofluorescence (IF) staining of yH2AX is a well-documented method of identifying dsDNA breaks (Rahmanian, Shokrzadeh and Eskandani, 2021). Staining was performed as in **Section 2.4.1** and the tails of the embryos were mounted and imaged. These results show that there is a significant increase in the number of yH2AX foci within the nuclei of embryos from an *rnaseh2a*$^{-/-}$ incross compared with those from the wild-type incross **(Figure 3.12A,B)**. This confirms that there is a large quantity of DNA damage occurring in the *MZrnaseh2a* embryos. In comparison, yH2AX staining and subsequent genotyping of embryos from a heterozygous incross show no difference in the yH2AX staining between homozygotes and their wild-type or heterozygote counter parts **(Figure 3.13A,B).**

3.2.6 *rnaseh2a*$^{-/-}$ adult zebrafish do not show any increase in DNA damage

Given the mild increase in rNMP incorporation seen in brain tissue from 15 month old adults, it was predicted that this may lead to an increase in dsDNA breaks. However, isolation, protein extraction and subsequent western blotting of adult zebrafish brains for yH2AX revealed that there is also no significant difference between *rnaseh2a*$^{-/-}$ and *rnaseh2a*$^{+/+}$ adult siblings suggesting that, despite the large numbers of rNMPs, these do not result in a significant increase of dsDNA breaks **(Figure 3.14A,B).** This may be due to the non-proliferative nature of adult brain cells such that there may be large number of ssDNA breaks that are not converted into dsDNA breaks due to not colliding with a replication fork. I conclude that despite the increase in rNMPs, these do not subsequently cause a high level of fragmentation of the DNA, in the brains of *rnaseh2a*$^{-/-}$ from heterozygous parents. A more accurate method may be to perform IF as seen in *MZrnaseh2a* embryos (**Figure3.12)**, allowing for higher sensitivity and specificity of dsDNA break identification.

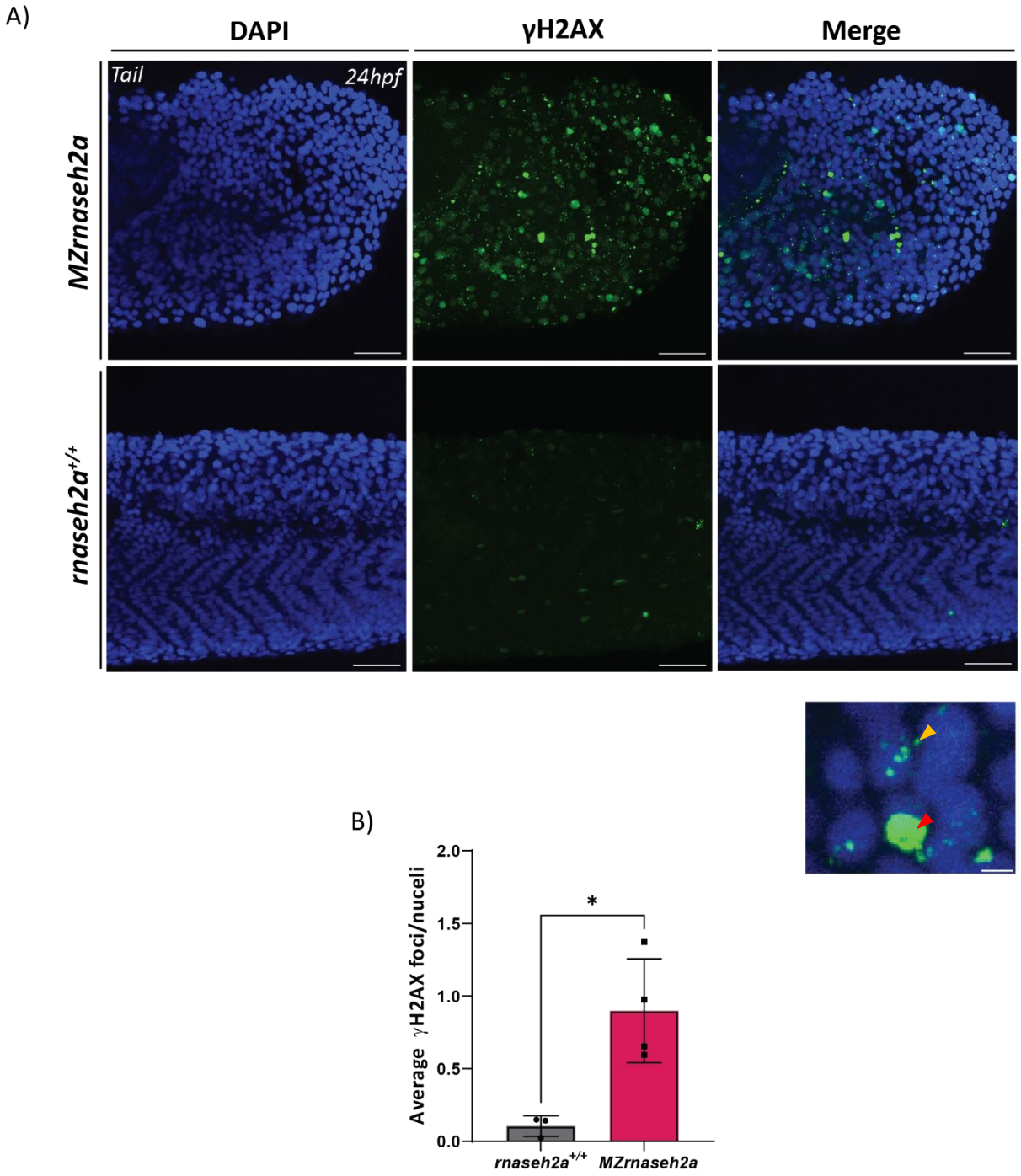

Figure 3.12: *MZrnaseh2a* embryos show more dsDNA breaks than *rnaseh2a*$^{+/+}$ embryos

A) γH2AX staining (Green) in tails of 24hpf *MZrnaseh2a* embryos. Nuclei stained with DAPI (Blue). Scale bar, 50µm. **B)** Quantification of γH2AX foci present within nuclei (Yellow arrow) whilst excluding apoptotic cells (Red). Scale bar, 5µm. Unpaired t-test, *p<0.01, ±SD. n=5, individual embryos.

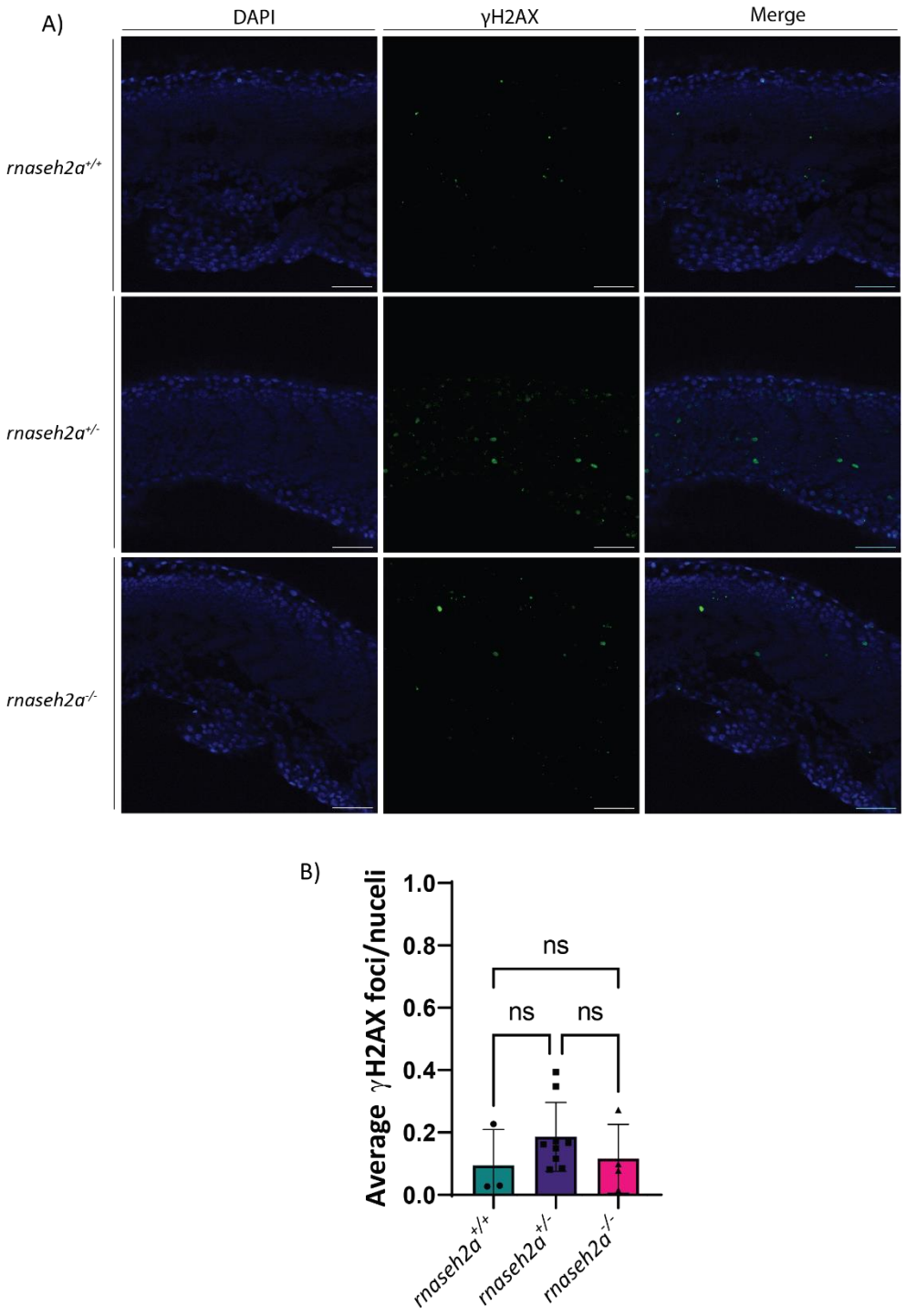

Figure 3.13: Larvae from *rnaseh2a*$^{+/-}$ parents show no significant difference in dsDNA breaks, regardless of genotype

A) γH2AX (Green) staining of 3dpf tails in embryos from *rnaseh2a*$^{+/-}$ parents. DAPI staining (Blue). Imaging was performed on an Olympus Confocal microscope as described in Section 2.9.1. Scale bar, 50um.**B)** Quantification of γH2AX foci per nuclei revealed no significant difference between genotypes. n= 3-8, individual embryos, One-Way ANOVA, ns p>0.05, ±SD.

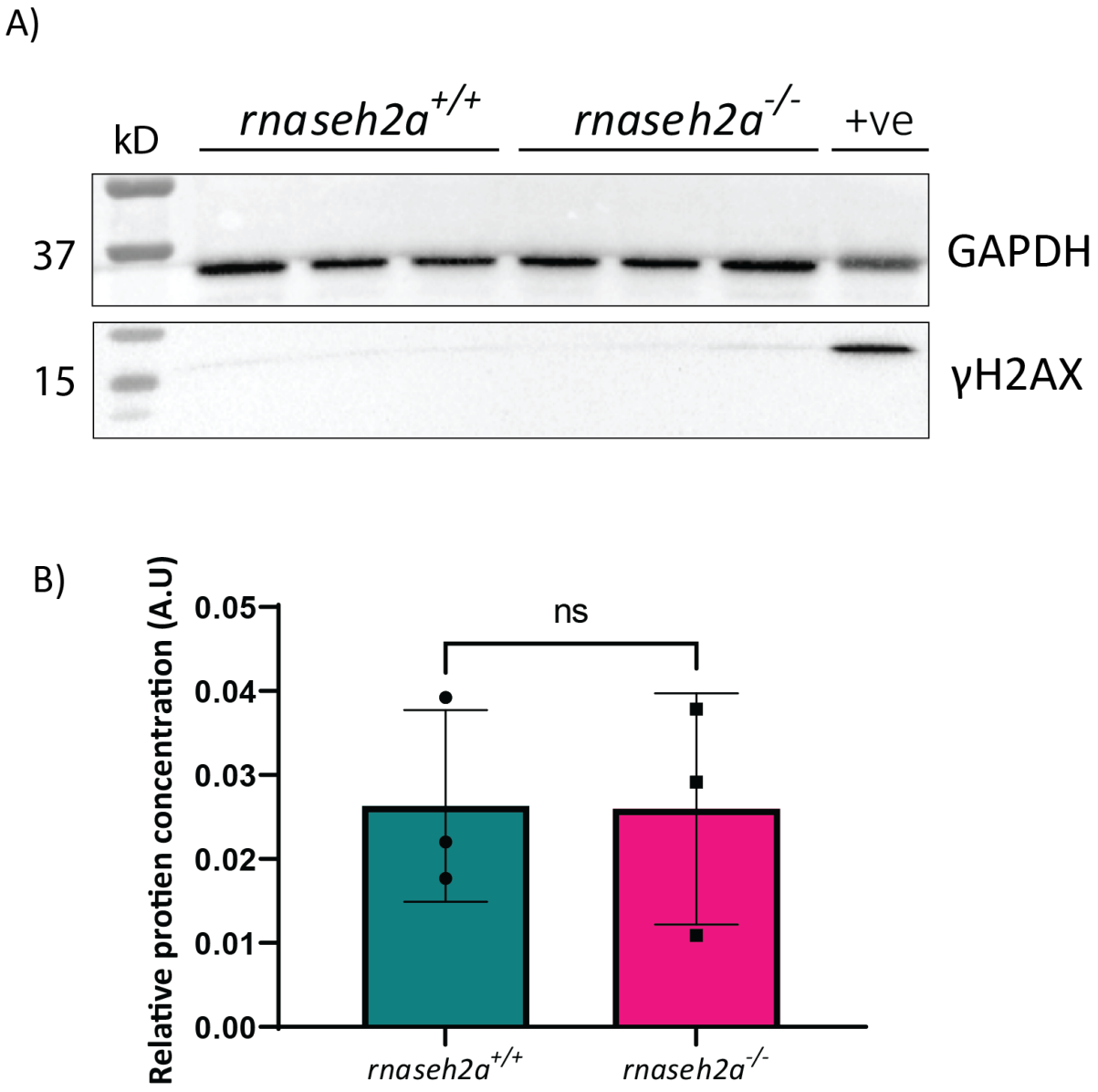

Figure 3.14: Western blot showing no significant increase in yH2AX between *rnaseh2a*$^{-/-}$ and *rnaseh2a*$^{+/+}$ adult zebrafish brains

A) Western blot showing yH2AX in individual adult zebrafish brains. GAPDH used as a loading control. Positive control of a significantly aged, wild-type zebrafish brain. **B)** Quantification of relative yH2AX expression against GAPDH shows no significant difference between *rnaseh2a*$^{-/-}$ and *rnaseh2a*$^{+/+}$ adult brains. Unpaired t-test, ns $p>0.05$, ±SD n=3, individual adult brains.

3.2.6 MZ*rnaseh2a* embryos have increased apoptosis

Given the large quantities of dsDNA breaks and bright field images of the *MZrnaseh2a* embryos depicting a large number of grey cells, it was hypothesised is that there is a large number of apoptotic cells. To confirm this, we used Acridine Orange (AO). It was previously reported that the emission wavelength depends on the pH of the solution. Between pH 5.7 and 8.0 apoptotic cells appear green, whereas dead, or necrotic, cells appear red. This allows AO to be able to distinguish between the two via fluorescent microscopy (Abel *et al.*, 1919; Abrams *et al.*, 1993; Wainwright, 2001; Tucker and Lardelli, 2007)**.** Importantly, AO is not able to intercalate to the DNA of living cells (Delic *et al.*, 1991).

When *MZrnaseh2a* embryos were incubated with AO, the number of dying cells was significantly increased compared with their wild-type counterparts **(Figure 3.15A,B)**. This supports the idea that the grey cells observed during bright field imaging were apoptotic and that embryos with homozygous parents are subjected to regulated cell death. This 100% increase of cell death will be one of the key elements in the early lethality of *MZrnaseh2a* embryos compared with their wild-type counterparts.

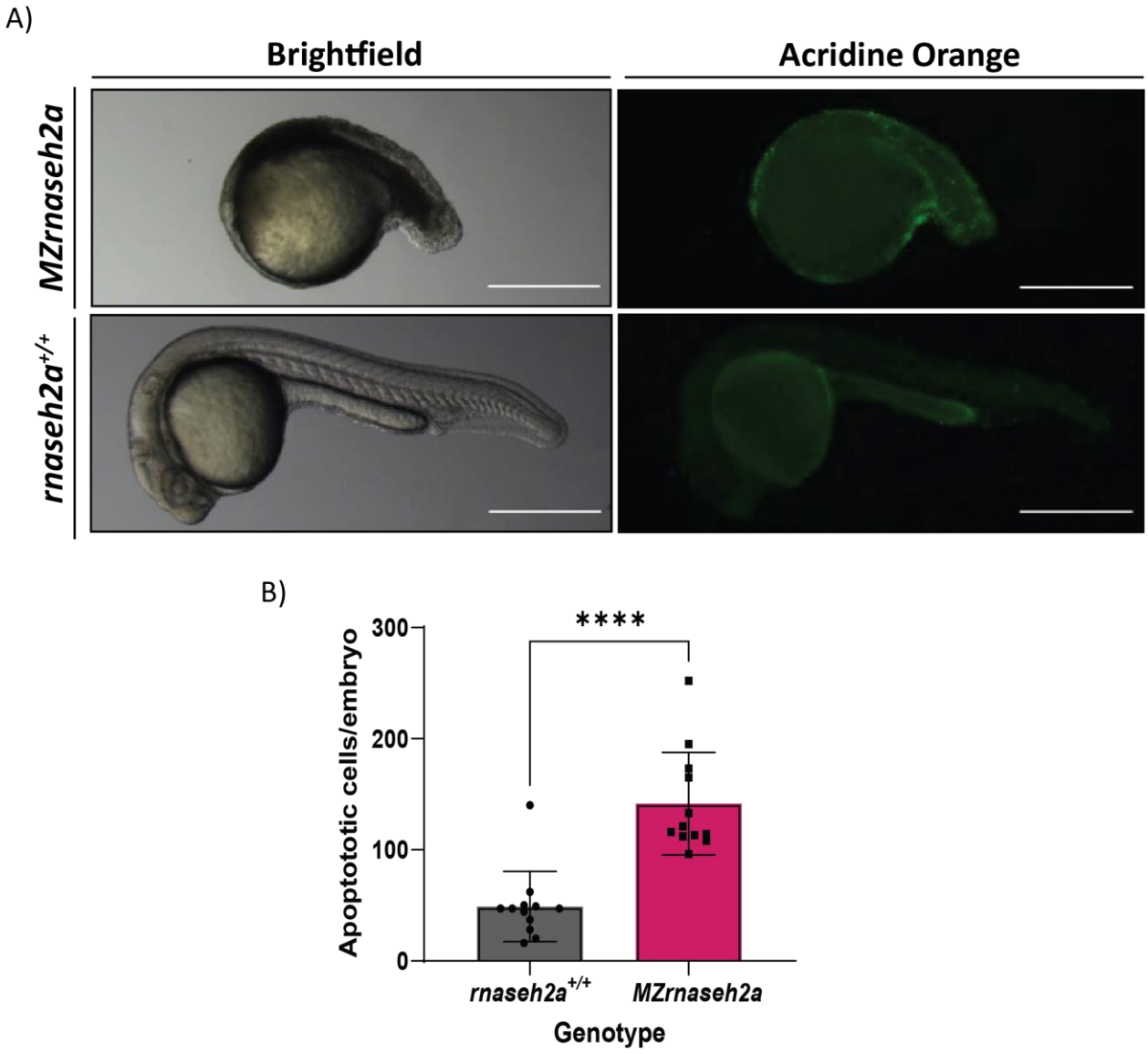

Figure 3.15: *MZrnaseh2a* embryos show more cell death after staining with Acridine Orange

A) Acridine Orange staining of dying cells (green) in 24hpf *MZrnaseh2a* and *rnaseh2a*$^{+/+}$ embryos **B)** Quantification of Acridine Orange positive cells shows a significant increase in the number of dying cells within *MZrnaseh2a* embryos compared with *rnaseh2a*$^{+/+}$ embryos. Unpaired t-test, ****p<0.0001, ±SD, n=12, individual embryos.

3.2.7 All offspring from *rnaseh2a*$^{-/-}$ are embryonic lethal

An initial hypothesis was that perhaps the loss of the maternal supply of RNaseH2a protein was preventing the survival of the *MZrnaseh2a* embryos. I therefore tested the crossing of *rnaseh2a*$^{-/-}$ male with an *rnaseh2a*$^{+/+}$ female to create a "paternal RNaseH2a mutant" (*Prnaseh2a*), predicting that this may result in improved embryo development as *Prnaseh2a* embryos would contain an active version of RNaseH2a, allowing for the efficient removal of rNMPs. Initially, the embryos appeared to be fertilized correctly and developed normally until at least 11hpf. However, from here, apoptotic cells become visible and the development of the embryos becomes very slow. Surprisingly, such embryos never develop to the extent that the embryos do from an *rnaseh2a*$^{-/-}$ incross (*MZrnaseh2a)* and show complete embryonic lethality by 24hpf **(Figure 3.16A)**. Following this surprising discovery, we also crossed an *rnaseh2a*$^{-/-}$ female and an *rnaseh2a* $^{+/+}$ male to produce a "maternal RNaseH2a mutant" (*Mrnaseh2a*) which resulted in embryos that are similar to those from an *rnaseh2a*$^{-/-}$ incross, with some looking slightly more developed but none that resemble a *wild-type* incross. All embryos from such crosses also show eventual lethality (**Figure 3.16B**). This result is inconsistent with scenario 1 as proposed in 3.2.2. This suggests that the phenotype in *MZrnaseh2a* embryos is not due to a missing maternal contribution of RNaseH2a. However, the observations could be explained via the fact that RNaseH2a is involved in the removal of single ribonucleotides in the DNA of the healthy *rnaseh2a*$^{-/-}$ adults, especially in the DNA in the gametes that subsequently contain a large number of ribonucleotides. In an *rnaseh2a*$^{-/-}$ incross the embryos are unable to remove these as neither the male not female could provide an active RNaseH2a.

When a male *rnaseh2a*$^{-/-}$, with large numbers of ribonucleotides incorporated into the sperm, is crossed with a *wild-type* female, with active RNaseH2a, the rNMPs are recognized and cleaved by the RNaseH2a present in the egg. This results in a large number of ssDNA breaks which, if in close proximity, can create extremely toxic dsDNA breaks. The repair pathway downstream of the cleavage event may not be able to cope with the number of breaks occurring or the DNA is fragmented into so many small pieces, the p53 response is activated and initiates the apoptotic pathway. However, if we cross a female *rnaseh2a*$^{-/-}$ with a wild-type male, the resulting embryos are slightly more developed than those resulting from an *rnaseh2a*$^{-/-}$ male and wild-type female but still not a healthy as a wild-type

embryo **(Figure 3.16C)**. This could be due to the fact that the DNA in the female gamete contains large numbers of incorporated ribonucleotides but the active RNaseH2a, which is provided via the DNA in the sperm of the male, is not yet active. This is due to the transcriptional delay in the zygotic embryo. For the first few hours of its development, it relies on the proteins provided by the mother. Therefore, by the time the active RNaseH2a coded for by the DNA in the male sperm has be transcribed and translated by the embryo, it has been able to develop slightly before the RNaseH2 begins cleaving the large numbers of rNMPs present in the newly formed embryo and the DNA provided by the female adult. This then triggers the same apoptotic arrest pathway as embryos from an *rnaseh2a*$^{-/-}$ male and wild-type female.

3.2.8 Rescue of *MZrnaseh2a*embryos with *wild-type* and non-functional *rnaseh2a*

If a lack of maternal RNaseH2 is the cause for the phenotypes of *MZrnaseh2a* embryos, reintroduction of that gene should lead to a partial rescue of the phenotype. However, given the previously established phenotypes (*Mrnaseh2a*, *Prnaseh2a*), an alternative prediction could be that the re-introduction of RNaseH2a would have a detrimental, rather than positive effect on the phenotype as it may attack the ribonucleotides in the DNA of the zygote.

To test this, I used the microinjection of mRNA coding for functional RNaseH2a into *MZrnaseh2a* embryos. This is predicted to result in embryos that are more developmentally delayed and die by 24hpf. mRNA for non-functional RNaseH2a was injected as a control. To create this non-functional version, analysis of the structure of RNaseH2a revealed a DNA binding domain which, if disrupted, should result in a non-functional protein. A two base pair deletion was created, causing a frameshift and truncated protein.

Injection of wild-type RNaseH2a mRNA into *rnaseh2a*$^{-/-}$ embryos resulted in significantly reduced development compared with wild-type embryos that showed no significant change in phenotype **(Figure 3.17A,B)**. Activity of the RNaseH2 after injection was measured using the activity assay described earlier **(Figure 3.17C)**. This supports the alternative hypothesis that introduction of a functional RNaseH2a into a homozygous mutant, rather than rescuing the knockout, attacks ribonucleotide laden DNA and contributes to an increase in apoptosis and subsequently reduced survival. Although the increase in cleavage after injection is mild,

due to the fragility of the *MZrnaseh2a* embryos, it is predicted that any increase in cleavage, even slight, is subsequently toxic.

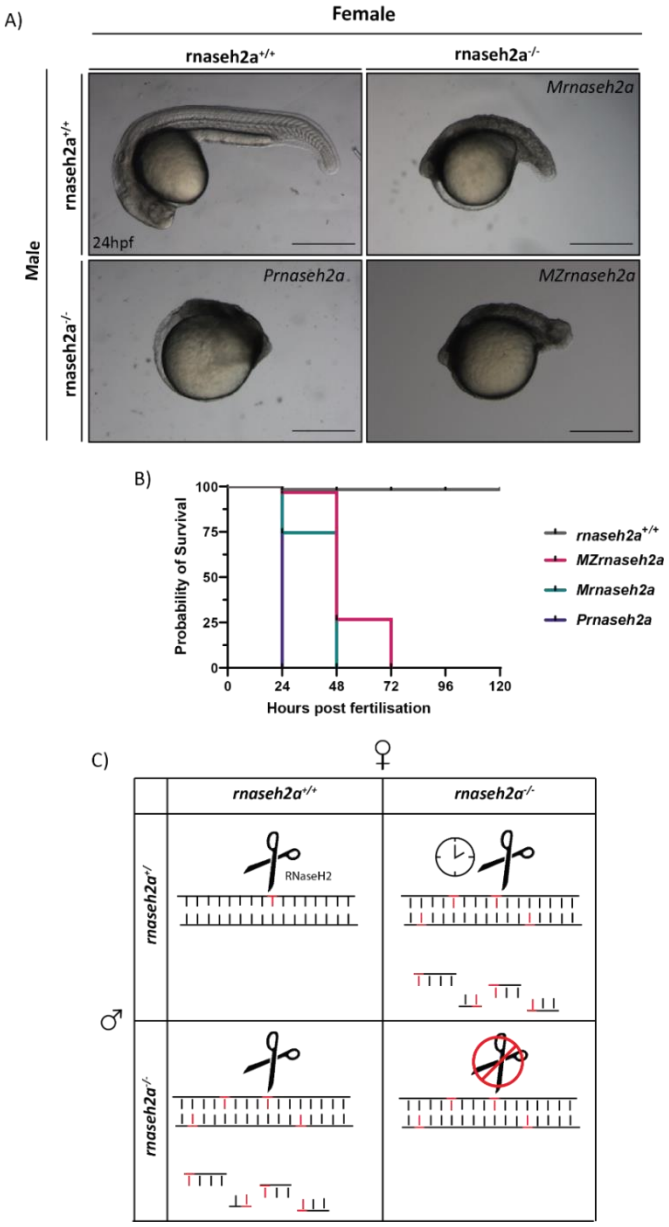

Figure 3.16: Embryos resulting from *rnaseh2a*$^{-/-}$ parents undergo early embryonic lethality

A) 24hpf Embryos from various crosses involving *rnaseh2a*$^{+/+}$ and *rnaseh2a*$^{-/-}$ parents. Genotype of adults indicated on the outer edge. Embryos resulting from an *rnaseh2a*$^{+/+}$ female; *rnaseh2a*$^{-/-}$ male (*Prnaseh2a), rnaseh2a*$^{-/-}$ female; *rnaseh2a*$^{+/+}$ male (*Mrnaseh2a*), and *rnaseh2a*$^{-/-}$ female; *rnaseh2a*$^{-/-}$ male (*MZrnaseh2a)* all show a lack of development by 24hpf. Scale bar = 0.5mm **B)** Survival curves of the resulting embryos show *Prnaseh2a* undergo lethality at 24hpf followed by *Mrnaseh2a* at 48hpf and *MZrnaseh2a* at 72hpf. n=120. **C)** Hypothesis of phenotypic severity shown by *Prnaseh2a*, *Mrnaseh2a* and *MZrnaseh2a* embryos.

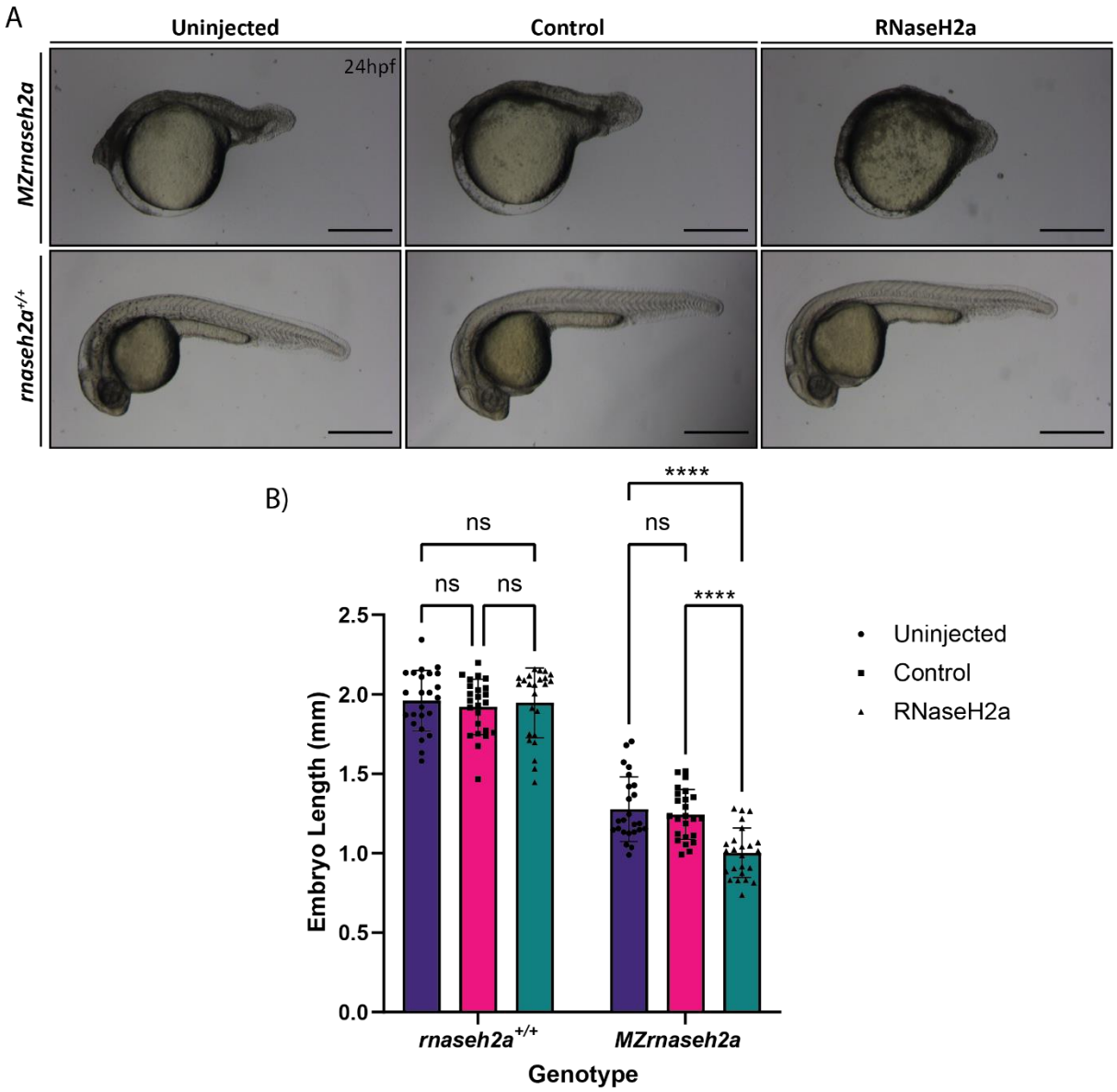

Figure 3.17: Re-introduction of RNaseH2a is unable to rescue the developmental phenotype

A) Microinjection of RNaseH2a mRNA caused a reduction in the development of *MZrnaseh2a* embryos compared with the control (non-functional RNaseh2a) or uninjected embryos. *rnaseh2a*$^{+/+}$ embryos were unaffected. **B)** Quantification of embryo size indicates a significant decrease in development in *MZrnash2a* embryos resupplied with RNaseH2a. Two-Way ANOVA, ****p<0.0001, ±SD, n=30, individual embryos.

3.2.9 *MZrnaseh2a* embryos have increased expression of p53

We have identified a large quantity of DNA damage and apoptotic cells. To determine the method by which the apoptosis of these cells is activated, we decided to look at one of the main regulators of apoptosis, the oncogene p53. p53 can be activated by DNA damage and is known to be involved in the activation of downstream genes that induce apoptosis of cells. Its overexpression has also been linked to various degenerative diseases such as arthritis, multiple sclerosis and also neuropathies (Mattson *et al.*, 2001; Wosik *et al.*, 2003)**.** The Δ113p53 isoform in particular has been shown to be significantly upregulated following DNA damage and has a role in the prevention of apoptosis and promote repair pathways (Gong *et al.*, 2015). This isoform has an n-terminal truncation that removes the MDM2-interacting motif, transactivation domain and partial deletion of the DNA-binding domain.

I therefore hypothesised that apoptosis in the *MZrnaseh2a* embryos would be accompanied by a large increase in Δ113p53 expression which would in turn, activate the apoptotic response. RT-qPCR was used to quantify gene expression, the primers used can be found in Chapter 2. A 100 fold increase was observed in p53 expression in *MZrnaseh2a* embryos. This is consistent with the severity of phenotype observed **(Figure 3.18B)**.

To confirm that activation of the p53 response is at least partially responsible for the phenotype of the embryos, I injected a well-established p53 morpholino into 1-cell stage embryos and imaged them at 24hpf (Robu *et al.*, 2007). This will lead to the downregulation of p53 function for the first few days of development.

After injection of the p53 MO at 0dpf, the embryos were imaged at 24hpf and visually appeared more developed that their uninjected siblings **(Figure 3.18A)**. This supports our hypothesis that p53 expression is at least partially responsible for the apoptosis observed. However, rescue was far from complete as the *MZrnash2a* embryos still showed a strong reduction in their body axis. Thus defects are not solely the result of p53 activation.

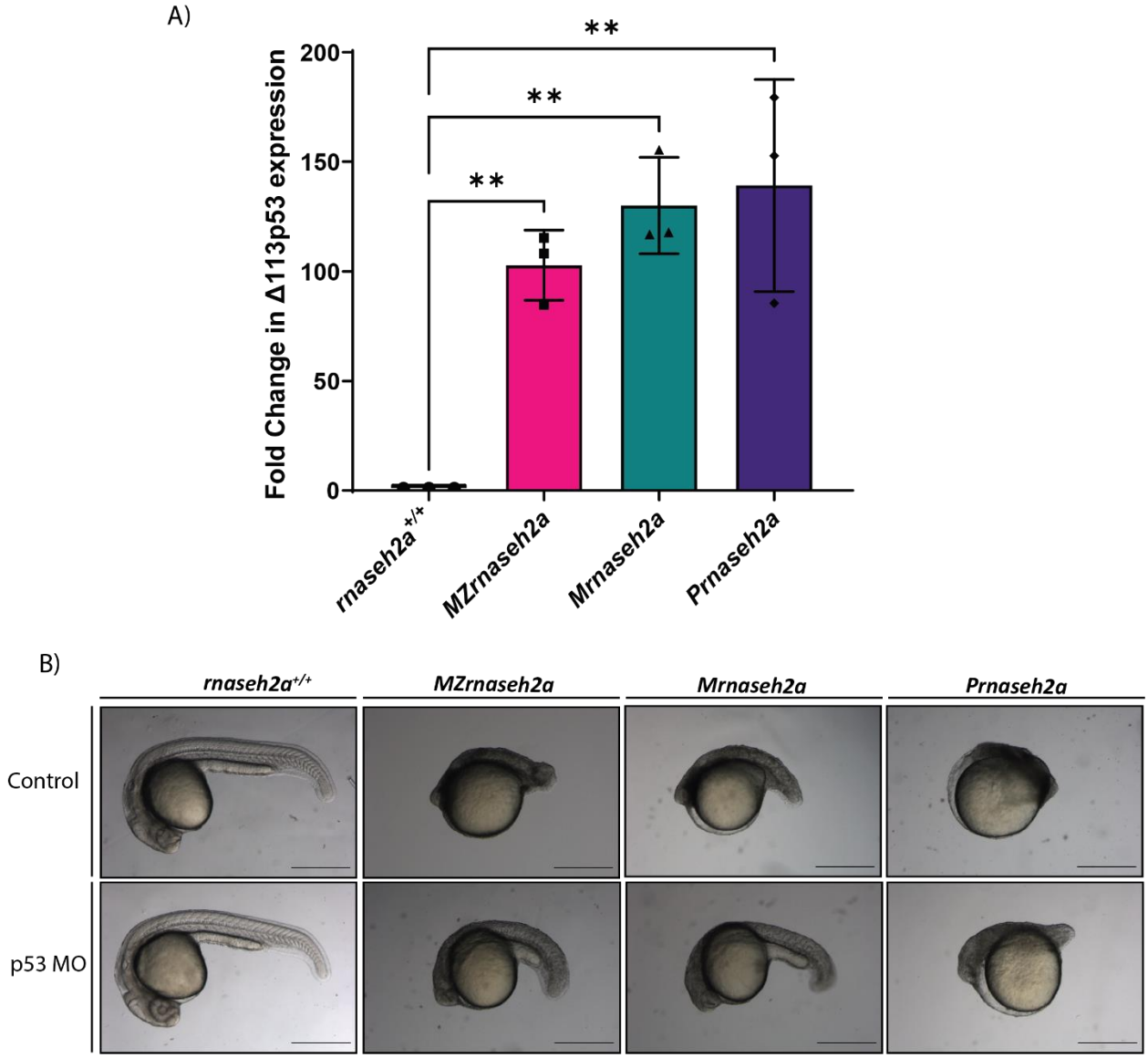

Figure 3.18: Knockdown of p53 significantly increases the development of embryos with *rnaseh2a*$^{-/-}$ parents.

A) Δ113p53 expression is significantly upregulated in all embryos with at least one *rnaseh2a*$^{-/-}$ parent compared with *rnaseh2a*$^{+/+}$ embryos n=3, 20 pooled embryos. p value calculated via a One-Way ANOVA **p<0.001, ±SD **B)** Microinjection of a p53 morpholino visibly improves the development of all embryos at 24hpf with one (*Prnaseh2a, Mrnaseh2a)* or two (*MZrnaseh2a*) *rnaseh2a*$^{-/-}$ parents.

3.2.10 *MZrnaseh2a* embryos have an increase in inflammatory genes

In the case of RNaseH2, its main role is to remove the ribonucleotides incorporated into DNA on a daily basis. If this is no longer possible, the rNMPs can spontaneously hydrolyse causing double strand breaks and the formation of DNA fragments. These fragments are then recognized by the cGas/STING pathway which in turn upregulate interferon stimulated genes.

As they aged, with a lack of RNaseH2a activity, it was expected that they would suffer from a large quantity of rNMP incorporation, DNA damage and subsequent activation of the cGas/STING pathway resulting in the upregulation of various interferon stimulated genes.

Using RT-qPCR I identified a significant upregulation in key interferon stimulated genes in *rnaseh2a*$^{-/-}$ embryos from homozygous parents (*MZrnaseh2a*) **(Figure 3.19)**. Interferon Stimulated Gene 15 (ISG15) showed significant upregulation compared with their wild-type counterparts, consistent with AGS patients.

ISG15 is small, ubiquitin-like protein that has been identified to have a key role in the antiviral response of the host cell and activates genes downstream such as p53 and p21 (Park *et al.*, 2016). We also identified upregulation in other interferon stimulated genes such as mxa, a GTP-binding protein and INFphi, a type 1 interferon. Both genes are thought to be involved in the anti-viral defence of the cell. Several inflammatory response genes including IL-1b, IL-6 and TNFα were also shown to have a slight upregulation in expression in *rnaseh2a*$^{-/-}$ embryos. We also identified a large upregulation in p21 however this is unsurprising due to studies suggesting that is activated downstream of ISG15.

However, *rnaseh2a*$^{-/-}$ homozygote embryos from a heterozygous incross did not show such a dramatic upregulation in interferon stimulated genes. RT-qPCR analysis revealed no significant upregulation in the regulation of genes in whole embryos at 5dpf **(Figure 3.20A)**. Analysis was also performed on various organs from adult zebrafish. Gut tissue showed a minor upregulation in a handful of genes but no upregulation was seen in the brains of homozygous adults compared with their wild-type siblings at 19 months **(Figure 3.20B)**. The data suggests that, despite the observed increase in ribonucleotide incorporation over time, this does not correlate with an upregulation of ISG expression.

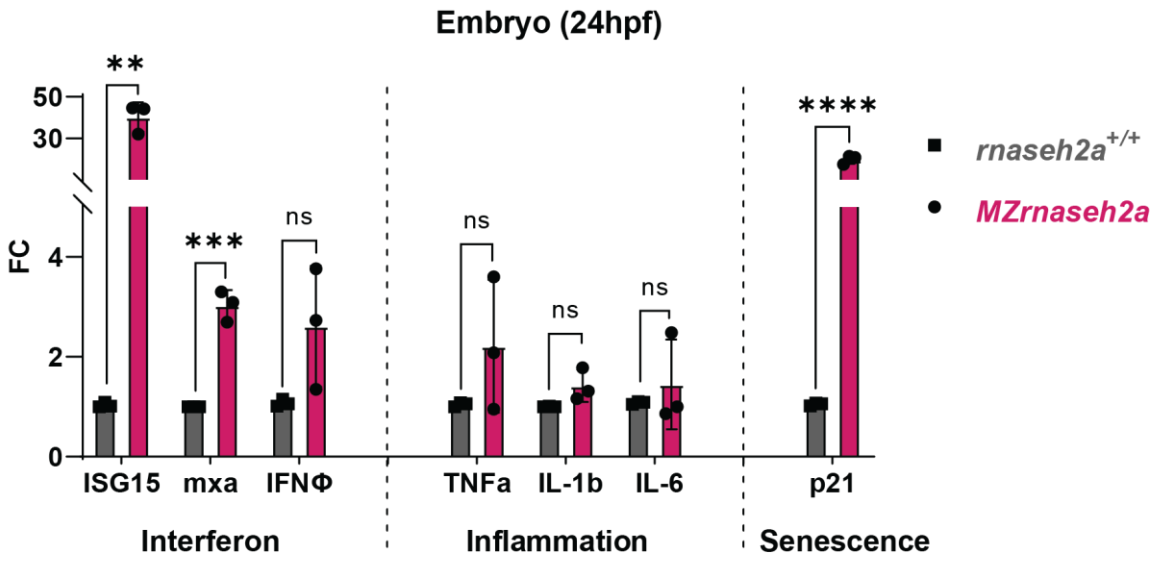

Figure 3.19: *MZrnaseh2a* embryos have a large upregulation in inflammatory response genes

A) RTqPCR analysis of interferon stimulated genes (ISG15, mxa and IFNΦ), inflammatory response genes (TNFα, IL-1b and IL-6) and senescence markers (p21) in 24hpf *MZrnaseh2a* embryos compared with wild-types. Multiple unpaired t-tests with Welch correction, ns $p>0.05$, *$p<0.05$, **$p<0.01$. ***$p<0.001$, ****$p<0.0001$ n=3, 20 pooled embryos, ±SD.

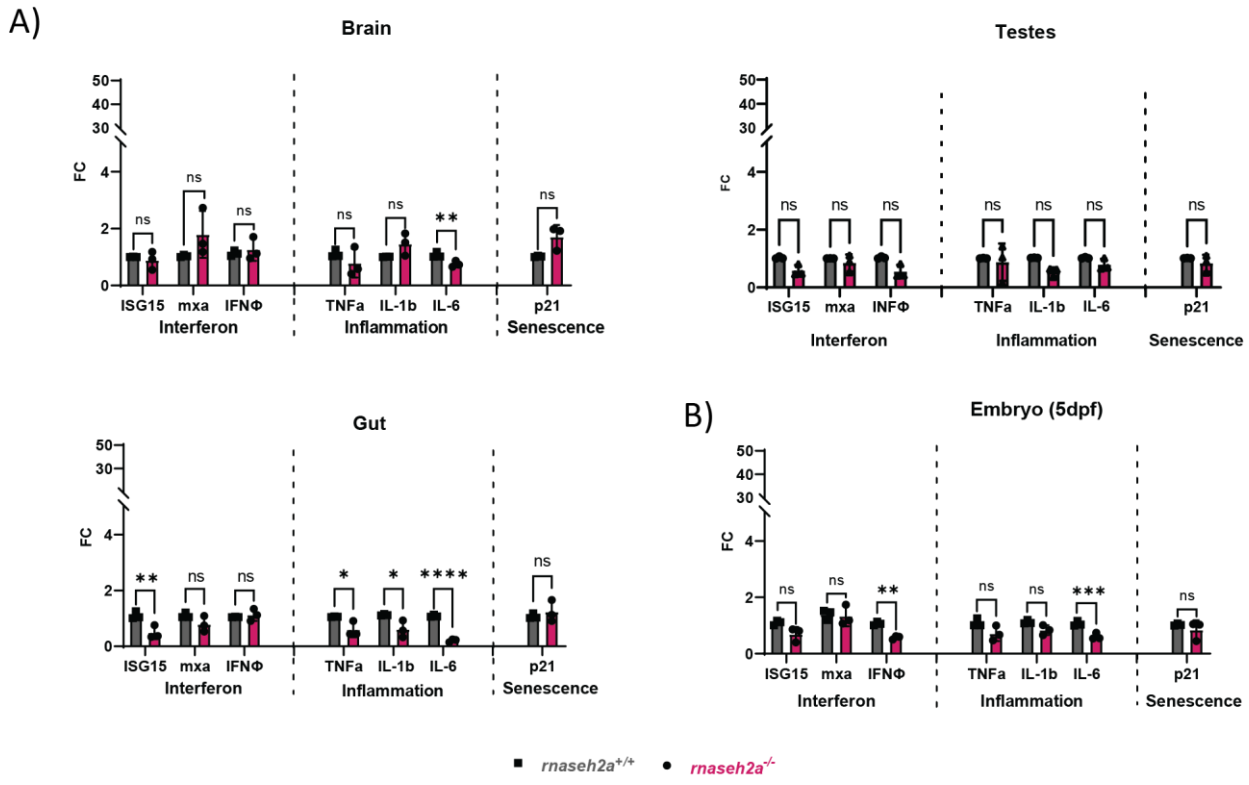

Figure 3.20: No upregulation of inflammatory response genes in adults or embryos from heterozygous parents

A) Expression of interferon stimulated genes (ISG15, mxa and IFNΦ), inflammatory response genes (TNFα, IL-1b and IL-6) and senescence markers (p21) were measured in tissues isolated from *rnaseh2a*$^{+/+}$ and *rnaseh2a*$^{-/-}$ 19 month adults. B) RTqPCR on 5dpf *rnaseh2a*$^{+/+}$ and *rnaseh2a*$^{-/-}$ embryos from a heterozygous incross. Multiple unpaired t-tests with Welch correction, ns p>0.05, *p<0.05, **p<0.01. ***p<0.001, ****p<0.0001 n=3, individual adult tissues or 20 pooled embryos (Embryo, 5dpf), ±SD.

3.2.11 *rnaseh2a*$^{-/-}$ adults have increased rNMPs in their testes compared with wild types

All the previous data suggest that embryos resulting from *rnaseh2a*$^{-/-}$ parents have severe embryonic defects due to the presence of ribonucleotides in the DNA of their parent's gametes. To test this hypothesis I analysed DNA from male *rnaseh2a*$^{-/-}$ adult testes. We predicted that the DNA isolated from these would be largely derived from germ cells or sperm. We found that the testes of *rnaseh2a*$^{-/-}$ adults from an *rnaseh2a*$^{+/-}$ incross contained more rNMPs than their *rnaseh2a*$^{+/+}$ siblings **(Figure 3.21A,B)**. This supports the hypothesis that the inheritance of rNMPs from the parents are a significant factor in the lethality of *MZrnaseh2a, Prnaseh2a* or *Mrnaseh2a* embryos.

3.2.12 Older adults produce offspring with higher phenotypic severity

As previously stated, offspring from maternal and paternal homozygote parents (*Mzrnaseh2a*) are embryonic lethal whereas first generation mutants are viable. If accumulation of rNMPs over time in this genome is driving the phenotype, the age of homozygous parents might influence the phenotype of the offspring. Indeed, I determined that, although still lethal, the embryos from younger parents are significantly more developed than those of the same genotype from older parents **(Figure 3.22A).** Furthermore, *Mzrnaseh2a* from older parents also had slightly higher expression levels of ISG15, suggesting a worse phenotype **(Figure 3.22B).** Although the difference in ISG15 expression between embryos from old and young parents was not significant, this may be because the baseline expression level of the inflammatory genes is already high, meaning a large increase in expression is not necessarily required for a significantly worse phenotype.

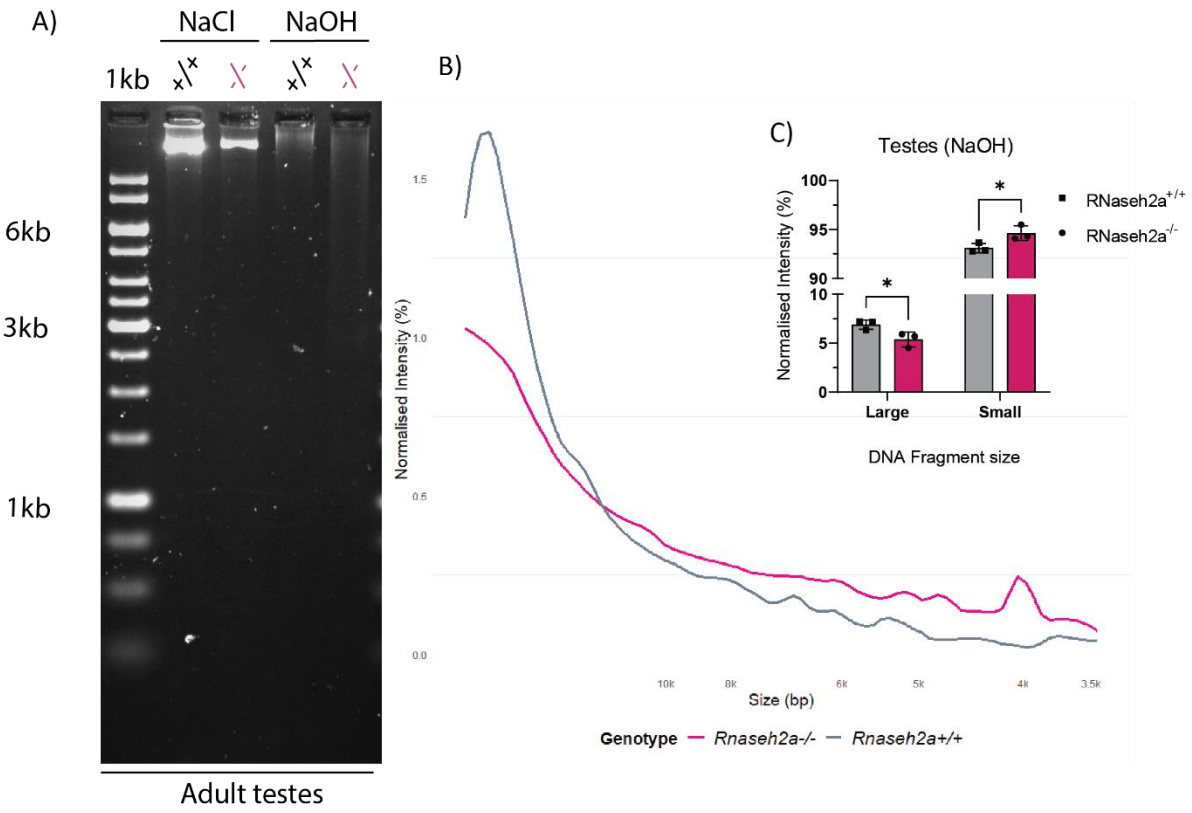

Figure 3.21: Testes of *rnaseh2a*$^{-/-}$ adults have increased rNMP incorporation compared with *rnaseh2a*$^{+/+}$

A) Representative agarose gel of DNA extracted from *rnaseh2a*$^{-/-}$ and *rnaseh2a* $^{+/+}$ testes **B)** Quantification of intensity from 3.21A and graphing of mean Normalised Intensity calculated from three biological replicates using R Studio (1 teste per replicate). **C)** Total normalised intensity of large and small DNA fragments as described in 3.10D. n=3, individual adults, Unpaired t-test, ±SD, p>0.05

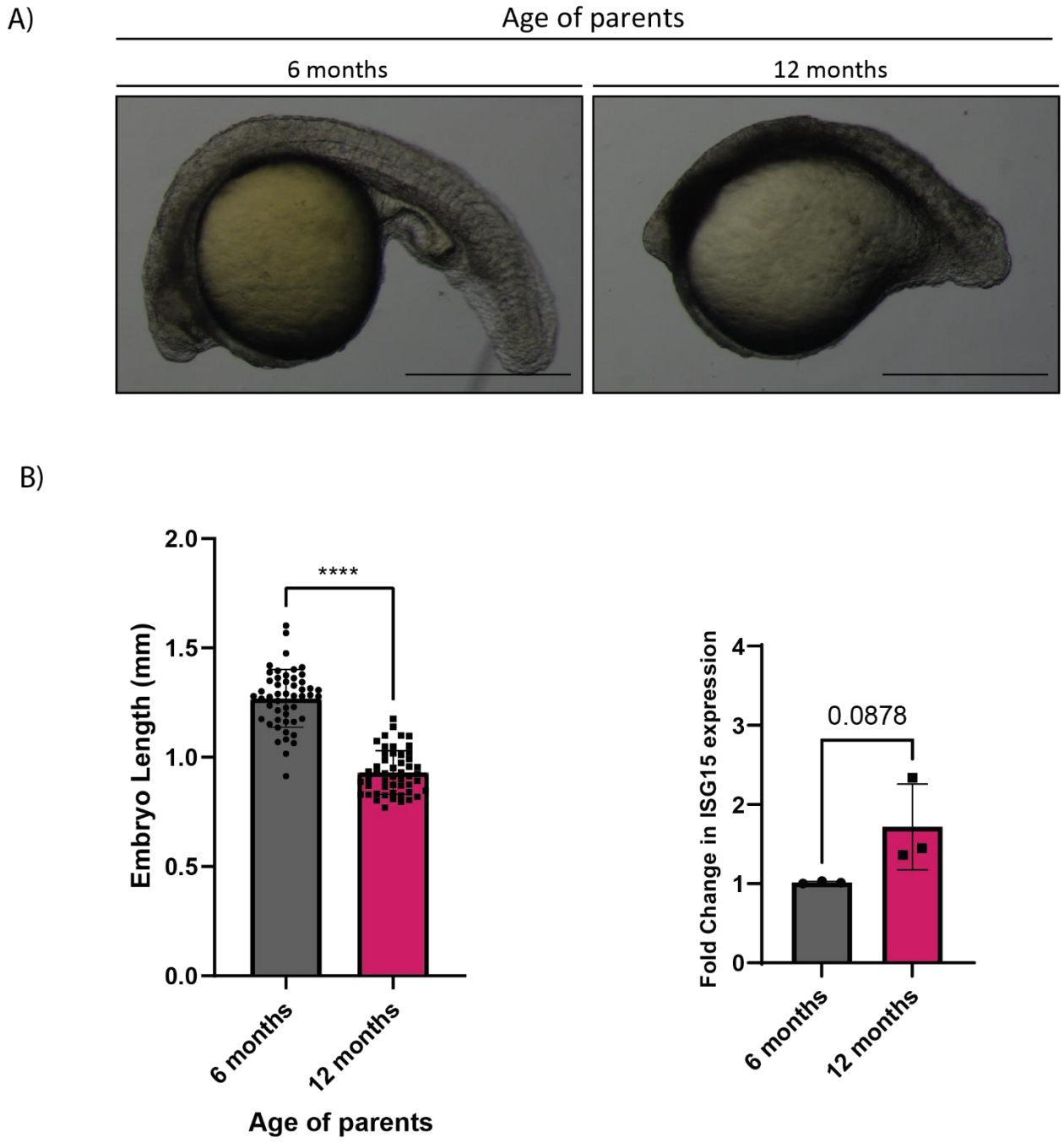

Figure 3.22: Embryos from older *rnaseh2a*$^{-/-}$ fish are significantly underdeveloped compared with embryos from younger fish

A) Representative images of *MZrnaseh2a* embryos from 6 month old and 12 month old parents. **B)** Quantification of embryo length from old and young zebrafish shows a decrease in embryo size from 12 month old parents. n=36, individual embryos**.** RTqPCR showing a mild increase in the expression level of ISG15 in embryos resulting from older *rnase2a*$^{-/-}$ adults. Scale Bar 0.5mm, n=3, 20 pooled embryos, Unpaired t-test, ****p<0.0001, ±SD.

3.2.13 Movement analysis in *rnaseh2a*$^{-/-}$ larvae and adults

Adult *rnaseh2a*$^{-/-}$ from a heterozygous incross are able to survive until 3 years with no outwardly apparent phenotype. This was surprising as data has shown a mild increase in the levels of ribonucleotides in their DNA. To see if more subtle phenotypes were present, their movement was analysed over three hours before their total distance travelled was compared with that of their wild-type siblings. It was seen that the *rnaseh2a*$^{-/-}$ adults travelled a significantly shorter distance than the wild-types **(Figure 3.23A)**. This movement defect was most prevalent when looking at the time they spent swimming at high speeds. This was a significantly shorter length of time than their wild-type siblings whereas there was no significant difference between their times spent inactive with a mild difference at normal speeds **(Figure 3.23B)**.

To determine whether a movement defect was present already at larval stages, we analysed the locomotion of 5dpf larvae from a heterozygous incross through light-dark cycles. This was done blindly as mutant cannot be identified by morphology. After analysis of movement, PCR analysis of the embryos was performed to identify their genotypes. It was identified that there was not a significant difference in the total distance moved by *rnaseh2a*$^{-/-}$ compared with *rnaseh2a*$^{+/+}$ at 5dpf **(Figure 3.24)**. This was the case at all movement speeds; inactive, normal and high speeds.

This continues to suggest that there is a secondary mechanism of removal that allows 5dpf embryos to survive with no accumulation of rNMPs in their genome and is only beginning to be overwhelmed in the adults, contributing to their movement phenotypes. Identification of the compensatory mechanism may aid the development of target identification for AGS patients suffering from locomotion symptoms.

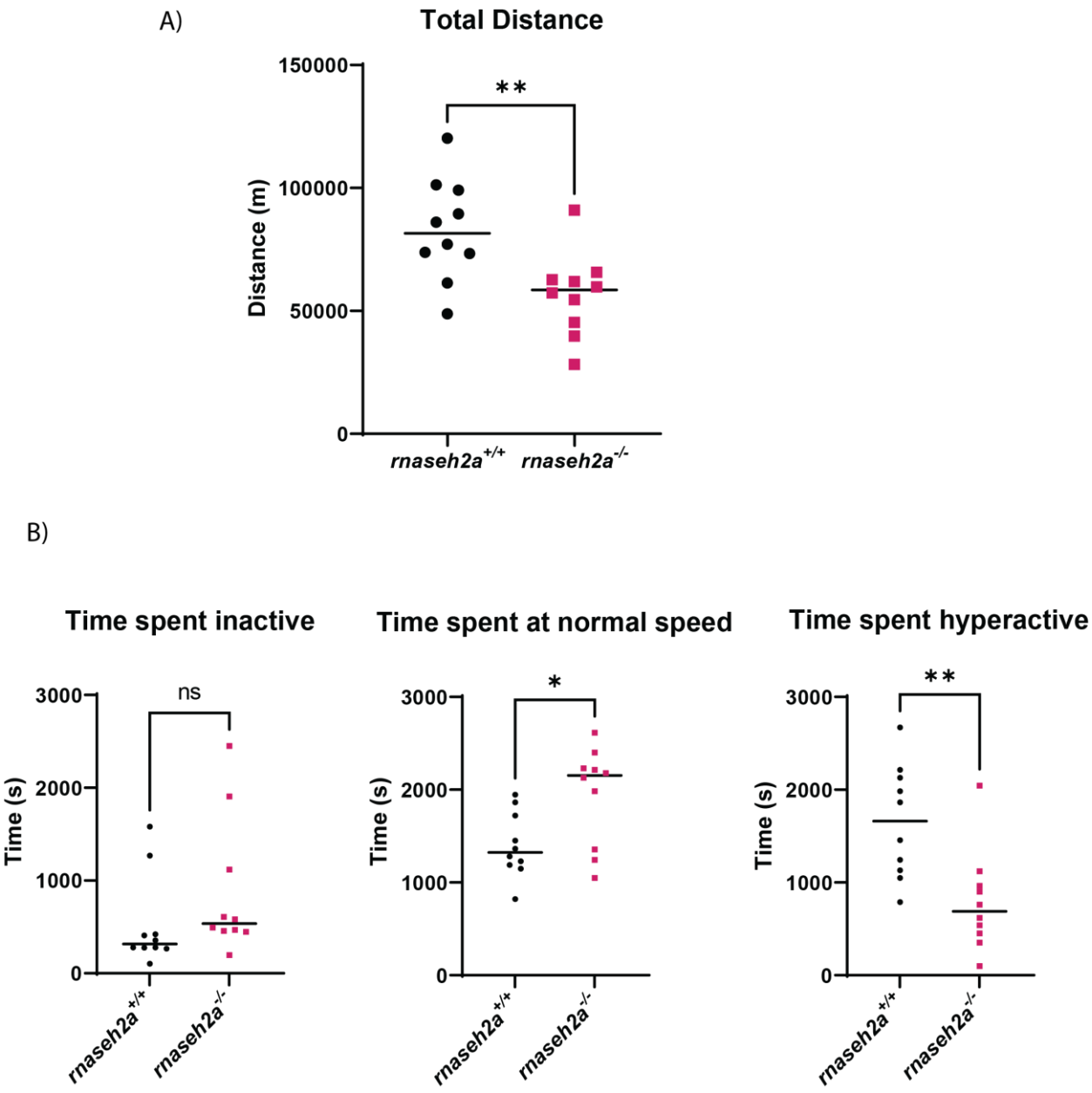

Figure 3.23: Movement analysis of adult *rnaseh2a*$^{-/-}$ show a significant reduction in movement compared with *rnaseh2a*$^{+/+}$ adults

A) Siblings from *rnaseh2a*$^{+/-}$ parents were filmed for three hours at 12 months old and the total distance moved by *rnaseh2a*$^{-/-}$ adults was significantly reduced when measured. **B)** Time periods spent inactive (<5cm/sec), normal (5-7cm/sec) and hyperactive >7cm/sec). n=10, individual adults, Unpaired t-test, ns p>0.05, *p<0.01, **p<0.01, ±SD.

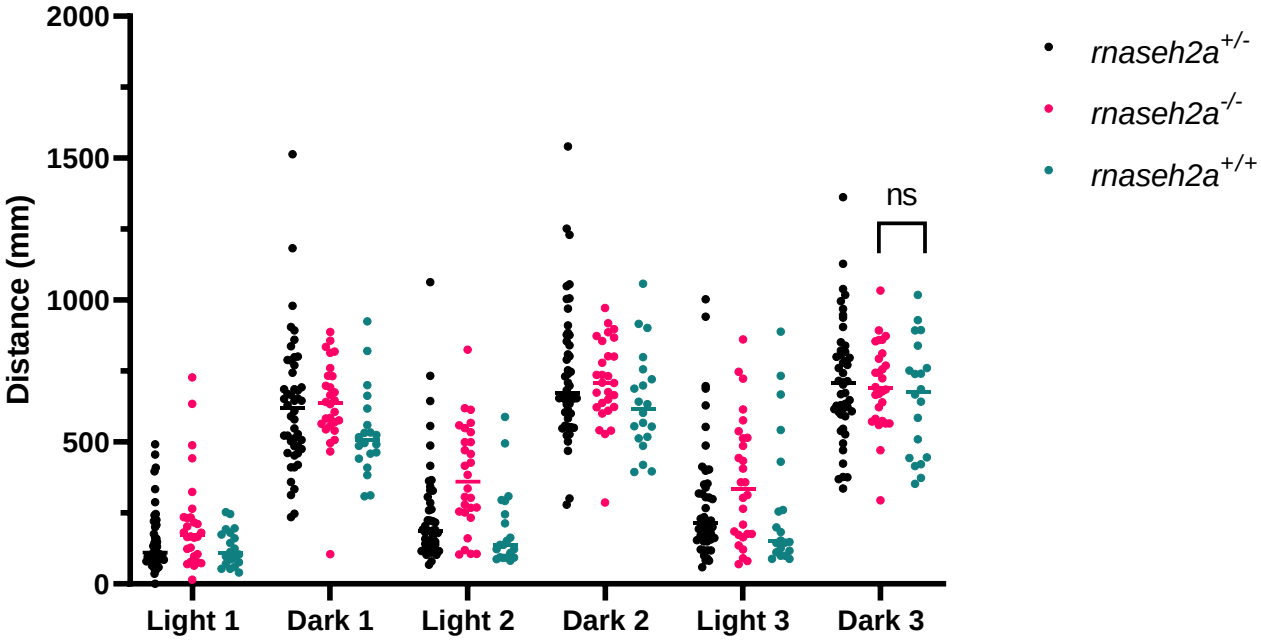

Figure 3.24: *rnaseh2a*$^{-/-}$ embryos show no movement phenotypes compared with *rnaseh2a*$^{+/+}$ at 5dpf

A) Photometric response measured in 5dpf embryos from a heterozygote cross show no significant difference between *rnaseh2a*$^{-/-}$ and *rnaseh2a*$^{+/+}$ embryos after genotyping. n=48, individual embryos, One-Way ANOVA, ns p>0.05, ±SD.

3.3 Discussion

Throughout this chapter I have described the creation and characterization of a novel ribonucleotide incision repair model. The first generation of *rnaseh2a*$^{-/-}$ zebrafish are viable to adulthood **(Figure 3.4)**, in contrast to previous animal models that have a lack of any of the three RNaseH2 subunits (Reijns *et al.*, 2012; Pokatayev *et al.*, 2016; Uehara *et al.*, 2018).

3.3.1 *MZrnaseh2a* show embryonic lethality and activation of ISGs

Surprisingly, any of the resulting offspring from female and male homozygous mutants (*MZrnaseh2a*) are embryonic lethal **(Figure 3.6)**. These results are consistent with the idea that *MZrnaseh2a* embryos are defective in removing single rNMPs incorporated into their DNA **(Figure 3.7)**, resulting in large quantities rNMPs **(Figure 3.10)**, subsequent DNA damage **(Figure 3.12)** and the upregulation of inflammatory response genes **(Figure 3.19)**. The *MZrnaseh2a* phenotype is consistent with previous models of AGS in mice (Hiller *et al.*, 2012; Reijns *et al.*, 2012; Pokatayev *et al.*, 2016; Bartsch *et al.*, 2018; Uehara *et al.*, 2018) and even partially recapitulates those seen in humans (Crow and Manel, 2015; Potenski *et al.*, 2019) showing that mutations in RNaseH2a cause an upregulation of Type 1 interferon regulated genes via the cGas/STING pathway (Crow and Manel, 2015; Uehara *et al.*, 2018). One prediction is that, due to the large number of rNMPs in the DNA of *MZrnaseh2a* embryos, the DNA spontaneously fragments due to the inherent instability of ribonucleotides. These fragments then 'leak' into the cytoplasm, thought to occur via micronuclei during cell division, activating the cGAS/STING pathway and causing an upregulation of ISGs (Mackenzie *et al.*, 2016). The high rate of cell division in embryos, along with their lack of maternally contributed RNaseH2, may be a contributing factor to their phenotypic severity **(Figure 3.25)**.

The strong upregulation of p53 expression in *MZrnaseh2a* embryos compared to wild-type controls also supports this hypothesis **(Figure 3.18)**, linking to the large quantities of apoptosis seen via acridine orange staining **(Figure 3.15)**. This again is consistent with the phenotype seen in mice that suggest the level of rNMP incorporation, once over a certain threshold, causes a dramatic upregulation of p53, increase cell death and ultimately embryonic lethality (Uehara *et al.*, 2018).

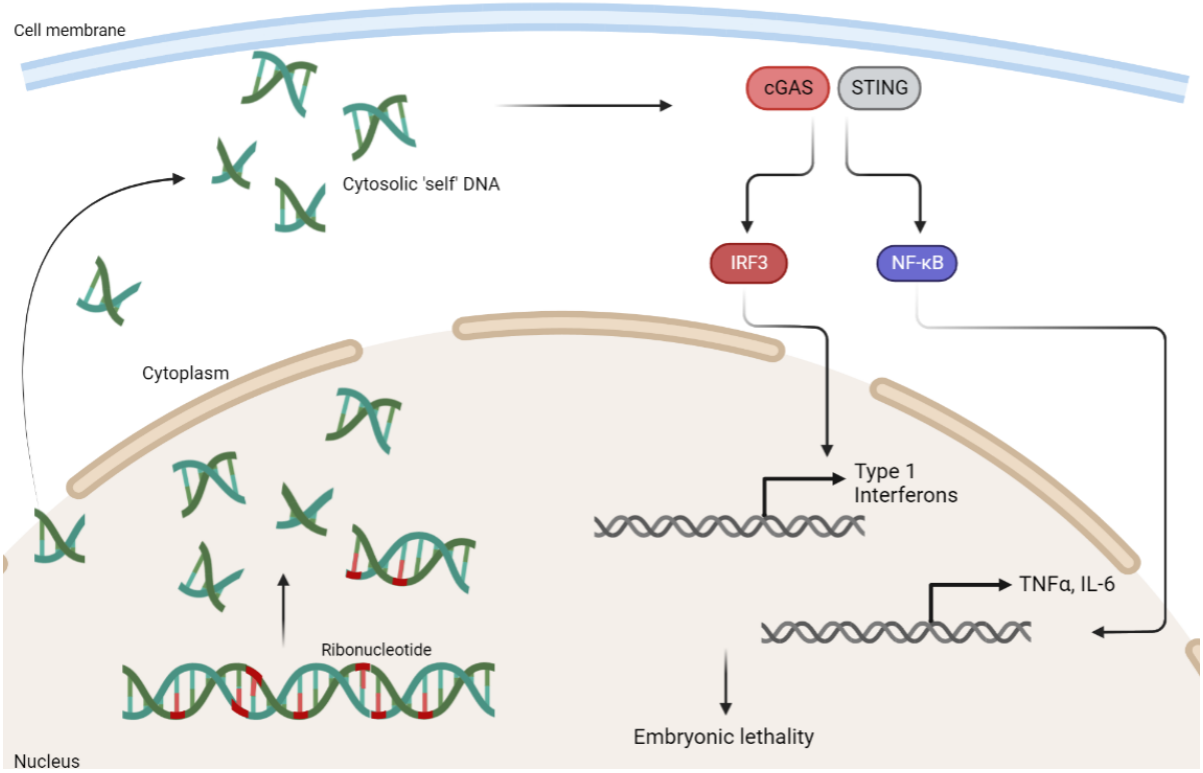

Figure 3.25**: Activation of the cGAS/STING inflammatory response pathway **via ribonucleotide incorporation in nuclear DNA

Increased ribonucleotide incorporation, without correct removal, can result in the fragmentation of DNA in the nucleus. These fragments then 'leak' through the nuclear pores, or are released into the cytoplasm during cell division. cGAS binds to the dsDNA fragments, causing the production of cGAMP (Not shown). This then activates the downstream receptor STING, ultimately causing the activation of IRF3 and NF-κβ that induce the expression of Type 1 interferons and inflammatory response genes such as TNFα and IL-6. Consistent overexpression of these factors leads to increased apoptosis (Not shown) and embryonic lethality of *MZrnaseh2a* embryos. Created with BioRender.com.

3.3.2 Embryos from any *rnaseh2a*$^{-/-}$ adult show lethality due to predicted ribodysgenesis

The early embryonic lethality was not limited to *MZrnaseh2a* embryos, those from two homozygous mutant parents. The same phenotype was also observed in embryos with paternal contribution of the mutation (*Prnaseh2a)* and maternal contribution (*Mrnaseh2a)* offspring where such embryos even showed an increase in severity and early death **(Figure 3.16)**. *Prnaseh2a* embryos survived the shortest length of time and *MZrnaseh2a* surviving the longest. The lethality of *Prnaseh2a* mutant was revealing to the reasons behind the rnaseh2a phenotype, as sperm cells contribute on two essential items to the egg: their DNA and a centrosome. Defects in the latter would disturb the earliest cell divisions in the embryo, and these were not observed. Therefore, errors in the DNA itself were the most likely cause. In this scenario, upon introduction of an active RNaseH2a, by one of the *rnaseh2a*$^{+/+}$ parents, the high levels of rNMPs in the mutant gamete DNA are recognised and cleaved, creating a large number of short DNA fragments, resulting in a large inflammatory response **(Figure 3.19)**.

Interestingly, in *Saccharomyces cerevisiae* strains that lack RNaseH2 (rnh202) and contain a polymerase delta edited to increase the incorporation of rNMPS (pol3-L612G), a recent report describes a similar phenotype, coined ribodysgenesis. Here they found that crosses from yeast strains where one was a wild-type and the other was an rnh202 pol3-L612G strain, resulted in the zygotes failing to divide. They were able to show that this was due to the incision of the large number of incorporated rNMPs in the rnh202 pol3-L612G strain by the introduction of an active RNaseH2, causing high levels of genome fragmentation (Sui *et al.*, 2022). Further experiments to confirm this phenomenon in *Mrnaseh2a and Prnaseh2a* embryos include alkaline assay analysis and γH2AX IF staining to identify higher levels of DNA cleavage than in *MZranseh2a* embryos.

3.3.3 *rnaseh2a*$^{-/-}$ embryos and adults are able to remove single rNMPs without RNaseH2

Unlike their offspring that were shown to be deficient in cleaving rNMPs, it was identified that *rnaseh2a*$^{-/-}$ zebrafish from *rnaseh2a*$^{+/-}$ parents were able to leave a single rNMP substrate, both at their embryonic (5dpf) and adult (19 months) stages (**Figure 3.8,3.9)**. The reduced cleavage efficiency in *rnaseh2a*$^{+/+}$ samples at 5dpf may be due to the reduced expression of *rnaseh2* and lower need for RNaseH2 activity as the rate of cell division, compared with 24hpf, is not as rapid. The expression of *rnaseh2* may then increase again

towards adulthood, allowing for the more efficient repair of differentiated cells. Despite this, the adults were shown to have an increased number of rNMPs incorporated into their brains, which was not present at 5dpf **(Figure 3.11)**. This suggested that there may be a secondary mechanism that allows them to remove rNMPs, but that this method is not as efficient as RNaseH2, leading to a build-up of rNMPs over time. This build up may also be the reason for the mild movement phenotypes seen in adult zebrafish that again, are not present at 5dpf. This can be related to the movement abnormalities seen in AGS patients. The slow accumulation of rNMPs may also explain their survival as, despite the increase in the number incorporated, the genome has not yet reached the threshold at which the p53 response is activated in *MZranseh2a* embryos, allowing the adults to survive. This is supported by the partial suppression of the phenotype in *MZrnaseh2a* embryos upon knockdown of p53 (**Figure 3.18)**. A key question to answer here would be if the accumulation of rNMPs in the brains of adults ever reach the threshold at which the p53 response is activated or are they able to tolerate the slow accumulation.

The increase of rNMPs in adults may be due to the predicted compensatory removal mechanism not being as efficient or being overwhelmed by ribonucleotide incorporation. If this is the case, it would also occur throughout adulthood, meaning that older fish have more rNMPs incorporated in their testes, ultimately causing their offspring to inherit a higher base level of rNMPs, triggering early apoptosis of developing cells.

This was supported when comparing the offspring from older *rnaseh2a*$^{-/-}$ adults (12 months) with younger *rnaseh2a*$^{-/-}$ adults (6 months). There was a significant reduction in the development of embryos from the 12 month of adults, and a mild increase in the interferon stimulated gene, ISG15 **(Figure 3.22)**.

3.3.4 Detrimental embryonic phenotypes predicted to be due to defective RER

RNaseH2a is not only involved in the removal of single rNMPs, but also in the cleavage and resolution of longer stretches of ribonucleotides and RNA/DNA hybrids such as R-loops. Previous separation of function mutants have been created that are unable to perform RER but are still able to resolve R-loops (RED). It was found that mice lacking the ability to remove single rNMPs undergo a large upregulation of the p53 response, causing early embryonic death (Uehara *et al.*, 2018). As the *MZrnaseh2a* embryos showed a significant upregulation in p53 expression, it suggests that their phenotypes are due to the lack of RER

ability rather than R-loop cleavage. However, to conclusively prove this, a RED mutant would have to be established that is unable to cleave single rNMPs, but maintains that other roles of RNaseH2, thus separating the phenotypes from individual functions.

3.3.5 Summary

We have created a viable *rnaseh2a*$^{-/-}$ zebrafish line, in contrast to all other current *in vivo* models against the subunits of RNaseH2 that show embryonic lethality. I have identified the potential for slow accumulation of rNMPs over the lifetime of these mutants which are ultimately inherited by their offspring. Upon the inheritance of such as large number of rNMPs, the embryos undergo large quantities of dsDNA breakage events, causing an increase in the expression of p53 and interferon stimulated genes, resulting in large quantities of cell death and loss of embryonic viability. This is perpetuated in the offspring of one *rnaseh2a*$^{-/-}$ and one *rnaseh2a*$^{+/+}$ parent where the active RNaseH2 recognises and cleaves the large quantity of rNMPs, known as ribodysgenesis **(Figure 3.26)**. In Chapter 4 I will discuss the potential reasons for the survival of *rnaseh2a*$^{-/-}$ adults before introducing further DNA break repair models.

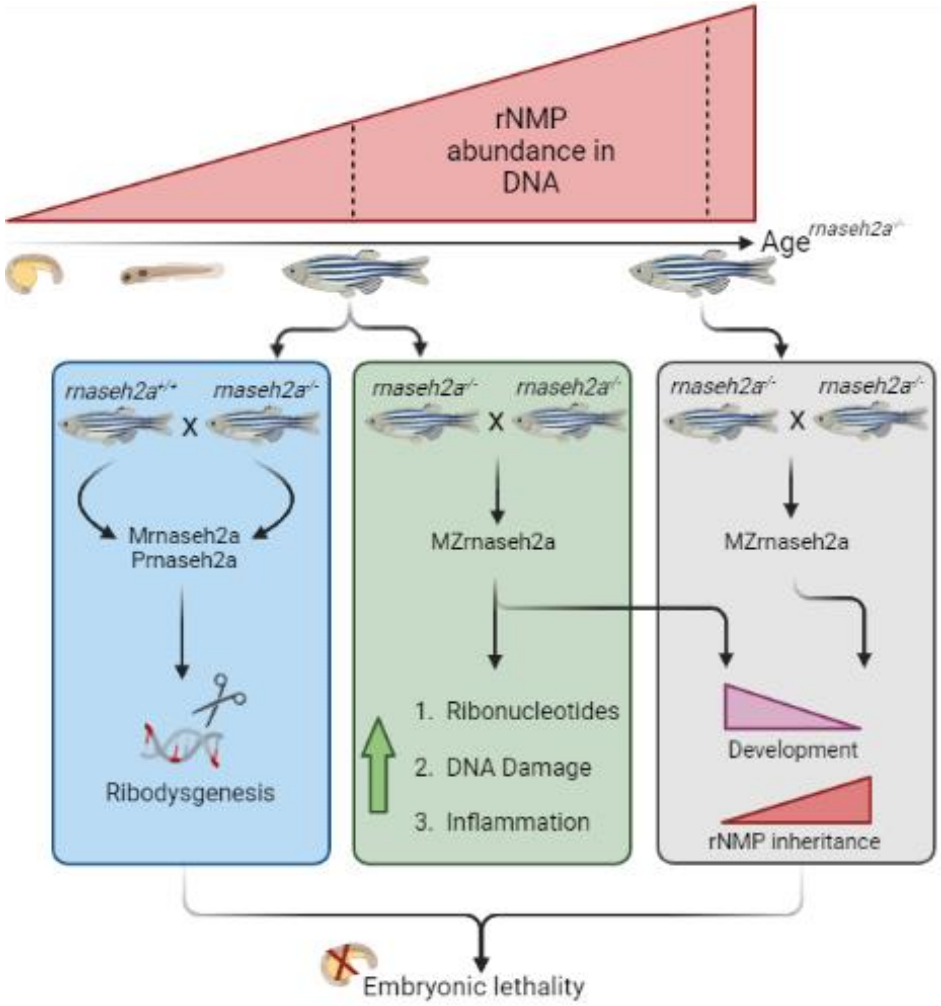

Figure 3.26: Schematic demonstrating how the predicted increase of rNMP incorporation in first generation *rnaseh2a*$^{-/-}$ adults leads to embryonic lethality in all second generation offspring

A schematic diagram indicating the predicted increase in rNMP incroperation into the DNA of *rnaseh2a*$^{-/-}$ zebrafish other their lifetime. Subsequent offspring from an *rnaseh2a*$^{-/-}$ and an *rnaseh2a*$^{+/+}$ adult (*Mrnaseh2a*, *Prnaseh2a*) result in early embryonic death via increased DNA cleavage events caused by an abundence of rNMPs in their genome. A process known as ribodysgenesis (Left, blue box). Alternatively, embyros from two *rnaseh2a*$^{-/-}$ parents (*MZrnaseh2a*) show increased rNMP incorperation, upregulation of DNA damage and subsequent, systemic activation of their inflammatory response (Central, green box). Preliminary work has shown this response to be enhanced in embryos from aged *rnaseh2a*$^{-/-}$ adults (Right, grey box). The reduced development observed is predicted to be caused by the inheritance of additional ribonucleotides. Created in Biorender.com.

Chapter 4

Alternative repair of ribonucleotides in RNaseH2a knockout zebrafish

4.1 Introduction

The removal of ribonucleotides from DNA is a key event in the survival of an individual cell. Although the main contributor to the removal of rNMPs in RNaseH2, there are other candidates known to have similar endonuclease activity.

The primary candidate is Topoisomerase 1 (TOP1) that has a well-defined role in the release of DNA torsional stress, generated by the replication and transcription complexes. It has also been shown to be able to remove single ribonucleotides, in the absence of RNaseH2.

The DNA-protein complexes formed after TOP1 cleavage of ribonucleotides can be reversed via the alignment of the tyrosine-DNA phosphodiester bond of the TOP1 with the 5'-hydroxyl group of the DNA allowing for nucleophilic attack by the latter on the former (**Figure 1.5)**. Although relegation and release of TOP1 is usually favoured, the resultant Top-1 Cleavage Complex (TOP1-cc) can become permanently bound if it collides with transcription machinery, is in close proximity to another ssDNA break or after treatment with topoisomerase inhibitors. One such inhibitor is camptothecin (CPT), which reversibly binds to TOP1 but prevents is release and religation, increasing DNA damage and apoptosis.

In the absence of RNaseH2, TOP1 has also been implicated in the removal of single rNMPs incorporated into the DNA (Kim *et al.*, 2011; Williams *et al.*, 2013). In yeast it was found that, in the presence of a modified Polε to increase rNMP incorporation, there was a distinct increase in the number deletions within 2-5bp tandem repeats which were shown to be produced by TOP1 (Kim *et al.*, 2011; Lippert *et al.*, 2011; Takahashi *et al.*, 2011). These indels characterise the cancer insertion-deletion mutation signature, ID4. These indels were also found to be present in both mammalian cells, an RER deficient mouse model (Reijns *et al.*, 2022) and cancer (Alexandrov *et al.*, 2020).

Although TOP1 is the main candidate for removal of rNMPs in the absence of RNaseH2, it is also mutagenic, as described above. In this case, there are also other candidates for enzymes that support the endolytic cleavage and removal of rNMPs by TOP1, preventing it from forming these repetitive deletions. In yeast, it was found that the Srs2 helicase can unwind the DNA on the 5' side of the nick created by TOP1 on an rNMP. In association with Exo1, this DNA gap can then be repaired in an error free manner (Potenski *et al.*, 2014). Studies have revealed that removal of RNaseH2 from biological systems causes synthetic

lethality when treated with ATR inhibitors (Wang *et al.*, 2018) and also upon treatment with PARP inhibitors as the rNMPs become PARP trapping lesions, associated with their repair by TOP1 (Zimmermann *et al.*, 2018).

At 5dpf and adulthood I have shown that *rnaseh2a*$^{-/-}$ larvae are able to remove rNMPs from their DNA, despite having a lack of active RNaseH2 **(Figure 3.8, 3.9).** The current hypothesis is that they contain a secondary mechanism that is able to cleave single rNMPs in the absence of RNaseH2. Given the current literature, the main candidate for this is Topoisomerase 1. Here I will describe the predicted role of TOP1 and other potential candidates in the viable *rnaseh2a*$^{-/-}$ line.

Hypothesis: *rnaseh2a*$^{-/-}$ embryos will be sensitive to an increased incorporation of rNMPs, induced by a reduction in the available dNTP pool. This can be performed via treatment with hydroxyurea. They will show sensitivity to TOP1 poisons such as CPT, suggesting TOP1 as the alternative method of rNMP removal.

Aims:

- Examine the sensitivity of *rnaseh2a*$^{-/-}$ embryos to a hydroxyurea treatment and subsequent increased incorporation of rNMPs.
- Investigate alternative methods of rNMP removal including Topoisomerase 1

4.2 Results

4.2.1 Hydroxyurea treatment does not adversely affect *rnaseh2a*$^{-/-}$ embryos

With a lack of active RNaseH2 to remove single rNMPs that are incorporated into the DNA, it is predicted that *rnaseh2a*$^{-/-}$ embryos will be significantly more sensitive to an increased incorporation of rNMPs. Hydroxyurea (HU) is known to increase the incorporation of ribonucleotides via decreasing the dNMP pool in cells (Sinha and Snustad, 1972).

Treatment of 24hpf embryos from heterozygous *rnaseh2a* parents with a range of HU concentration (5uM-50uM) and imaging at 5dpf revealed no significant increase in severely affected (reduced head growth, spinal curvature, cell death, lack of swim bladder) *rnaseh2a*$^{-/-}$ embryos compared with their wild-type siblings **(Figure 4.1)**. Although this disproves the initial hypothesis, due to the ability of *rnaseh2a*$^{-/-}$ embryos to cleave rNMPs at the same rate as their *rnaseh2a*$^{+/+}$ siblings **(Figure 3.7)**, subsequently preventing a build-up of rNMPS, it is therefore not too surprising that they are able to cope with an artificial increase in rNMPs as efficiently as wild-types.

4.2.2 Topoisomerase 1 inhibition does not adversely affect *rnaseh2a*$^{-/-}$ embryos

Topoisomerase 1 is known to have the ability to remove single ribonucleotides from DNA, particularly when RNaseH2 is not present. Removal of rNMPs by TOP1 is usually a reversible process **(Figure 1.5)** but if the resulting topoisomerase 1 cleave complex becomes permanent, it can lead to increased DNA damage and reduced genome stability. Upon treatment with CPT, TOP1-cc's become stabilized, creating a DNA-protein complex and resultant ssDNA break. If TOP1 is significantly compensating for the lack of RNaseH2a in the zebrafish, then treatment with the topoisomerase 1 inhibitor, CPT should have a significantly more detrimental effect on the *rnaseh2a*$^{-/-}$ embryos form a heterozygous incross than their wild-type siblings.

Embryos from an *rnaseh2a*$^{+/-}$ cross were treated with CPT overnight. The next day the most severely affected embryos were imaged and genotyped **(Figure 4.2A,B)**. After genotyping, it was established that the morphological effects of the treatment did not differ between genotypes **(Figure 4.2C)** and that *rnaseh2a*$^{-/-}$ was not significantly enriched in those most severely affected **(Figure 4.2D)**. This suggests that there is not a significantly increased number of TOP1-cc's formed in the *rnaseh2a*$^{-/-}$ embryos.

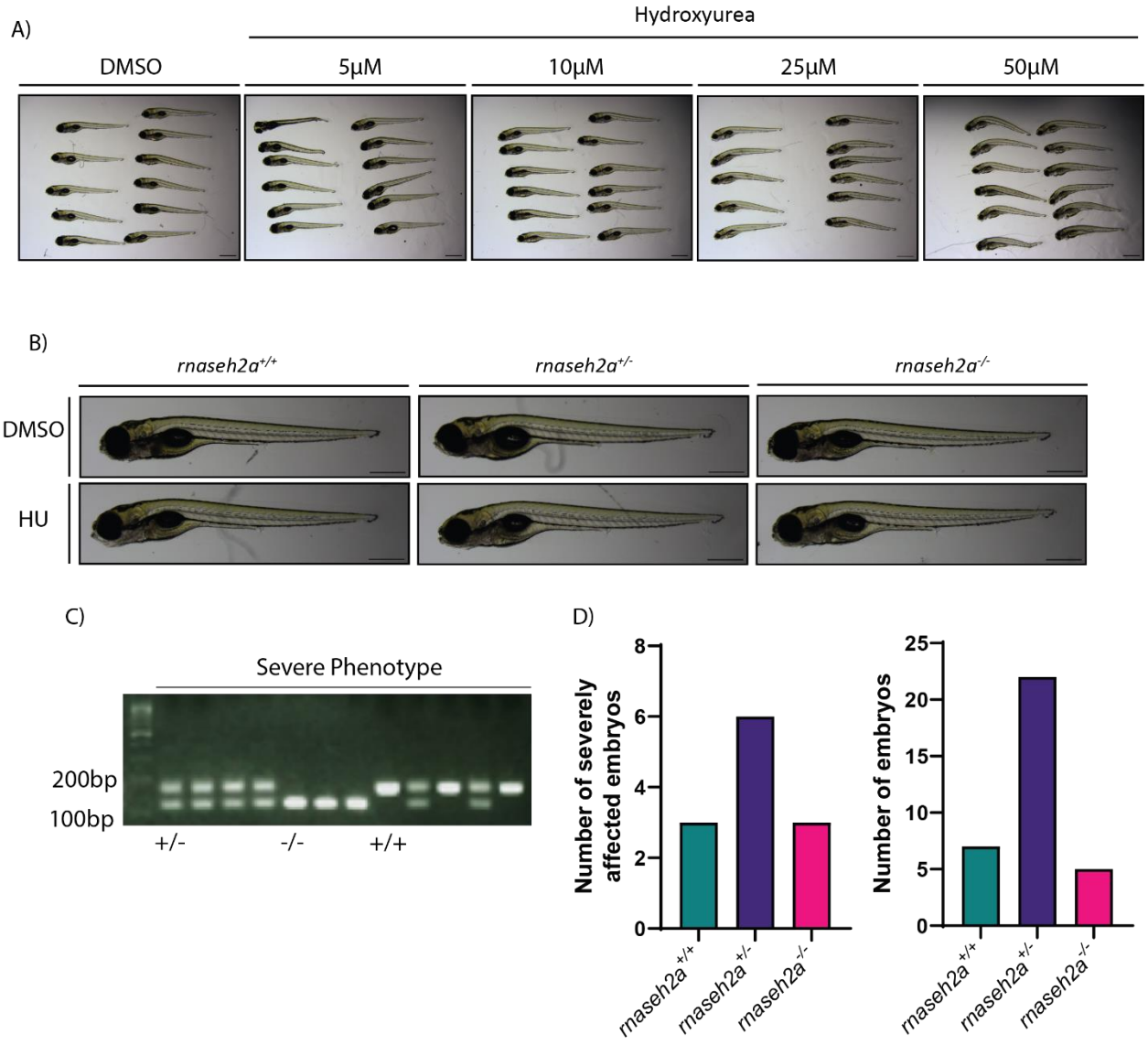

Figure 4.1: Treatment of embryos with hydroxyurea from *rnaseh2a*$^{+/-}$ parents revealed no significant difference in phenotypic severity

A) Treatment of embryos from *rnaseh2a*$^{+/-}$ parents with increasing concentrations of Hydroxyurea showing an increase in severity of phenotype with concentration. Embryos were treated at 4.5dpf overnight (16hrs) and imaged at 5dpf **B)** Phenotypic analysis of the most severely affected embryos (10uM) showed no significant gross morphological phenotypic difference between *rnaseh2a*$^{+/+}$ and *rnaseh2a*$^{-/-}$ after genotyping. Scale Bar, 0.5mm **C+D)** Genotyping of the most severely affected embryos showed no enrichment for the *rnaseh2a*$^{-/-}$ genotype compared to other genotypes.

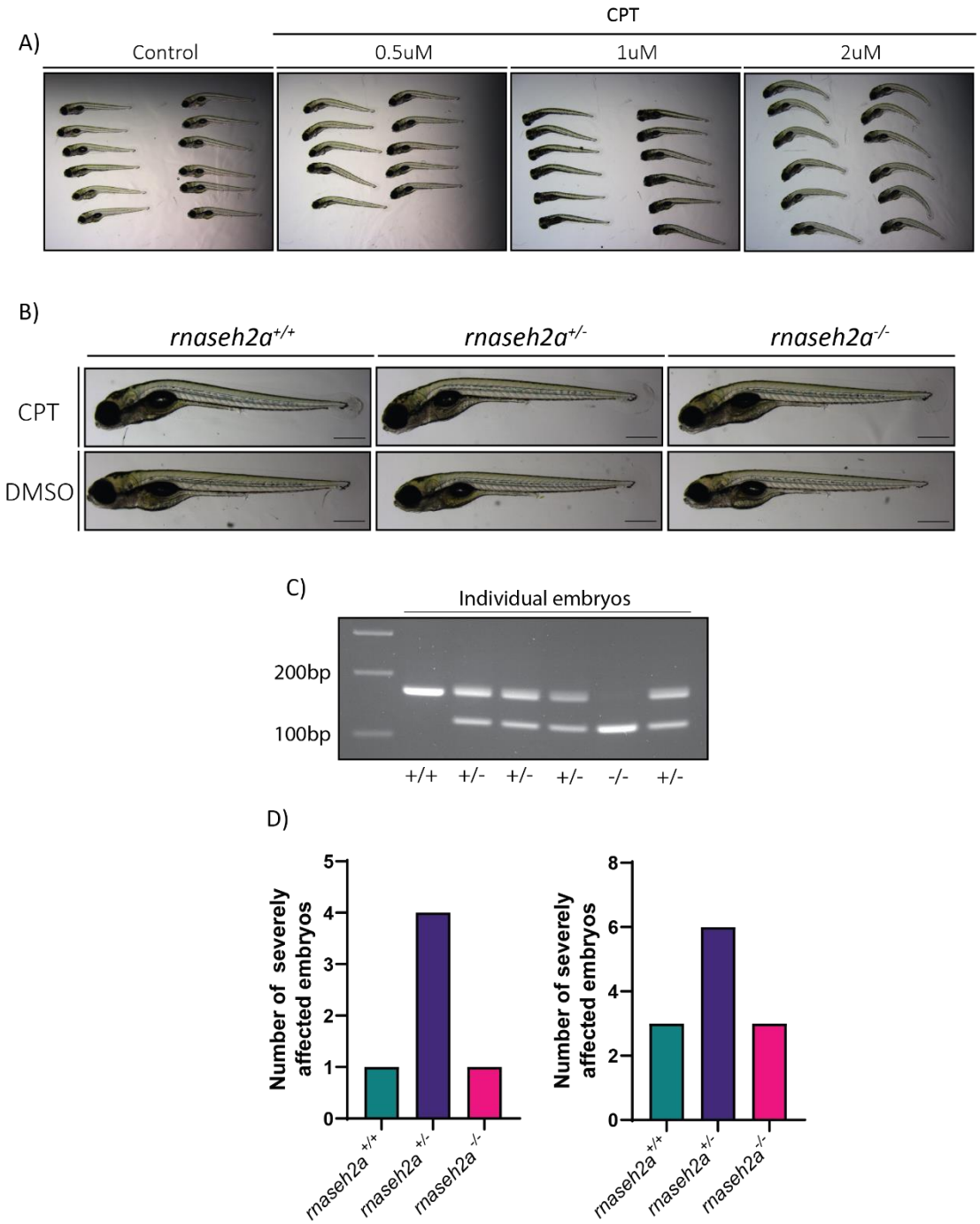

Figure 4.2: Treatment of embryos with CPT from *rnaseh2a*$^{+/-}$ parents revealed no significant difference in phenotypic severity

A) Treatment of embryos from *rnaseh2a*$^{+/-}$ parents with increasing concentrations of CPT showing an increase in phenotypic severity with concentration **B)** Phenotypic analysis of the most severely affected embryos (0.5 µM) showed no visually significant difference between genotypes. Scale Bar, 0.5mm **C+D)** Genotyping of severely affected embryos did not show an enrichment for *rnaseh2a*$^{-/-}$ mutants compared with the other genotypes.

4.2.3 *rnaseh2a*$^{-/-}$ embryos are not significantly sensitive to ATR inhibition

ATR has a key role in DNA repair, particularly in response to stress acquired during DNA replication (Saldivar, Cortez and Cimprich, 2017; Técher *et al.*, 2017) but also in regulating cell cycle checkpoints, telomere maintenance and mechanical stresses (Wright *et al.*, 1998; Brown and Baltimore, 2000; De Klein *et al.*, 2000). Given its key roles in cell survival, ATR inhibition has been a promising target for cancer therapies but has shown to be essential in human and mouse cells (Wright *et al.*, 1998; Brown and Baltimore, 2000; De Klein *et al.*, 2000; Saldivar, Cortez and Cimprich, 2017). A genome wide study aimed to identify genes which, upon ATR inhibition, display synthetic lethality. One of the prominent genes emerging from this study was RNaseH2 (Wang *et al.*, 2018).

Therefore, I decided to investigate whether the *rnaseh2a*$^{-/-}$ larvae were hypersensitive to an ATR inhibitor (ATRi) compared with their wild-type siblings. Treatment of embryos from an *rnaseh2a*$^{+/-}$ incross were treated in a blinded fashion from 24hpf-3dpf with 10uM of ATRi **(Figure 4.3A,B)**. This treatment revealed a variety of sick phenotypes and the most severely affected fish were selected for genotyping. Unlike the previous findings in cell lines, it emerged that the severely affected fish had a range of genotypes; there was no enrichment for *rnaseh2a*$^{-/-}$ larvae **(Figure 4.3C,D,E)**.

Although these results contradict previous literature (Wang *et al.*, 2018), it is not totally surprising. One instance of DNA damage repair that ATR is involved with is the repair of ssDNA breaks. An example of this, is the stalling of a TOP1 bound complex to form a TOP-cc, potentially via collision with the replication machinery (Shao *et al.*, 1999). This ssDNA is recognized and bound by the Replication protein A (RPA) which localizes ATR, shown in both yeast and human cells (Zou and Elledge, 2003). ATR is then activated and stimulates downstream ssDNA repair complexes **(Figure 1.2)**.

Given that we have previously shown no significant sensitivity to the stalling of TOP1 complexes, and no increase in rNMPs in *rnaseh2a*$^{-/-}$ larvae, it is therefore not too surprising that they are not very sensitive to ATR inhibition. This lends further support the hypothesis that TOP1 is not the main contributor to the removal of rNMPs in *rnaseh2a*$^{-/-}$ upon the depletion of RNaseH2a or if it is, the levels of rNMPs are tolerated at embryonic stages when their levels are still low, but begin to pose problems into adulthood, when levels appear higher.

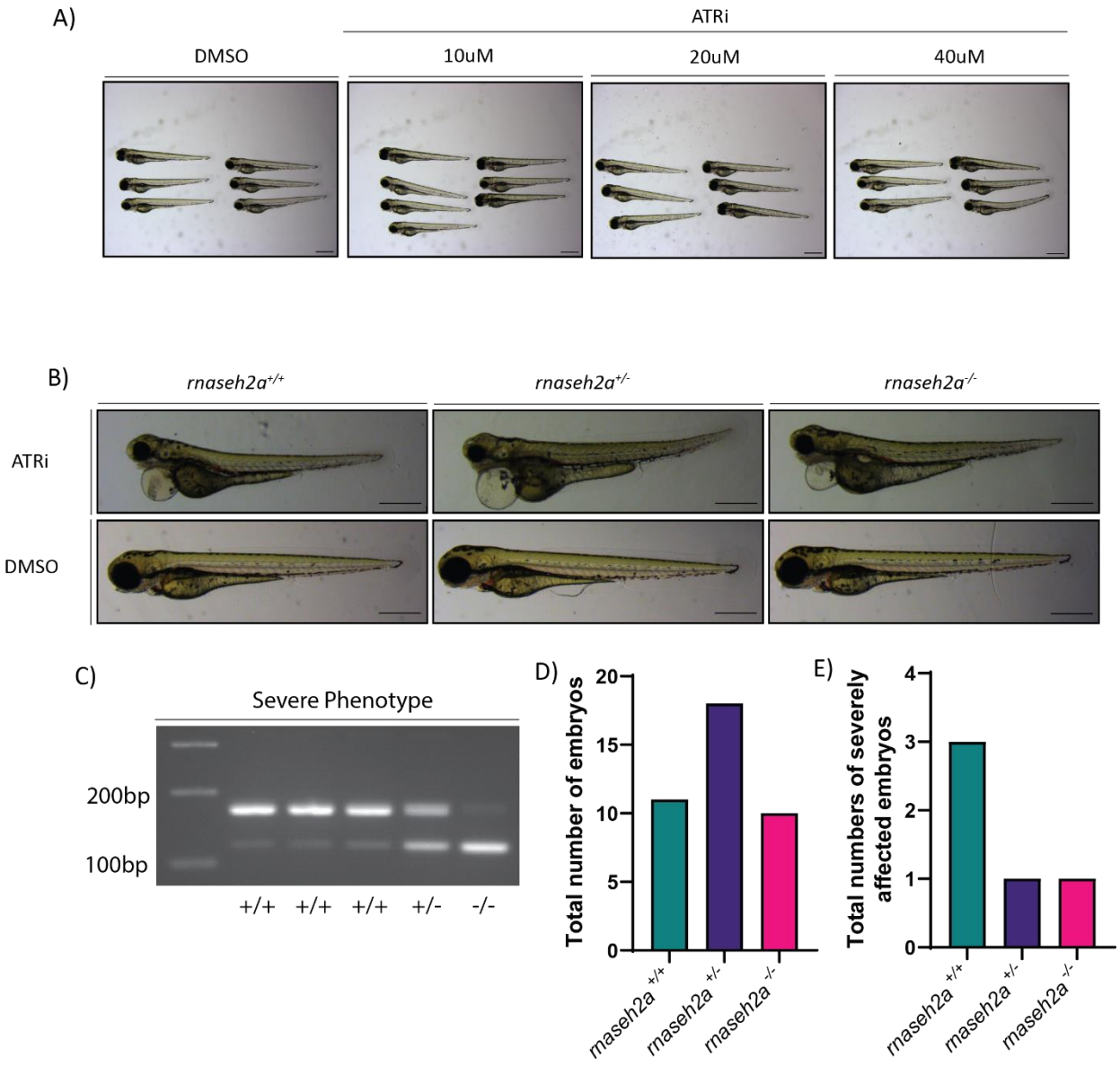

Figure 4.3: *rnaseh2a*$^{-/-}$ embryos show no enhanced detrimental phenotype upon treatment with ATRi

A) Treatment with increasing concentrations of ATRi shows increasing toxicity. **B)** Examples of the most severely affected embryos after treatment with 10µM ATRi. **C)** Genotyping revealed no significant link between the severity of the phenotype and genotype of the embryo. **D, E)** *rnaseh2a*$^{-/-}$ embryos are not enriched in the most severely affected class.

4.2.4 *rnaseh2a*$^{-/-}$ embryos are not overly sensitive to PARP inhibition

Poly (ADP-ribose) polymerase catalyses the polymerization of ADP-ribose (PAR) polymers onto both itself and other proteins, recruiting DNA repair components and regulating their activity. It has been described to have many roles in the detection and resolution of several DNA lesions including TOP1-cc's and genomic ribonucleotides (Pommier *et al.*, 2014; Das *et al.*, 2016; Ray Chaudhuri and Nussenzweig, 2017; Zimmermann *et al.*, 2018). TOP1-cc's are removed by the activity of TDP1 which hydrolyses the phosphodiester bond, allowing the removal of TOP1 from the DNA. PARP1 targets TDP1 and, through PARylation, stabilizes and enhances its recruitment to the TOP1-cc. This complex is essential for maintaining DNA stability (Ray Chaudhuri and Nussenzweig, 2017). Recent studies have also identified single rNMPs as a key source of PARP trapping lesions, due to their repair by TOP1 in the absence of RNaseH2 (Zimmermann *et al.*, 2018).

Treatment of embryos from *rnaseh2a*$^{+/-}$ parents with increasing concentrations of Talazoparib revealed a dose dependent increase of phenotypic severity **(Figure 4.4A)**. Blinded treatment of such embryos with 500nM from 24hpf to 3dpf revealed a variety of phenotypes **(Figure 4.4A,B)**. Upon selection and genotyping of the most severe phenotypes, it revealed that the severity was not genotype dependent **(Figure 4.4C,D,E)**.

Although this result is in contradiction to previous studies on RNaseH2a deficient cell lines, it is in keeping with the previous results seen in this thesis upon *treatment* of embryos with an ATRi. Given the lack of rNMP accumulation **(Figure 3.6)** and resistance to TOP1 inhibitors such as camptothecin already seen **(Figure 4.2)**, it was relatively unsurprising that treatment with PARP inhibitors does not adversely affect *rnaseh2a*$^{-/-}$ embryos. This continues to suggest an alternative pathway used by *rnaseh2a*$^{-/-}$ for the removal of rNMPs.

4.2.5 Loss of *APEX2* does not significantly decrease survival *rnaseh2a*$^{-/-}$ embryos

Another protein involved in the repair of protein linked DNA complexes formed by TOP1 resolution of rNMPs is the Apurinic/Apyrimidinic Endodeoxyribonuclease 2 (APEX2). APEX2 does not directly cleave single ribonucleotides, but is involved in the repair of the 2'-3'-cyclic phosphate formed by TOP1 cleavage of rNMPs, helping to prevent mutagenic repair (Li *et al.*, 2019).

Microinjection of four guides targeting the two isoforms of APEX2 in zebrafish (APEX201 (present in humans) and APEX202 (not present in humans)), in combination with the CRISPR/Cas9 system, aimed to create first generation mutant knockouts of overall APEX2 (both APEX201 and APEX202). After genotyping, no difference in phenotypic severity or survival was seen between the *rnaseh2a*$^{-/-}$ larvae and their *wild-type* siblings at 5dpf **(Figure 4.5A,B)**. Analysis of *rnaseh2a*$^{+/+}$ and *rnaseh2a*$^{-/-}$ embryos revealed decrease in expression of APEX201 but no significant difference in overall APEX2 expression after qPCR analysis **(Figure 4.5C).**

4.2.6 DDX3X is not upregulated in *rnaseh2a*$^{-/-}$ embryos

Given the absence in sensitivity of *rnaseh2a*$^{-/-}$ to TOP1 inhibitors such as CPT, there is the hypothesis that there is a secondary mechanism of repair that does not involve TOP1. Candidates include the DEAD-box helicase DDX3X. DEAD-box helicases are known to be involved in several processes involved in RNA metabolism including mRNA export, transcriptional and translational regulation and ribosome biogenesis (Rocak and Linder, 2004) as well as being implicated in the resolution of RNA:DNA hybrids and RNA degradation (Schröder, 2010). More recently, DDX3X has been shown to have RNaseH2-like activity, allowing it to perform RER *in vitro*. Knockout of DDX3X in mammalian cells also causes the accumulation of rNMPs in the genome, corroborating the suggestion that DDX3X could be involved in the removal of single ribonucleotides (Riva *et al.*, 2020). However, analysis of gene expression in *rnaseh2a*$^{-/-}$ embryos showed no significant upregulation of DDX3X in the absence of RNaseH2 in our zebrafish model **(Figure 4.6).** Unfortunately, there was no time to perform functional experiments with this gene.

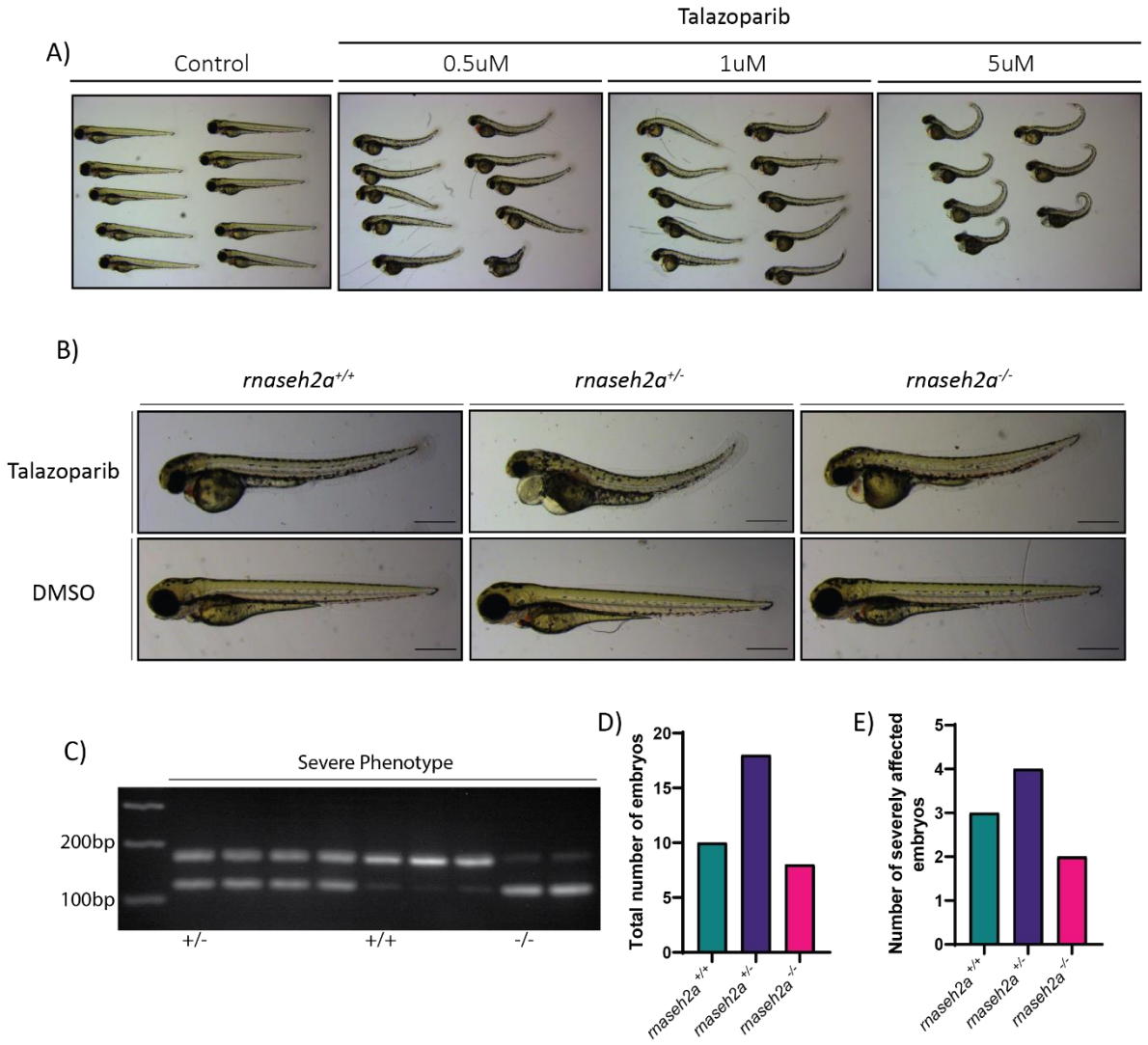

Figure 4.4: *rnaseh2a*$^{-/-}$ embryos show no significantly detrimental phenotype upon treatment with Talazoparib

A) Treatment with increasing concentrations of Talazoparib shows increasing toxicity. **B)** Examples of the most severely affected embryos after treatment with 500nM Talazoparib. Scale bar, 0.5mm **C)** Genotyping revealed no significant link between severe phenotypes and genotype. **D, E)** The number of genotypes were present at a Mendelian ratio, regardless of phenotype.

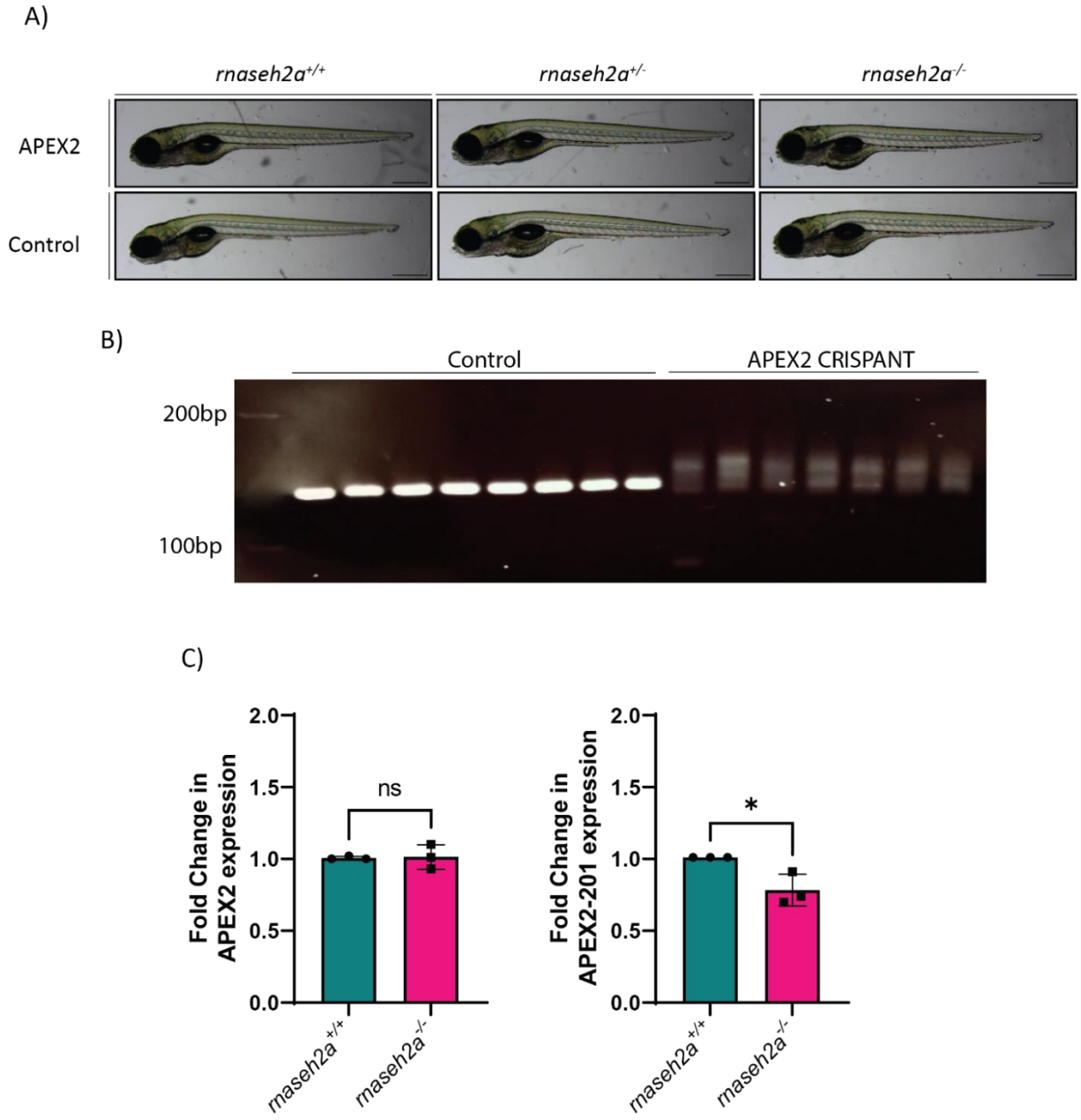

Figure 4.5: *rnaseh2a*$^{-/-}$ embryos show no significantly detrimental phenotype upon creation of APEX2 CRISPANTs

A) Creation of APEX2 CRISPANTs in an *rnaseh2a*$^{-/-}$ background does not have a significantly detrimental effect compared with controls injected with guides targeting *lamb1b* **B)** PCR of the APEX2 gene shows a large number of indels (smear) that are predicted to create early stop codons and a truncated, non-functional APEX protein. Scale bar, 0.5mm **C)** qPCR analysis showed no significant upregulation of either APEX201 or overall APEX2 (201 and 202) expression in *rnaseh2a*$^{-/-}$ embryos compared with *rnaseh2a*$^{+/+}$ siblings. n=3, 20 pooled embryos, Unpaired t-test, ns $p>0.05$ *$p<0.01$, ±SD.

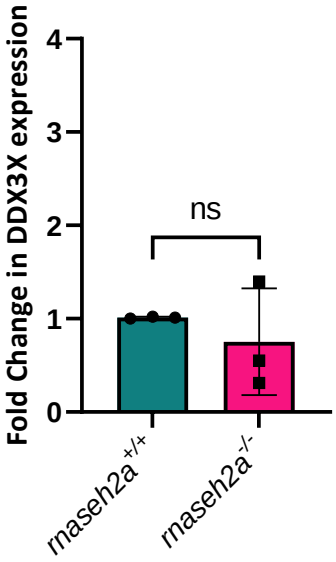

Figure 4.6: Expression levels of other potential repair factors not significantly upregulated in *rnaseh2a*$^{-/-}$ embryos

A) RTqPCR analysis revealed DDX3X mRNA level does not increase in *rnaseh2a*$^{-/-}$ embryos from *rnaseh2a*$^{+/-}$ parents compared with their wild-type siblings. n=3, 20 pooled embryos, Unpaired t-test, p>0.05, ±SD.

4.3 Discussion

In this chapter I have analysed pathways that may be involved in the survival of zebrafish lacking an active RNaseH2 enzyme. Previously in Chapter 3 I have described how, despite containing a deletion that causes an early stop codon in RNaseH2a, removing key amino acids, a *D.rerio rnaseh2a* knockout is still able to survive to adulthood, unlike previously established models (Hiller *et al.*, 2012; Reijns *et al.*, 2012; Pokatayev *et al.*, 2016; Bartsch *et al.*, 2018; Uehara *et al.*, 2018). It was also established that they can cleave single rNMPs **(Figure 3.7)**, but this does not stop them from slowly accumulating in the genome over time **(Figure 3.10, 3.11)**. This lead to the hypothesis that there is a secondary repair mechanism, performing RER in the absence of RNaseH2.

4.3.1 Inhibition of TOP1 has no significant effect on *rnaseh2a*$^{-/-}$ embryos

This in itself is not a new concept, Topoisomerase 1 has been implicated in the removal of rNMPs in the absence of RNaseH2 (Kim *et al.*, 2011; Williams *et al.*, 2013). TOP1 cleavage of rNMPs can result in the reversible TOP1-cc complex which can then be stalled by inhibitors such as CPT, becoming toxic. If TOP1 was the primary backup pathway in *rnaseh2a*$^{-/-}$ embryos then treatment with CPT should increase TOP1-cc's, subsequent dsDNA breaks and reduced survival. However, *rnaseh2a*$^{-/-}$ embryos do not have increased sensitivity to CPT **(Figure 4.2)**. Although this is in contrast to cell lines whose CPT sensitivity is rescued by overexpression of RNaseH2a (Kimura *et al.*, 2022), it may be explained by the incidental nature of TOP1 cleavage at rNMPs. Given that it is not thought to be a directed process, the levels of TOP1ccs may not be dependent on rNMP incorporation. This could be investigated via TOP1-cc analysis in CPT treated and untreated samples, as well as base levels of TOP1ccs in *rnase2a*$^{+/+}$ and *MZrnaseh2a* embryos. However, this could initially imply that TOP1 may not be the primary mechanism of removal in absences of RNaseH2 in zebrafish at an embryonic level.

4.3.2 Inhibition of DNA damage signally pathways show no specificity to *rnaseh2a*$^{-/-}$

Our results with zebrafish *rnaseh2a*$^{-/-}$ mutants also contradict previous experiments showing synthetic lethality of RNaseH2a knockout with inhibition of PARP, known to aid the repair of TOP1-cc's, as treatment with Talazoparib showed no significant difference in severity

between *rnaseh2a*$^{+/+}$ and *rnaseh2a*$^{-/-}$ embryos **(Figure 4.4)**. The same is observed with ATR inhibition, known to aid the repair of single-strand DNA breaks and has shown synthetic lethality in *rnaseh2a*$^{-/-}$ cell lines (Wang *et al.*, 2018) **(Figure 4.3)**.
Both of these also suggest an alternative repair mechanism that is not TOP1 dependent.

4.3.3 Alternative secondary repair pathways show no upregulation in *rnaseh2a*$^{-/-}$ embryos

A recently published report detailed a Dead-box helicase with RNase like activity (Riva *et al.*, 2020). Despite there being no difference in mRNA expression (Figure 4.6), DDX3X may be upregulated at the protein level or functionally "step-in". Analysis via western blot, knocking out DDX3X via CRISPANT analysis or creating a double knockout zebrafish line would go further into analysing whether or not this enzyme is the cause of *rnaseh2a*$^{-/-}$ survival.
APEX2 is involved in the repair of the 2'-3'-cyclic phosphate formed by TOP1 cleavage of rNMPs and therefore knocking out APEX2 was thought to cause a significantly detrimental phenotype in *rnaseh2a*$^{-/-}$ but this was not the case **(Figure 4.5)**. The decrease in APEX201 expression may be due to an increase in APEX202 expression in zebrafish, which overall meant no significant change in overall APEX2 expression in *rnaseh2a*$^{-/-}$ embryos. Given the indication that *rnaseh2a*$^{-/-}$ embryos have no natural increase in rNMPs, it is unsurprising that APEX2 does not play a large role in their survival. Though, if stressed with hydroxyurea, subsequently increasing the number of rNMPs, we predicted that APEX2 may play a more significant role.

4.3.4 Summary

Given the current literature, in this chapter I have targeted the most likely candidates for rNMP removal in the absence of RNaseH2 including TOP1, APEX2 and DDX3X. I have also investigated the reported synthetic lethality of RNaseH2a knockout with the inhibition of PARP or ATR. This warrants further analysis via the use of large-scale mRNA analysis such as microarrays and analysis of RNA-seq datasets with other experimental techniques that will be discussed at the end of this thesis to help identify the secondary mechanism allowing for the survival of *rnaseh2a*$^{-/-}$ zebrafish.

Chapter 5

Alternative repair mechanisms in tdp1$^{-/-}$ embryos

5.1 Introduction

As discussed in Chapter 4, TOP1 has roles in release of torsional stress and the removal of single ribonucleotides in the absence of RNaseH2 (Williams *et al.*, 2013). Although normally reversible **(Figure 1.4)**, TOP1 can become permanently attached to the DNA after collision with replication machinery or being in close proximity to other ssDNA breaks. Thereby, a permanent protein-linked DNA break complex is formed, the TOP1 cleavage complex (Debéthune *et al.*, 2002). Tyrosyl-DNA phosphodiesterase 1 (TDP1) is a key component in resolving stalled TOP1 cleavage complexes.

Mutations in TDP1 have also been associated with the rare neurodegenerative disorder spinocerebellar ataxia with axonal neuropathy (SCAN1) in which patients suffer from neurodegeneration, resulting in an ataxic gait (Takashima *et al.*, 2002).

Previous work has shown that *tdp1*$^{-/-}$ mouse models develop mild cerebellar degeneration, similar to the phenotype shown in humans, and show sensitivity to TOP1 poisons (Hirano *et al.*, 2007; Katyal *et al.*, 2007; Hawkins *et al.*, 2009). On the other hand, knockout of TDP1 in other models such as *Arabidopsis thaliana* and yeast have shown no sensitivity to Top1 poisons upon removal of TDP1 (Liu, Pouliot and Nash, 2002; Vance and Wilson, 2002; Deng *et al.*, 2005; Enderle *et al.*, 2019). Recently, a *tdp1*$^{-/-}$ zebrafish model was created and shows that, at embryonic stages, they also do not show sensitivity to TOP1 poisons such as CPT However, once reaching adulthood, the *tdp1*$^{-/-}$ zebrafish showed sensitivity to the TOP1 poison, topotecan. In embryos it was identified that, after treatment with the TOP1 inhibitor CPT, there was a significant decrease in *tdp1* mRNA levels. This suggests that at the embryonic stage, TDP1 is not significantly involved in repairing TOP1-cc's. Concurrently, the expression levels of two genes *apex2* and *ercc4* were upregulated upon CPT treatment. (Zaksauskaite *et al.*, 2021).

Here I will investigate the potential role of *apex2* and *ercc4* for resolving TOP1cc's formed by TOP1 poisons in *tdp1*$^{-/-}$ larvae.

Aim:

- Create CRISPANT knockouts against APEX2 and ERCC4 in *tdp1*$^{-/-}$ embryos and measure their response to CPT treatment

5.2 Results

5.2.1 Mosaic *apex2* CRISPANTS in *tdp1*$^{-/-}$ background show mild locomotion defects upon treatment with CPT

As previously described in Chapter 4, APEX2 has a role in the repair of single strand breaks, particularly in the repair of TOP1-cc's as reported in yeast, mice and chicken (Liu, Pouliot and Nash, 2002; Vance and Wilson, 2002; Hartsuiker, Neale and Carr, 2009; Nakamura *et al.*, 2010; Li *et al.*, 2019; Álvarez-Quilón *et al.*, 2020). Expression of APEX2 was found to be upregulated in *tdp1*$^{-/-}$ zebrafish embryos after treatment with the topoisomerase inhibitor, CPT (Zaksauskaite *et al.*, 2021). To investigate the role of APEX2 further, CRISPANT knockouts of APEX2 were created in *tdp1*$^{-/-}$ embryos. The injected embryos initially showed no outwardly gross phenotypes, which persisted after treatment with CPT **(Figure 5.1A)**. PCR of APEX2 suggested a knockout efficiency of >42% **(Section 2.3.2) (Figure 5.1B)**. However, after the analysis of movement between CPT treated APEX2 knockout and CPT treated controls (Lamb1b CRISPANT), there was a mild difference in their locomotive ability, with APEX2 CRISPANT embryos travelling a reduced distance compared with the controls **(Figure 5.1C)** (Zaksauskaite *et al.*, 2021). This suggests that, at an embryonic stage, APEX2 has a role in the repair of TOP1 associated breaks in the absence of TDP1.

5.2.1 Mosaic *ERCC4* CRISPANTS in *tdp1*$^{-/-}$ background show mild locomotion defects upon treatment with CPT

ERCC4 is a homolog of the human XPF gene and is part of the ERCC1-XPF complex that is formed of ERCC1 and XPF (ERCC4). It is known to be involved in both the global-genome (Naegeli and Sugasawa, 2011) and transcription coupled nucleotide excision repair pathways (Hanawalt and Spivak, 2008). Repair of TOP1-cc's via the ERCC1-XPF complex is thought to occur via the removal of the nucleotides containing the tyrosyl-phosphodiester bond that forms on the 3' end of the break by cleavage directly 5' to the break (Vance and Wilson, 2002; Zhang *et al.*, 2011). In yeast it has been shown that, upon the inactivation of TDP1, the cells do not show an increase in sensitivity to CPT, unless the ERCC1-XPF (ERCC4) orthologue complex, Rad1-Rad10 (Ciccia, McDonald and West, 2008), is also removed (Liu, Pouliot and Nash, 2002; Vance and Wilson, 2002; Deng *et al.*, 2005)

This corroborates the findings that in zebrafish embryos, there is no increase in sensitivity to CPT at an embryonic level upon the knockout of TDP1. It was also identified that there was a

mild upregulation of ERCC4 in embryos post treatment with CPT (Zaksauskaite *et al.*, 2021). Given the current literature, it was predicted that ERCC4 may be involved in a compensatory pathway to remove TOP1-cc's in zebrafish embryos, in the absence of TDP1.

To study this, CRISPANT knockouts of ERCC4 were produced via the microinjection of three guides targeting early exons in the ERCC4 gene. Phenotypic analysis of 5dpf embryos revealed no gross abnormalities in ERCC4 CRISPANTS, before or after treatment with CPT **(Figure 5.2A)**. PCR analysis revealed a knockout of ERCC4 via the identification of potential indels, indicated by the DNA smearing on an agarose gel. **(Figure 5.2B)**. However, upon analysis of their locomotion, it was identified that there is a significant reduction in the distance travelled by *tdp1*$^{-/-}$*;ercc4 CRISPANT* compared with the controls after CPT treatment **(Figure 5.2C)**.

This suggests that, in agreement with the current literature, ERCC4 plays a compensatory role in the removal of TOP1-cc's in the absence of TDP1 and after treatment with a topoisomerase inhibitor.

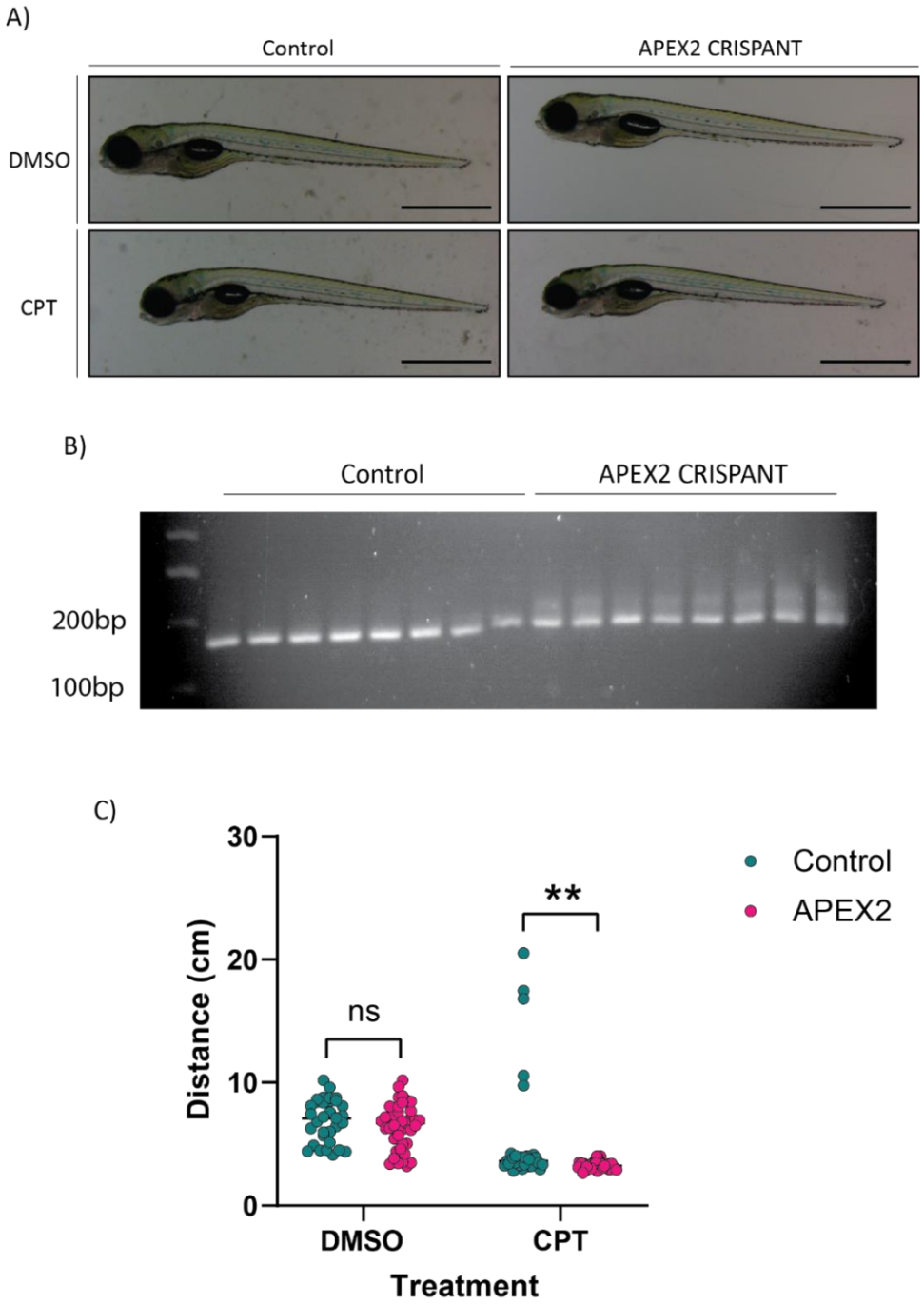

Figure 5.1: APEX2 CRISPANTs show mild sensitivity to CPT when in a *tdp1*$^{-/-}$ background

A) Representative images of 5dpf *tdp1*$^{-/-}$ control (Lamb1b CRISPANT) and APEX2 CRISPANT embryos after treatment with 500nM DMSO or CPT overnight. **B)** PCR of the APEX2 gene in control and APEX2 CRISPNAT. 4% TBE agarose gel shows predicted indels via smearing of wild-type band. **C)** Embryos were videoed for 30 seconds and their distance moved measured. Distance measured via Image J. Scale bar 1mm. n=38, individual embryos, Two-way ANOVA, ns $p>0.05$, ** $p<0.001$, ±SD.

The work in this figure has been published in (Zaksauskaite *et al.*, 2021).

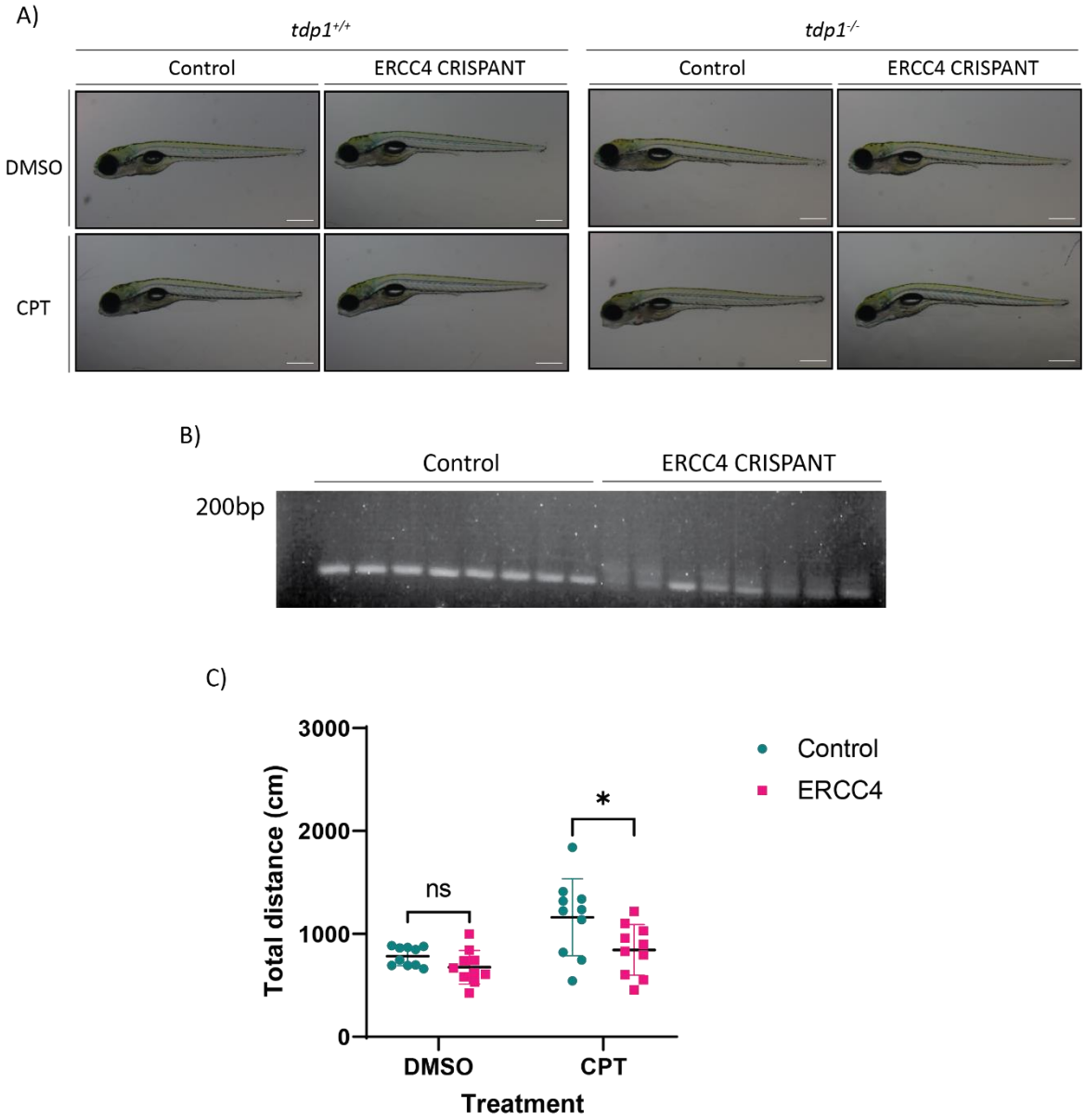

Figure 5.2: ERCC4 CRISPANT show mild sensitivity to CPT when in a *tdp1*$^{-/-}$ background.

A) Representative images of 5dpf *tdp1*$^{+/+}$and *tdp1*$^{-/-}$ control (Lamb1b CRISPANT) and ERCC4 CRISPANT embryos after treatment with 500nM DMSO or CPT overnight. **B)** PCR of the ERCC4 gene in control and ERCC4 CRISPANT. 4% TBE agarose gel shows predicted indels via smearing of wild-type band. **C)** Embryos were videoed for 30 minutes and their distance moved measured. Distance measured via ViewPoint software. Scale Bar 0.5mm. n=10, individual embryos, Two-way ANOVA, ns p>0.05, **p<0.001, ±SD.

5.3 Discussion

Topoisomerase 1 is involved in the relaxation of torsional stress and removal of single ribonucleotides in the absence of RNaseH2 (Debéthune *et al.*, 2002; Williams *et al.*, 2013). Although this process is usually reversible, if the cleavage product is involved in transcriptional collisions, is in close proximity to another single stranded break or undergoes inhibition via chemical treatment (CPT) then the complex can no longer remove itself and becomes a covalently bound TOP1 cleavage complex. At this time, repair components such as TDP1 are required to aid release of the TOP1-cc's and allow successful DNA repair. Mutations in TDP1 can cause the neurodegenerative disease SCAN1 (Takashima *et al.*, 2002). Previous work in our lab established a larval *tdp1*$^{-/-}$ zebrafish model that showed no increased sensitivity to TOP1 poisons but did show an upregulation in *apex2* and *ercc4* (Zaksauskaite *et al.*, 2021).

5.3.1 Mild locomotion deficiencies seen in *tdp1*$^{-/-}$ when treated with CPT after APEX2 knockout

APEX2 has been shown to be capable of removing the 3' DNA phosphotyrosine bond formed in a TOP1-cc. It has also shown activity on the 2',3'-cyclic phosphates created upon TOP1 removal of rNMPs (Li *et al.*, 2019). Upon knockout of APEX2 in *tdp1*$^{-/-}$ zebrafish, there were no significant phenotypic differences with their wild-type siblings. However, they did show a mild decrease in locomotive response upon treatment with CPT **(Figure 5.1)**. This suggests that, in the absence of TDP1, zebrafish in their embryonic stages utilize APEX2 as one of the secondary mechanisms for the resolution of stalled TOP1-cc's. This correlates with the findings in mammalian cell lines that double knockout of APEX2 and TDP1 show significantly more sensitivity to CPT than TDP1 knockout alone (Álvarez-Quilón *et al.*, 2020; Zhang *et al.*, 2022). However, an issue with our results was the unusual distribution, where the difference was mainly due to a few highly active larvae in the control. It would be useful to further back this up by performing the experiment with a longer timeframe and more sensitive equipment (as seen in **Figure 5.2**) or with a complete knockout of APEX2 through the creation of a *tdp1*$^{-/-}$*;apex*$^{-/-}$ zebrafish line.

Unlike mammalian cells however, zebrafish do not display synthetic lethality, suggesting there is more than one pathway that may be compensating for the lack of TDP1 activity.

3.3.2 Mild locomotion deficiencies seen in *tdp1*$^{-/-}$ when treated with CPT after ERCC4 knockout

ERCC4 is an orthologue of XPF and part of the ERCC1-XPF (ERCC4) complex. This has been shown to be involved in the nucleotide excision repair pathway and repair the tyrosyl-phosphodiester bond by nucleotide removal or direct cleavage in associated with RPA (Vance and Wilson, 2002; Takahata *et al.*, 2015). In mammalian cells, depletion of both TDP1 and XPF (ERCC4) result in a higher sensitivity to CPT treatment than TDP knockout alone but to a lesser extent than the TDP1;APEX2 double knockout (Zhang *et al.*, 2022). This correlates with our findings that after ERCC4 knockout and treatment with CPT, *tdp1*$^{-/-}$ embryos show a mild locomotion defect **(Figure 5.2)** but to a less significant extent that APEX2. This may suggest a role APEX2 in the repair of TOP1-cc's in the absence of TDP1 with minor backup repair performed by the ERCC1-XPF (ERCC4) complex. However, given the variable efficiencies of CRISPANT guides that could create different percentage knockouts and the differences between how the assays were performed, further experiments would have to be performed to draw more definitive conclusions. This may include movement analysis of APEX2 and ERCC4 CRISPANTS simultaneously and an increase in n numbers to mitigate the shifts in CRISPANT efficiencies between embryos.

Chapter 6

Creation and characterisation of a NuMA knockout zebrafish

6.1 Introduction

The Nuclear Mitotic Apparatus Protein (NuMA) is a high molecular weight (236kDa) protein that was first discovered to localize to the interphase nucleus but becomes localized at the mitotic spindle poles during cell division (Kallajoki *et al.*, 1993) (Lydersen and Pettijohn, 1980) **(Figure 6.1)**. NuMA has been identified as an essential protein in the maintenance of spindle poles via siRNA screening (Harborth *et al.*, 2001) and the creation of knockout mice that demonstrated early embryonic lethality (Silk, Holland and Cleveland, 2009). It has also been found to localize to the interphase nucleus where it is thought to act as a key regulator of nuclear morphology (Merdes and Cleveland, 1998; Serra-Marques *et al.*, 2020) whilst also being reported to be involved in DNA damage repair through homologous recombination (Vidi *et al.*, 2014; Moreno *et al.*, 2019).

More recently, work in our lab has revealed that NuMA interacts with single-strand break repair components such as the previously described TDP1 (Ray *et al.*, 2022). Identification of an S/TPXX motif, involved in DNA binding and found in proteins involved in gene regulation (Luderus *et al.*, 1994) lead to the prediction that NuMA was somehow involved in regulating the expression of a certain subset of genes. A recent report from our lab revealed that this is indeed the case as it regulates the transcription of genes, particularly those involved in the repair of oxidative damage (Ray *et al.*, 2022).

Many of these findings resulted from the use of cell lines or *in vitro* work. Although this has given a new insight into the role of NuMA in DNA repair, there are limited studies on the role of NuMA in whole organisms. Although previously identified as an essential gene in mice (Silk, Holland and Cleveland, 2009), there has been no investigation into the role of NuMA in DNA repair. This could lead to more interesting discoveries about the activity of NuMA in different tissues and the phenotypic effects shown upon its deletion *in vivo*.

Hypothesis: Depletion of NuMA in zebrafish will lead to early embryonic lethality. Re-introduction of full-length NuMA will rescue the phenotype and introduction of truncated versions of NuMA will reduce the DNA damage burden.

Aims:

- To investigate the role of NuMA in DNA repair using an *in vivo* model
    - Create and characterize a *numa*$^{-/-}$ zebrafish line
    - Link phenotypes seen to the role of NuMA in DNA repair
    - Investigate the response of *numa*$^{-/-}$ to oxidative damage
    - Rescue via re-introduction of full length *numa*
    - Separate the two functions of NuMA and their resulting phenotypes via introduction of truncation mutants

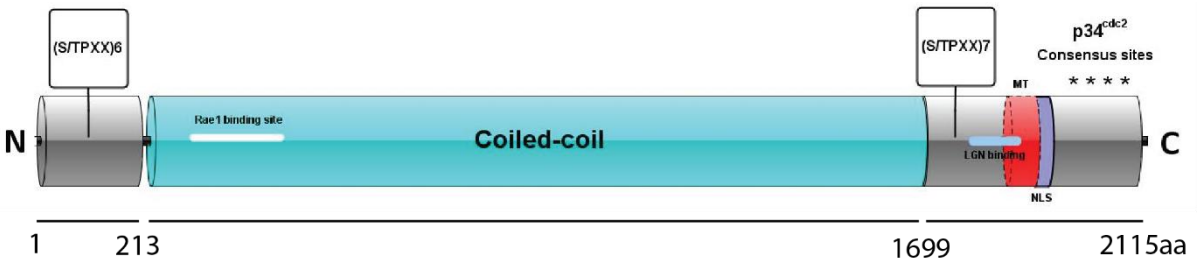

Figure 6.1: Schematic Representation of the Protein Domains in human NuMA

Coiled coil domain (Teal). Globular N and C terminal domains (Grey). S/TPXX DNA-binding motif which occurs with six repeats in the N terminus and seven repeats in the C terminus. Microtubule (MT) binding domain (1900-1971aa) (Red). Nuclear localisation signal (1971-1991aa) (Purple). Rae1 binding domain (325-829aa), critical for spindle formation (White line). LGN binding domain (1878-1910aa), where binding of LGN inhibits microtubule binding function (Blue line). Asterix indicate consensus sequence of $P34^{cdc2}$ phosphorylation sites, known to regulate localisation to mitotic spindle sites. Modified from (Radulescu and Cleveland, 2010).

6.2 Results

6.2.1 Creation of a homozygous NuMA knockout

Zebrafish contain one copy of the *numa* gene. It is 7806bp in length and produces a protein of 2450aa. The gene is made up of 23 exons, 22 of which are coding (Ensembl). Due to the c-terminal playing such an important role in both the microtubule binding and predicted DNA repair function of NuMA, the aim was to try and create a truncation mutant of the full length NuMA. In most cases, targeting the gene as close to the initial start site as possible, yields the best chance of creating a truncated, non-functional protein. However, there is a risk of alternative start sites being utilized by the host, creating a still functional protein. It was therefore decided to target two exons, exon 2 and exon 14 **(Figure 6.2A)**. The former was an attempt to target an N-terminal region to truncate the protein as much as possible. The latter targeted the largest, central exon in which a CRISPR/Ca9 indel would be unlikely to yield a transcript with an alternative start site. Guide RNAs (gRNAs) were designed and selected using Chop Chop (chopchop.cbu.uib.no) and ordered from Sigma Aldrich **(Figure 6.2B)**. The guide RNAs were injected into the one cell stage of LWT embryos with a Cas9 protein. The resultant embryos were checked for abnormalities at 24hpf and several with greying heads, a visual sign of cell death, were visible.

At this point, the Cas9 cleavage in Exon 14 appeared to provide a large range of clear insertions and deletions (indels) via PCR in the injected embryos, indicating a highly likelihood that these embryos will contain an indel creating an early stop codon and significant truncation of NuMA. A selection of injected healthy embryos were raised to adulthood. Genotyping of these adults revealed a selection of indels and two adults with 112bp insertion were selected as heterozygote founders (SH678) **(Figure 6.2C)**. This insertion resulted in a frameshift and an early stop codon situated 5aa downstream of the insertion creating a significantly truncated NuMA protein including removing the c-terminal domain essential for both its functions. The 5aa directly after the insertion will also be changed due to the frameshift.

Given that NuMA has previously been shown to be an essential protein (Silk, Holland and Cleveland, 2009), it was expected that the phenotypes of *numa*$^{-/-}$ embryos would be severely detrimental to survival.

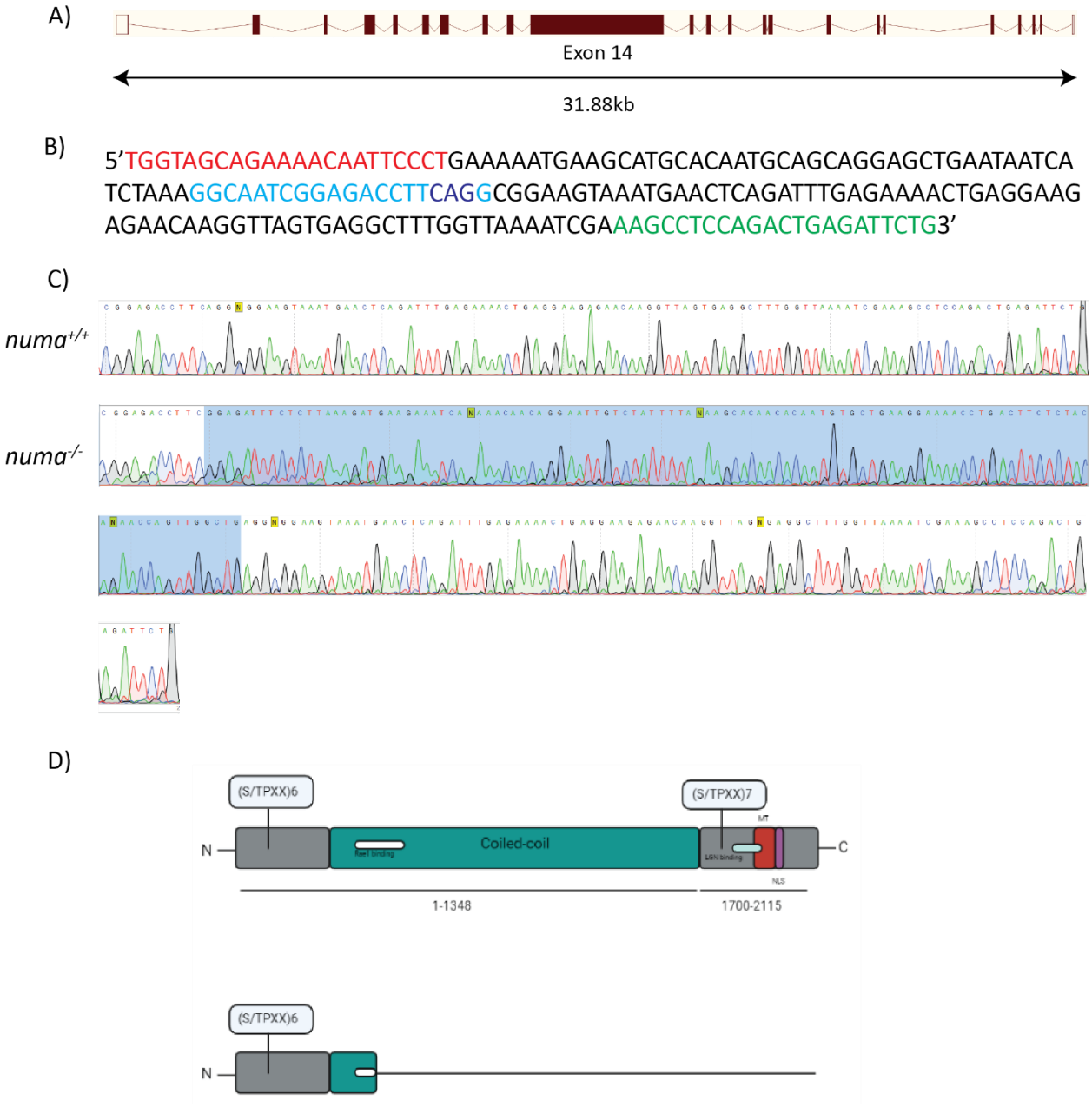

Figure 6.2: Generation of *numa*$^{-/-}$ zebrafish using the CRISPR/Cas9 system

A) Intron-exon structure of zebrafish *numa* (Ensembl, transcript ID:ENSDART00000166209.2). Exon 14 (black) was selected as a target for CRSIPR/Cas9 restriction. **B)** Target sequence within Exon 14 with forward primer (red) reverse primer (green) and gRNA target (blue). The gRNA sequence contained a diagnostic restriction site (dark blue) enabling identification of homozygous mutants. **C)** DNA sequence of the target region in *numa*$^{+/+}$ and the 112bp insertion (blue box) which resulted in a frameshift and premature stop codon 5 amino acids downstream of the insertion and a subsequently truncated protein. **D)** Schematic of full length NuMA protein and truncated version induced via the premature stop codon.

6.2.2 NuMA knockouts have severe abnormalities in neural development

NuMA has been found to be highly expressed in the cerebellum (Ray *et al.*, 2022) and localized to post mitotic Purkinje cells (Radulescu and Cleveland, 2010). Therefore, removal of the NuMA gene was predicted to have a large impact on the neurological function of the zebrafish.

A cross of the two heterozygous adults resulted in offspring with instantly identifiable embryos that showed high levels of cell death in the brains and curly tails (**Figure 6.3A**). These embryos were predicted to be homozygotes as they appeared in a Mendelian ratio but were unable to survive to 5dpf (**Figure 6.3C**). To confirm that this prediction was correct, DNA was isolated from a selection of embryos with a severe phenotype and also from those indistinguishable from wild-types. The region of interest was amplified and after the products were run on a 3% agarose gel, three distinct genotypes could be identified (**Figure 6.3B**). The single band at 180bp is indicative of the $numa^{+/+}$ gene. The three bands in the central lane indicate a $numa^{+/SH678}$ embryos, containing one *wt* allele and one gene containing the 112bp insertion, resulting in a band at 292bp. The middle band is predicted to be a heterodimer, a combination of the PCR products of the $numa^{+/+}$ and mutated alleles. All embryos with a severe phenotype that were selected resulted in just one PCR product at 292bp, concluding that they were homozygotes knockout for *numa*. This enabled confirmation of a genotypic linkage to the observed phenotype. Due to the fact that $numa^{+/+}$ and $numa^{+/SH678}$ are indistinguishable from each other in terms of phenotype, they will be pooled from now on and referred to as the siblings of $numa^{SH678/SH678}$ embryos from a heterozygous incross or, $numa^{sibs}$. Only one mutated allele resulting in a frameshift was able to be identified and therefore all future reference to $numa^{SH678/SH678}$ will be as $numa^{-/-}$. All work was performed on 48hpf embryos due to the phenotype being clear and embryonic death not yet occurring.

The curly tail up (cup) phenotype has previously been associated with spindle defects in zebrafish models (Metzner *et al.*, 2020) and it is hypothesized that the majority of the severity of this phenotype can be linked to the role that NuMA has in cell division via the stabilization of mitotic spindle poles. Loss of this role will also cause large quantities of cell death in $numa^{-/-}$ embryos. However, it has also been found that single strand break repair such as TDP1 are highly expressed in the brain, particularly the cerebellum. Mutations in

humans cause neurological diseases such as SCAN1 (Takashima *et al.*, 2002; El-Khamisy *et al.*, 2005; Ray *et al.*, 2022). This suggests that, given its high levels of expression in the cerebellum, the large quantities of cell death in the brain of the *numa*$^{-/-}$ embryos could also be linked to its role in single strand break repair (Ray *et al.*, 2022).

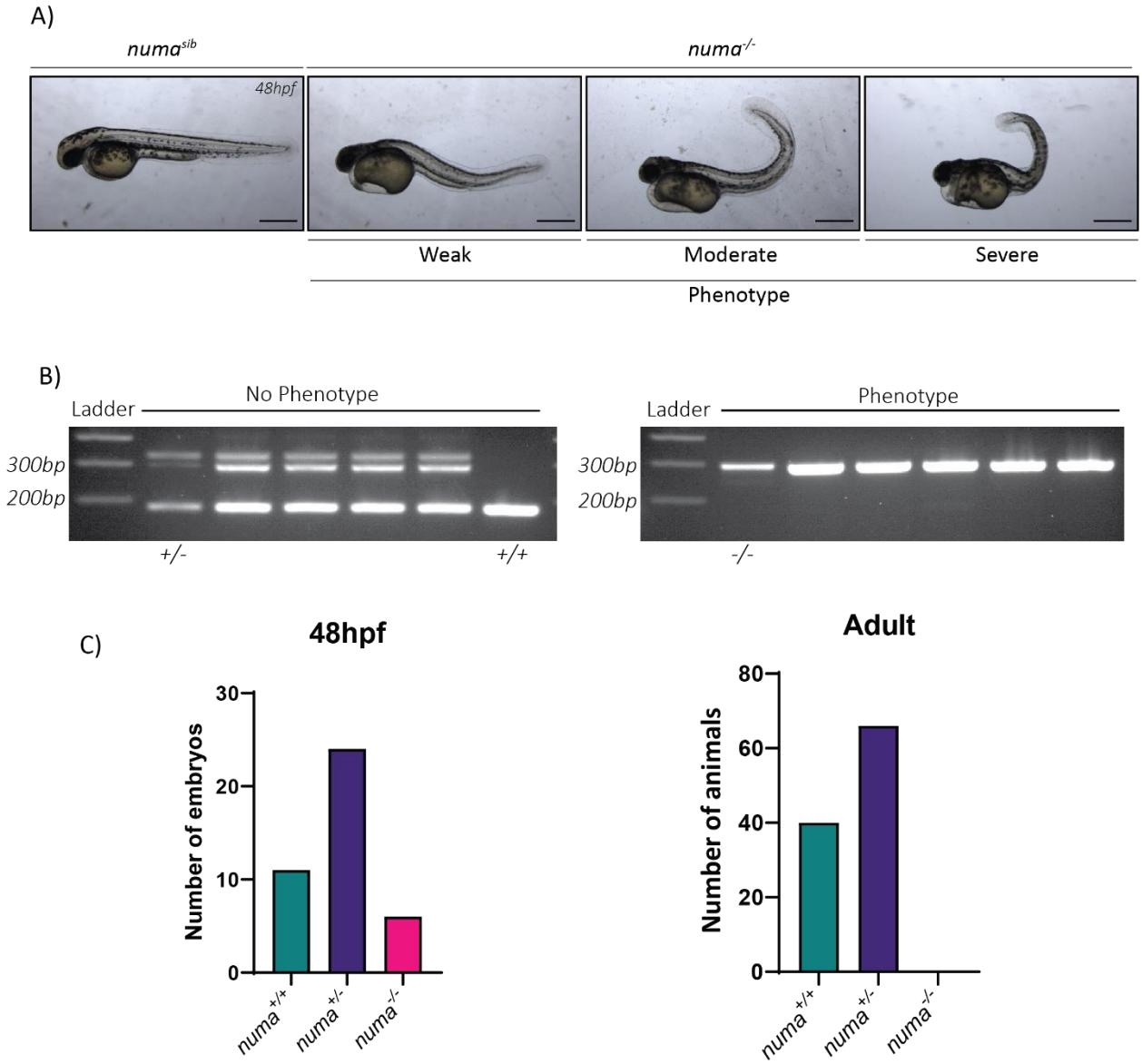

Figure 6.3: *numa*$^{-/-}$ embryos show severe neuronal degeneration and curly tails

(A) 48hpf *numa*$^{-/-}$ embryos show severe neuronal degeneration and curly tails, visible by 24hpf. The majority have died by 4dpf, those that do survive have severe motility issues, no swim bladders and a large volume of yolk remaining which represents a lack of development. Scale bar, 0.5mm. (**B)** Genotypic confirmation of the phenotype in panel A being linked to homozygous mutants via HOTSHOT DNA extraction and PCR. The 112bp insertion is visible via gel electrophoresis. *numa*$^{+/+}$ are displayed as one single lower band (180bp), *numa*$^{-/-}$ are one single higher band (292bp). *numa*$^{+/-}$ display both the *numa*$^{+/+}$ and *numa*$^{-/-}$ bands as well as an additional third band situated above the *numa*$^{-/-}$ band. This is predicted to be a heterodimer of the two. **(C)** Genotyping of embryos at 48hpf show inheritance at a Mendelian ratio. $X^2 = 1.62$, with two degrees of freedom; 2-tailed P value of 0.529. Adult genotypes show lack of survival of *numa*$^{-/-}$.

6.2.3 *numa*$^{-/-}$ embryos have increased apoptosis

One of the main identifiable phenotypes in *numa*$^{-/-}$ embryos is the large quantity of grey cells, visible under a light microscope. These are predicted to be apoptotic, which can be stained with acridine orange (AO) which is taken up into live cells. After staining of 48hpf embryos with acridine orange, it was clear to see a large increase of fluorescence in the *numa*$^{-/-}$ embryos compared with the *numa*^{sibs} **(Figure 6.4A,B)**. This confirms the initial hypothesis that the greying cells seen in the heads of embryos are apoptotic.
Apoptosis of brain cells is severely detrimental to a whole organism and is the phenotype associated with many neurological diseases. Association of the loss of NuMA with such a phenotype correlates with its high levels of cerebellum expression and the associated neurological diseases linked with the loss of other highly expressed cerebella genes such as TDP1 (Takashima *et al.*, 2002; El-Khamisy *et al.*, 2005).

6.2.4 *numa*$^{-/-}$ embryos have an increase in DNA damage

Histones can be found in abundance within the nucleus and are important in the compaction and organization of chromatin (Mariño-Ramírez *et al.*, 2005). Phosphorylated Histone2AX (γH2AX) localizes in particular to dsDNA breaks and signals the recruitment of further repair factors. Therefore, antibodies against γH2AX are an excellent way to identify any changes in the activation of DNA damage repair pathways (Valdiglesias *et al.*, 2013).

Despite *numa* being highly expressed in the brain and the clear morphological phenotypes seen in the heads of early embryos, the quantity of apoptotic cells make the brain a difficult region to perform immunofluorescence. Given the gross phenotypes seen throughout the rest of the embryos, I decided instead to use the tails of 48hpf embryos.

Tails of *numa*$^{-/-}$ and *numa*^{sibs} were stained with an antibody against γH2AX and DAPI to identify the nucleus **(Figure 6.5A).** Visualization of the tails identified an increase in γH2AX foci in *numa*$^{-/-}$ embryos compared with *numa*^{sibs} **(Figure 6.5B)**. Quantification of the number of individual foci per nuclei show a trend increase of foci in *numa*$^{-/-}$ compared with *numa*^{sibs} confirming the visual assumption **(Figure 6.5B)**.

Considering the large quantity of apoptosis occurring in the embryos, an increase in DNA damage is unsurprising. Although the apoptotic cells will primarily be due to errors in mitosis, the levels of DNA damage may lend further support the role of NuMA in DNA repair.

It would also suggest an increase in the expression of genes such as p53 that are involved in the apoptotic and DNA repair pathways.

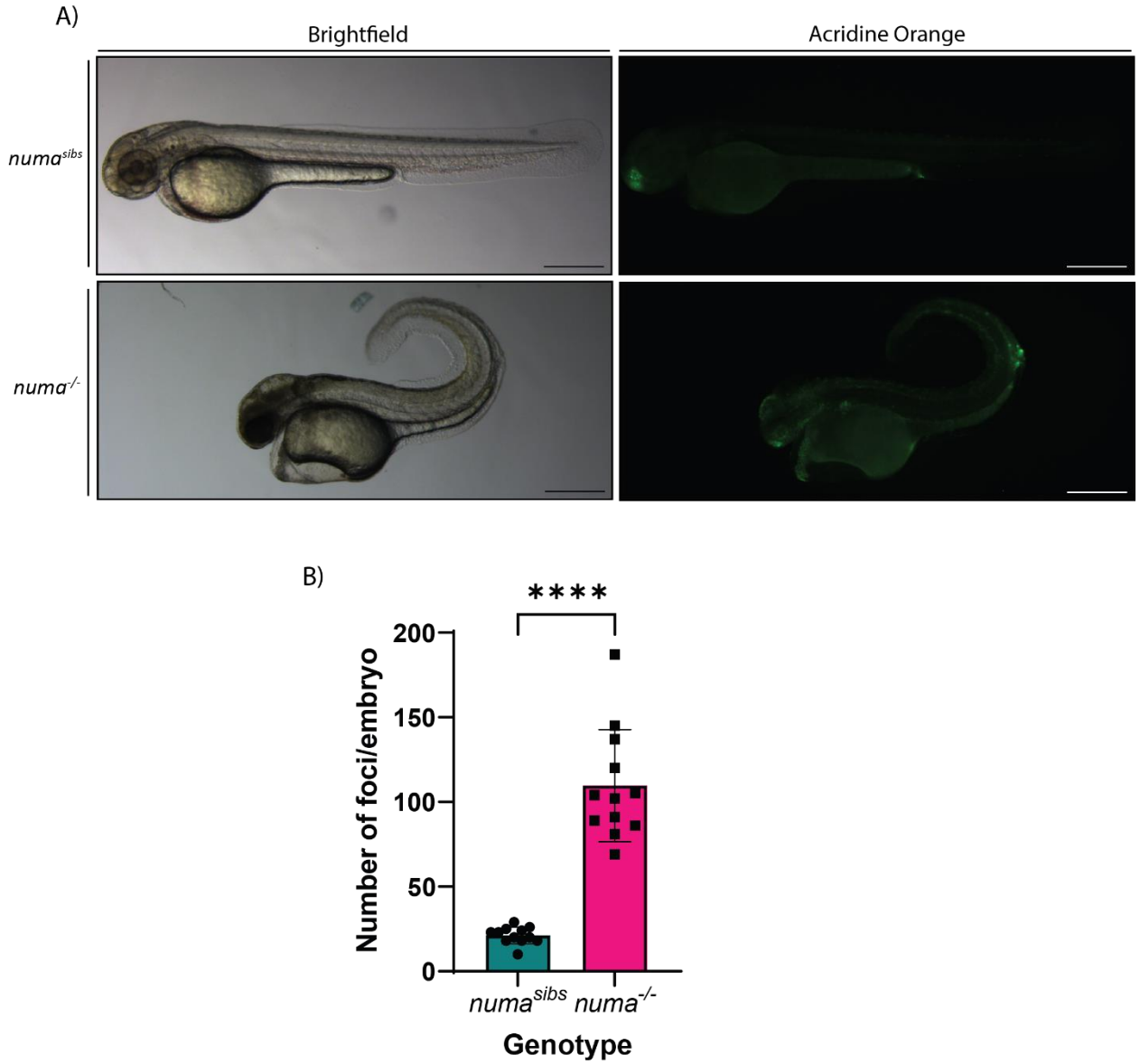

Figure 6.4: *numa*$^{-/-}$ have an increased number of apoptotic cells compared with *numa*^{sibs}

(A) *numa*^{sibs} and *numa*$^{-/-}$ embryos were staining with AO and separated via brightfield analysis of phenotype **(B)** Quantification of apoptotic cells seen in green (AO) with ImageJ. Unpaired t-test performed ****p<0.0001, n=12, individual embryos, ±SD. Scale bar, 0.5mm.

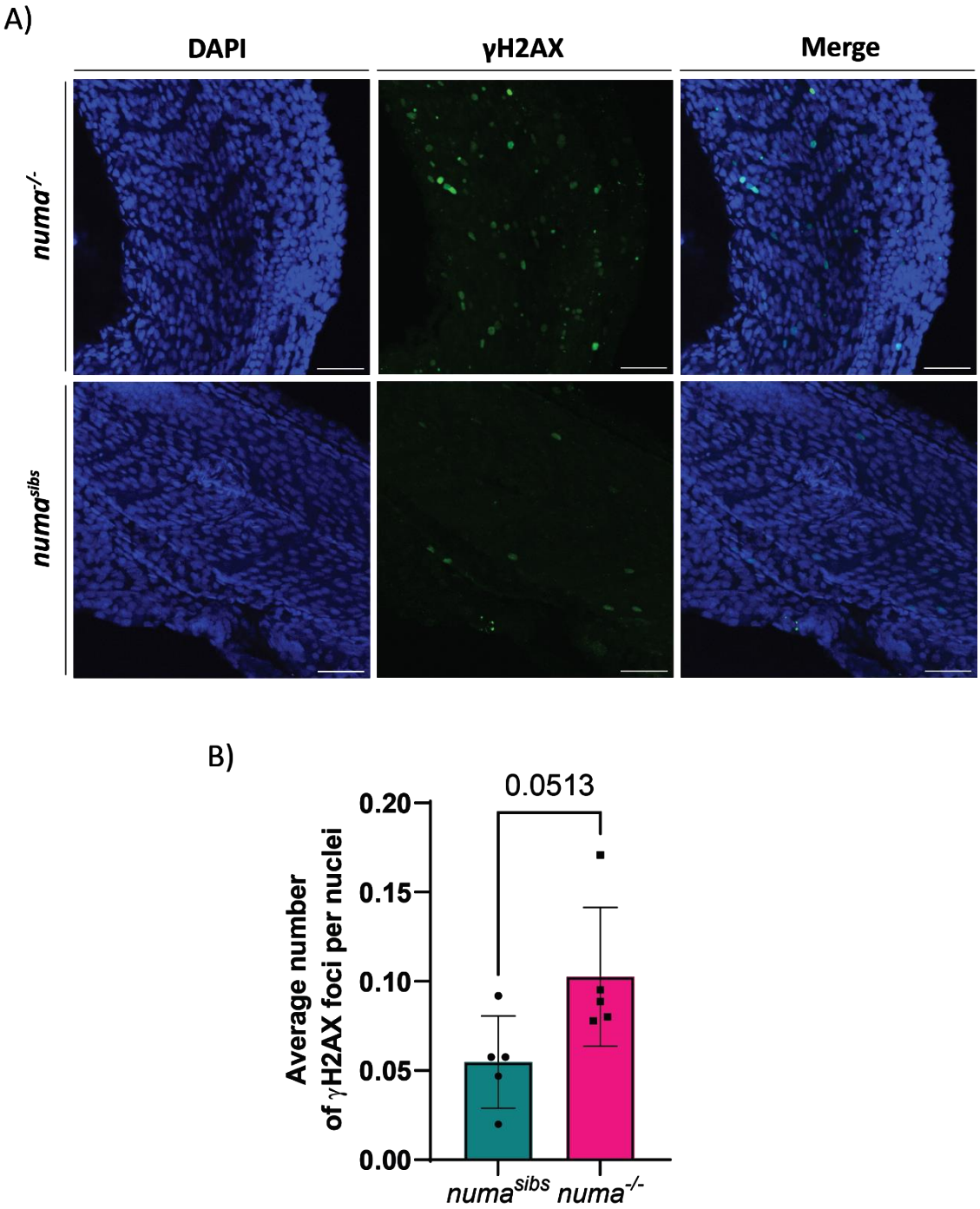

Figure 6.5: *numa*$^{-/-}$ embryos have more γH2AX foci than *numa*^{sibs}

(A) γH2AX staining of a *numa*^{sibs} and *numa*$^{-/-}$ (Green) and nuclear staining (Blue). Scale bar, 50um **(B)** Quantification of γH2AX foci reveals an increase in dsDNA breaks within *numa*$^{-/-}$ embryos at 48hpf. Apoptotic cells excluded during analysis via ImageJ maxima diameter. Only foci within nuclei counted. Unpaired t-test, n=5, individual embryos, p=0.0513, ±SD.

6.2.5 *numa*$^{-/-}$ embryos have increased expression of p53

The tumour suppressor gene, p53, has been implicated in the prevention of cancer formation and thus, is important for maintenance of genome stability in multicellular organisms. p53 has roles in the initiation of apoptosis, prevention of continuation of the cell cycle, activation of downstream factors such as p21 and activation of DNA repair components (He *et al.*, 2005). So, given the large upregulation of γH2AX foci in *numa*$^{-/-}$ embryos, it is predicted that they will also have an upregulation in the expression of Δ113p53.

As predicted, RT-qPCR on 48hpf *numa*$^{-/-}$ embryos also shows a significant, almost 60 fold increase in Δ113p53 expression compared with *numa*^{sibs} embryos **(Figure 6.6A)**. This also correlates with the increase in apoptosis seen in the heads of *numa*$^{-/-}$ as identified earlier **(Figure 6.4A).** This suggests that, upon knockout of NuMA, large quantities of DNA damage occur, activating the p53 response and increasing apoptosis of cells in areas that would have high levels of NuMA expression. This increase in p53 may also have alternative downstream effects.

6.2.6 Increased gene expression of p21 in *numa*$^{-/-}$ suggests senescence present in embryos

One of the main mechanisms in which p53 enables the maintenance of genome integrity is through the stalling of the cell cycle in G1 phase. This is done via activating the transcription of the cyclin dependent kinase (Cdk) inhibitory protein p21. An increase in p21 expression inhibits cdk2 kinases preventing the promotion of cell cycle progression. This stalling allows for the correct repair of damaged DNA before the cell continues in the cell cycle. Upon knockout of NuMA in our zebrafish model, a large increase in p21 expression was identified. **(Figure 6.6B)**. Given the large increase in p53 expression reported earlier, this is predicted to be the pathway by which p21 is upregulated. This supports previous findings from the literature where upon oxidative stress of cells, NuMA has been shown to upregulate P21 expression via p53, helping to stall the cell cycle in order for repair of oxidative damage. (Ohata *et al.*, 2013; Jayaraman *et al.*, 2017).

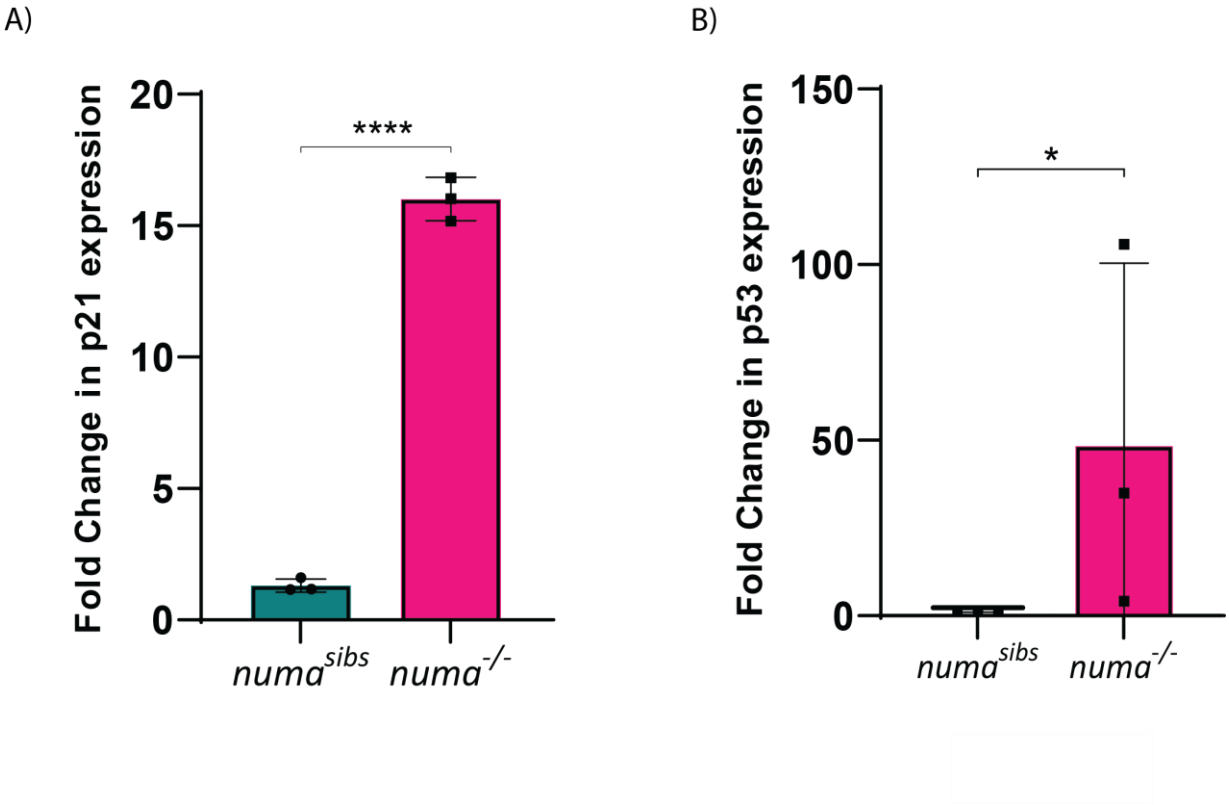

Figure 6.6: *numa*$^{-/-}$ embryos show an increase in p53 and p21 compared with their siblings

(A) 48hpf *numa*$^{-/-}$ embryos show a significant increase in p21 expression after RTqPCR analysis. **(A)** 48hpf *numa*$^{-/-}$ embryos show a significant increase in p53 expression. Unpaired t-test. n=3, 20 pooled embryos, *p<0.01, ****p<0.00001, ±SD

6.2.7 Mass Spectrometry of *numa*$^{-/-}$ embryos reveals an increase in 8 oxo-guanine sites

Oxidative damage is primarily caused by reactive oxygen species (ROS) that are generated as a natural by-product of metabolism. The most commonly oxidized DNA base is Guanine, leading to the creation of 7,8-dihydrro-8-oxoguanine (8-oxoG) (Margolin *et al.*, 2006). These oxidized bases can result in the mismatch pairing of subsequently replicated DNA and are therefore targeted for repair (Substitutions *et al.*, 1992). Repair of 8-oxo-guanine sites occurs via 8-oxoguanine DNA glycosylase (OGG1) which converts the 8-oxo-guanine sites to apurinic and apyrimidinic (AP) sites that are then subsequently repaired by single strand break repair components, including TDP1 (El-Khamisy *et al.*, 2005). It has been noted however, that these 8-oxo-guanine sites are also found in abundance at guanine rich promoter regions and are heavily involved in the regulation of pro-inflammatory genes (Pan *et al.*, 2016; Fleming, Ding and Burrows, 2017). Recent reports have implicated NuMA in the regulation and repair of oxidative damage at these gene regulatory elements (Ray *et al.*, 2022).

Three biological replicates of DNA from *numa*^{sibs} and *numa*$^{-/-}$ were isolated and underwent analysis via HPLC-QQQ mass spectrometry in the Kriaucionis lab at the University of Oxford. It was found that there was a significant increase in the number of 8-oxo-guanine sites in *numa*$^{-/-}$ embryos compared with their siblings **(Figure 6.7)**. This supports the hypothesis that NuMA is involved in the removal of oxidative DNA damage, potentially at the regulatory elements of inflammatory response genes using an *in vivo* whole organism.

6.2.8 Increased expression of inflammatory genes in *numa*$^{-/-}$ embryos

Removal of oxidative damage such as 8-oxoG is important for the maintenance of DNA stability. It has been previously shown that 8-oxoG sites in gene regulatory regions interact with and are removed by OGG1 in both nuclear and mitochondrial DNA (Hazra *et al.*, 1998). An increase in 8-oxo-G sites has been implicated with the premature aging phenotype of the neurodegenerative disorder Cockayne syndrome (Stevnsner *et al.*, 2002) and mouse models have displayed an upregulation in inflammatory response markers (Kajitani *et al.*, 2021).

Mutations in OGG1 were suspected to show a marked increase in 8-oxoG sites and this was positively identified in OGG1-deficient mice (Klungland *et al.*, 1999; Minowa *et al.*, 2000). Surprisingly however, despite this increase in 8-oxoG sites, the mice only showed moderate phenotypes with no significant difference in their lifespan and have no significant

upregulation in inflammatory response markers (Mabley *et al.*, 2005; Touati *et al.*, 2006; Li *et al.*, 2012; Bacsi *et al.*, 2013). It was also identified that, *in vivo*, they were still able, albeit slowly, to remove 8-oxo-G sites (Klungland *et al.*, 1999). This lead to the prediction that there was a secondary mechanism of removal of these sites, allowing for a slow accumulation over time rather than a dramatic increase that would overwhelm individual cells, promoting apoptosis and clinical malignancies.

It has also been shown that the repair of 8-oxoG sites by OGG1 promotes the expression of proinflammatory molecules and the innate immune system (Aguilera-Aguirre *et al.*, 2014) via activation of the NF-κB pathway. It has also been identified that inhibition of OGG1 by a small molecule has anti-inflammatory effects (Visnes *et al.*, 2018).

The hypothesis emerged that there would also be an increase in inflammatory response markers due to the predicted 8-oxoG sites present at their promoters. RTqPCR analysis of IL-6 and TNFα revealed an increase in expression in *numa*$^{-/-}$ embryos **(Figure 6.8A,B)**. Although these results are not significant, this can be explained by the large range of phenotypes seen within *numa*$^{-/-}$ embryos **(Figure 6.3A)**. The variation in apoptosis in the brains and severity of their curly tail phenotype is predicted to be responsible for the range of gene expression levels seen in the RTqPCR data.

The prediction is that NuMA is part of the pathway that facilitates the removal of 8-oxoG sites, subsequently leading to the increased activation of OGG1 in an attempt to remove these sites and causing an upregulation of inflammatory response genes in *numa*$^{-/-}$embryos compared with *numa*^{sibs}.

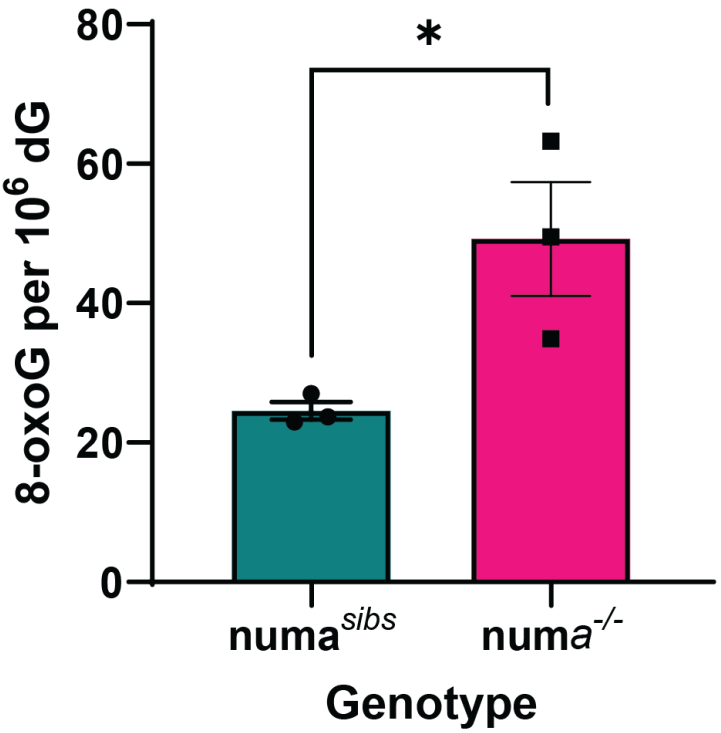

Figure 6.7: numa$^{-/-}$ embryos show an increase in 8-oxo-G sites compared with their siblings

Proteinase K DNA extraction from 48hpf embryos collected from *numa*$^{+/-}$ parents. *numa*^{sibs} and *numa*$^{-/-}$ were separated based on phenotype before extraction of genomic DNA. Samples underwent HPLC-QQQ Mass Spectrometry. Data calculated as 8OG/dG ppm. Unpaired t-test, *p<0.05, n=3, 10 pooled embryos, ±SD.

My thanks to the members of the Kriaucionis Lab at the University of Oxford for performing the Mass Spectrometry analysis.

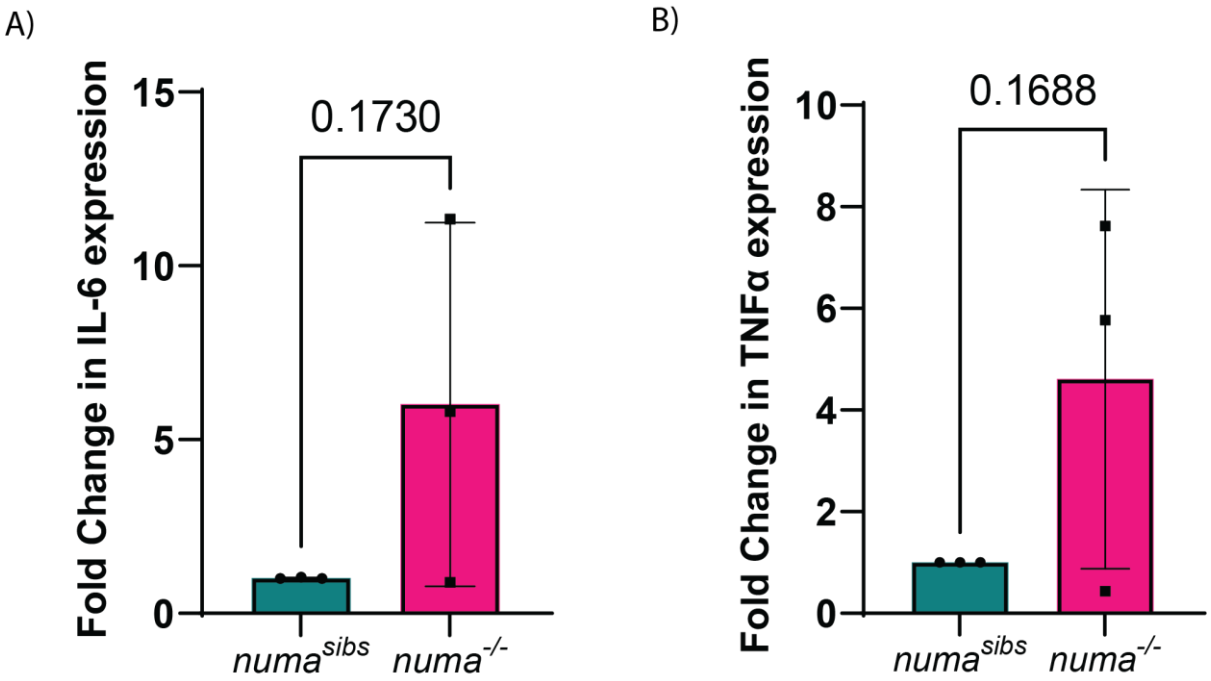

Figure 6.8: *numa*$^{-/-}$ embryos show a mild increase in the inflammatory markers IL-6 and TNFα compared with their siblings

48hpf embryos show a mild increase in inflammatory markers **(A)** IL-6 and **(B)** TNFα. Due to the large spread of expression measured, likely due to the range of phenotypes seen, they are not statistically significant but do show a trend increase. n=3, 20 pooled embryos, Unpaired t-test, p>0.05, ±SD.

6.3 Discussion

NuMA has long been known as a component of the nuclear apparatus, stabilizing spindle poles during mitosis (Lydersen and Pettijohn, 1980; Kallajoki *et al.*, 1993). More recently, it has also been shown to interact with single strand break repair factors such as TDP1 and recruit repair factors to DNA containing oxidative damage at gene regulatory elements (Ray *et al.*, 2022)

6.3.1 Knockout of NuMA *in vivo* recapitulates the *in vitro* role in oxidative stress

During this chapter I have described the creation of *numa*$^{-/-}$ zebrafish line. The resultant embryos display large quantities of apoptosis in their brain and have a curly tail phenotype that correlates with the embryonic lethality of most embryos by 4dpf **(Figure 6.3)**. This is concurrent with descriptions in the literature of the NuMA gene being essential in eukaryotic cells due to its significant role in mitosis (Harborth *et al.*, 2001; Silk, Holland and Cleveland, 2009). Increased DNA damage is also seen in *numa*$^{-/-}$ embryos **(Figure 6.5)**, supporting the proposal that NuMA is involved in DNA repair (Vidi *et al.*, 2014; Moreno *et al.*, 2019). More specifically, NuMA has shown involvement in the repair of single-strand breaks, shown to occur via interaction with other single strand break repair factors such as TDP1, XRCC1 and PARP1 (Ray *et al.*, 2022). An increase of 8-oxo-guanine sites was established in *numa*$^{-/-}$ zebrafish **(Figure 6.7)** that corroborates the finding that a loss of NuMA results in the accumulation of the oxidative damage sites, even without exposure to ROS inducing agents such as H_2O_2. In the presence of NuMA and oxidative stress, a sub-set of NuMA regulated genes (NRGs) have been identified that are required for recovery from oxidative stress and are down regulated upon NuMA depletion. These include SSBR factors such as TDP1, XRCC1 and FEN1. In future, it will be interesting to study any potential NRGs to identify whether this phenomenon is also corroborated *in vivo*. A mild increase in inflammatory response genes was also identified. The range of expression is initially thought to be due to the range of phenotypes established in *numa*$^{-/-}$ embryos. In future, increased sample numbers or the selection of specific phenotypic groups may help to reduce this variability.

6.3.2 *In vivo* analysis of NuMA as a nuclear matrix protein

Upregulation of p21 was also identified in the *numa*$^{-/-}$ embryos **(Figure 6.6A,B)**. Since the identification that NuMA localizes to the interphase nucleus, one theory is that it could

somehow be involved in the structural organization in a nuclear matrix form has been discussed (Radulescu and Cleveland, 2010). One of the front runners in the search for a nuclear matrix candidate is the nuclear lamins, particularly Lamin A. Mutations in lamins can lead to defects in cell proliferation, apoptosis and senescence (Dechat *et al.*, 2010). More specifically, mutations in Lamin A have been associated with degenerative disorders such as Emery-Dreifuss muscular dystrophy, neuropathies and the premature aging phenotype of Hutchinson-Gilford progeria syndrome (HGPS) (Bonne *et al.*, 1999; Rankin and Ellard, 2006). A zebrafish model for Hutchinson-Gilford progeria syndrome in which they knocked down Lamin A has been produced and it was shown that there was a large increase in p21 expression and an increase in senescent cells using a SA-βGal staining assay (Koshimizu *et al.*, 2011). Given the increased expression of p21 in the *numa*$^{-/-}$ embryos compared with their siblings, it could be suggested that NuMA may play a role in the organisation of the nuclear matrix, in a similar way to Lamin A. To further investigate this theory, SA-βGal staining would need to be performed in *numa*$^{-/-}$ embryos compared with their siblings.

6.3.3 Separation of NuMA functions allowing, link between phenotype and role

One of the largest drawbacks of the research described in this chapter is the inability to separate the two main functions of NuMA. Previous literature describes the role of NuMA in cell division in detail with more recent research outlining the DNA repair aspect to this large protein. Given the essential functions of this protein in eukaryotic cells, it is hard to definitively place any of the phenotypes seen as being due to the DNA repair role. Previous attempts to rescue the phenotypes seen in *numa*$^{-/-}$ embryos including mRNA injection and plasmid insertion via the Tol2 system have so far been unsuccessful. Firstly, a rescue via a full length NuMA construct would confirm that the phenotypes seen are due to the lack of NuMA. Secondly, rescue by a domain that supports DNA repair (Ray *et al.*, 2022) would allow a link between the DNA damage role of NuMA and the phenotypes associated. The repair domain is situated in the globular c-terminal end which has been found to be essential for binding to TDP1 (Palazzo *et al.*, 2018; Hendriks, Larsen and Nielsen, 2019).

6.3.4 Summary

In summary, I have developed a knockout of *numa* in the model organism *D.rerio* that shows severe developmental phenotypes and increased oxidative damage. Once a rescue has been shown via the re-introduction of NuMA, it will give confidence to the phenotypes described

in this chapter. Re-introduction of the c-terminal domain in particular will allow the separation of the cell division and DNA repair roles of NuMA. This model paves the way for the study of NuMA and confirms the previously described *in vitro* roles *in vivo*.

Chapter 7
General Discussion

7.1 Overview

Faithful transmission of genetic material is essential for organisms to reproduce and survive. DNA can be damaged by both internal and external sources which are, to some extent, unavoidable. The majority of lesions created are repaired by the interlinking DNA damage response systems. However, if there are mutations in key damage response components it can lead to neurological disease, premature aging and immunodeficiency.

One of the most common lesions is the incorporation of ribonucleotides. These are significantly more unstable than deoxyribonucleotides and can lead to spontaneous breakage of DNA stands via their 5'OH group (Li and Breaker, 1999). Removal of ribonucleotides usually occurs via the Ribonucleotide Excision Repair pathway, of which RNaseH2 is a key component. Mutations in any of the three subunits of RNaseH2 has been shown to cause the severe neuroinflammatory disorder, Aicardi-Goutières Syndrome (Goutières *et al.*, 1998).

Current *in vivo* models to study AGS have all shown embryonic lethality upon knockout of RNaseH2 subunits (Hiller *et al.*, 2012; Reijns *et al.*, 2012; Pokatayev *et al.*, 2016; Bartsch *et al.*, 2018; Uehara *et al.*, 2018). This recapitulates the severe form of AGS but does not allow for investigation of the molecular consequences *in vivo*. It has also been shown that, in the absence of RNaseH2, topoisomerase 1 has a key role in the removal of ribonucleotides, although in a mutagenic fashion.

The aim of this thesis was to characterise the RNaseH2a knockout zebrafish line previously created in the lab that, unlike previous *in* vivo knockout models, are viable to adulthood. Secondly, I would investigate why they are viable, and why this is in contradiction to other *in vivo* models. Thirdly, I would investigate the reason for survival of the *tdp1*$^{-/-}$ line previously established in the lab through the use of CRISPANTs and drug screening. Finally, I aimed to create a novel *in vivo* knockout model of the recently identified TDP1 interaction partner, NuMA. I would then characterise this knockout and draw comparisons with the previously identified *in vitro* role of NuMA in DNA repair (Ray *et al.*, 2022).

7.2 Lessons from RNaseH2a knockout zebrafish

In Chapter 3 I described an *in vivo* zebrafish knockout of the A subunit of the heterotrimeric protein RNaseH2. Here I showed that *rnaseh2a*$^{-/-}$ zebrafish are viable to adulthood at which point they display a mild locomotive phenotype **(Figure 3.4, 3.23)**. The overall survival of these knockout zebrafish is in contradiction to previous RNaseH2a knockout mouse models (Hiller *et al.*, 2012; Reijns *et al.*, 2012; Pokatayev *et al.*, 2016; Bartsch *et al.*, 2018; Uehara *et al.*, 2018) which all show embryonic lethality. The initial hypothesis included several options: A) The fish have a compensatory mechanism of single ribonucleotide removal that is upregulated in the absence of RNaseH2. B) They can tolerate high levels of ribonucleotides C) The maternal contribution of RNaseH2a allows them to survive through the larval stages of cell division.

Data presented in this thesis shows that the offspring of any *rnaseh2a*$^{-/-}$ adults zebrafish were embryonic lethal **(Figure 3.16)**. They also showed an increase in rNMP incorporation **(Figure 3.10)**, an increase in DNA damage **(Figure 3.12)** and significant upregulation of interferon stimulated genes (ISGs) **(Figure 3.19)**. These results are more consistent with previous *in vivo* models that demonstrate similar phenotypes (Hiller *et al.*, 2012; Reijns *et al.*, 2012; Pokatayev *et al.*, 2016; Bartsch *et al.*, 2018; Uehara *et al.*, 2018). It also agrees with studies in yeast that show an increase in rNMP incorporation upon the knockout of RNaseH2 (*rnaseh201)*.

I have also identified an increase in the number of rNMPs incorporated into the DNA from 5dpf to adulthood in *rnaseh2a*$^{-/-}$ zebrafish **(Figure 3.11)** but this does not correlate with an increase in DNA damage **(Figure 3.13, 3.14)**. It does however correlate with a unique paternal (*Prnaseh2a*) phenotype resulting from an *rnaseh2a*$^{-/-}$ male and *rnaseh2a*$^{+/+}$ female that resulted in an even more severe development defect than maternal zygotic (*Mzrnaseh2a*) embryos **(Figure 3.16)**. This was predicted to be due to an increase of rNMPs in the sperm of the male coming into contact with an active RNaseH2 protein from the female, resulting in high levels of DNA fragmentation as it tries to repair the large quantities of rNMPs. This is a phenomenon also seen in yeast and has been coined ribodysgenesis (Sui *et al.*, 2022). It also appeared to be exacerbated in embryos from older adults, suggesting the accumulation of ribonucleotides in their DNA increased over time **(Figure 3.22)**.

7.2.1 Investigation of secondary removal mechanisms

In Chapter 4 I aimed to identify the molecular reasoning behind the survival of *rnaseh2a*$^{-/-}$ zebrafish by investigating the predicted secondary repair pathways. Increased incorporation of rNMPs via hydroxyurea treatment did not adversely affect the *rnaseh2a*$^{-/-}$ embryos which is in agreement with there being a secondary mechanism of removal that is highly active in embryos **(Figure 4.1)**.

The most well studied secondary rNMP repair mechanism is that performed by TOP1. This topoisomerase can cleave single ribonucleotides but tends to do so in an error prone manner (Reijns *et al.*, 2022). Treatment with a topoisomerase inhibitor (CPT) did not show any significantly detrimental phenotype in *rnaseh2a*$^{-/-}$ embryos compared with *rnaseh2a*$^{+/+}$ suggesting that it did not cause a significant increase in TOP1-cc's in *rnaseh2a*$^{-/-}$ zebrafish and that TOP1 may not be the primary mechanism of repair **(Figure 4.2)**.
Cell lines deficient in RNaseH2a have also shown synthetic lethality with PARP and ATR inhibitors and APEX2 knockout, all involved in single strand break repair after TOP1 removal of rNMPs. I found that, in contrast to previous studies, neither of these inhibitors nor knockout of APEX2 created a significant phenotype in the *rnaseh2a*$^{-/-}$ zebrafish at 5dpf **(Figure 4.3, 4.4, 4.5)**.

7.2.2 Future directions utilising the RNaseH2a knockout zebrafish

Previous work in an RNaseH2b knockout mouse line (*rnaseh2b*$^{Nes\text{-}cre}$) also identified an upregulation of inflammatory response genes and DNA damage markers. They also observed the decreased size of the cerebellum compared with controls (Aditi *et al.*, 2021). To determine the cause of this neuropathology, they knocked out *cGAS* to produce *rnaseh2b*$^{Nez\text{-}cre}$*;cGAS*$^{-/-}$ mice, reducing their inflammatory response. These did not show a rescue in the size of their cerebellum, therefore concluding that the neuropathology is mainly driven by the increase in DNA damage, rather than inflammation.

Given the upregulation of both ISGs and DNA damage events, it would be interesting to investigate which, if either, is more responsible for the detrimental phenotype seen in *Mzrnaseh2a* embryos. Despite attempts to treat with STING inhibitors, create CRISPANT STING mutants and morpholino injections to knockdown STING, none were successful in reducing the expression levels of ISG15 in the *Mzrnaseh2a* embryos. This may be due to the severity of their phenotype before manipulation and may limit studies surrounding this

area. This could potentially be approached instead by the induction of inflammation in *rnaseh2a*$^{-/-}$ embryos from a heterozygous cross.
Another interesting investigation would be whether the *rnaseh2a*$^{-/-}$ adults that already have increased rNMP incorporation are more sensitive to HU treatment compared with their *rnaseh2a*$^{+/+}$ siblings. If this was the case then the repair mechanism may have higher activity in developing embryos that in aged adults.

It would also be useful to quantify the number of TOP1-cc's produced after treatment of *rnaseh2a*$^{-/-}$ with CPT to confirm what only a predicted increase is currently identified. Also, to investigate whether simultaneous treatment with HU and CPT would be more detrimental to *rnaseh2a*$^{-/-}$ embryos compared with their siblings due to the combined increase of rNMPs and lack of potential repair mechanisms such as the formation and resolution of TOP1-cc's.

Again, treatment of *rnaseh2a*$^{-/-}$ after APEX2 knockout with HU may reveal that with increased rNMPs a phenotype may be present upon the removal of a secondary repair mechanisms. This would also be interesting to study into adulthood.
Investigation into the potential compensatory mechanisms allowing for the survival of *rnaseh2a*$^{-/-}$ embryos should also be prioritised. The small size and large numbers of offspring produced by zebrafish lends them to be a good *in vivo* model for large scale drug screening. Here the use of embryos from an *rnaseh2a*$^{+/-}$ cross would also for the blind selection of embryos effected by inhibitors of potential ribonucleotide removal candidates. Any hits identified could then be used as CRISPANT targets in *rnaseh2a*$^{-/-}$ embryos or in the creation of full double knockouts using the CRISPR/Cas9 system. Characterisation of these double knockouts and investigation of their sensitivity to increased ribonucleotide load via treatment with HU would allow for the identification of secondary mechanism involved in the removal if single ribonucleotides in the absence of RNaseH2a.

In the literature, RNaseH2 has a defined role in the resolution of RND:DNA hybrids (R-loops). As we have seen that *rnaseh2a*$^{-/-}$ embryos are able to remove single ribonucleotides, despite a lack of RNaseH2, it would be interesting to use S9.6 IF and S9.6 slot blot analysis to investigate the levels of R-loops present in the RNaseH2a knockout and see if these differ to their wild-type siblings. The creation of the Ribonucleotide Excision Defective (*RNaseH2a*^{RED}) line allowed for the separation of the two functions of RNaseh2a in mice (Uehara *et al.*,

2018). If R-loops appear to be upregulated, particularly in *Mzrnaseh2a* embryos, creation of this separation of function mutant would allow for the main candidate of their embryonic lethality to be identified.

Finally, the increased severity of the embryonic phenotype from aged adults may suggest a premature aging phenotype. I have already shown a mild locomotive phenotype in *rnaseh2a*$^{-/-}$ adults compared with their *rnaseh2a*$^{+/+}$ siblings. If repeated at stages throughout the life of the zebrafish (6 months, 12 months, 18 months, 24 months) it may be possible to identify if this phenotype is exacerbated with age. The same time points can be used to deduce whether the embryos produced by aged adults continue to decline in their ability to develop.

7.3 Lessons from TDP1 knockout zebrafish

As described earlier, TDP1 is required for the removal of TOP1 covalent complexes that have become irreversibly attached to the DNA after release of torsional stress or removal of single ribonucleotides. Mutation of TDP1 in humans cause the neurodegenerative disorder SCAN1. On one hand, *tdp1*$^{-/-}$ mice show mild cerebellar degradation and sensitivity to TOP1 poisons, similar to the human phenotype (Hirano *et al.*, 2007; Katyal *et al.*, 2007; Hawkins *et al.*, 2009) but on the other hand, knockouts in *A.thaliana* and yeast models show no sensitivity (Liu, Pouliot and Nash, 2002; Vance and Wilson, 2002; Deng *et al.*, 2005; Enderle *et al.*, 2019).

Recent work in our lab has produced a *tdp1*$^{-/-}$ zebrafish model that demonstrates no sensitivity to TOP1 poisons at a larval level but a mild effect is seen in adults, showing similarities to both results shown previously. This suggested an alternative mechanism of TOP1-cc repair was occurring at the larval stage. Two genes, *apex2 and ercc4* were found to be upregulated in *tdp1*$^{-/-}$ embryos (Zaksauskaite *et al.*, 2021).

I utilised the CRISPANT technique to produce first generation knockouts of APEX2 and ERCC4. Although no difference was seen in their overall morphology with just the knockout, after treatment with CPT, mild locomotion phenotypes were seen in both cases **(Figure 5.1, 5.2).** This correlates with the mild upregulation seen in both genes through microarray analysis (Zaksauskaite *et al.*, 2021).

In the case of the APEX2 embryos in particular, the significance in movement came from a few highly active embryos in the control **(Figure 5.1)**. This result could be further qualified via the creation of a full APEX2 zebrafish knockout in the *tdp1*$^{-/-}$ background. Although mild effects were seen in both APEX2 and ERCC4 knockouts, neither appear to be totally responsible for the lack of sensitivity to TOP1 poisons by *tdp1*$^{-/-}$ larvae. Triple knockouts are possible in zebrafish so it may be interesting to investigate the effect of removing both APEX2 and ERCC4 in *tdp1*$^{-/-}$ zebrafish. Alternatively, there may be a further mechanism of repair that could be identified through large scale drug screening that could then be used a kits in CRISPANT analysis or CRISPR knockout targets.

The results of the microarray performed in (Zaksauskaite *et al.*, 2021) also suggest that

there may not be one pathway that is compensating but a mild upregulation of many factors, all contributing to the overall phenotype.

7.4 Lessons from NuMA knockout zebrafish

NuMA has recently been identified as a novel interaction partner of TDP1. It has a previously well-defined role in the formation and maintenance of mitotic spindles and knockout of NuMA has been shown to cause embryonic lethality in mice (Silk, Holland and Cleveland, 2009). The recent analysis performed by the El-Khamisy lab demonstrated a new role of NuMA in single strand break repair and the regulation of genes involved in the repair of oxidative damage (Ray *et al.*, 2022).

In this thesis I have described a new *in vivo* $numa^{-/-}$ model. In contrast to previous animal models, the $numa^{-/-}$ embryos are able to survive to 4dpf. However, up until lethality they demonstrate severe neurological damage and curly tails **(Figure 6.3)**. I have also identified an increase in oxidative damage sites, namely 8-oxoG in $numa^{-/-}$ embryos **(Figure 6.7)**, in agreement with previous *in vitro* analysis as well as a mild upregulation in inflammatory response genes IL-6 and TNFα **(Figure 6.8)** (Ray *et al.*, 2022).

7.4.1 Future directions utilising the NuMA knockout zebrafish

One of the key future experiments will be to rescue the phenotype seen in $numa^{-/-}$ embryos via the reintroduction of a wild-type NuMA. Previous rescue attempts including the microinjection of mRNA and plasmid containing a CMV promoter were unsuccessful. Although expression occurred, it was in a mosaic fashion and no difference in the overall phenotype was observed. Utilisation of the Tol2 system may be possible, causing the integration of *numa* into the $numa^{-/-}$ embryos. However, again this is likely to be a mosaic integration and may not rescue the severe developmental phenotype. Raising of $numa^{+/-}$ zebrafish and crossing to produce $numa^{-/-}$ resupplied with wild-type NuMA may produce a rescue of the $numa^{-/-}$ phenotype. One of the main challenges with this is the size of wild-type NuMA. At over 7KB the insertion of *numa* may disrupt other genes, masking any benefit provided by its insertion. However, analysis with various truncated versions would allow for the integration of smaller DNA fragments. This would also allow the investigation of ineffective DNA repair and TDP1 binding whilst maintaining the mitotic spindle function allowing cell division.

Investigation into the expression profile of genes predicted to be regulated by NuMA (NRGs) (Ray *et al.*, 2022) would go further to validating the $numa^{-/-}$ as an *in vivo* model that reliably reproduces previously identified results *in vitro.*

Use of this model in the future will be valuable in validating *in vitro* findings in an *in vivo* setting, isolation of individual functions of NuMA as its characterisation as a DNA repair factor continues and as a model for the effect of oxidative stress in a whole organism.

7.5 Summary

In summary, I have created and/or characterised several novel zebrafish models to investigate the role of ribonucleotide removal and its associated factors. Firstly, I have identified the unusual ability of first generation *rnaseh2a*$^{-/-}$ zebrafish to survive to adulthood, unlike previous models, and discovered a second generation lethality via an increased inheritance of ribonucleotides and ribodysgenesis. I have also shown that a build-up of ribonucleotides may be occurring over the lifetime of *rnaseh2a*$^{-/-}$ zebrafish. This will require analysis of further time points but may be an indication of premature aging, allowing the utilisation of this model for further disease analysis. I have also identified partial secondary repair mechanisms of TOP1-cc's via APEX2 and ERCC4 in the absence of TDP1. Finally, I have produced a novel *in vivo* NuMA knockout zebrafish and used it to validate findings such as increased oxidative damage and expression of inflammatory response genes seen only before *in vitro*. Further utilisation of this model will help to confirm these findings and investigate the molecular role of NuMA in DNA repair.

All three models will allow the investigation of the molecular causes of DNA repair related human disease via the utilisation of *in vivo* models.

References

Abel, L. *et al.* (1919) *Bell Blair, ' The Pituitary*, *Lieben, ' Centralblatt f. Physiol*. Hooker. Available at: https://royalsocietypublishing.org/.

Abrams, J.M. *et al.* (1993) 'Programmed cell death during Drosophila embryogenesis', *Development*, 117(1), pp. 29–43. Available at: https://doi.org/10.1242/DEV.117.1.29.

Aditi *et al.* (2021) 'Genome instability independent of type I interferon signaling drives neuropathology caused by impaired ribonucleotide excision repair', *Neuron*, 109(24), pp. 3962-3979.e6. Available at: https://doi.org/10.1016/j.neuron.2021.09.040.

Aguilera-Aguirre, L. *et al.* (2014) 'Innate Inflammation Induced by the 8-Oxoguanine DNA Glycosylase-1–KRAS–NF-κB Pathway', *The Journal of Immunology*, 193(9), pp. 4643–4653. Available at: https://doi.org/10.4049/JIMMUNOL.1401625.

Aguilera, A. and García-Muse, T. (2012) 'R Loops: From Transcription Byproducts to Threats to Genome Stability', *Molecular Cell*, 46(2), pp. 115–124. Available at: https://doi.org/10.1016/J.MOLCEL.2012.04.009.

Alexandrov, L.B. *et al.* (2020) 'The repertoire of mutational signatures in human cancer', *Nature 2020 578:7793*, 578(7793), pp. 94–101. Available at: https://doi.org/10.1038/s41586-020-1943-3.

Álvarez-Quilón, A. *et al.* (2020) 'Endogenous DNA 3' Blocks Are Vulnerabilities for BRCA1 and BRCA2 Deficiency and Are Reversed by the APE2 Nuclease', *Molecular cell*, 78(6), pp. 1152-1165.e8. Available at: https://doi.org/10.1016/J.MOLCEL.2020.05.021.

Babin, P.J., Goizet, C. and Raldúa, D. (2014) 'Zebrafish models of human motor neuron diseases: advantages and limitations', *Progress in neurobiology*, 118, pp. 36–58. Available at: https://doi.org/10.1016/J.PNEUROBIO.2014.03.001.

Bacsi, A. *et al.* (2013) 'Down-regulation of 8-oxoguanine DNA glycosylase 1 expression in the airway epithelium ameliorates allergic lung inflammation', *DNA repair*, 12(1), pp. 18–26. Available at: https://doi.org/10.1016/J.DNAREP.2012.10.002.

Bai, P. (2015) 'Biology of Poly(ADP-Ribose) Polymerases: The Factotums of Cell Maintenance', *Molecular cell*, 58(6), pp. 947–958. Available at: https://doi.org/10.1016/J.MOLCEL.2015.01.034.

Balk, B. *et al.* (2013) 'Telomeric RNA-DNA hybrids affect telomere-length dynamics and senescence', *Nature Structural & Molecular Biology 2013 20:10*, 20(10), pp. 1199–1205. Available at: https://doi.org/10.1038/nsmb.2662.

Bartsch, K. *et al.* (2017) 'Absence of RNase H2 triggers generation of immunogenic micronuclei removed by autophagy', *Human Molecular Genetics*, 26(20), pp. 3960–3972. Available at: https://doi.org/10.1093/HMG/DDX283.

Bartsch, K. *et al.* (2018) 'RNase H2 loss in murine astrocytes results in cellular defects reminiscent of nucleic acid mediated autoinflammation', *Frontiers in Immunology*, 9(MAR), p. 29. Available at: https://doi.org/10.3389/FIMMU.2018.00587/FULL.

Behrendt, R. *et al.* (2013) 'Mouse SAMHD1 has antiretroviral activity and suppresses a spontaneous cell-intrinsic antiviral response', *Cell Reports*, 4(4), pp. 689–696. Available at: https://doi.org/10.1016/j.celrep.2013.07.037.

Bonne, G. *et al.* (1999) 'Mutations in the gene encoding lamin A/C cause autosomal dominant Emery-Dreifuss muscular dystrophy', *Nature genetics*, 21(3), pp. 285–288. Available at: https://doi.org/10.1038/6799.

Bower, N.I. *et al.* (2017) 'Vegfd modulates both angiogenesis and lymphangiogenesis during zebrafish embryonic development', *Development (Cambridge, England)*, 144(3), pp. 507–518.

Available at: https://doi.org/10.1242/DEV.146969.

Breen, A.P. and Murphy, J.A. (1995) 'Reactions of oxyl radicals with DNA', *Free Radical Biology and Medicine*, 18(6), pp. 1033–1077. Available at: https://doi.org/10.1016/0891-5849(94)00209-3.

Brown, E.J. and Baltimore, D. (2000) 'ATR disruption leads to chromosomal fragmentation and early embryonic lethality', *Genes & Development*, 14(4), p. 397. Available at: https://doi.org/10.1101/gad.14.4.397.

Brown, J.A. and Suo, Z. (2011) 'Unlocking the sugar "steric gate" of DNA polymerases', *Biochemistry*, 50(7), pp. 1135–1142. Available at: https://doi.org/10.1021/bi101915z.

Bubeck, D. *et al.* (2011) 'PCNA directs type 2 RNase H activity on DNA replication and repair substrates', *Nucleic Acids Research*, 39(9), p. 3652. Available at: https://doi.org/10.1093/NAR/GKQ980.

Burma, S. *et al.* (2001) 'ATM Phosphorylates Histone H2AX in Response to DNA Double-strand Breaks', *Journal of Biological Chemistry*, 276(45), pp. 42462–42467. Available at: https://doi.org/10.1074/JBC.C100466200.

Caldecott, K.W. (2008) 'Single-strand break repair and genetic disease', *Nature Reviews Genetics 2008 9:8*, 9(8), pp. 619–631. Available at: https://doi.org/10.1038/nrg2380.

Cannan, W.J. *et al.* (2014) 'Nucleosomes suppress the formation of double-strand DNA breaks during attempted base excision repair of clustered oxidative damages', *Journal of Biological Chemistry*, 289(29), pp. 19881–19893. Available at: https://doi.org/10.1074/jbc.M114.571588.

Cayuela, M.L. *et al.* (2019) 'The Zebrafish as an Emerging Model to Study DNA Damage in Aging, Cancer and Other Diseases', *Frontiers in Cell and Developmental Biology*, 6. Available at: https://doi.org/10.3389/fcell.2018.00178.

Cerritelli, S.M. and Crouch, R.J. (2009) 'Ribonuclease H: the enzymes in Eukaryotes', *The FEBS journal*, 276(6), p. 1494. Available at: https://doi.org/10.1111/J.1742-4658.2009.06908.X.

Chabes, A. *et al.* (2003) 'Survival of DNA damage in yeast directly depends on increased dNTP levels allowed by relaxed feedback inhibition of ribonucleotide reductase', *Cell*, 112(3), pp. 391–401. Available at: https://doi.org/10.1016/S0092-8674(03)00075-8.

Champoux, J.J. (2001) 'DNA Topoisomerases: Structure, Function, and Mechanism', *Annual Review of Biochemistry*, 70(1), pp. 369–413. Available at: https://doi.org/10.1146/annurev.biochem.70.1.369.

Chang, H.H.Y. *et al.* (2017) 'Non-homologous DNA end joining and alternative pathways to double-strand break repair'. Available at: https://doi.org/10.1038/nrm.2017.48.

Chapman, A.L. *et al.* (2013) 'Axonal Transport Defects in a Mitofusin 2 Loss of Function Model of Charcot-Marie-Tooth Disease in Zebrafish', *PLoS ONE*, 8(6), p. 67276. Available at: https://doi.org/10.1371/journal.pone.0067276.

Chatterjee, N. and Walker, G.C. (2017) 'Mechanisms of DNA damage, repair, and mutagenesis', *Environmental and Molecular Mutagenesis*, pp. 235–263. Available at: https://doi.org/10.1002/em.22087.

Cheng, K.C. *et al.* (1992) '8-Hydroxyguanine, an abundant form of oxidative DNA damage, causes G → T and A → C substitutions', *Journal of Biological Chemistry*, 267(1), pp. 166–172. Available at: https://doi.org/10.1016/s0021-9258(18)48474-8.

Chon, H. *et al.* (2009) 'Contributions of the two accessory subunits, RNASEH2B and RNASEH2C, to the activity and properties of the human RNase H2 complex', *Nucleic Acids Research*, 37(1), pp. 96–

110. Available at: https://doi.org/10.1093/nar/gkn913.

Ciccia, A., McDonald, N. and West, S.C. (2008) 'Structural and Functional Relationships of the XPF/MUS81 Family of Proteins', *https://doi.org/10.1146/annurev.biochem.77.070306.102408*, 77, pp. 259–287. Available at: https://doi.org/10.1146/ANNUREV.BIOCHEM.77.070306.102408.

Clausen, A.R. *et al.* (2013) 'Ribonucleotide incorporation, proofreading and bypass by human DNA polymerase δ', *DNA repair*, 12(2), pp. 121–127. Available at: https://doi.org/10.1016/J.DNAREP.2012.11.006.

Cooke, M.S. *et al.* (2003) 'Oxidative DNA damage: mechanisms, mutation, and disease', *The FASEB Journal*, 17(10), pp. 1195–1214. Available at: https://doi.org/10.1096/FJ.02-0752REV.

Cortez, D. *et al.* (2001) 'ATR and ATRIP: partners in checkpoint signaling', *Science (New York, N.Y.)*, 294(5547), pp. 1713–1716. Available at: https://doi.org/10.1126/SCIENCE.1065521.

Cristini, A. *et al.* (2022) 'RNase H2, mutated in Aicardi-Goutières syndrome, resolves co-transcriptional R-loops to prevent DNA breaks and inflammation', *Nature Communications 2022 13:1*, 13(1), pp. 1–14. Available at: https://doi.org/10.1038/s41467-022-30604-0.

Crossley, M.P., Bocek, M. and Cimprich, K.A. (2019) 'R-Loops as Cellular Regulators and Genomic Threats', *Molecular Cell*. Cell Press, pp. 398–411. Available at: https://doi.org/10.1016/j.molcel.2019.01.024.

Crow, Y.J. *et al.* (2006) 'Mutations in genes encoding ribonuclease H2 subunits cause Aicardi-Goutières syndrome and mimic congenital viral brain infection', *Nature Genetics 2006 38:8*, 38(8), pp. 910–916. Available at: https://doi.org/10.1038/ng1842.

Crow, Y.J. *et al.* (2015) 'Characterization of human disease phenotypes associated with mutations in TREX1, RNASEH2A, RNASEH2B, RNASEH2C, SAMHD1, ADAR, and IFIH1', *American journal of medical genetics. Part A*, 167A(2), pp. 296–312. Available at: https://doi.org/10.1002/AJMG.A.36887.

Crow, Y.J. and Manel, N. (2015) 'Aicardi–Goutières syndrome and the type I interferonopathies', *Nature Reviews Immunology 2015 15:7*, 15(7), pp. 429–440. Available at: https://doi.org/10.1038/nri3850.

Dalgaard, J.Z. (2012) 'Causes and consequences of ribonucleotide incorporation into nuclear DNA', *Trends in Genetics*, 28(12), pp. 592–597. Available at: https://doi.org/10.1016/j.tig.2012.07.008.

Das, B.B. *et al.* (2014) 'PARP1-TDP1 coupling for the repair of topoisomerase I-induced DNA damage', *Nucleic acids research*, 42(7), pp. 4435–4449. Available at: https://doi.org/10.1093/NAR/GKU088.

Das, S.K. *et al.* (2016) 'Poly(ADP-ribose) polymers regulate DNA topoisomerase I (Top1) nuclear dynamics and camptothecin sensitivity in living cells', *Nucleic acids research*, 44(17), pp. 8363–8375. Available at: https://doi.org/10.1093/NAR/GKW665.

Debéthune, L. *et al.* (2002) 'Processing of nucleopeptides mimicking the topoisomerase I-DNA covalent complex by tyrosyl-DNA phosphodiesterase', *Nucleic acids research*, 30(5), pp. 1198–1204. Available at: https://doi.org/10.1093/NAR/30.5.1198.

Dechat, T. *et al.* (2010) 'Nuclear lamins', *Cold Spring Harbor perspectives in biology*, 2(11). Available at: https://doi.org/10.1101/CSHPERSPECT.A000547.

Delic, J. *et al.* (1991) 'Impossibility of acridine orange intercalation in nuclear DNA of the living cell', *Experimental cell research*, 194(1), pp. 147–153. Available at: https://doi.org/10.1016/0014-4827(91)90144-J.

Deng, C. *et al.* (2005) 'Multiple endonucleases function to repair covalent topoisomerase I

complexes in Saccharomyces cerevisiae', *Genetics*, 170(2), pp. 591–600. Available at: https://doi.org/10.1534/GENETICS.104.028795.

Dorsemans, A.-C. *et al.* (2017) 'Impaired Constitutive and Regenerative Neurogenesis in Adult Hyperglycemic Zebrafish', *J. Comp. Neurol*, 525, pp. 442–458. Available at: https://doi.org/10.1002/cne.24065.

Du, Q. *et al.* (2002) 'LGN blocks the ability of NuMA to bind and stabilize microtubules: A mechanism for mitotic spindle assembly regulation', *Current Biology*, 12(22), pp. 1928–1933. Available at: https://doi.org/10.1016/S0960-9822(02)01298-8.

Dudley, D.D. *et al.* (2005) 'Mechanism and control of V(D)J recombination versus class switch recombination: Similarities and differences', *Advances in Immunology*, 86, pp. 43–112. Available at: https://doi.org/10.1016/S0065-2776(04)86002-4.

Egli, M., Usman, N. and Rich, A. (1993) 'Conformational Influence of the Ribose 2'-Hydroxyl Group: Crystal Structures of DNA-RNA Chimeric Duplexess', *Biochemistry*, 32(13), pp. 3221–3237. Available at: https://doi.org/10.1021/BI00064A004/ASSET/BI00064A004.FP.PNG_V03.

El-Khamisy, S.F. *et al.* (2005) 'Defective DNA single-strand break repair in spinocerebellar ataxia with axonal neuropathy-1', *Nature*, 434(7029), pp. 108–113. Available at: https://doi.org/10.1038/NATURE03314.

El-Khamisy, S.F. and Caldecott, K.W. (2006) 'TDP1-dependent DNA single-strand break repair and neurodegeneration', *Mutagenesis*, 21(4), pp. 219–224. Available at: https://doi.org/10.1093/mutage/gel024.

Enderle, J. *et al.* (2019) 'The Protease WSS1A, the Endonuclease MUS81, and the Phosphodiesterase TDP1 Are Involved in Independent Pathways of DNA-protein Crosslink Repair in Plants', *The Plant Cell*, 31(4), p. 775. Available at: https://doi.org/10.1105/TPC.18.00824.

Feitsma, H. *et al.* (2007) 'Mlh1 deficiency in zebrafish results in male sterility and aneuploid as well as triploid progeny in females', *Genetics*, 175(4), pp. 1561–1569. Available at: https://doi.org/10.1534/genetics.106.068171.

Fenech, M. *et al.* (2011) 'Molecular mechanisms of micronucleus, nucleoplasmic bridge and nuclear bud formation in mammalian and human cells', *Mutagenesis*, 26(1), pp. 125–132. Available at: https://doi.org/10.1093/mutage/geq052.

Flanagan, J.M. *et al.* (2009) 'Genomics screen in transformed stem cells reveals RNASEH2A, PPAP2C, and ADARB1 as putative anticancer drug targets', *Molecular Cancer Therapeutics*, 8(1), pp. 249–260. Available at: https://doi.org/10.1158/1535-7163.MCT-08-0636.

Fleming, A.M., Ding, Y. and Burrows, C.J. (2017) 'Oxidative DNA damage is epigenetic by regulating gene transcription via base excision repair', *Proceedings of the National Academy of Sciences of the United States of America*, 114(10), pp. 2604–2609. Available at: https://doi.org/10.1073/PNAS.1619809114.

Fousteri, M. and Mullenders, L.H. (2008) 'Transcription-coupled nucleotide excision repair in mammalian cells: molecular mechanisms and biological effects', *Cell Research*, 18(1), pp. 73–84. Available at: https://doi.org/10.1038/cr.2008.6.

Gall, A. *et al.* (2012) 'Autoimmunity Initiates in Nonhematopoietic Cells and Progresses via Lymphocytes in an Interferon-Dependent Autoimmune Disease', *Immunity*, 36(1), pp. 120–131. Available at: https://doi.org/10.1016/j.immuni.2011.11.018.

García-Muse, T. and Aguilera, A. (2016) 'Transcription–replication conflicts: how they occur and how

they are resolved', *Nature Reviews Molecular Cell Biology 2016 17:9*, 17(9), pp. 553–563. Available at: https://doi.org/10.1038/nrm.2016.88.

Garg, P. *et al.* (2004) 'Idling by DNA polymerase δ maintains a ligatable nick during lagging-strand DNA replication', *Genes & Development*, 18(22), p. 2764. Available at: https://doi.org/10.1101/GAD.1252304.

Ghodgaonkar, M.M. *et al.* (2013) 'Ribonucleotides Misincorporated into DNA Act as Strand-Discrimination Signals in Eukaryotic Mismatch Repair', *Molecular Cell*, 50(3), p. 323. Available at: https://doi.org/10.1016/J.MOLCEL.2013.03.019.

Ghosh, D., Kumari, S. and Raghavan, S.C. (2022) 'Depletion of RNASEH2 Activity Leads to Accumulation of DNA Double-strand Breaks and Reduced Cellular Survivability in T Cell Leukemia', *Journal of Molecular Biology*, 434(12), p. 167617. Available at: https://doi.org/10.1016/j.jmb.2022.167617.

Giglia-Mari, G., Zotter, A. and Vermeulen, W. (2011) 'DNA damage response.', *Cold Spring Harbor perspectives in biology*, 3(1), p. a000745. Available at: https://doi.org/10.1101/cshperspect.a000745.

Gong, L. *et al.* (2015) 'p53 isoform Δ113p53/Δ133p53 promotes DNA double-strand break repair to protect cell from death and senescence in response to DNA damage', *Nature Publishing Group*, 25, pp. 351–369. Available at: https://doi.org/10.1038/cr.2015.22.

GoutièRes, F. *et al.* (1998) 'Aicardi-Goutières syndrome: An update and results of interferon-α studies', *Annals of Neurology*, 44(6), pp. 900–907. Available at: https://doi.org/10.1002/ana.410440608.

Gueth-Hallonet, C., Weber, K. and Osborn, M. (1996) 'NuMA: A bipartite nuclear location signal and other functional properties of the tail domain', *Experimental Cell Research*, 225(1), pp. 207–218. Available at: https://doi.org/10.1006/excr.1996.0171.

Gueven, N. *et al.* (2004) 'Aprataxin, a novel protein that protects against genotoxic stress', *Human Molecular Genetics*, 13(10), pp. 1081–1093. Available at: https://doi.org/10.1093/hmg/ddh122.

Hamilton, N. *et al.* (2020) 'The failure of microglia to digest developmental apoptotic cells contributes to the pathology of RNASET2-deficient leukoencephalopathy', *Glia*, 68(7), p. 1531. Available at: https://doi.org/10.1002/GLIA.23829.

Hanawalt, P.C. and Spivak, G. (2008) 'Transcription-coupled DNA repair: Two decades of progress and surprises', *Nature Reviews Molecular Cell Biology*, pp. 958–970. Available at: https://doi.org/10.1038/nrm2549.

Harborth, J. *et al.* (2001) 'Identification of essential genes in cultured mammalian cells using small interfering RNAs', *Journal of Cell Science*, 114(24), pp. 4557–4565.

Hartner, J.C. *et al.* (2004) 'Liver Disintegration in the Mouse Embryo Caused by Deficiency in the RNA-editing Enzyme ADAR1', *Journal of Biological Chemistry*, 279(6), pp. 4894–4902. Available at: https://doi.org/10.1074/jbc.M311347200.

Hartsuiker, E., Neale, M.J. and Carr, A.M. (2009) 'Distinct requirements for the Rad32(Mre11) nuclease and Ctp1(CtIP) in the removal of covalently bound topoisomerase I and II from DNA', *Molecular cell*, 33(1), pp. 117–123. Available at: https://doi.org/10.1016/J.MOLCEL.2008.11.021.

Hatch, E.M. *et al.* (2013) 'Catastrophic Nuclear Envelope Collapse in Cancer Cell Micronuclei', *Cell*, 154(1), p. 47. Available at: https://doi.org/10.1016/J.CELL.2013.06.007.

Hawkins, A.J. *et al.* (2009) 'In vitro complementation of Tdp1 deficiency indicates a stabilized enzyme-DNA adduct from tyrosyl but not glycolate lesions as a consequence of the SCAN1

mutation', *DNA Repair*, 8(5), pp. 654–663. Available at: https://doi.org/10.1016/j.dnarep.2008.12.012.

Hazra, T.K. *et al.* (1998) 'The presence of two distinct 8-oxoguanine repair enzymes in human cells: their potential complementary roles in preventing mutation', *Nucleic acids research*, 26(22), pp. 5116–5122. Available at: https://doi.org/10.1093/NAR/26.22.5116.

He, G. *et al.* (2005) 'Induction of p21 by p53 following DNA damage inhibits both Cdk4 and Cdk2 activities', *Oncogene*, 24(18), pp. 2929–2943. Available at: https://doi.org/10.1038/sj.onc.1208474.

Hendriks, I.A., Larsen, S.C. and Nielsen, M.L. (2019) 'An Advanced Strategy for Comprehensive Profiling of ADP-ribosylation Sites Using Mass Spectrometry-based Proteomics', *Molecular & cellular proteomics : MCP*, 18(5), pp. 1010–1024. Available at: https://doi.org/10.1074/MCP.TIR119.001315.

Hiller, B. *et al.* (2012) 'Mammalian RNase H2 removes ribonucleotides from DNA to maintain genome integrity', *Journal of Experimental Medicine*, 209(8), pp. 1419–1426. Available at: https://doi.org/10.1084/jem.20120876.

Hirano, R. *et al.* (2007) 'Spinocerebellar ataxia with axonal neuropathy: consequence of a Tdp1 recessive neomorphic mutation?', *The EMBO Journal*, 26(22), pp. 4732–4743. Available at: https://doi.org/10.1038/sj.emboj.7601885.

Holmes, J.B. *et al.* (2015) 'Primer retention owing to the absence of RNase H1 is catastrophic for mitochondrial DNA replication', *Proceedings of the National Academy of Sciences of the United States of America*, 112(30), pp. 9334–9339. Available at: https://doi.org/10.1073/pnas.1503653112.

Hovatter, K.R. and Martinson, H.G. (1987) 'Ribonucleotide-induced helical alteration in DNA prevents nucleosome formation.', *Proceedings of the National Academy of Sciences of the United States of America*, 84(5), p. 1162. Available at: https://doi.org/10.1073/PNAS.84.5.1162.

Howe, K. *et al.* (2013) 'The zebrafish reference genome sequence and its relationship to the human genome', *Nature*, 496(7446), pp. 498–503. Available at: https://doi.org/10.1038/nature12111.

Hua, S. *et al.* (2020) 'Identification of hub genes in hepatocellular carcinoma using integrated bioinformatic analysis', *Aging (Albany NY)*, 12(6), p. 5439. Available at: https://doi.org/10.18632/AGING.102969.

Huang, S.-Y.N. *et al.* (2017) 'Topoisomerase I-mediated cleavage at unrepaired ribonucleotides generates DNA double-strand breaks', *The EMBO Journal*, 36, pp. 361–373. Available at: https://doi.org/10.15252/embj.201592426.

Imlay, J.A., Chin, S.M. and Linn, S. (1988) 'Toxic DNA damage by hydrogen peroxide through the Fenton reaction in vivo and in vitro', *Science (New York, N.Y.)*, 240(4852), pp. 640–642. Available at: https://doi.org/10.1126/SCIENCE.2834821.

Imseng, S., Aylett, C.H. and Maier, T. (2018) 'Architecture and activation of phosphatidylinositol 3-kinase related kinases', *Current opinion in structural biology*, 49, pp. 177–189. Available at: https://doi.org/10.1016/J.SBI.2018.03.010.

Interthal, H. *et al.* (2005) 'SCAN1 mutant Tdp1 accumulates the enzyme--DNA intermediate and causes camptothecin hypersensitivity', *The EMBO journal*, 24(12), pp. 2224–2233. Available at: https://doi.org/10.1038/SJ.EMBOJ.7600694.

Interthal, H., Chen, H.J. and Champoux, J.J. (2005) 'Human Tdp1 cleaves a broad spectrum of substrates, including phosphoamide linkages', *The Journal of biological chemistry*, 280(43), pp. 36518–36528. Available at: https://doi.org/10.1074/JBC.M508898200.

Interthal, H., Pouliot, J.J. and Champoux, J.J. (2001) 'The tyrosyl-DNA phosphodiesterase Tdp1 is a

member of the phospholipase D superfamily', *Proceedings of the National Academy of Sciences of the United States of America*, 98(21), pp. 12009–12014. Available at: https://doi.org/10.1073/PNAS.211429198/SUPPL_FILE/4291METHODS.PDF.

Ishikawa, H., Ma, Z. and Barber, G.N. (2009) 'STING regulates intracellular DNA-mediated, type I interferon-dependent innate immunity', *Nature*, 461(7265), p. 788. Available at: https://doi.org/10.1038/NATURE08476.

Jackson, S.P. (2002) 'Sensing and repairing DNA double-strand breaks', *Carcinogenesis*, 23(5), pp. 687–696. Available at: https://doi.org/10.1093/CARCIN/23.5.687.

Jayaraman, S. *et al.* (2017) 'The nuclear mitotic apparatus protein NuMA controls rDNA transcription and mediates the nucleolar stress response in a p53-independent manner', *Nucleic Acids Research*, 45(20), p. 11725. Available at: https://doi.org/10.1093/NAR/GKX782.

Jeong, H.S. *et al.* (2004) 'RNase H2 of Saccharomyces cerevisiae is a complex of three proteins', *Nucleic Acids Research*, 32(2), p. 407. Available at: https://doi.org/10.1093/NAR/GKH209.

Jinks-Robertson, S. and Bhagwat, A.S. (2014) 'Transcription-Associated Mutagenesis'. Available at: https://doi.org/10.1146/annurev-genet-120213-092015.

Johnson, M.K., Kottur, J. and Nair, D.T. (2019) 'A polar filter in DNA polymerases prevents ribonucleotide incorporation', *Nucleic Acids Research*, 47, pp. 10693–10705. Available at: https://doi.org/10.1093/nar/gkz792.

Kajitani, G.S. *et al.* (2021) 'Neurovascular dysfunction and neuroinflammation in a Cockayne syndrome mouse model', *Aging (Albany NY)*, 13(19), p. 22710. Available at: https://doi.org/10.18632/AGING.203617.

Kallajoki, M. *et al.* (1993) 'Microinjection of a monoclonal antibody against SPN antigen, now identified by peptide sequences as the NuMA protein, induces micronuclei in PtK2 cells', *Journal of Cell Science*, 104(1), pp. 139–150.

Katyal, S. *et al.* (2007) 'TDP1 facilitates chromosomal single-strand break repair in neurons and is neuroprotective in vivo', *The EMBO Journal*, 26(22), pp. 4720–4731. Available at: https://doi.org/10.1038/sj.emboj.7601869.

Keeney, S. and Neale, M.J. (2006) 'Initiation of meiotic recombination by formation of DNA double-strand breaks: mechanism and regulation', *Biochemical Society transactions*, 34(Pt 4), pp. 523–525. Available at: https://doi.org/10.1042/BST0340523.

Kim, H.R. *et al.* (2020) 'Investigation of the role of VHL-HIF signaling in DNA repair and apoptosis in zebrafish', *Oncotarget*, 11(13), pp. 1109–1130. Available at: https://doi.org/10.18632/ONCOTARGET.27521.

Kim, N. *et al.* (2011) 'Mutagenic processing of ribonucleotides in DNA by yeast topoisomerase I', *Science (New York, N.Y.)*, 332(6037), pp. 1561–1564. Available at: https://doi.org/10.1126/SCIENCE.1205016.

Kimmel, C.B. *et al.* (1995) 'Stages of embryonic development of the zebrafish', *Developmental Dynamics*, 203(3), pp. 253–310. Available at: https://doi.org/10.1002/aja.1002030302.

Kimura, N. *et al.* (2022) 'Ribonuclease H2 Subunit A Preserves Genomic Integrity and Promotes Prostate Cancer Progression', *Cancer Research Communications*, 2(8), pp. 870–883. Available at: https://doi.org/10.1158/2767-9764.CRC-22-0126.

De Klein, A. *et al.* (2000) 'Targeted disruption of the cell-cycle checkpoint gene ATR leads to early embryonic lethality in mice', *Current biology : CB*, 10(8), pp. 479–482. Available at:

https://doi.org/10.1016/S0960-9822(00)00447-4.

Klein, H.L. (2017) 'Genome Instabilities Arising from Ribonucleotides in DNA', *DNA repair*, 56, p. 26. Available at: https://doi.org/10.1016/J.DNAREP.2017.06.004.

Klungland, A. *et al.* (1999) 'Accumulation of premutagenic DNA lesions in mice defective in removal of oxidative base damage', *Proceedings of the National Academy of Sciences of the United States of America*, 96(23), pp. 13300–13305. Available at: https://doi.org/10.1073/PNAS.96.23.13300/ASSET/663AF3FA-E18B-43EC-B3A3-4EF1B4E07135/ASSETS/GRAPHIC/PQ2394015005.JPEG.

Koshimizu, E. *et al.* (2011) 'Embryonic senescence and laminopathies in a progeroid zebrafish model', *PLoS ONE*, 6(3). Available at: https://doi.org/10.1371/journal.pone.0017688.

Kunkel, T.A. (1999) 'The high cost of living', *Trends in Genetics*, 15(3), pp. 93–94. Available at: https://doi.org/10.1016/S0168-9525(98)01664-3.

Kunkel, T.A. (2004) 'DNA replication fidelity', *The Journal of biological chemistry*, 279(17), pp. 16895–16898. Available at: https://doi.org/10.1074/JBC.R400006200.

Kunkel, T.A. (2009) 'Evolving views of DNA replication (in)fidelity', *Cold Spring Harbor symposia on quantitative biology*, 74, pp. 91–101. Available at: https://doi.org/10.1101/SQB.2009.74.027.

Kunkel, T.A. (2011) 'Balancing eukaryotic replication asymmetry with replication fidelity', *Current opinion in chemical biology*, 15(5), pp. 620–626. Available at: https://doi.org/10.1016/J.CBPA.2011.07.025.

Kwan, K.M. *et al.* (2007) 'The Tol2kit: A multisite gateway-based construction kit forTol2 transposon transgenesis constructs', *Developmental Dynamics*, 236(11), pp. 3088–3099. Available at: https://doi.org/10.1002/dvdy.21343.

Lazzaro, F. *et al.* (2012) 'RNase H and Postreplication Repair Protect Cells from Ribonucleotides Incorporated in DNA', *Molecular Cell*, 45(1), p. 99. Available at: https://doi.org/10.1016/J.MOLCEL.2011.12.019.

Lebon, P. *et al.* (1988) 'Intrathecal synthesis of interferon-alpha in infants with progressive familial encephalopathy', *Journal of the Neurological Sciences*, 84(2–3), pp. 201–208. Available at: https://doi.org/10.1016/0022-510X(88)90125-6.

Lee, J.H. and Paull, T.T. (2005) 'ATM activation by DNA double-strand breaks through the Mre11-Rad50-Nbs1 complex', *Science (New York, N.Y.)*, 308(5721), pp. 551–554. Available at: https://doi.org/10.1126/SCIENCE.1108297.

Lempiäinen, H. and Halazonetis, T.D. (2009) 'Emerging common themes in regulation of PIKKs and PI3Ks', *The EMBO journal*, 28(20), pp. 3067–3073. Available at: https://doi.org/10.1038/EMBOJ.2009.281.

Li, F. *et al.* (2019) 'Apn2 resolves blocked 3' ends and suppresses Top1-induced mutagenesis at genomic rNMP sites', *Nature Structural and Molecular Biology*, 26(3), pp. 155–163. Available at: https://doi.org/10.1038/s41594-019-0186-1.

Li, G. *et al.* (2012) '8-Oxoguanine-DNA glycosylase 1 deficiency modifies allergic airway inflammation by regulating STAT6 and IL-4 in cells and in mice', *Free radical biology & medicine*, 52(2), pp. 392–401. Available at: https://doi.org/10.1016/J.FREERADBIOMED.2011.10.490.

Li, T. and Chen, Z.J. (2018) 'The cGAS–cGAMP–STING pathway connects DNA damage to inflammation, senescence, and cancer', *The Journal of Experimental Medicine*, 215(5), p. 1287. Available at: https://doi.org/10.1084/JEM.20180139.

Li, Y. and Breaker, R.R. (1999) 'Kinetics of RNA Degradation by Specific Base Catalysis of Transesterification Involving the 2'-Hydroxyl Group', *Journal of the American Chemical Society*, 121(23), pp. 5364–5372. Available at: https://doi.org/10.1021/JA990592P.

Liddicoat, B.J. *et al.* (2015) 'RNA editing by ADAR1 prevents MDA5 sensing of endogenous dsRNA as nonself', *Science*, 349(6252), pp. 1115–1120. Available at: https://doi.org/10.1126/science.aac7049.

Lieschke, G.J. and Currie, P.D. (2007) 'Animal models of human disease: zebrafish swim into view', *Nature reviews. Genetics*, 8(5), pp. 353–367. Available at: https://doi.org/10.1038/NRG2091.

Lindahl, T. (1993) 'Instability and decay of the primary structure of DNA', *nature.com* [Preprint]. Available at: https://www.nature.com/articles/362709a0 (Accessed: 24 October 2018).

Lippert, M.J. *et al.* (2011) 'Role for topoisomerase 1 in transcription-associated mutagenesis in yeast', *Proceedings of the National Academy of Sciences of the United States of America*, 108(2), pp. 698–703. Available at: https://doi.org/10.1073/PNAS.1012363108/-/DCSUPPLEMENTAL.

Liu, B. *et al.* (2017) 'Direct Visualization of RNA-DNA Primer Removal from Okazaki Fragments Provides Support for Flap Cleavage and Exonucleolytic Pathways in Eukaryotic Cells', *The Journal of biological chemistry*, 292(12), pp. 4777–4788. Available at: https://doi.org/10.1074/JBC.M116.758599.

Liu, C., Pouliot, J.J. and Nash, H.A. (2002) 'Repair of topoisomerase I covalent complexes in the absence of the tyrosyl-DNA phosphodiesterase Tdp1', *Proceedings of the National Academy of Sciences of the United States of America*, 99(23), pp. 14970–14975. Available at: https://doi.org/10.1073/PNAS.182557199.

Liu, Q. *et al.* (2000) 'Chk1 is an essential kinase that is regulated by Atr and required for the G2/M DNA damage checkpoint', *Genes & Development*, 14(12), p. 1448. Available at: https://doi.org/10.1101/gad.14.12.1448.

Livingston, J.H. and Crow, Y.J. (2016) 'Neurologic Phenotypes Associated with Mutations in TREX1, RNASEH2A, RNASEH2B, RNASEH2C, SAMHD1, ADAR1, and IFIH1: Aicardi-Goutières Syndrome and Beyond', *Neuropediatrics*, 47(6), pp. 355–360. Available at: https://doi.org/10.1055/S-0036-1592307.

Lockhart, A. *et al.* (2019) 'RNase H1 and H2 Are Differentially Regulated to Process RNA-DNA Hybrids', *Cell Reports*, 29(9), pp. 2890-2900.e5. Available at: https://doi.org/10.1016/j.celrep.2019.10.108.

Lovejoy, C.A. and Cortez, D. (2009) 'Common mechanisms of PIKK regulation', *DNA repair*, 8(9), pp. 1004–1008. Available at: https://doi.org/10.1016/J.DNAREP.2009.04.006.

Lucas-Lledó, J.I. and Lynch, M. (2009) 'Evolution of mutation rates: phylogenomic analysis of the photolyase/cryptochrome family.', *Molecular biology and evolution*, 26(5), pp. 1143–53. Available at: https://doi.org/10.1093/molbev/msp029.

Luderus, M E Eva *et al.* (1994) *Binding of Matrix Attachment Regions to Lamin Polymers Involves Single-Stranded Regions and the Minor Groove*, *MOLECULAR AND CELLULAR BIOLOGY*. Available at: http://mcb.asm.org/ (Accessed: 27 March 2020).

Lujan, S.A. *et al.* (2013) 'Ribonucleotides are signals for mismatch repair of leading-strand replication errors', *Molecular cell*, 50(3), pp. 437–443. Available at: https://doi.org/10.1016/J.MOLCEL.2013.03.017.

Luo, X. and Lee Kraus, W. (2012) 'On PAR with PARP: cellular stress signaling through poly(ADP-ribose) and PARP-1', *Genes & development*, 26(5), pp. 417–432. Available at:

https://doi.org/10.1101/GAD.183509.111.

Lydersen, B.K. and Pettijohn, D.E. (1980) 'Human-specific nuclear protein that associates with the polar region of the mitotic apparatus: Distribution in a human/hamster hybrid cell', *Cell*, 22(2), pp. 489–499. Available at: https://doi.org/10.1016/0092-8674(80)90359-1.

Mabley, J.G. *et al.* (2005) 'Potential role for 8-oxoguanine DNA glycosylase in regulating inflammation', *FASEB journal : official publication of the Federation of American Societies for Experimental Biology*, 19(2), pp. 1–18. Available at: https://doi.org/10.1096/FJ.04-2278FJE.

Mackenzie, K.J. *et al.* (2016) ' Ribonuclease H2 mutations induce a cGAS / STING -dependent innate immune response ', *The EMBO Journal*, 35(8), pp. 831–844. Available at: https://doi.org/10.15252/embj.201593339.

MacKenzie, K.J. *et al.* (2017) 'cGAS surveillance of micronuclei links genome instability to innate immunity', *Nature*, 548(7668), p. 461. Available at: https://doi.org/10.1038/NATURE23449.

Mannion, N.M. *et al.* (2014) 'The RNA-Editing Enzyme ADAR1 Controls Innate Immune Responses to RNA', *Cell Reports*, 9(4), pp. 1482–1494. Available at: https://doi.org/10.1016/j.celrep.2014.10.041.

Margolin, Y. *et al.* (2006) 'Paradoxical hotspots for guanine oxidation by a chemical mediator of inflammation', *Nature chemical biology*, 2(7), pp. 365–366. Available at: https://doi.org/10.1038/NCHEMBIO796.

Mariño-Ramírez, L. *et al.* (2005) 'Histone structure and nucleosome stability', *Expert Review of Proteomics*. NIH Public Access, pp. 719–729. Available at: https://doi.org/10.1586/14789450.2.5.719.

Martín-Jiménez, R., Campanella, M. and Russell, C. (2015) 'New Zebrafish Models of Neurodegeneration', *Current Neurology and Neuroscience Reports*, 15(6), pp. 1–7. Available at: https://doi.org/10.1007/S11910-015-0555-Z/FIGURES/1.

Matsuoka, S. *et al.* (2007) 'ATM and ATR substrate analysis reveals extensive protein networks responsive to DNA damage', *Science (New York, N.Y.)*, 316(5828), pp. 1160–1166. Available at: https://doi.org/10.1126/SCIENCE.1140321.

Matsuoka, S., Huang, M. and Elledge, S.J. (1998) 'Linkage of ATM to cell cycle regulation by the Chk2 protein kinase', *Science*, 282(5395), pp. 1893–1897. Available at: https://doi.org/10.1126/SCIENCE.282.5395.1893/ASSET/50019E18-A1B2-4077-9B9F-C9FD35CA4B78/ASSETS/GRAPHIC/SE4987064004.JPEG.

Mattson, M.P. *et al.* (2001) 'Neurodegenerative disorders and ischemic brain diseases', *Apoptosis 2001 6:1*, 6(1), pp. 69–81. Available at: https://doi.org/10.1023/A:1009676112184.

Mccormick, J.P. *et al.* (1976) 'Characterization of a Cell-Lethal Product from the Photooxidation of Tryptophan: Hydrogen Peroxide', *Science*, 191(4226), pp. 468–469. Available at: https://doi.org/10.1126/SCIENCE.1108203.

McElhinny, Stephanie A. Nick *et al.* (2010) 'Abundant ribonucleotide incorporation into DNA by yeast replicative polymerases', *Proceedings of the National Academy of Sciences*, 107(11), pp. 4949–4954. Available at: https://doi.org/10.1073/PNAS.0914857107.

McElhinny, Stephanie A Nick *et al.* (2010) 'Genome instability due to ribonucleotide incorporation into DNA', *Nature Chemical Biology 2010 6:10*, 6(10), pp. 774–781. Available at: https://doi.org/10.1038/nchembio.424.

Merdes, A. and Cleveland, D.W. (1998) 'The role of NuMA in the interphase nucleus', *Journal of cell science*, 111 (Pt 1)(1), pp. 71–79. Available at: https://doi.org/10.1242/JCS.111.1.71.

Meroni, A. *et al.* (2017) 'The Incorporation of Ribonucleotides Induces Structural and Conformational Changes in DNA', *Biophysical Journal*, 113(7), p. 1373. Available at: https://doi.org/10.1016/J.BPJ.2017.07.013.

Metzner, A. *et al.* (2020) 'A high throughput zebrafish chemical screen reveals ALK5 and non-canonical androgen signalling as modulators of the pkd2−/− phenotype', *Scientific Reports 2020 10:1*, 10(1), pp. 1–14. Available at: https://doi.org/10.1038/s41598-019-56995-7.

Michael Hagmann *et al.* (1998) 'Homologous Recombination and DNA-End Joining Reactions in Zygotes and Early Embryos of Zebrafish (Danio rerio) and Drosophila melongaster', *Biological Chemistry* , Volume 379(Issue 6).

Minowa, O. *et al.* (2000) 'Mmh/Ogg1 gene inactivation results in accumulation of 8-hydroxyguanine in mice', *Proceedings of the National Academy of Sciences of the United States of America*, 97(8), pp. 4156–4161. Available at: https://doi.org/10.1073/PNAS.050404497.

Mirkin, E. V. and Mirkin, S.M. (2007) 'Replication Fork Stalling at Natural Impediments', *Microbiology and Molecular Biology Reviews*, 71(1), pp. 13–35. Available at: https://doi.org/10.1128/MMBR.00030-06/ASSET/2C2D65C4-7C52-4DE3-985B-8C043EDCB4CB/ASSETS/GRAPHIC/ZMR0010721430010.JPEG.

Moreno, N.S. *et al.* (2019) 'The nuclear structural protein NuMA is a negative regulator of 53BP1 in DNA double-strand break repair', *Nucleic acids research*, 47(6), pp. 2703–2715. Available at: https://doi.org/10.1093/NAR/GKZ138.

Morita, M. *et al.* (2004) 'Gene-Targeted Mice Lacking the Trex1 (DNase III) 3′→5′ DNA Exonuclease Develop Inflammatory Myocarditis', *Molecular and Cellular Biology*, 24(15), pp. 6719–6727. Available at: https://doi.org/10.1128/mcb.24.15.6719-6727.2004.

Morsli, S. *et al.* (2022) 'A p21-GFP zebrafish model of senescence for rapid testing of senolytics in vivo', *bioRxiv*, p. 2022.09.19.506911. Available at: https://doi.org/10.1101/2022.09.19.506911.

Motwani, M., Pesiridis, S. and Fitzgerald, K.A. (2019) 'DNA sensing by the cGAS–STING pathway in health and disease', *Nature Reviews Genetics 2019 20:11*, 20(11), pp. 657–674. Available at: https://doi.org/10.1038/s41576-019-0151-1.

Naegeli, H. and Sugasawa, K. (2011) 'The xeroderma pigmentosum pathway: Decision tree analysis of DNA quality', *DNA Repair*, 10, pp. 673–683. Available at: https://doi.org/10.1016/j.dnarep.2011.04.019.

Nakamura, K. *et al.* (2010) 'Collaborative action of Brca1 and CtIP in elimination of covalent modifications from double-strand breaks to facilitate subsequent break repair', *PLoS genetics*, 6(1). Available at: https://doi.org/10.1371/JOURNAL.PGEN.1000828.

Neff, M.M. *et al.* (1998) 'dCAPS, a simple technique for the genetic analysis of single nucleotide polymorphisms: Experimental applications in Arabidopsis thaliana genetics', *Plant Journal*, 14(3), pp. 387–392. Available at: https://doi.org/10.1046/j.1365-313X.1998.00124.x.

Nowotny, M. *et al.* (2005) 'Crystal Structures of RNase H Bound to an RNA/DNA Hybrid: Substrate Specificity and Metal-Dependent Catalysis', *Cell*, 121(7), pp. 1005–1016. Available at: https://doi.org/10.1016/J.CELL.2005.04.024.

Ohata, H. *et al.* (2013) 'NuMA is required for the selective induction of p53 target genes', *Molecular and cellular biology*, 33(12), pp. 2447–2457. Available at: https://doi.org/10.1128/MCB.01221-12.

Palazzo, L. *et al.* (2018) 'Serine is the major residue for ADP-ribosylation upon DNA damage', *eLife*, 7. Available at: https://doi.org/10.7554/ELIFE.34334.

Pan, L. *et al.* (2016) 'Oxidized Guanine Base Lesions Function in 8-Oxoguanine DNA Glycosylase-1-mediated Epigenetic Regulation of Nuclear Factor κB-driven Gene Expression', *The Journal of biological chemistry*, 291(49), pp. 25553–25566. Available at: https://doi.org/10.1074/JBC.M116.751453.

Park, J.H. *et al.* (2016) 'Positive feedback regulation of p53 transactivity by DNA damage-induced ISG15 modification', *Nature Communications*, 7(1), pp. 1–13. Available at: https://doi.org/10.1038/ncomms12513.

Park, J.W. and Ames, B.N. (1988) '7-Methylguanine adducts in DNA are normally present at high levels and increase on aging: analysis by HPLC with electrochemical detection.', *Proceedings of the National Academy of Sciences*, 85(20), pp. 7467–7470. Available at: https://doi.org/10.1073/PNAS.85.20.7467.

Pokatayev, V. *et al.* (2016) 'RNase H2 catalytic core Aicardi-Goutières syndrome–relatedmutant invokes cGAS–STING innate immune-sensing pathway inmice', *The Journal of Experimental Medicine*, 213(3), p. 329. Available at: https://doi.org/10.1084/JEM.20151464.

Pommier, Y. *et al.* (2014) 'Tyrosyl-DNA-phosphodiesterases (TDP1 and TDP2)', *DNA repair*, 19, pp. 114–129. Available at: https://doi.org/10.1016/J.DNAREP.2014.03.020.

Pommier, Y. *et al.* (2016) 'Roles of eukaryotic topoisomerases in transcription, replication and genomic stability', *Nature Reviews Molecular Cell Biology*, 17(11), pp. 703–721. Available at: https://doi.org/10.1038/nrm.2016.111.

Pommier, Y. *et al.* (2022) 'Human topoisomerases and their roles in genome stability and organization', *Nature Reviews Molecular Cell Biology 2022 23:6*, 23(6), pp. 407–427. Available at: https://doi.org/10.1038/s41580-022-00452-3.

Potenski, C.J. *et al.* (2014) 'Avoidance of rNMP-induced mutations via RNaseH2 and Srs2-Exo1 dependent mechanisms', *Nature*, 511(7508), p. 251. Available at: https://doi.org/10.1038/NATURE13292.

Potenski, C.J. *et al.* (2019) 'Genome Instability Consequences of RNase H2 Aicardi-Goutières Syndrome Alleles', *DNA repair*, 84, p. 102614. Available at: https://doi.org/10.1016/J.DNAREP.2019.04.002.

Pryor, J.M. *et al.* (2018) 'Ribonucleotide incorporation enables repair of chromosome breaks by nonhomologous end joining', *Science*, 361(6407), pp. 1126–1129. Available at: https://doi.org/10.1126/science.aat2477.

Qiu, J. *et al.* (1999) 'Saccharomyces cerevisiae RNase H(35) Functions in RNA Primer Removal during Lagging-Strand DNA Synthesis, Most Efficiently in Cooperation with Rad27 Nuclease', *Molecular and Cellular Biology*, 19(12), p. 8361. Available at: https://doi.org/10.1128/MCB.19.12.8361.

Raab, M. *et al.* (2016) 'ESCRT III repairs nuclear envelope ruptures during cell migration to limit DNA damage and cell death', *Science*, 352(6283), pp. 359–362. Available at: https://doi.org/10.1126/science.aad7611.

Radulescu, A.E. and Cleveland, D.W. (2010) 'NuMA after 30 years: The matrix revisited', *Trends in Cell Biology*, 20(4), pp. 214–222. Available at: https://doi.org/10.1016/j.tcb.2010.01.003.

Rahmanian, N., Shokrzadeh, M. and Eskandani, M. (2021) 'Recent advances in γH2AX biomarker-based genotoxicity assays: A marker of DNA damage and repair', *DNA Repair*, 108, p. 103243. Available at: https://doi.org/10.1016/J.DNAREP.2021.103243.

Rankin, J. and Ellard, S. (2006) 'The laminopathies: a clinical review', *Clinical genetics*, 70(4), pp. 261–

274. Available at: https://doi.org/10.1111/J.1399-0004.2006.00677.X.

Ray Chaudhuri, A. and Nussenzweig, A. (2017) 'The multifaceted roles of PARP1 in DNA repair and chromatin remodelling', *Nature Reviews Molecular Cell Biology*. Nat Rev Mol Cell Biol, pp. 610–621. Available at: https://doi.org/10.1038/nrm.2017.53.

Ray, S. *et al.* (2022) 'A mechanism for oxidative damage repair at gene regulatory elements', *Nature 2022 609:7929*, 609(7929), pp. 1038–1047. Available at: https://doi.org/10.1038/s41586-022-05217-8.

Rehwinkel, J. *et al.* (2013) 'SAMHD1-dependent retroviral control and escape in mice', *EMBO Journal*, 32(18), pp. 2454–2462. Available at: https://doi.org/10.1038/emboj.2013.163.

Reijns, M.A.M. *et al.* (2011) 'The structure of the human RNase H2 complex defines key interaction interfaces relevant to enzyme function and human disease', *Journal of Biological Chemistry*, 286(12), pp. 10530–10539. Available at: https://doi.org/10.1074/JBC.M110.177394.

Reijns, M.A.M. *et al.* (2012) 'Enzymatic Removal of Ribonucleotides from DNA Is Essential for Mammalian Genome Integrity and Development', *Cell*, 149(5), p. 1008. Available at: https://doi.org/10.1016/J.CELL.2012.04.011.

Reijns, M.A.M. *et al.* (2022) 'Signatures of TOP1 transcription-associated mutagenesis in cancer and germline', *Nature*, 602(7898), p. 623. Available at: https://doi.org/10.1038/S41586-022-04403-Y.

Reinhardt, H.C. *et al.* (2007) 'p53-deficient cells rely on ATM- and ATR-mediated checkpoint signaling through the p38MAPK/MK2 pathway for survival after DNA damage', *Cancer cell*, 11(2), pp. 175–189. Available at: https://doi.org/10.1016/J.CCR.2006.11.024.

Riva, V. *et al.* (2020) 'Novel alternative ribonucleotide excision repair pathways in human cells by DDX3X and specialized DNA polymerases', *Nucleic acids research*, 48(20), pp. 11551–11565. Available at: https://doi.org/10.1093/NAR/GKAA948.

Robu, M.E. *et al.* (2007) 'activation by knockdown technologies', *PLoS Genet*, 3(5), p. 78. Available at: https://doi.org/10.1371/journal.pgen.

Rocak, S. and Linder, P. (2004) 'DEAD-box proteins: the driving forces behind RNA metabolism', *Nature Reviews Molecular Cell Biology 2004 5:3*, 5(3), pp. 232–241. Available at: https://doi.org/10.1038/nrm1335.

Rumbaugh, J.A. *et al.* (1997) 'Creation and Removal of Embedded Ribonucleotides in Chromosomal DNA during Mammalian Okazaki Fragment Processing', *Journal of Biological Chemistry*, 272(36), pp. 22591–22599. Available at: https://doi.org/10.1074/JBC.272.36.22591.

Rydberg, B. and Lindahl, T. (1982) 'Nonenzymatic methylation of DNA by the intracellular methyl group donor S-adenosyl-L-methionine is a potentially mutagenic reaction.', *The EMBO Journal*, 1(2), p. 211. Available at: https://doi.org/10.1002/J.1460-2075.1982.TB01149.X.

Safari, R., Hoseinifar, S.H. and Kavandi, M. (2016) 'Modulation of antioxidant defense and immune response in zebra fish (Danio rerio) using dietary sodium propionate', *Fish Physiology and Biochemistry*, 42(6), pp. 1733–1739. Available at: https://doi.org/10.1007/s10695-016-0253-z.

Saldivar, J.C., Cortez, D. and Cimprich, K.A. (2017) 'The essential kinase ATR: ensuring faithful duplication of a challenging genome', *Nature reviews. Molecular cell biology*, 18(10), pp. 622–636. Available at: https://doi.org/10.1038/NRM.2017.67.

Schröder, M. (2010) 'Human DEAD-box protein 3 has multiple functions in gene regulation and cell cycle control and is a prime target for viral manipulation', *Biochemical Pharmacology*, 79(3), pp. 297–306. Available at: https://doi.org/10.1016/J.BCP.2009.08.032.

Segal, A.W. (2005) 'How neutrophils kill microbes', *Annual review of immunology*, 23, pp. 197–223. Available at: https://doi.org/10.1146/ANNUREV.IMMUNOL.23.021704.115653.

Sekiguchi, J.A. and Shuman, S. (1997) 'Site-specific ribonuclease activity of eukaryotic DNA topoisomerase I', *Molecular cell*, 1(1), pp. 89–97. Available at: https://doi.org/10.1016/S1097-2765(00)80010-6.

Serra-Marques, A. *et al.* (2020) 'The mitotic protein NuMA plays a spindle-independent role in nuclear formation and mechanics', *The Journal of cell biology*, 219(12). Available at: https://doi.org/10.1083/JCB.202004202.

Shao, R.G. *et al.* (1999) 'Replication-mediated DNA damage by camptothecin induces phosphorylation of RPA by DNA-dependent protein kinase and dissociates RPA:DNA-PK complexes', *The EMBO Journal*, 18(5), pp. 1397–1406. Available at: https://doi.org/10.1093/EMBOJ/18.5.1397.

Silk, A.D., Holland, A.J. and Cleveland, D.W. (2009) 'Requirements for NuMA in maintenance and establishment of mammalian spindle poles', *Journal of Cell Biology*, 184(5), pp. 677–690. Available at: https://doi.org/10.1083/jcb.200810091.

Sinha, N.K. and Snustad, D.P. (1972) 'Mechanism of inhibition of deoxyribonucleic acid synthesis in Escherichia coli by hydroxyurea', *Journal of bacteriology*, 112(3), pp. 1321–1324. Available at: https://doi.org/10.1128/JB.112.3.1321-1334.1972.

Sparks, J.L. *et al.* (2012) 'RNase H2-Initiated Ribonucleotide Excision Repair', *Molecular cell*, 47(6), p. 980. Available at: https://doi.org/10.1016/J.MOLCEL.2012.06.035.

Sparks, J.L. and Burgers, P.M. (2015) 'Error-free and mutagenic processing of topoisomerase 1-provoked damage at genomic ribonucleotides', *The EMBO Journal*, 34(9), p. 1259. Available at: https://doi.org/10.15252/EMBJ.201490868.

Stetson, D.B. *et al.* (2008) 'Trex1 Prevents Cell-Intrinsic Initiation of Autoimmunity', *Cell*, 134(4), pp. 587–598. Available at: https://doi.org/10.1016/j.cell.2008.06.032.

Stevnsner, T. *et al.* (2002) 'Mitochondrial repair of 8-oxoguanine is deficient in Cockayne syndrome group B', *Oncogene*, 21(57), pp. 8675–8682. Available at: https://doi.org/10.1038/SJ.ONC.1205994.

Substitutions, A.+ C. *et al.* (1992) '8-Hydroxyguanine, an abundant form of oxidative DNA damage, causes G-T and A-C substitutions.', *Journal of Biological Chemistry*, 267, pp. 166–172. Available at: https://doi.org/10.1016/S0021-9258(18)48474-8.

Sui, Y. *et al.* (2022) 'Ribodysgenesis: sudden genome instability in the yeast Saccharomyces cerevisiae arising from RNase H2 cleavage at genomic-embedded ribonucleotides', *Nucleic acids research*, 50(12), pp. 6890–6902. Available at: https://doi.org/10.1093/NAR/GKAC536.

Takahashi, T. *et al.* (2011) 'Topoisomerase 1 provokes the formation of short deletions in repeated sequences upon high transcription in Saccharomyces cerevisiae', *Proceedings of the National Academy of Sciences of the United States of America*, 108(2), pp. 692–697. Available at: https://doi.org/10.1073/PNAS.1012582108/-/DCSUPPLEMENTAL.

Takahata, C. *et al.* (2015) 'Repair synthesis step involving ERCC1-XPF participates in DNA repair of the Top1-DNA damage complex', *Carcinogenesis*, 36(8), pp. 841–851. Available at: https://doi.org/10.1093/CARCIN/BGV078.

Takashima, H. *et al.* (2002) 'Mutation of TDP1, encoding a topoisomerase I-dependent DNA damage repair enzyme, in spinocerebellar ataxia with axonal neuropathy', *Nature genetics*, 32(2), pp. 267–272. Available at: https://doi.org/10.1038/NG987.

Técher, H. *et al.* (2017) 'The impact of replication stress on replication dynamics and DNA damage in

vertebrate cells', *Nature reviews. Genetics*, 18(9), pp. 535–550. Available at: https://doi.org/10.1038/NRG.2017.46.

Thyme, S.B. and Schier, A.F. (2016) 'Polq-Mediated End Joining Is Essential for Surviving DNA Double-Strand Breaks during Early Zebrafish Development', *Cell Reports*, 15(4), pp. 707–714. Available at: https://doi.org/10.1016/j.celrep.2016.03.072.

Touati, E. *et al.* (2006) 'Deficiency in OGG1 protects against inflammation and mutagenic effects associated with H. pylori infection in mouse', *Helicobacter*, 11(5), pp. 494–505. Available at: https://doi.org/10.1111/J.1523-5378.2006.00442.X.

Truong, L.N. *et al.* (2013) 'Microhomology-mediated End Joining and Homologous Recombination share the initial end resection step to repair DNA double-strand breaks in mammalian cells', *Proceedings of the National Academy of Sciences of the United States of America*, 110(19), pp. 7720–7725. Available at: https://doi.org/10.1073/PNAS.1213431110/-/DCSUPPLEMENTAL.

Tucker, B. and Lardelli, M. (2007) 'A Rapid Apoptosis Assay Measuring Relative Acridine Orange Fluorescence in Zebrafish Embryos', *https://home.liebertpub.com/zeb*, 4(2), pp. 113–116. Available at: https://doi.org/10.1089/ZEB.2007.0508.

Tumbale, P. *et al.* (2014) 'Aprataxin resolves adenylated RNA-DNA junctions to maintain genome integrity', *Nature*, 506(7486), pp. 111–115. Available at: https://doi.org/10.1038/nature12824.

Uehara, R. *et al.* (2018) 'Two RNase H2 Mutants with Differential rNMP Processing Activity Reveal a Threshold of Ribonucleotide Tolerance for Embryonic Development', *Cell Reports*, 25(5), pp. 1135-1145.e5. Available at: https://doi.org/10.1016/j.celrep.2018.10.019.

Uziel, T. *et al.* (2003) 'Requirement of the MRN complex for ATM activation by DNA damage', *The EMBO journal*, 22(20), pp. 5612–5621. Available at: https://doi.org/10.1093/EMBOJ/CDG541.

Valdiglesias, V. *et al.* (2013) 'γH2AX as a marker of DNA double strand breaks and genomic instability in human population studies', *Mutation Research - Reviews in Mutation Research*. Elsevier, pp. 24–40. Available at: https://doi.org/10.1016/j.mrrev.2013.02.001.

Vance, J.R. and Wilson, T.E. (2002) 'Yeast Tdp1 and Rad1-Rad10 function as redundant pathways for repairing Top1 replicative damage', *Proceedings of the National Academy of Sciences of the United States of America*, 99(21), pp. 13669–13674. Available at: https://doi.org/10.1073/PNAS.202242599.

Vidi, P.A. *et al.* (2014) 'NuMA promotes homologous recombination repair by regulating the accumulation of the ISWI ATPase SNF2h at DNA breaks', *Nucleic acids research*, 42(10), pp. 6365–6379. Available at: https://doi.org/10.1093/NAR/GKU296.

Visnes, T. *et al.* (2018) 'Small-molecule inhibitor of OGG1 suppresses proinflammatory gene expression and inflammation', *Science*, 362(6416), pp. 834–839. Available at: https://doi.org/10.1126/SCIENCE.AAR8048/SUPPL_FILE/AAR8048S1.MP4.

Wainwright, M. (2001) 'Acridine-a neglected antibacterial chromophore', *The Journal of antimicrobial chemotherapy*, 47(1), pp. 1–13. Available at: https://doi.org/10.1093/JAC/47.1.1.

Walkley, C.R., Liddicoat, B. and Hartner, J.C. (2012) 'Role of ADARs in Mouse development', *Current Topics in Microbiology and Immunology*, 353(1), pp. 197–220. Available at: https://doi.org/10.1007/82_2011_150.

Wang, C. *et al.* (2018) 'Genome-wide CRISPR screens reveal synthetic lethality of RNASEH2 deficiency and ATR inhibition', *Oncogene 2018 38:14*, 38(14), pp. 2451–2463. Available at: https://doi.org/10.1038/s41388-018-0606-4.

Williams, J.S. *et al.* (2012) 'Proofreading of ribonucleotides inserted into DNA by yeast DNA

polymerase ε', *DNA repair*, 11(8), pp. 649–656. Available at: https://doi.org/10.1016/J.DNAREP.2012.05.004.

Williams, J.S. *et al.* (2013) 'Topoisomerase 1-Mediated Removal of Ribonucleotides from Nascent Leading-Strand DNA', *Molecular Cell*, 49(5), pp. 1010–1015. Available at: https://doi.org/10.1016/J.MOLCEL.2012.12.021.

Wosik, K. *et al.* (2003) 'Oligodendrocyte injury in multiple sclerosis: a role for p53', *Journal of neurochemistry*, 85(3), pp. 635–644. Available at: https://doi.org/10.1046/J.1471-4159.2003.01674.X.

Wright, J.A. *et al.* (1998) 'Protein kinase mutants of human ATR increase sensitivity to UV and ionizing radiation and abrogate cell cycle checkpoint control', *Proceedings of the National Academy of Sciences of the United States of America*, 95(13), pp. 7445–7450. Available at: https://doi.org/10.1073/PNAS.95.13.7445.

Wu, J. *et al.* (2013) 'Cyclic-GMP-AMP Is An Endogenous Second Messenger in Innate Immune Signaling by Cytosolic DNA', *Science (New York, N.Y.)*, 339(6121), pp. 826–830. Available at: https://doi.org/10.1126/SCIENCE.1229963.

Wu, L. (2013) 'Samhd1 knockout mice: Modeling retrovirus restriction in vivo', *Retrovirology*, 10(1), pp. 1–5. Available at: https://doi.org/10.1186/1742-4690-10-142.

Xi, Y., Noble, S. and Ekker, M. (2011) 'Modeling neurodegeneration in zebrafish', *Current neurology and neuroscience reports*, 11(3), pp. 274–282. Available at: https://doi.org/10.1007/S11910-011-0182-2.

Yang, C.A. *et al.* (2018) 'Prognostic Value of RNASEH2A-, CDK1-, and CD151-Related Pathway Gene Profiling for Kidney Cancers', *International Journal of Molecular Sciences 2018, Vol. 19, Page 1586*, 19(6), p. 1586. Available at: https://doi.org/10.3390/IJMS19061586.

Yang, C.H., Lambie, E.J. and Snyder, M. (1992) 'NuMA: An unusually long coiled-coil related protein in the mammalian nucleus', *Journal of Cell Biology*, 116(6), pp. 1303–1317. Available at: https://doi.org/10.1083/jcb.116.6.1303.

Yang, N., Galick, H. and Wallace, S.S. (2004) 'Attempted base excision repair of ionizing radiation damage in human lymphoblastoid cells produces lethal and mutagenic double strand breaks', *DNA Repair*, 3(10), pp. 1323–1334. Available at: https://doi.org/10.1016/J.DNAREP.2004.04.014.

Yue, F. *et al.* (2014) 'A comparative encyclopedia of DNA elements in the mouse genome', *Nature*, 515(7527), p. 355. Available at: https://doi.org/10.1038/NATURE13992.

Zaksauskaite, R. *et al.* (2021) 'Tdp1 protects from topoisomerase 1-mediated chromosomal breaks in adult zebrafish but is dispensable during larval development', *Science Advances*, 7(5). Available at: https://doi.org/10.1126/SCIADV.ABC4165.

Zhang, H. *et al.* (2022) 'TDP1-independent pathways in the process and repair of TOP1-induced DNA damage', *Nature Communications 2022 13:1*, 13(1), pp. 1–18. Available at: https://doi.org/10.1038/s41467-022-31801-7.

Zhang, L. *et al.* (2018) 'Identification of Common Genes Refers to Colorectal Carcinogenesis with Paired Cancer and Noncancer Samples', *Disease Markers*, 2018. Available at: https://doi.org/10.1155/2018/3452739.

Zhang, Y.-W. *et al.* (2011) 'Poly(ADP-ribose) polymerase and XPF-ERCC1 participate in distinct pathways for the repair of topoisomerase I-induced DNA damage in mammalian cells'. Available at: https://doi.org/10.1093/nar/gkq1304.

Zhang, Y. *et al.* (2005) 'Reconstitution of 5'-directed human mismatch repair in a purified system', *Cell*, 122(5), pp. 693–705. Available at: https://doi.org/10.1016/j.cell.2005.06.027.

Zhang, Y. *et al.* (2016) 'Manipulating the air-filled zebrafish swim bladder as a neutrophilic inflammation model for acute lung injury', *Cell Death & Disease 2016 7:11*, 7(11), pp. e2470–e2470. Available at: https://doi.org/10.1038/cddis.2016.365.

Zimmermann, M. *et al.* (2018) 'CRISPR screens identify genomic ribonucleotides as a source of PARP-trapping lesions', *Nature*, 559(7713), p. 285. Available at: https://doi.org/10.1038/S41586-018-0291-Z.

Zou, L. and Elledge, S.J. (2003) 'Sensing DNA damage through ATRIP recognition of RPA-ssDNA complexes', *Science (New York, N.Y.)*, 300(5625), pp. 1542–1548. Available at: https://doi.org/10.1126/SCIENCE.1083430.